Green Energy and Technology

Marcello De Falco
Angelo Basile *Editors*

Enriched Methane

The First Step Towards the Hydrogen Economy

Springer

Green Energy and Technology

More information about this series at http://www.springer.com/series/8059

Marcello De Falco · Angelo Basile
Editors

Enriched Methane

The First Step Towards the Hydrogen Economy

Springer

Editors
Marcello De Falco
University Campus Bio-Medico of Rome
Rome
Italy

Angelo Basile
ITM-CNR
University of Calabria
Rende
Italy

ISSN 1865-3529 ISSN 1865-3537 (electronic)
Green Energy and Technology
ISBN 978-3-319-22191-5 ISBN 978-3-319-22192-2 (eBook)
DOI 10.1007/978-3-319-22192-2

Library of Congress Control Number: 2015951769

Springer Cham Heidelberg New York Dordrecht London

Printed on acid-free paper

Springer International Publishing AG Switzerland is part of Springer Science+Business Media (www.springer.com)

Preface

The massive use of hydrogen as an energy vector would be the last step towards the energy decarbonisation process, solving once and for all the greenhouse gases and pollutant emissions in our industrial and civil systems.

On the other hand, technological development of the production processes, storage, distribution and use of hydrogen is still quite far from a real competitiveness compared to traditional fossil fuels. To date, in fact, there is no market for hydrogen as an energy carrier and, in the near term, hydrogen economy will hardly replace fossil fuels, even if the environmental and societal issues related to energy production are perceived as urgent and solutions are absolutely required in the next years.

Enriched methane could be an intermediate step able to introduce hydrogen in our energy systems, using the consolidated natural gas infrastructures at competitive costs and leading to a significant reduction of the pollution, immediately applicable and without high structural costs: the new blend is a necessary step towards the "dream of hydrogen".

The scope of this book is to present the most interesting and advanced technologies of enriched methane production and use, in order to update the readers on this topic and to clarify what is already available and on what the international scientific and technological communities have still to work at. At the end, the readers should have a clear panorama of both the enriched methane potentialities and on the step forward to be taken.

The realization of the book would have been impossible without the support of Profs. Luigi Marrelli and Prof. Diego Barba, who helped us in understanding and defining the focal and critical points of enriched methane production and applications.

The book aims to inspire young engineers and scientists to face the next technological challenges balancing the environmental requirements, the technological specifics and the market needs, always considering that any good idea should then be introduced in the market respecting its rules and should interact with the environment, reducing the impacts and the resources use.

Marcello De Falco
Angelo Basile

Contents

Enriched Methane: A Ready Solution for the Transition Towards the Hydrogen Economy

Mauro Capocelli and Marcello De Falco

Abstract The extensive use of hydrogen as an energy vector has the potential to minimize the world's addiction to crude oil mitigating the global warming as well as economic crisis and conflicts. Nonetheless, at least in the near term, hydrogen economy will hardly replace fossil fuels because of the high production cost, the difficulty of storing at high energy density, the lack of extensive distribution infrastructure. R&D advances do not satisfy policies, investors and consumer's needs. The potential for methane enrichment by mixing with hydrogen is an interesting alternative to the complete replacement of conventional fuels and to the increased need of exploiting renewable energies. This solution can rapidly find a market collocation to renewable production (from gasification and steam reforming), low-cost storage and delivery through existent technologies, whereas improving the environmental impact of "methane/natural gas" applications. In this chapter, we present the application potentialities of the enriched methane in the four areas characterizing the evaluation of alternative fuels: production, storage, distribution and utilization. We present the main advances in this framework and the near perspectives indicating the enriched methane as a promising route towards the hydrogen economy and an immediate solution for the mitigation of climate changes.

Keywords Hydrogen economy · Methane enrichment · Energy production · Storage · Distribution and use

List of Symbols

CCS	Carbon Capture and Storage
DOE	US Department of Energy
EU	European Union
FCH JU	Fuel Cell and Hydrogen Joint Undertaking
GTL	Gas to Liquid

M. Capocelli · M. De Falco (✉)
University of Rome "Campus Bio-Medico", Via Alvaro del Portillo 21,
00128 Rome, Italy
e-mail: m.defalco@unicampus.it

M. De Falco and A. Basile (eds.), *Enriched Methane*,
Green Energy and Technology, DOI 10.1007/978-3-319-22192-2_1

ICE	Internal Combustion Engine
IEA	International Energy Agency
LPG	Liquefied Petroleum Gas
NG	Natural Gas
PV	Photovoltaic
SI	Spark Ignition
USD	United States Dollar

1 Introduction

Hydrogen can be produced from all energy resources, from fossil to renewables (biomass, wind, solar and nuclear energy). It can be converted to power and heat with high efficiency and zero emissions. It is used as an energy carrier (Fig. 1) increasing, at the same time the security of supply by decoupling demand from resources and the chance to exploit renewables and offering a solution to the energy fluctuations [1–3].

Since the nineteenth century, the hydrogen potentialities were clear to scientist (J.B.S. Haldane advocated the hydrogen production from water splitting using wind energy) as well as writers (J. Verne prospected the energy self-sufficiency of Europe with hydrogen exploitation in his novel "The Mysterious Island"). The 1950s saw the development of hydrogen applications towards the realization of the first fuel cell of 5 kW by F. Bacon in 1959. The expression "hydrogen economy" was minted in 1970 by J. Bockris (General Motors), who saw hydrogen as the fuel for all types of transport. The 1973 oil crisis boosted the hydrogen exploitation, one year later the first "Hydrogen Economy" conference was organized in Miami. Many researchers advocated the production of hydrogen via electrolysis from nuclear power reactors; governments in the United States, Europe and Japan began to fund hydrogen research [1, 4]. The hydrogen economy became a popular "green utopia" after the words of many scientific and economic essayists and disseminators. J. Rifkin in 2002 promoted it for the realization of a national energy web towards democratic power redistribution. According to him, hydrogen showed the potential to end world's reliance on imported oil, mitigate the global warming and cool down geopolitical conflicts [5].

In 2003 the US strengthened the R&D efforts in hydrogen production by water electrolysis and started to link the hydrogen economy to the abundant nuclear power after the commitment of $720 million by G. Bush [6]. At the same time, believing in the strategic economic opportunities of the hydrogen technologies, the European Commission established the European hydrogen and fuel cell technology platform in 2003 to create a hydrogen-oriented energy system by 2050 [7, 8].

Since then, industries (as well as researchers) have made several steps forward in the use of hydrogen as an automotive fuel and in the coupling of its production to

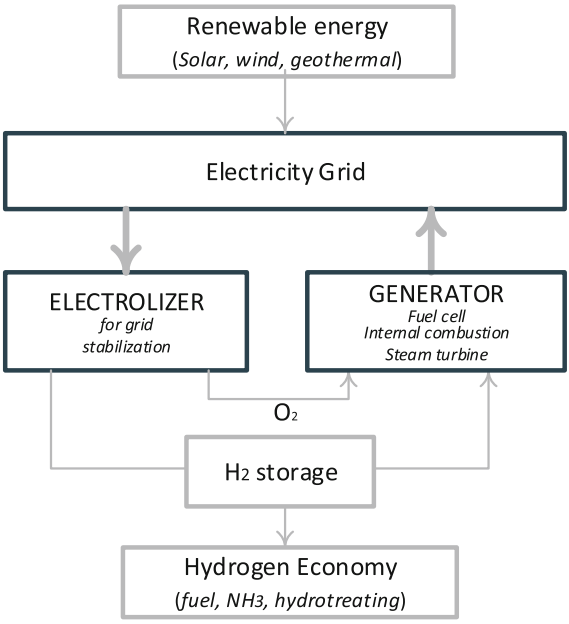

Fig. 1 Storage of renewable energy with hydrogen

renewable energies, two keystones of hydrogen economy [1, 8]. Nowadays, several types of fuel cells have been developed, cleaner and quitter car and buses are now travelling in our cities, hydrogen-fueled forklifts are now replacing battery-powered forklifts and different countries are accelerating the construction of hydrogen-fueling station [7, 9–11].

In the early twenty-first century, hydrogen energy has been linked to the decarbonating pathways of industrialized countries after the Kyoto Protocol in 2003 [4]. Coupled with Carbon Capture and Storage (CCS), the hydrogen production can be obtained also by biomass and waste gasification with a double industrial and environmental benefit [9–11]. Indeed, the hydrogenation of CO_2 to valuable products is a paradigm to the complete independence from fossil fuels and the insertion of renewable energy into the production cycle [12–16].

Despite these promising prospects, economical and research efforts did not payback the investors and the milestone in worldwide hydrogen roadmaps have been repeatedly postponed. Till date, hydrogen economy is still linked to fossil fuels: more than 95 % of the global H_2 production involves fossil fuels resulting in high carbon dioxide emissions [1, 2, 6–8, 17]. Moreover, the storage and delivery infrastructures suffer from the classical chicken-egg problem in a world where the hydrogen demand is not significantly growing. Therefore, although the utilization in vehicle is ready, the H_2 delivery will be economically unfair until it is seen as a common energy carrier (by the producers as well as actually perceived by the users). In the last years, oil prices dropped back down to historical lows and the recent accidents have highlighted the hidden costs of nuclear power.

Considering the problem of the high cost and, in some case, low efficiency of the production methods, storage and end-use technologies, it is clear that the transition towards a hydrogen economy will pass through the use of hybrid technologies [17, 18]. One of the most promising is the Enriched Methane (EM), a mixture of methane with the addition of a limited percentage of H_2, thought to avoid the drawbacks related to hydrogen transport and storage (and partially production). These kinds of mixtures can be transported, stored and used with the actual gas infrastructure. Moreover, available storage systems for compressed natural gas can be employed and no compressors are needed in the medium- or low-pressure distribution grid. The addition of H_2 in limited percentage in internal combustion engines can be realized with little modifications and high advantages. Hence, according to the most recent and developing scientific literature, the enriched mixture presents numerous advantages that can affirm it as a ready and sustainable solution in the transition phase towards the hydrogen economy [19].

On this basis, the following sections present an insight into the "EM economy" by discussing the peculiarity of enriched methane with a parallelism to the hydrogen. A summary of the R&D and political efforts in this context is presented. The discussion tackles the main topic: the production, the storage, the delivery/distribution and the end use/consumption. This logical sequence characterizes the description of hydrogen advantages as well as the barriers still limiting its application. The chapter eventually presents the way EM could overcome these issues keeping some advantages of the pure H_2 implementation and, on the other hand, offering a ready solution for the investor payback as well as the insertion of renewables in the production cycle.

2 Hydrogen

2.1 Production

Hydrogen is present in very small quantities in natural sources and is commonly produced from hydrocarbons (C_xH_y) and water. The production can follow different pathways by maximizing the local energy sources and the availability of renewable energy. Figure 2 shows the hydrogen production map. The processes can be grouped into thermochemical (dark blue), electrochemical (light blue) and photochemical (green). Although water appease as the most abundant and convenient source, hydrocarbons and fossil fuels are the most used as both raw materials and energy source.

Because of the lack of refuelling infrastructure and the delivery issues (mainly safety and low energy density), the hydrogen is commonly produced near the site of utilization by reformation of fossil fuels and biomasses. Up to now, almost the total production is located at the consumer-owned and consumer-operated refinery plants (captive production is almost the 50 % of the total) and ammonia (and partly

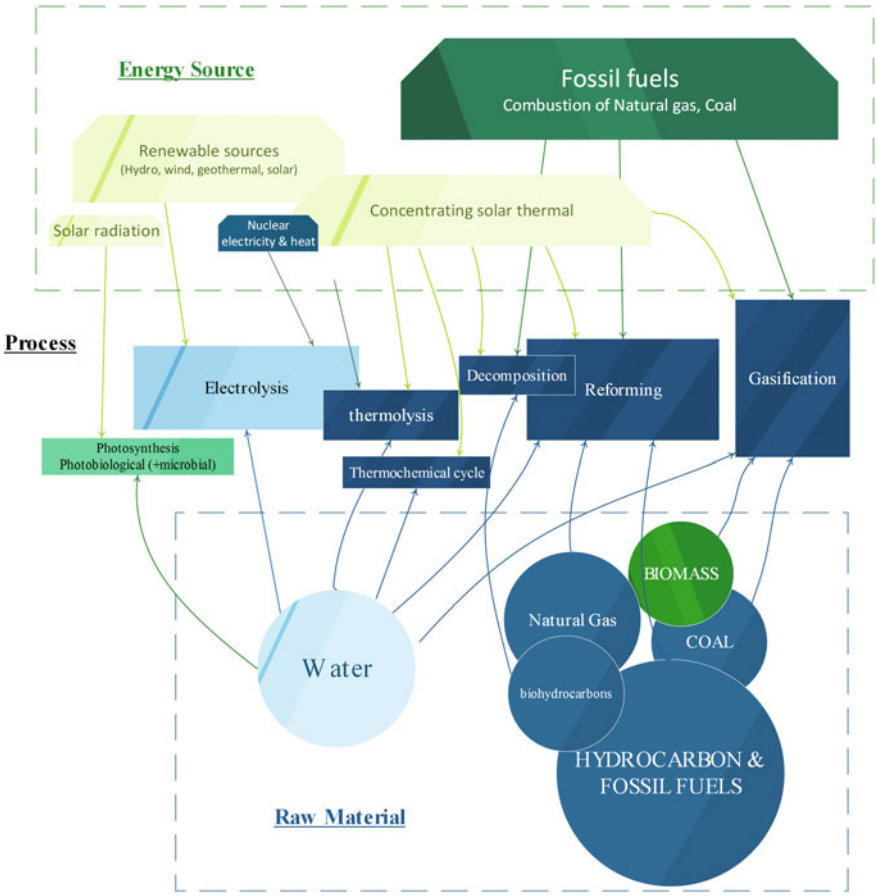

Fig. 2 Hydrogen production: *raw materials*, *processes* and *energy sources*

methanol) producers. Globally, the on-site production overcome the 90 % of the total and a very small quantity is supplied as compressed gas or cryogenic liquid by industrial gas companies, as shown in Fig. 3, that report both the captive (stationary refinery) capacity and the merchant capacity. The H_2 manufacture expansion does not confirm the global forecast: production of hydrogen has slightly increased in the last decade, while the hydrogen fuelling stations are still limited in a small number all over the world (mainly in Europe and Japan) [16–20].

The reforming breaks the hydrocarbon molecules into hydrogen through endothermic reactions needing an external heat source and a catalyst bed in order to reach the desired selectivity. Erickson et al. give an extended review of hydrocarbon reformation for H_2 production [21]. The reformation process can be directly combined to carbon dioxide capture and sequestration [11, 13]. Main feedstocks are natural gas/methane and refinery oil (partial oxidation). Production yield from

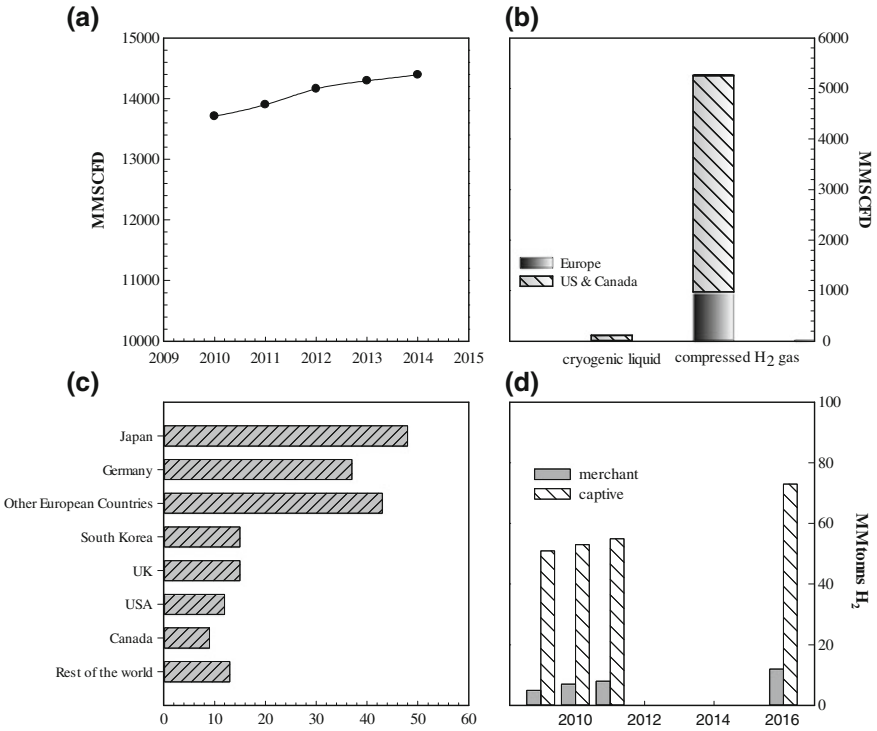

Fig. 3 **a** Installed refinery capacity **b** merchant capacity **c** fueling station **d** global market production [10, 16–20]

methanol and ethanol are not competitive if compared with the SR of gasoline or diesel but both alcohols can be reformed at very low temperature compatible with renewable energies. In a typical methane steam reformer, the process is carried at 800–1000 °C at 20–45 bar in a Ni-based catalyst, then the water-gas shift reaction is carried out to increase the H_2 yield by CO conversion [22–24]. R&D efforts in the field of hydrogen stationary production characterize the area of renewable energy coupling [21, 25], CO_2 capture [11–15], reactor optimization and membrane reactor development for the pure H_2 production [22, 23, 26–28]. Furthermore, the chance of on-board production via reforming (internal reforming) would enable the ambient storage and transportation of high energy density fuels and the utilization with low environmental impact and heat losses. High temperature fuel cells based on molten carbonate or solid oxide technology operate at sufficiently high temperatures to run directly on methane [20, 29].

Valuable synthesis gas containing H_2 can be obtained through steam gasification of coal and biomasses [17, 30]; recent advances in this field regard high temperature water-gas shift, the supercritical and the plasma gasification [12, 14, 20]. According to Gnanagrapasam et al., in the next future the coal gasification with CCS will reach

production cost competitive with the same process applied to natural gas; in the same paper, the authors give and extensive analysis of hydrogen production from solid fuels from the techno-economic analysis to the waste management system integration [31].

In the electrolysis process, the electric current splits water into hydrogen and oxygen with a typical efficiency of 70–80 %. This process is modular and suitable for large-scale production with a wide range of capacity and different chances for renewable energy coupling. The Alkaline, PV, solid polymer and high-temperature electrolysis are among the main recent advances in this field [20, 29, 32].

The thermochemical cycle consists of the water splitting reaction for H_2 and O_2 production with recycling and regeneration of intermediate compounds. Mirabel et al. give a comprehensive review of this topic [32].

Biohydrogen can be obtained through photolysis (H_2 from water and sunlight), photo- and dark fermentation. In the photobiological water splitting, microbes, such as green algae, consume water in the presence of sunlight with hydrogen as a by-product [32, 33]. Over the past decades, many publications have focused on microbial H_2 production but a number of obstacles have to be overcome for the realization on a practical scale. Dark fermentation is considered of a great interest because realizable in the absence of light (all day long) at anaerobic conditions, producing cheap H_2 and valuable metabolites [32].

Current decentralized production costs are more than 50 USD/GJ representing still a limiting factor towards the affirmation of the hydrogen economy paradigm. At the state of the art, to produce hydrogen costs more than to produce electricity as well as other fuels from biomass or fossils [34]. Although it is predicted that natural gas steam reforming will decrease to about 15 USD/GJ, electrolysis processes to less than 20 using solar or nuclear heat as some gasification processes, this will happen a consolidate technological scenario. At this stage, H_2 production costs remain still higher than other conventional and alternative fuels (Fig. 4 shows the comparison at two different gasoline prices). Moreover, the end-use cost (as described in further paragraphs) would remain high in the near future because of the overall (capital) cost of storage and delivery infrastructures necessary for the market consolidation [34].

2.2 Storage

Hydrogen has a low molecular weight and is in the gaseous phase at normal usage and storage temperatures. It has a very low normal density, although it has the highest mass lower heating values (Fig. 5), the volumetric density is lower in comparison to the conventional fuels. Gasoline has a specific energy of 42 MJ/kg approximately and a volumetric energy density of 32 MJ/L, a 10^3 magnitude higher than H_2. As aforementioned, in order to overcome the low-density issue, hydrogen is mainly produced at the use point.

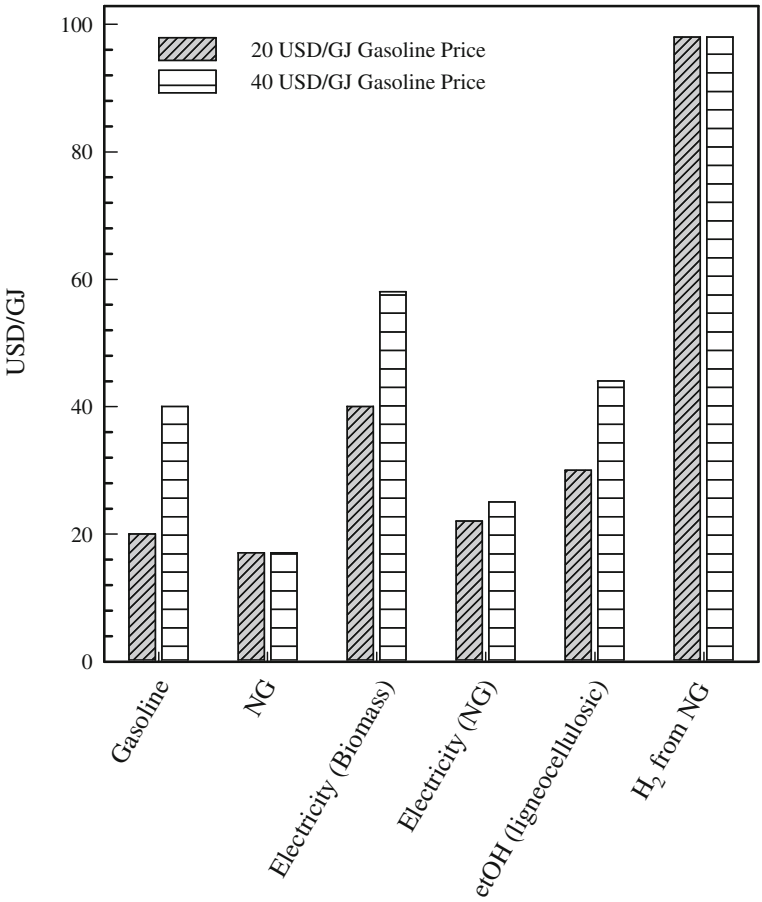

Fig. 4 Cost of production from different sources at two levels of crude oil prices (extracted from [34])

Alternatively, it can be liquefied at cryogenic temperatures (20 K, p = 200 kPa) and compressed in the gas phase at 15–25 MPa. Since the hydrogen molecules migrate within the steel structure, the long-term exposure of hydrogen to carbon steel can promote embrittlement and cause stress corrosion cracks and failures. Bends in piping or welded joints are susceptible to failure as well. Hoses for hydrogen should be non-porous to prevent leakage. Both these physical storage systems require high volume and/or high pressure, low temperatures and, consequently, expensive materials (e.g. to maintain cryogenic conditions, liquid H_2 is typically stored in double-walled superinsulating Dewar vessels). Non-ferrous metals as aluminium, copper and alloys like bronze and brass are compatible with hydrogen. Although the liquid form is the most valuable, it is confined to niche applications such as space program and high energy nuclear physics because H_2

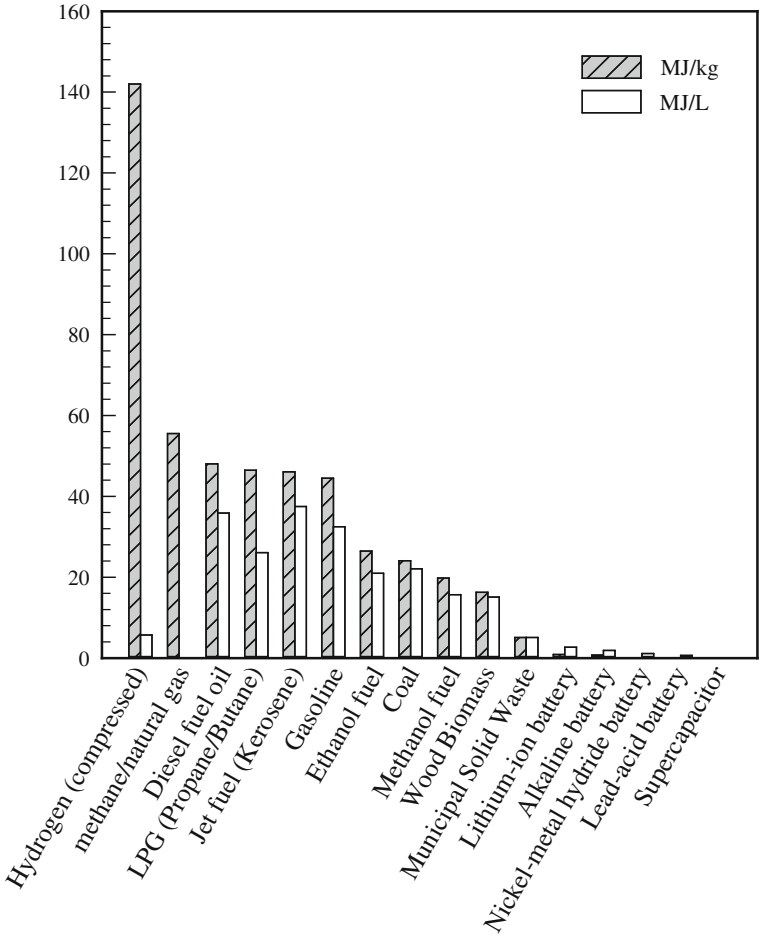

Fig. 5 Energy density of fuels

liquefaction requires more than 10 kWh/kg consuming 33 % of H_2 heating value. Moreover, heat transfer issues must be addressed (liquid hydrogen requires the use of vacuum jacketed piping to minimize heat gain) and, particularly for the liquid form, the hydrogen delivery and consumption rates should be carefully matched (H_2 must be used at a sufficiently high rate at the point of consumption in order to avoid the boiling off from containment vessels). Liquid hydrogen presents another set of safety issues, such as risk of cold burns and the increased duration of leaked cryogenic fuel or the violent explosion of expanding vapours in case of a pressure relief valve failure [1–3, 32, 35]. The consolidated storage costs in the range of 2.5–40 USD/kWh for liquid hydrogen storage and compressed terrestrial tanks. Geological storage and salt cavern have a lower storing cost (0.05–0.5 USD/kWh).

In the presence of some metals and alloys, H_2 can form metal hydrides splitting in H atoms in the lattice. Taking into account the mass of the metal, this process does not bring a great advantage in mass density of the storage system: the best gravimetric storage density achieved is 0.07 kgH_2/kg of metal for a high-temperature hydride MgH_2 [36]. This method is considered the safest because the chemical binding avoids flame propagation in case of tank damage. The process also needs heat removal in the storage process and energy supply during the releasing one (in case of the on-board storage this can be achieved by using exhaust gases). Carbon nanotubes capable to store 75 % H_2 also in a reversible way are under development [35–37]. The reversible storage option involves adsorbing hydrogen on a carbon surface; adsorbed H_2 can be increased as the temperature is lowered (cryogenic temperatures are not required) and can be dissociative (conventional metal hydrides, complex hydrides, Low-Z hydrides, hydrocarbons) or molecular (oxides, carbon-based and hybrid material). Such materials (e.g. activated carbon or small glass sphere) can be heated on-board to release the hydrogen gas. A great deal of literature reported that materials such as carbon nanotubes and pyrolized conducting polymers could provide high-capacity ambient-temperature hydrogen storage [36, 37].

2.3 Distribution

The road map of hydrogen supply represents a trade-off between centralized and distributed production to consider [34, 36]. Furthermore, the unique hydrogen properties present unique challenges to pipeline materials and compressor design. Producing hydrogen centrally in large plants cuts production costs but boosts distribution costs. On the other hand, the production at the fuelling stations cuts distribution costs but boosts production costs. Up to now, most hydrogen used is produced at or close to where it is used, typically at large industrial sites, and the hydrogen distribution through pipelines is limited to the transportation to nearby utilization sites (10–20 km) in stainless steel piping [35–38].

The prerequisite for establishment of a widespread hydrogen economy is the development of the infrastructure needed for distributing hydrogen to the nationwide network of fueling stations required for the widespread use of fuel cell vehicle. Without both actual and perceived fueling capability (convenient station location, fueling speed and safety), consumers will be reluctant to purchase fuel cell vehicles. Since the demand is influenced by both the perceived availability and the economy, this is a classical chicken-and-egg problem. Furthermore, building a new hydrogen pipeline network involves high initial capital costs (1.5–1.8 times higher costs than large-scale natural gas transmission) more than political efforts to overcome. Natural gas reciprocating compressors can be used for H_2, while centrifugal compressors instead may cause greater problems. Attention is needed for the sealing and to the fatigue stressed materials and embrittlement by pure H_2 at

high pressure. In order to minimize leaks, compression fittings and flanged joints are preferred on pipes instead of threaded joints [38].

Elgowainy et al. studied the delivery cost of hydrogen as a function of hydrogen vehicle market penetration [39] by individuating nine possible pathways of hydrogen delivery from the point of view of production, storage, transmission and distribution (compressed H_2 gas in tube trailers, via pipelines and Liquid H_2 trucks' transportation). They concluded that in the early market all delivery modes show 5–10 USD/kgH_2 and, for a mature market conditions with H_2 sufficient penetration, the best option is the pipeline delivery showing 2–4 USD/kgH_2. For pipeline delivery, tube trailer delivery and liquid hydrogen delivery, the energy consumption corresponds to a significant amount of the delivered energy, respectively, the 30, 35 and 80 %.

2.4 End Use

The electrochemical conversion through fuel cell produces directly electrical energy with a reverse electrolysis. Type of fuel cells are: Alkaline fuel cells, proton exchange membrane, phosphoric acid fuel cells, molten-carbonate fuel cells, solid oxide fuel cells. This topic embraces the principal investigation and R&D recent efforts [39, 40].

Hydrogen-fired internal combustion engines are more efficient than conventional gasoline engines with higher compression ratio and specific heat ratio. Hydrogen has a low self-ignition temperature and can burn in lean mixture. It basically produces H_2O and small amount of NOx that can be controlled through gas recirculation. Very small amount of hydrocarbons and CO_2 are formed by lubricating oil combustion. By adding water to control the temperature, saturated and supersaturated steam can be produced from the oxygen combustion product (steam at 3000 °C). Hydrogen steam generation with very high energy efficiency can be used for peak load electricity generation, industrial steam supply network, spinning reserve in power plant and microgeneration (as well as in some biotechnology and medical applications).

3 Barriers Towards the Hydrogen Economy

Although someone could think that the falling oil price is responsible for the braking in renewable investments, the biggest threat to the investment in low-carbon energy is the financial crisis. Renewable energy subsidies cut or revoked are among the first choice in a framework of global recession.

This critical framework partially slows down the expansion of the hydrogen economy. As a matter of fact, the production of hydrogen as energy carrier would require an increase in production rate by several orders of magnitude. In a

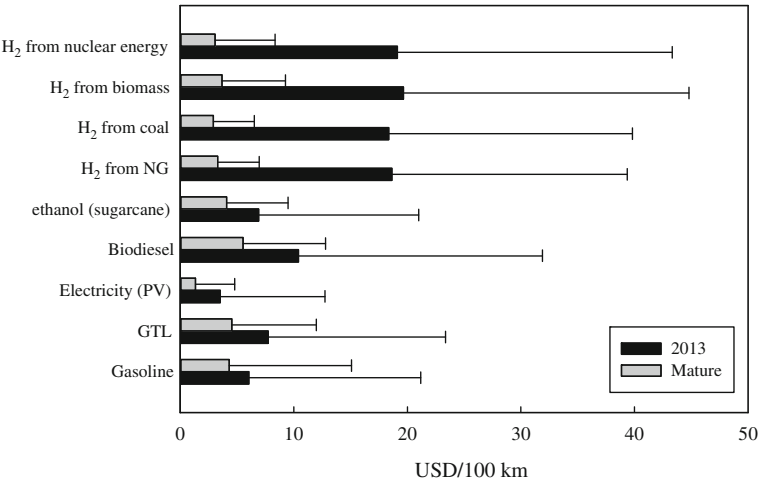

Fig. 6 Fuel total driving cost [34]

market-driven economy, the hydrogen faith will be connected to the final cost perceived by the users. Although the production cost will decrease in a mature technological scenario, the overall investment in infrastructure (DOE estimated its order of magnitude in the trillion of USD) will weigh on the end-user cost. The technological limit described in the previous sections are evident in the calculation of the final H_2 cost calculated by IEA (total cost of driving by taking into account the production, the storage, the delivery and utilization). The simulations are repeated for different fuels in the 2013 scenario (at two different gasoline prices) and considering a fully mature technological supply chain. Main results are reported in Fig. 6; the upper value is calculated in high petroleum cost scenario, a mature scenario for hydrogen would be achieved by 2030. Their results state the higher hydrogen cost in the current scenario at any possible fuel price is well above the conventional fuels and will be comparable only in the 2030, when most probably the electricity will defeat all the other competitors [34].

More than the technological barriers highlighted in the previous paragraphs, some crucial aspects should be considered analysing the strategy of hydrogen economy development. A consistent portion of R&D effort in hydrogen economy has been linked to nuclear energy and recent accidents have highlighted the hidden costs of nuclear power. In 2009, USA was the first investor in FCH diverting much of the funding into battery research. Now, all the US decarbonized pathways assume a percentage of hydrogen sources below the 15 % (comparable to biofuels) with a predominance of electrical energy source from batteries. Indeed, since the 2011, the majority of the alternative US fueling station in USA is electrical. Figure 7 reports the incidence of major fuels in the US in 1992 and 2011. Although increased in the last decades, the hydrogen utilization is not comparable to the other fuels (fossil as well as alternative).

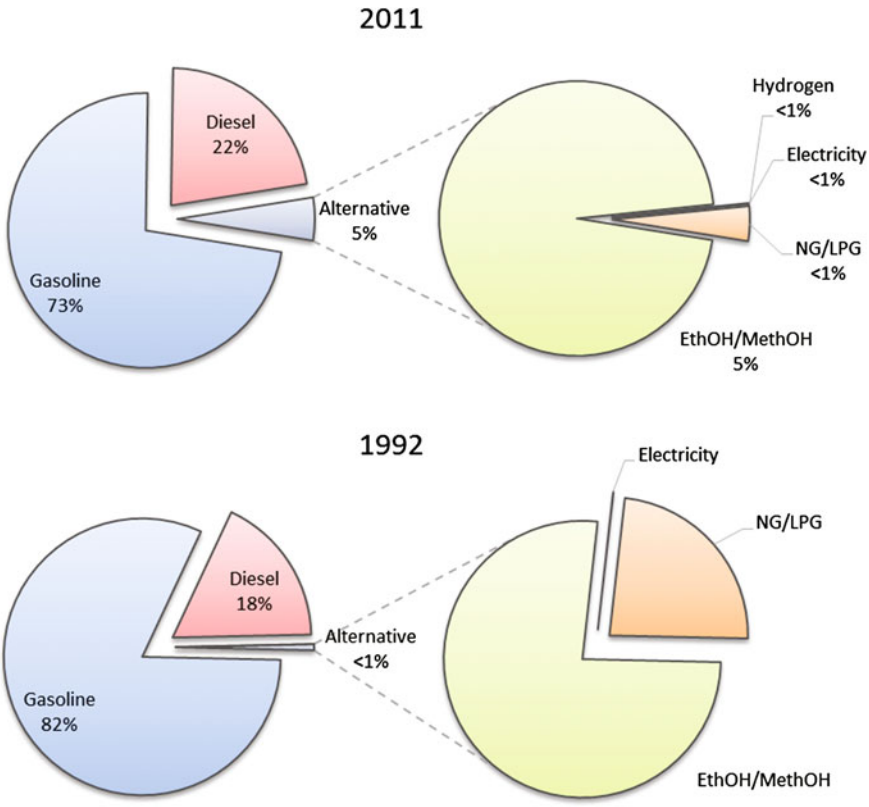

Fig. 7 Consumption of conventional and alternative fuels for highway vehicles (thousand gasoline-equivalent gallons) [41]

Moreover, the hydrogen production faith has been tight to a "not ready" technological area: the carbon capture and storage, CCS. Nowadays, more than 90 % of the world's hydrogen is produced from fossil fuels through steam reforming of hydrocarbons (mostly natural gas) producing carbon dioxide. Therefore, the high costs of CCS technologies pose a real brake on the development of the hydrogen economy.

Up to now, the hydrogen economy has not been self-sustained neither market-driven but hanging on the thread of political decisions. In order to achieve the market applications, it is common that the cash flow of an innovative technology goes negative if not supported by this kind of investment; a public investment is required to make a breakthrough technology escape from "the valley of death". Figure 8 depicts this approach adopted by the EU to estimate the required investments in hydrogen and fuel cell technologies. In 2007, the HFP estimated that the required R&D effort (until 2015) to achieve the objectives of the hydrogen economy costed around €7.4 billion. The calculation method is based on the

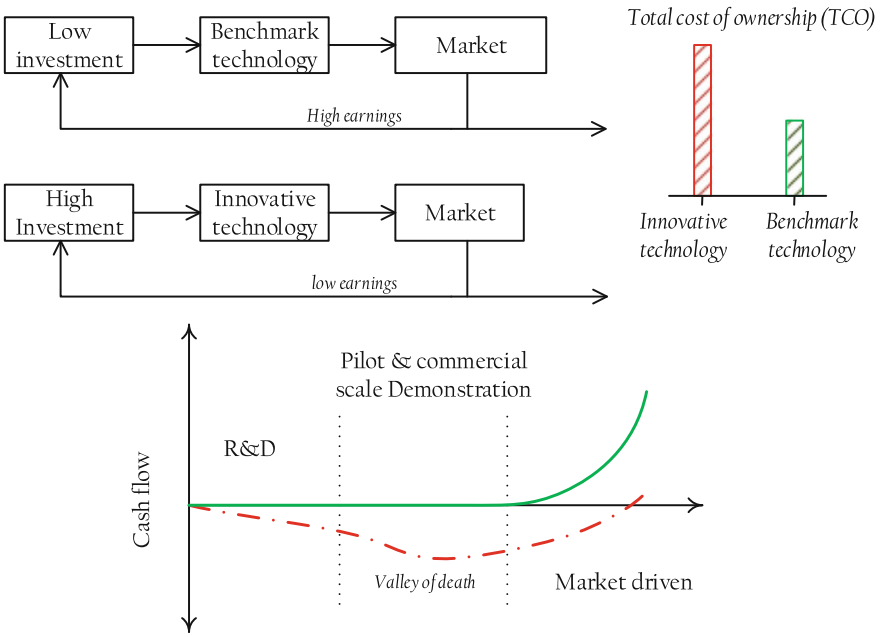

Fig. 8 Financing approach of the EU

evaluation of the cost of research projects needed to achieve the technology performances considering the total "Cost of Ownership" (both the acquisition cost and the operational costs) comparison between breakthrough and benchmark technology.

Following the approach promoted by HFP, EU created the Fuel Cells and Hydrogen Joint Undertaking (FCH JU) as the first Industrial Initiative under the EU SET Plan with a dedicated budget of public and private partnership supporting R&D in a coordinated manner (fundamental/basic as well as demonstration and policy, pre-market study) in 2008. The JU spent more than 400 M€ in R&D, supporting more than 130 projects between 2008 and 2013:

- 45 Project in Transportation for 202 M€ (H_2 consumption down to 11 kg/100 km for buses, more than ten refuelling station with H_2 cost less than 10 €/kg)
- 87 in energy for 210 M€ (more than 1000 micro CHP for domestic application; fuel cell improvement in electrical efficiency)
- 19 Project in Cross-Cutting Priorities for 20 M€.

Although the great economic effort, 940 M€ considering the private co-funding, the available amounts were still insufficient to facilitate a market breakthrough and to overcome the significant commercialization gap; a significant difference remains between the necessary €7.4 billion and the allocated 1 [8, 20].

4 The Enriched Methane

Considering the above-mentioned difficulties in harnessing hydrogen as a transportation fuel, it has become necessary to examine near-term alternatives. The addition of hydrogen to mixture of other fuels (hydrogen enrichment) is a ready alternative that can act as a route towards the hydrogen economy (being a compromise between the full objectives and the fast commercialization). According to the literature, H_2 is considered the best gaseous candidate for natural gas/methane enrichment due to its rare burning peculiarities. A brief insight into the blend of 15–20 % H_2 and 80–85 % CH_4 is presented in this section. An overall comparison of their fuel properties is given in Table 1 (the properties of their mixtures lay within those values). In the cited proportion, hydrogen contributes only about 5–7 % of the total heat of combustion but enables the exploitation of all the existent infrastructures and conversion technologies with improved results in terms of efficiency and emission (with respect to the pure methane).

Table 1 Hydrogen and methane property comparison

	Hydrogen	Methane
Density (kg/m^3)	0.084	0.65
Heat of vaporization ($kJ \times kg^{-1}$)	445.6	509.9
Lower heating value ($kJ \times kg^{-1}$)	119.93×10^3	50.02×10^3
Higher heating value ($kJ \times kg^{-1}$)	141.8×10^3	55.3×10^3
Thermal conductivity ($mW \times cm^{-1}\ K^{-1}$)	1.897	0.33
Diffusion coefficient in air ($cm^2 \times s^{-1}$)	0.61	0.16
Flammability limits in air (vol.%)	4.0–75	5.3–15
Detonability limits in air (vol.%)	18.3–59	6.3–13.5
Limiting oxygen index (vol.%)	5	12.1
Stoichiometric composition in air (vol.%)	29.53	9.48
Minimum energy for ignition in air (mJ)	0.02	0.29
Autoignition temperature (K)	858	813
Flame temperature in air (K)	2318	2148
Maximum burning velocity in air ($m \times s^{-1}$)	3.46	0.45
Detonation velocity in air ($km \times s^{-1}$)	1.48–2.15	1.4–1.64
Energy of explosion, mass-related (gTNT/g)	24	11
Energy of explosion, volume-related ($gTNT \cdot m^3(STP)$)	2.02	7.03

4.1 Production

If compared to the production of pure hydrogen, the enrichment is easier connectable with renewable energy.

As reported in the previous paragraphs, the steam methane reforming at high temperatures over Ni-based catalyst is today the most important commercial massive hydrogen production process. However, if just a limited volumetric content of hydrogen (15–20 %) is requested, a limited methane conversion and lower operating temperature is needed. Therefore, different efficiently matching with low-quality energy sources can be implemented if the enrichment is chosen instead of pure hydrogen. De Falco et al. studied the coupling options with solar-derived heat available at temperatures lower than 600 °C for the production of 17 % H_2 enriched methane. They proposed the optimization of an innovative reactor coupled with CSP technology using molten salt stream as heat carrier [18], as better described in Chaps. 2 and 3. The same research group also underlined the environmental benefit of this technology for the large-scale implementation (1.5 hectare plants for more than 2500 domestic users and more than 6000 ICE-based vehicles) [42]. Generating hydrogen enrichment by on-board reformation is energetically practicable if the increase in efficiency cover the energy required for reformation. In order to generate the 5 % energy of hydrogen using a reformation process with thermal efficiency of 80 % it would be required to convert the 6.25 % of the incoming primary fuel. An integrated production strategy with waste heat recovery has been depicted by Vernon and Erickson et al. [43].

The enrichment finds a great development in gasification process which can be used to exploit renewable energy sources. Biomass steam gasification is already predisposed to produce hydrogen-rich product gas. CaO-based chemical looping gasification (CaO-based CLG) has been proven due to its energy-efficient and environment-friendly aspects [13, 14].

Cavinato et al. proposed a long-term pilot scale demonstration of thermophilic dark fermentation and anaerobic digestion of food waste (refer to Chap. 4). They produce a daily gas composition of methane, hydrogen and carbon dioxide respectively at 58, 6.9 and 36 % (gas production of 0.80 m^3/kgTVS) [33].

4.2 Storage

A viable hydrogen storage technology has not yet implemented: H_2 hydride storage suffer from high-desorption temperatures, while physic-sorption in nanoporous adsorbents (such as carbon) can meet required storage densities and deliveries only at low temperatures [44].

The main safety issue related to the storage is that the hydrogen/air mixture can burn in relatively wide volume ratios between 4 and 75 % of hydrogen. Hydrogen has a very low ignition energy (0.02 mJ reaches minimum at about 25–30 %

hydrogen content in air), about one order of magnitude lower than other fuels. Hydrogen has a flame velocity 7 times faster than that of natural gas or gasoline and would therefore be more likely to progress to a deflagration or even a detonation than other fuels. Moreover, the hydrogen burns in invisible flames and has a great tendency to escape if stored as compressed gas. Because hydrogen suffers from real and perceived economic and safety issues, the storage represents a strong barrier to its diffusion [36, 37, 46].

Logistically, methane can be easier to work with than hydrogen. Methane's boiling point is about 110 K, compared to hydrogen's 20 K; this means that nitrogen can be used as purge gas for both fuel and oxidizer lines. It has a higher energy volumetric density, favourable for the on-board storage.

From the safety point of view, the addition of hydrogen to methane results in a negligible increase of the explosion risks up to 30 % (without any mitigation actions). Little differences in overpressure for methane/hydrogen mixture containing 20 % have been observed and no transition to detonation [45, 46].

Besides the conventional storage methods (related to methane and natural gas) many innovative storage methods under development for hydrogen can be suitable for EM. Kowalcycs and Bhatia studied the carbon nanopores storage of hydrogen methane mixture for the increasing of volumetric energy density [44]. Their computational studies suggest the utilization of H_2–CH_4 mixture physisorbed in a vessel with an extra container filled with pure free/adsorbed methane, a possible configuration for bus on-board fuel storaging near ambient pressures.

4.3 Distribution

As aforementioned, the distribution infrastructures are crucial for driving the H_2 production and increasing the overall market. Besides the on-site generation (SR and electrolyser) or the H_2 carrying by track/rail or new pipeline, the ready solution is the transport into methane and natural gas existent pipeline networks. Nonetheless, according to the pertinent literature, this last is possible only below a limit of H_2 concentration.

The FP7 project named Naturally formed a consortium of 39 European partners, including 15 from the gas business company for the investigation of hydrogen enrichment of the natural gas system. The project individuates the fatigue behaviour as the main critical issue concluding that the maximum percentage of H_2 added to natural gas is limited by (in order of increasing stringency) pipeline materials, safety and end use. About the transmission pipelines, the final results give confidence to the technical feasibility of injecting H_2 in NG pipes. The most critical situation is the fatigue behaviour that limit the H_2 below the 50 % vol. The safety issues for the increased permeation losses limit the practical concentration to the 20 % (in this range, no substantial issues were observed). These considerations give emphasizes the practicability of H_2 blending with CH_4 (or natural gas) in existent delivery systems [45, 46].

4.4 End Use

Hydrogen enrichment, when performed properly, promotes complete combustion and extends the lean/dilute operating limits. It can be applied to different types of combustion processes: internal combustion engines (ICEs), spark ignition (SI) and compressed ignition (CI), turbine system and burners [19]. Major effects are the increase of thermal efficiency and the reduction of pollutant emissions. Pre-mixed hydrogen enrichment in a direct injection stratified methane engine increases efficiency, reduces CO and HC. The NOx increases should be controlled by retarding ignition timing. Munshi demonstrated that it is possible to lower NOx and hydrocarbon emission (keeping constant the engine torque and fuel economics) in a lean-burn SI engine with natural gas enriched 20–30 % [47]. Through hydrogen addition it is possible to ameliorate the mixing conditions of fuel jet [48].

The H_2 enrichment brings more complete combustion, reduced CO and NOx emission in lean conditions, with potential increased gas recirculation [42]. In SI ICEs hydrogen increases free radical production with extension of the lean limit, shortening of the flame nucleation period, thereby increasing the heat release/burn rate. The hydrogen addition does not change the general trends but typically shift them towards higher efficiency. Hydrogen enrichment in stoichiometric conditions can increase peak temperatures causing moderate NOx emission increase. On the other hand, by using ultra lean mixtures close to the dilution limit the peak can be reduced to minimize NOx formation [47–52]. Temperature dependence of laminar burning velocity of EM mixtures were predicted by Kumar Jadav et al. [49], providing how to improve stability and lean flammability limits of low heating value fuels like biogas, gasification gas and producer gas by blending them with hydrogen. The promotion of chemical reaction with hydrogen addition is due to the increase of H, O and OH mole fractions in the flame as hydrogen is added. The mole fraction of CH_2O and CH_3CHO is decreased as hydrogen is added to reduce the aldehydes emissions; the methane oxidation pathways move towards lower carbon reactions reducing the soot formation [47–52]. Several studies investigate the effect of hydrogen addition to methane from the theoretical and experimental point of view [50–54].

On the other hand, the use of any gaseous fuel reduces the power output per unit volume. The degree of power reduction depends on the difference in volumetric energy density in the enriched air–fuel mixture (an enrichment of 25 % reduces approximately the amount of energy per unit volume of 4 %). Increasing in efficiency associated with hydrogen enrichment partially compensates the reduction of overall energy volume density.

From the safety point of view, pre-ignition leading knock can be caused by hot spot gases in the cylinder that, in H_2–CH_4 case, should be cooled. Flame flashback is also possible into the intake manifold or premix chamber. Nevertheless, an overall hydrogen enrichment below 20 % showed similar knock resistance as the primary fuel and similar potential risks. For properly adjusted appliances and favourable conditions of natural gas quality, also conventional domestic utilities can accommodate up to 20 % H_2 blends.

5 Conclusions

The hydrogen economy is progressing slowly towards a full affirmation. Many technological and economical barriers are limiting the H_2 utilization and are mining the investors' confidence. From the brief review of the last decade developments, the main limit appeared to be:

- low impact of renewable energy in the hydrogen production. Currently, 96 % of hydrogen is generated from fossil fuels, while less than 4 % of hydrogen is made from water via electrolysis;
- the high costs of transport and storage equipment and infrastructures;
- no breakthrough innovations in the last years have lowered the attention of policy and markets;
- high R&D effort still needed (CCS, lower cost composite material for hydrogen pipeline and storage vessels as well as new methods in high efficiency renewable hydrogen liquefaction).

In this context, the hydrogen enrichment can act as a catalyst for the hydrogen economy bringing a compromise between the market and the technical/environmental benefits. EM diffusion as fuel could constitute a crucial step towards a more sustainable economy worldwide with the following strategic objectives:

- to increase the renewable share in the hydrogen production system;
- to offer a market-driven solution capable to payback the investment towards the hydrogen economy;
- to contribute to the decarbonating and depolluting of emission, particularly in the automotive sector;
- to prepare the public opinion to accept hydrogen as fuel (mainly overcoming perceived safety issues).

References

1. Marbán G, Valdés-Solís T (2007) Towards the hydrogen economy? Int J Hydrogen Energy 32 (12):1625–1637
2. Steinfeld A (2005) Solar thermochemical production of hydrogen—a review. Sol Energy 78 (5):603–615
3. Barreto L, Makihira A, Riahi K (2002) The hydrogen economy in the 21st century : a sustainable development scenario. Int J Hydrogen Energy 28(43):1–10
4. McDowall W, Eames M (2006) Forecasts, scenarios, visions, backcasts and roadmaps to the hydrogen economy: a review of the hydrogen futures literature. Energy Policy 34(11):1236–1250
5. Clark WW, Rifkin J (2006) A green hydrogen economy. Energy Policy 34(17):2630–2639
6. DOE (2006) Hydrogen posture plan. An Integrated Research, Development and Demonstration Plan
7. DOE (2011) Breakthrough Technology Institute Inc. 2010 Fuel Cell Technologies Market Report

8. EU (2013) Second interim evaluation of the fuel cell and hydrogen joint undertaking. Publications Office of the European Union, Luxembourg
9. DOE (2008) Effects of a transition to a hydrogen economy on employment in the United States report to congress
10. Bromaghim G, Gibeault K, Serfass J, Serfass P, Wagner E (2010) Hydrogen and fuel cells the U.S. market report. National Hydrogen Association, Washington
11. Rose R, Gangi J, Curtin S (2013) 2012 Fuel cell technologies market report, DoE EERE
12. Andrés MB, Boyd T, Grace JR, Jim Lim C, Gulamhusein A, Wan B, Kurokawa H, Shirasaki Y (2011) In-situ CO2 capture in a pilot-scale fluidized-bed membrane reformer for ultra-pure hydrogen production. Int J Hydrogen Energy 36(6):4038–4055
13. Hanaoka T, Yoshida T, Fujimoto S, Kamei K, Harada M, Suzuki Y, Hatano H, Yokoyama S, Minowa T (2005) Hydrogen production from woody biomass by steam gasification using a CO2 sorbent. Biomass Bioenergy 28(1):63–68
14. Molburg JC, Doctor RD (2003) Hydrogen from steam-methane reforming with CO 2 capture. In: 20th annual international Pittsburgh coal conference
15. Gallucci F, Fernandez E, Corengia P, van Sint Annaland M (2013) Recent advances on membranes and membrane reactors for hydrogen production. Chem Eng Sci 92:40–66
16. Centi G, Perathoner S (2009) Opportunities and prospects in chemical recycling of carbon dioxide to fuels. Catal Today 148:191–205
17. Chianese S, Loipersböck J, Malits M, Rauch R, Hofbauer H, Molino A, Musmarra D (2015) Hydrogen from the high temperature water gas shift reaction with an industrial Fe/Cr catalyst using biomass gasification tar rich synthesis gas Fuel Process. Technology 132:39–48
18. De Falco M, Piemonte V (2010) Solar enriched methane production : assessment of plant potentialities and applications. Appl Technol Innovations J 1(1):1–8
19. Mariani A, Morrone B, Unich A (2012) A review of hydrogen-natural gas blend fuels in internal combustion engines fossil fuel and the environment. ISBN 978-953-51-0277-9
20. EU FCHJ (2013) Programme review 2013. Fuel cells and hydrogen
21. Erickson W, Tang PA, Vernon Reformation of hydrocarbon fuels. In: Handbook of hydrogen energy. CRC Press, Taylor & Francis Group, Boca Raton
22. Gallucci F, Comite A, Capannelli G, Basile A (2006) Steam reforming of methane in a membrane reactor: an industrial case study. Ind Eng Chem Res 45(9):2994–3000
23. Balasubramanian B, Ortiz L, Kaytakoglu S, Harrison DP (1999) Hydrogen from methane in a single-step process. Chem Eng Sci 54(15–16):3543–3552
24. Piemonte V, De Falco M, Favetta B, Basile A (2010) Counter-current membrane reactor for WGS process: membrane design. Int J Hydrogen Energy 35(22):12609–12617
25. Ghribi D, Khelifa A, Diaf S, Belhamel M (2013) Study of hydrogen production system by using PV solar energy and PEM electrolyser in Algeria. Int J Hydrogen Energy 38(20):8480–8490
26. Kyriakides AS, Rodríguez-García L, Voutetakis S, Ipsakis D, Seferlis P, Papadopoulou S (2014) Enhancement of pure hydrogen production through the use of a membrane reactor. Int J Hydrogen Energy 39(9):4749–4760
27. De Falco M, Piemonte V, Di Paola L, Basile A (2014) Methane membrane steam reforming: heat duty assessment. Int J Hydrogen Energy 39(9):4761–4770
28. Basile A, Campanari S, Manzolini G, Iulianelli A, Longo T, Liguori S, De Falco M, Piemonte V (2011) Methane steam reforming in a Pd-Ag membrane reformer: an experimental study on reaction pressure influence at middle temperature. Int J Hydrogen Energy 36 (2):1531–1539
29. Offer GJ, Howey D, Contestabile M, Clague R, Brandon NP (2010) Comparative analysis of battery electric, hydrogen fuel cell and hybrid vehicles in a future sustainable road transport system. Energy Policy 38(1):24–29
30. Salemme L, Simeone M, Chirone R, Salatino P (2014) Analysis of the energy efficiency of solar aided biomass gasification for pure hydrogen production. Int J Hydrogen Energy 39 (27):14622–14632

31. Gnanapragasam NV, Reddy BV, Rosen MA (2015) Hydrogen production from solid fuels. Handbook of hydrogen Energy. CRC Press Taylor & FRrancis Group, Boca Raton
32. Mirabel ST, Goel N, Ingley A, Goswami D (2004) Utilization of domestic fuels for hydrogen production. Int J Power and Energy Syst 24(2):239–245
33. Cavinato A, Giuliano A, Bolzonella D, Pavan P, Cecchi F (2012) Bio-hythane production from food waste by dark fermentation coupled with anaerobic digestion process: a long-term pilot scale experience. Int J Hydrogen Energy 37(15):11549–11555
34. International Energy agency (IEA) (2013) Production costs of alternative transportation fuel & influence of crude oil price and technology maturity, pp. 1–51
35. Barckholtz T, Burgunder A, Casey D, Dillich S, Elgowainy A, Merritt J, Parks G, Pawel S, Simnick J, Soto H, Sutherland E (2013) Hydrogen delivery hydrogen storage technologies technical team roadmap. Roadmap, p 54
36. Penev M (2013) Hybrid hydrogen energy storage. All-Energy, Aberdeen
37. Chen (2005) Hydrogen delivery infrastructure options analysis. Doe Energy Program Review, Washington
38. Schoenung S (2011) Economic analysis of large-scale hydrogen storage for renewable utility applications, 1196–1199
39. Elgowainy A, Mintz M, Gardiner M (2015) Distribution networking. Handbook of hydrogen energy. CRC Press Taylor & Francis Group, Boca Raton, pp 935–955
40. Lipman TE, Edwards JL, Kammen DM (2004) Fuel cell system economics: comparing the costs of generating power with stationary and motor vehicle PEM fuel cell systems. Energy Policy 32(1):101–125
41. U.S. Department of Energy, Energy Information Administration, Alternatives to Traditional Transportation Fuels 2011, table C-1 and similar tables in earlier editions. http://www.eia.gov/renewable/afv/index.cfm. Accessed 17 April 2013
42. Piemonte V, De Falco M, Giaconia A, Basile A, Iaquaniello G (2012) Production of enriched methane by a molten-salt concentrated solar power plant coupled with a steam reforming process: an LCA study. Int J Hydrogen Energy 37(15):11556–11561
43. Vernon DR, Erickson PA (2015) Hydrogen enrichment. Handbook of hydrogen energy. CRC Press Taylor & Francis Group, Boca Raton, pp 903–933
44. Kowalczyk P, Bhatia SK (2006) Optimization of slitlike carbon nanopores for storage of hythane fuel at ambient temperatures. J Phys Chem B 110(47):23770–23776
45. Florisson O, Gasunie NVN (2010) A step towards the hydrogen economy by using the existing natural gas grid (the NATURALHY-project)
46. Kema OF (2010) NATURALHY: Assessing the potential of the existing natural gas network for hydrogen delivery
47. Munshi S (2006) Medium/heavy duty hydrogen enriched natural gas spark ignition IC engine operation. Gratz, Austria, pp 71–82
48. Yon S, Sautet J (2012) Effects of hydrogen addition to the fuel jet on the velocity field in a two separated jets configuration in non-reacting flow, pp 9–12
49. Raut-Jadhav S, Saharan VK, Pinjari D, Sonawane S, Saini D, Pandit A (2013) Synergetic effect of combination of AOP's (hydrodynamic cavitation and H_2O_2) on the degradation of neonicotinoid class of insecticide. J Hazard Mater 261:139–147
50. Yadav VK, Singha R, Pandey AK (2014) Hydrogen enriched methane mixtures, vol. 5, pp. 2010–2014
51. Di Sarli V, Di Benedetto A (2007) Laminar burning velocity of hydrogen-methane/air premixed flames. Int J Hydrogen Energy 32(5):637–646
52. Sabia P, de Joannon M, Fierro S, Tregrossi A, Cavaliere A (2007) Hydrogen-enriched methane mild combustion in a well stirred reactor. Exp Thermal Fluid Sci 31:469–475
53. Wang J, Huang Z, Tang C, Miao H, Wang X (2009) Numerical study of the effect of hydrogen addition on methane-air mixtures combustion. Int J Hydrogen Energy 34(2):1084–1096
54. Ceper, BA (2012) Use of hydrogen-methane blends in internal combustion engines. hydrogen energy—challenges and perspectives licensee InTech

Enriched Methane Production Through a Low Temperature Steam Reforming Reactor

Marcello De Falco

Abstract An innovative hybrid plant, composed by a solar section for heating up a molten salt stream through a Concentrating Solar Power (CSP) plant, a chemical section for the production of 1000 Nm^3/h of Enriched Methane (EM) with a 20 %vol. content of hydrogen, and an electrical section for the electricity production by means of an Organic Rankine Cycle unit (conversion efficiency = 28 %) is presented and assessed. The core of the process is the low-temperature solar steam reformer, where a feedstock composed by methane and water steam is partially converted to hydrogen. The reactor is modeled in detail, the equations set is described and commented, together with the boundary conditions. Then, the reactors' behavior is simulated. By applying 15 reformers in parallel and imposing a Gas Hourly Space Velocity (GHSV) of 40,965 h^{-1}, it is possible to produce a stream of EM (20 %vol. H_2) equal to 1000 Nm^3/h and 500 kW approximately of net electrical power output. The molten salt stream is heated up to 550 °C by the CSP plant, then it supplies the reforming process heat duty (reactor heat duty, feedstock preheating, and reactant steam generation) and, finally, it generates the electricity by exploiting its residual sensible heat. By the simulation of the reformers under industrial conditions, the feasibility of the proposed architecture is demonstrated and its potentialities are assessed.

Keywords Enriched methane production · CSP · Hybrid plant · Natural gas steam reforming

List of Symbols

C_i	i-component composition (mol m^{-3})
c_p	Gas mixture specific heat (J kg^{-1} K^{-1})
$c_{p,MS}$	Molten salt specific heat (J kg^{-1} K^{-1})
CSP	Concentrating Solar Plant
D_{er}	Effective radial diffusivity (m^2 s^{-1})

M. De Falco (✉)
University of Rome "Campus Bio-Medico", via Alvaro del Portillo 21, 00128 Rome, Italy
e-mail: m.defalco@unicampus.it

M. De Falco and A. Basile (eds.), *Enriched Methane*,
Green Energy and Technology, DOI 10.1007/978-3-319-22192-2_2

d_p	Equivalent catalyst particle diameter (m)
EM	Enriched Methane
f	Friction factor
G	Superficial mass flow velocity (kg s^{-1} m^{-2})
GHSV	Gas Hourly Space Velocity (h^{-1})
MDEA	Methyl diethanolamine
$n_{\text{reformers}}$	Number of reformers inside the shell
ORC	Organic Rankine Cycle
P	Reaction pressure (Pa)
PDE	Partial Differential Equation
PSA	Pressure Swing Adsorption
r	Radial coordinate (m)
r_i	Total reaction rate of the i-component (mol kg_{cat}^{-1} s^{-1})
r_j	Reaction rate of reaction j (mol kg_{cat}^{-1} s^{-1})
r_t	Catalytic tube radius (m)
T	Gas mixture temperature (K)
T_{MS}	Molten salt temperature (K)
U	Global heat exchange coefficient between the molten salt and reaction packed bed (J m^{-2} s^{-1} K^{-1})
u_s	Gas velocity (m s^{-1})
w_{MS}	Molten salt mass flow rate (kg/s)
z	Axial coordinate (m)
ΔH_j	Enthalpy of reaction j (J mol^{-1})
ε	Void fraction of the catalytic bed
λ_{er}	Effective thermal conductivity (J m^{-1} h^{-1} K^{-1})
μ_g	Gas mixture viscosity (kg m^{-1} K^{-1})
ρ_B	Catalytic bed density (kg m^{-3})
ρ_g	Gas density (kg m^{-3})

1 Introduction

Many biological processes are proposed to produce enriched methane, as anaerobic fermentation of food wastes [1, 2], fermentation from waste lactose in cyclic-batch reactors [3], from xylose [4], or from wheat straw hydrolysate [5]. But, all the traditional chemical and electrochemical hydrogen production processes, as water electrolysis [6], hydrocarbons steam- and auto-thermal reforming [7, 8], and thermochemical cycles [9], can be used to produce enriched methane streams, simply adding methane at the end of the process or, if the methane is the feedstock, avoiding the last separation step between the hydrogen produced and the unreacted methane.

Among the traditional process for the massive industrial production of hydrogen, the natural gas steam reforming is the most used and technologically consolidated.

The process is composed of the Steam Reforming (SR) reaction (1)

$$CH_4 + H_2O \leftrightarrow CO + 3H_2 \qquad \Delta H^0_{298\,K} = 206\,\frac{kJ}{mol} \tag{1}$$

which is strongly endothermic; and by the exothermic water gas shift (WGS) reaction (2)

$$CO + H_2O \leftrightarrow CO_2 + H_2 \qquad \Delta H^0_{298\,K} = -41\,\frac{kJ}{mol} \tag{2}$$

The global reaction, described as follow:

$$CH_4 + 2H_2O \leftrightarrow CO_2 + 4H_2 \qquad \Delta H^0_{298\,K} = 165\,\frac{kJ}{mol} \tag{3}$$

is endothermic and needs a high-temperature thermal flux to be supported. Traditionally, the reactions are performed in catalytic tubular reactors placed inside a furnace, where the reactions (1–3) occur fast over Ni-based catalyst and when equilibrium conditions are quickly reached, so that high methane conversions (>90 %) are achieved only at high operating temperatures (850–1000 °C) [7].

But, if an enriched methane stream with a hydrogen content of 20–30 %vol. has to be produced instead of pure hydrogen, high methane conversions are not required and, consequently, the reactions can be performed at milder operating temperatures. From the thermodynamic analysis of the reactions (1–3) shown in Fig. 1, it can be noticed that a methane conversion of 10–20 %, enough to reach the process specification (20–30 %vol. of hydrogen in the outlet enriched methane mixture), is

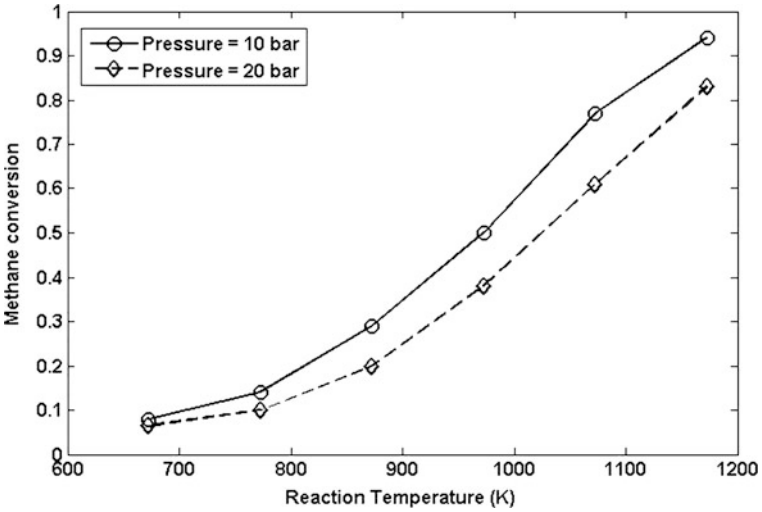

Fig. 1 Methane conversion at equilibrium conditions versus reaction temperature (H_2O to CH_4 ratio in the inlet feedstock equal to two)

achieved, at equilibrium conditions, at a reaction temperature within the range 500 °C (773 K) at 10 bar—550 °C (823 K) at 20 bar, leading to the possibility to avoid the use of a furnace for supplying the reactor heat duty.

The heat can be supplied coupling the methane steam reforming reaction with the Concentrating Solar Power (CSP) plant developed by ENEA and able to heat a thermal fluid (molten salt) up to 550 °C (823 K). Refer to chapter "Methane/Hydrogen Mixtures from Concentrated Solar Energy: The METISOL Project" for details about the CSP technology. By this configuration, the reaction operating temperature can reach 500–520 °C (773–793 K) and the equilibrium methane conversion is 15 % and more.

Such a solution leads to the following main benefits:

1. Since methane is the reaction feedstock, enriched methane mixture is directly produced in the reactor. Therefore, after the reaction, only separation steps to remove CO, CO_2, and steam water and to reach the final composition are required.
2. Natural gas steam reforming is a consolidated and widely applied process, so that the technology is well-known and a wide industrial experience is available.
3. The coupling between the enriched methane production process and the molten salt-based CSP technology is feasible since the thermal flow generated by the solar plant has the proper thermal level for the EM production through steam reforming.

In this chapter, after the description of the process configuration and its comparison with the traditional natural gas steam reforming plant, a mathematical model of the low-temperature solar steam reforming reactor for the enriched methane (EM) mixture production is presented and described. Then, some simulations imposing industrial conditions (1.000 Nm^3/h of EM production) are reported and results are discussed, demonstrating the feasibility of the technological solution.

2 Solar Steam Reforming Process

As above mentioned, the natural gas steam reforming is a consolidated industrial process widely applied for the massive production of pure hydrogen. Figure 2 shows a layout of the complete process, which is composed by

- A pretreatment section, where the methane is compressed (C-1), the water stream is pumped (P-1), and then vaporized (E-1); the two streams are mixed and pre-heated (E-2) before entering into the reactor;
- A reaction section, composed by the catalytic tubular reactors (R-1) placed inside a furnace, where the required high operating temperatures are reached;
- A purification section, where unreacted steam is separated by condensation (E-3 + V-1), CO_2 by an ammine separation unit (MDEA, S-1), while produced hydrogen and un-reacted methane are separated by a Pressure Swing Adsorption (PSA) unit (S-2).

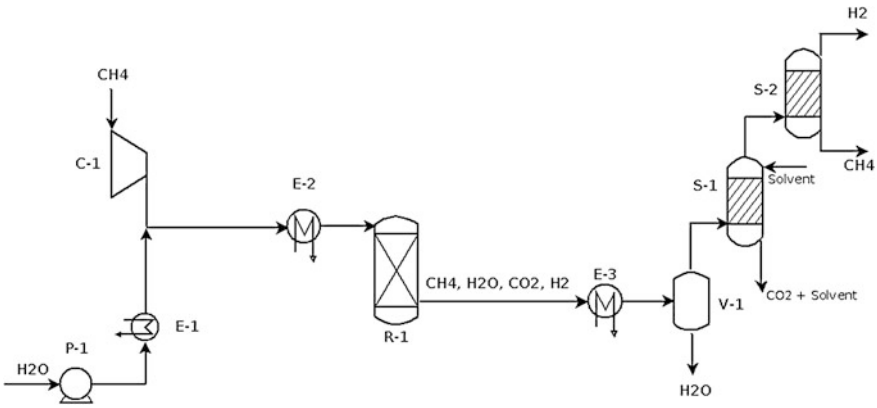

Fig. 2 Methane steam reforming traditional process layout

When the scope of the process is the production of EM instead of pure hydrogen, the last separation step (PSA) can be avoided and replaced by a methane stream addition, needed to modulate the hydrogen content in the final mixture. Moreover, the reactors are not placed in a furnace but they are tubes-and-shell shaped, with the hot molten salt stream fed through the shell. The molten salt supplies the heat for the reactor duty, for the preheating of the feedstock (E-2) and for the reactant steam generation (E-1).

Figure 3 reports a layout of the steam reforming process for the enriched methane production

- the feedstock is compressed (CH_4) and pumped (H_2O) up to the reaction pressure;
- the liquid water is vaporized by means of the boiler E-1;
- then, the reactant mixture is preheated by E-2 up to the reactor's operating temperature;

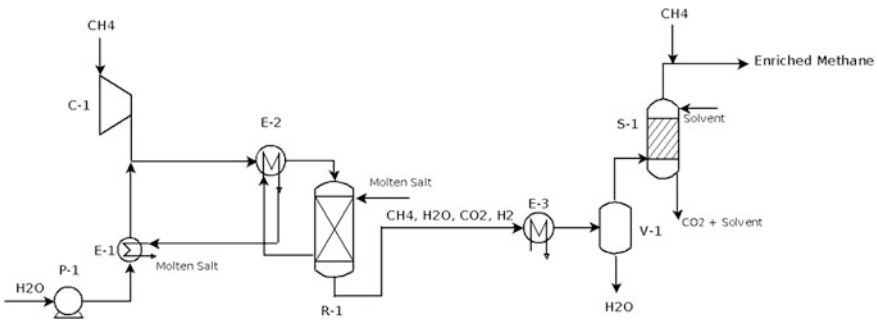

Fig. 3 Solar steam reforming for enriched methane production process layout

- the reactants are fed to the reactor R-1, where the low-temperature steam reforming reactions (1–3) are supported by exploiting the sensible heat of the hot molten salt stream, heated up by the CSP plant;
- the un-reacted water is separated by condensation;
- the CO_2 is separated in an MDEA unit (S-1);
- at the end, a methane stream is added to the final mixture to modulate the hydrogen content in the EM stream.

After supplying the heat needed for the enriched methane generation, the molten salt stream still has a high level of sensible heat, which can be exploited to produce medium pressure steam to be sent to a steam turbine for electricity production. By this configuration, the CSP-EM production plant is cogenerative, since it is able to produce both the hydrogen in the EM mixture and an electricity output exploiting solar energy.

The core of the process is the low-temperature steam reforming reactor, heated up by the molten salt stream and where the reactions occur at a temperature within the range 500–520 °C. In the next paragraph, a detailed mathematical model for the design and simulation of the reformer behavior is presented and discussed.

3 Solar Steam Reforming Reactor Modeling

The low-temperature steam reforming reactor is modeled by means of material, energy, and momentum balances. The reformer is assumed to be a tubes-and-shell unit, where the molten salt stream is fed through the shell and the reactants mixture through the tubes, as shown in Fig. 4.

The model is composed by a set of Partial Differential Equations (PDEs) able to simulate the axial and radial profiles (two-dimensional model) of components' concentration, temperature, and pressure inside the cylindrical reformers. The balances are imposed with the following assumptions:

- steady-state conditions;
- a single tube is representative of any other tube;

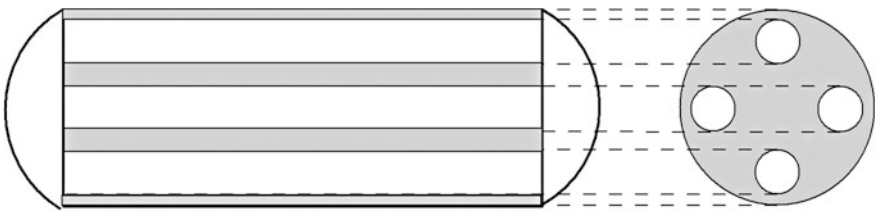

Fig. 4 Solar reformer tubes-and-shell shaped configuration

- pseudo-homogenous conditions, i.e., the packed bed reactor is described without considering the existence of two different phases (gas mixture and catalytic solid). The balances are imposed for one single pseudo-phase and the chemical–physical properties and transport coefficients are calculated by applying empirical expressions reported in the literature [10, 11];
- plug-flow is imposed for the gas velocity profiles, leading to a uniform pressure profile in the radial coordinate;
- axial mixing is neglected, and the only transport mechanism along the axial coordinate is the convective flux;
- pressure drop in the shell is neglected;
- one-dimensional energy balance in the shell is imposed.

A complete description of the model is reported in [12]. Here, the main equations composing the PDEs set to be solved, together with the boundary conditions, are listed

Material balances in the tubes

$$\frac{\varepsilon D_{\text{er}}}{u_s}\left(\frac{\partial^2(u_s C_i)}{\partial r^2}+\frac{1}{r}\frac{\partial(u_s C_i)}{\partial r}\right)-\frac{d(u_s C_i)}{dz}=\rho_B r_i \tag{4}$$

where ε is the void fraction of the catalytic bed, D_{er} the effective radial diffusivity of the pseudo-homogeneous phase [10], u_s the gas velocity, C_i the i-component composition, r the radial coordinate, z the axial coordinate, ρ_B the catalytic bed density, and r_i the total reaction rate of the i-component, calculated according to the Xu-Froment mechanism [13].

Energy balance in the tubes

$$-\lambda_{\text{er}}\left(\frac{\partial^2 T}{\partial r^2}+\frac{1}{r}\frac{\partial T}{\partial r}\right)+u_s\rho_g c_p\frac{dT}{dz}=\sum_{j=1}^{n_r}\left(-\Delta H_j\right)\rho_B r_j \tag{5}$$

where λ_{er} is the effective thermal conductivity of the pseudo-homogeneous phase [10], T the gas mixture temperature, ρ_g the gas density, c_p the gas mixture specific heat, ΔH_j, and r_j the enthalpy and the reaction rate of reaction j (=1, 2, 3), respectively.

Energy balance in the shell

$$w_{\text{MS}}c_{p,\text{MS}}\frac{dT_{\text{MS}}}{dz}=\pm U\cdot n_{\text{reformers}}\cdot 2\cdot\pi\cdot r_t\cdot\left(T_{\text{MS}}-T\right) \tag{6}$$

where w_{MS} is the mass flow rate of the molten salt stream, $c_{p,\text{MS}}$ its specific heat, T_{MS} the temperature of the molten salt, U the global heat exchanging coefficient between the tubes and the shell [14], $n_{\text{reformers}}$ the number of the tubes inside the

shell, and r_t the tubes radius. The sign ± represents that the molten salt stream can be fed co-currently (−) or counter-currently (+).

Momentum balance in the tubes

$$\frac{dP}{dz} = -\frac{f \cdot G \cdot \mu_g}{\rho_g d_p^2} \cdot \frac{(1-\varepsilon)^2}{\varepsilon^3} \tag{7}$$

where P is the reaction pressure, f the friction factor, G the superficial mass flow velocity, μ_g the gas mixture viscosity, d_p the equivalent catalyst particle diameter.

The boundary conditions to be imposed to solve the PDEs set (4)–(7) are

$$\begin{aligned} &z = 0, \forall r: \\ &\quad u_s C_i = (u_s C_i)_{\text{in}} \\ &\quad T = T_{\text{in}} \\ &\quad P = P_{\text{in}} \\ &\quad T_{\text{MS}} = T_{\text{MS,in}} \qquad \text{heat exchange co-current configuration} \end{aligned} \tag{8}$$

$$\begin{aligned} &z = L, \forall r: \\ &\quad T_{\text{MS}} = T_{\text{MS,in}} \qquad \text{heat exchange counter-current configuration} \end{aligned} \tag{9}$$

$$\begin{aligned} &r = r_t, \forall z: \\ &\quad \frac{\partial (u_s \cdot c_i)}{\partial r} = 0 \\ &\lambda_{\text{er}} \cdot \frac{\partial T_{\text{reac}}}{\partial r} = U \cdot (T_{\text{MS}} - T_{|r_t}) \end{aligned} \tag{10}$$

$$\begin{aligned} &r = 0, \forall z: \\ &\quad \frac{\partial (u_s \cdot c_i)}{\partial r} = 0 \\ &\quad \frac{\partial T}{\partial r} = 0 \end{aligned} \tag{11}$$

Solving the proposed PDEs set by applying the boundary conditions (8)–(11) it is possible to calculate the radial and axial profiles of the components' concentration and of the reaction temperature, the axial profile of the reaction pressure, and the axial profile of the molten salt temperature.

In the following, some simulations imposing industrial conditions (1.000 Nm^3/h of EM production) are reported in order to assess the low-temperature steam reforming reactor behavior and the technology potentialities.

4 Industrial Reactor Simulation and Performance Analysis

A deep analysis of the effect of the main operating conditions as the reaction temperature and pressure, the reactants mixture residence time, the inlet feedstock composition, etc. is reported in [15]. Here, a preliminary design of the low-temperature solar reformer operating under industrial conditions is proposed by exploiting the mathematical model described in the previous paragraph.

It is assumed that after the reformer, a WGS reactor able to convert the 99 % of CO produced by reaction (1) in CO_2 and H_2 by supporting the reaction (2) is integrated. Moreover, the molten salt stream, after supplying the reaction heat duty, is fed to the reactant steam generator and then to an Organic Rankine Cycle (ORC) for the production of electricity with a conversion efficiency, calculated as the ratio between the electrical output and the residual sensible heat of the molten salt stream, equal to 28 %, so that the produced electrical power is

$$P_{\mathrm{el}} = 0.28 \cdot w_{\mathrm{MS}} c_{p,\mathrm{MS}} \left(T_{\mathrm{out,MS}} - 290\,^{\circ}\mathrm{C}\right) \tag{12}$$

where $T_{\mathrm{out,MS}}$ is the temperature of the molten salt stream after the EM production plant.

The fixed parameters for the reactor simulation are summarized in Table 1.

The process specific is the production of 1000 Nm^3/h of EM with a content of 20 %vol. H_2. Such specificity is obtained by modulating the following operation and configuration parameters

- the Gas Hourly Space Velocity, i.e.,

$$\mathrm{GHSV} = \frac{Q_{\mathrm{feedstock}}}{V_{\mathrm{reformers}}} \quad \left(\mathrm{h}^{-1}\right) \tag{13}$$

  where $Q_{\mathrm{feedstock}}$ is the total volumetric inlet flow rate and $V_{\mathrm{reformers}}$ is the total volume of the number of installed reformers ($n_{\mathrm{reformers}}$);
- the number of reformers $n_{\mathrm{reformers}}$ installed inside the shell of the tubes-and-shell shaped reactor (refer to Fig. 4).

Table 1 Process parameters fixed in the simulation

Inlet temperature T_{in} (°C)	500
Inlet pressure P_{in} (bar)	10
Steam to carbon ratio	3
Molten salt mass flow rate w_{MS} (kg/s), fed co-currently with the reactants flow	6
Molten salt inlet temperature $T_{\mathrm{MS,in}}$ (°C)	550
Reactor length L (m)	2.05
Reactor external radius r_t (cm)	4.8

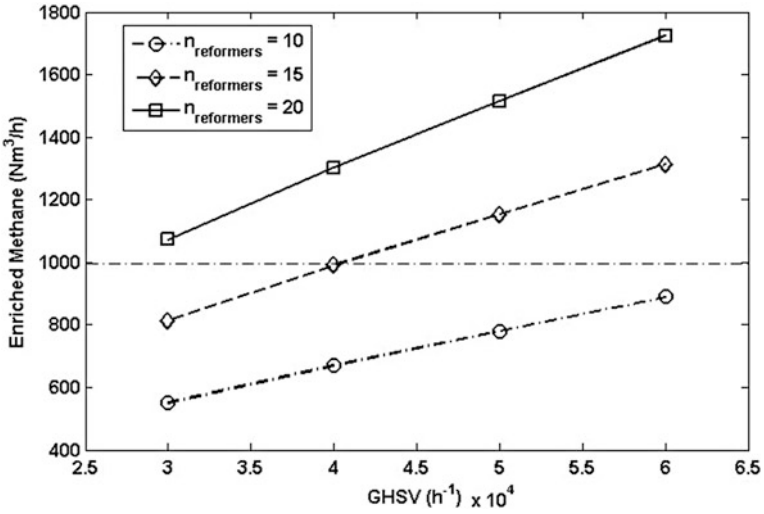

Fig. 5 Enriched methane production versus Gas Hourly Space Velocity at various number of reformers in parallel

Figure 5 shows the total enriched methane (20 %vol. of H_2) produced varying the GHSV and imposing $n_{reformers}$ = 10, 15, and 20 in parallel.

Increasing the GHSV leads to an increase of EM production since, fixing the reformers volume, increasing GHSV means that higher methane and steam flow rates are fed to the reactors. Moreover, installing more reformers in parallel leads to an increase in EM production.

Fixing a number of reformer equal to 15 and a GHVS of 40,965 h^{-1} (359 Nm^3/h of methane + 1077.7 Nm^3/h of steam water), which is a realistic value for an industrial application, the following results are obtained:

- methane conversion = 14.02 %
- hydrogen outlet flow rate = 201.54 Nm^3/h
- hydrogen content in the EM mixture after the reactor and the separation steps = 39.5 %vol.
- final molten salt temperature = 483.6 °C

As shown in the Fig. 3, after the reaction and H_2O and CO_2 separation, a methane flow is added to regulate the final H_2 composition in the EM mixture: therefore, 497.3 Nm^3/h of methane is added and the final target of 1000 Nm^3/h of EM with 20 %vol. of H_2 is achieved (as shown in Fig. 5).

Then, the residual molten salt stream sensible heat is used to generate an electrical power output equal to 499.8 kW_{el}.

Figure 6 shows the axial profile of the temperature inside the reactor in three different radial coordinates and the axial profile of the molten salt temperature. It is clear that the axial profiles present a "cold spot" in the first part of the reactor, where the endothermic reaction is strongly supported; then, the reaction kinetics is low,

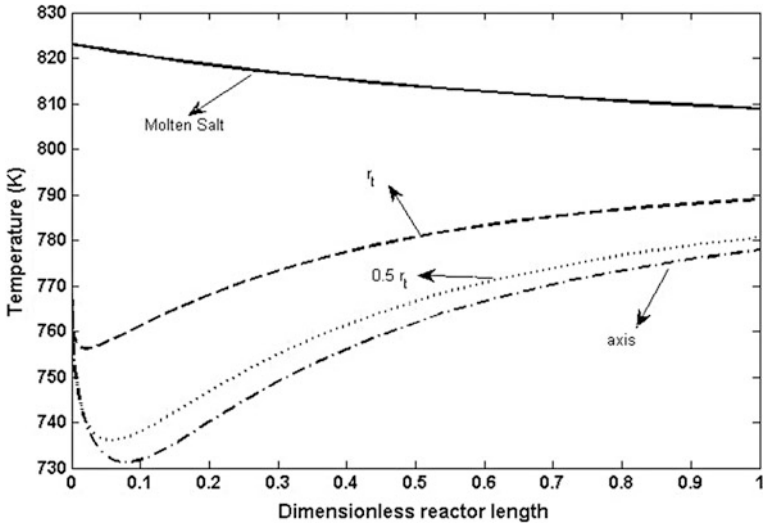

Fig. 6 Temperature profiles of the molten salt stream and inside the reactor

since the products composition increases and the temperature grows, thanks to the heat flow from the molten salt. In the radial direction, it has to be noticed that a high-temperature radial gradient is present (12 °C approximately from the reformer wall to the center).

Figure 7 illustrates the components' molar fraction inside the reactor (averaged on the radial coordinate). It is worth the assessment that a steep increase of

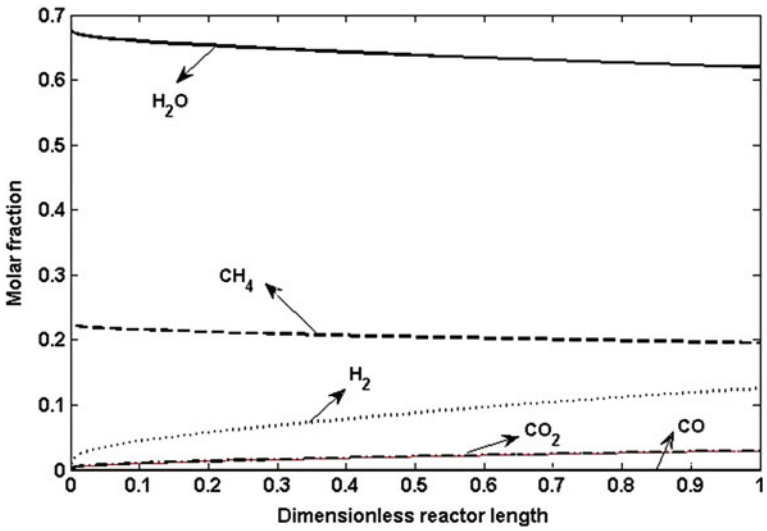

Fig. 7 Molar fraction of the components inside the reactor

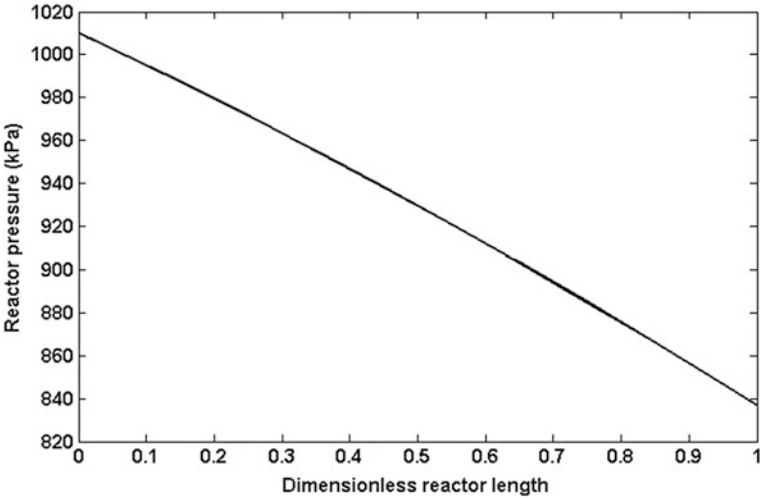

Fig. 8 Reaction pressure profile inside the reactor (1 bar = 100 kPa)

hydrogen content in the mixture occurs inside the reactor, while the CO_2 and mainly the CO molar fraction are always low: in the outlet stream, the molar fraction of CO_2 is 0.03, while the molar fraction of CO is 10^{-5}.

Finally, the pressure axial profile inside the reactor is shown in Fig. 8. A pressure drop equal to 2.4 bar approximately occurs inside the reactor, which is an admissible value for the application.

5 Conclusions

A low-temperature solar steam reformer, heated up by the molten salt stream of a CSP plant, has been modeled and simulated under industrial environments.

Imposing the conditions listed in Table 1, by applying 15 reformers and a GHSV of 40,965 h^{-1}, it is possible to produce a stream of EM equal to 1000 Nm^3/h and 500 kW approximately of electrical power output, generated by exploiting the residual sensible heat of the molten salt stream.

The simulation has demonstrated the feasibility of the proposed hybrid architecture, composed by a solar section for heating up the molten salt, a chemical section for the EM production, and an electrical section for the electricity production.

The EM produced can be stored in traditional methane storage system or fed to the natural gas medium pressure distribution network [16] and used as a feedstock for the natural gas fuelled Internal Combustion Engines (ICE), with an improvement of the engine conversion efficiency and a reduction of carbon dioxide and pollutants emissions [17, 18].

The plant proposed is composed by consolidated technologies (molten salt CSP, natural gas steam reforming process, and ORC unit), leading to a high level of operational reliability.

References

1. Cavinato C, Bolzanella D, Fatone F, Cecchi F, Pavan P (2011) Optimization of two-phase thermophilic anaerobic digestion of biowaste for hydrogen and methane production through reject water recirculation. Bioresour Technol 102:8605–8611
2. Cavinato C, Giuliano A, Bolzonella D, Pavan P, Cecchi F (2012) Bio-hythane production from food waste by dark fermentation coupled with anaerobic digestion process: a long-term pilot scale experience. Int J Hydrogen Energy 37:11549–11555
3. Clark IC, Zhang RH, Upadhyaya SK (2012) The effect of low pressure and mixing on biological hydrogen production via anaerobic fermentation. Int J Hydrogen Energy 37:11504–11513
4. Kongjan P, Min B, Angelidaki I (2009) Biohydrogen production from xylose at extreme thermophilic temperatures (70 C) by mixed culture fermentation. Water Res 43:1414–1424
5. Pawar SS, van Niel EWJ (2013) Thermophilic biohydrogen production: how far are we? Appl Microbiol Biotechnol 97:7999–8009
6. Zeng K, Zhang D (2010) Recent progress in alkaline water electrolysis for hydrogen production and applications. Prog Energy Combust Sci 36:307–326
7. Rostrup-Nielsen JR (1984) Catal Steam Reform. Catalysis 5:1–117
8. Li Y, Wang Y, Zhang X, Mi Z (2008) Thermodynamic analysis of autothermal steam and CO_2 reforming of methane. Int J Hydrogen Energy 33:2507–2514
9. Steinfeld A (2005) Solar thermochemical production of hydrogen—a review. Sol Energy 78:603–615
10. Kulkarni B, Doraiswamy L (1980) Estimation of effective transport properties in packed bed reactors. Catal Rev Sci Eng 22:431–483
11. Dixon A, Cresswell D (1979) Theoretical prediction of effective heat transfer parameters in packed beds. AIChE J 25:663–675
12. De Falco M, Giaconia A, Marrelli L, Tarquini P, Grena R, Caputo G (2009) Enriched methane production using solar energy: an assessment of plant performance. Int J Hydrogen Energy 34:98–109
13. Xu J, Froment G (1989) Methane steam reforming, methanation and water-gas shift: I intrinsic kinetics. AIChE J 35:88–96
14. De Falco M (2011) Membrane reactor modeling. In: De Falco M, Marrelli L, Iaquaniello G (eds) Membrane reactors for hydrogen production processes. Springer, New York. ISBN:978-0-85729-150-9
15. De Falco M, Piemonte V (2011) Solar enriched methane production by steam reforming process: reactor design. Int J Hydrogen Energy 36:7759–7762
16. Haeseldonckx D, D'haeseleer W (2007) The use of natural-gas pipeline infrastructure for hydrogen transport in a changing market structure. Int J Hydrogen Energy 32:1381–1386
17. Orhan Akansu S, Dulger Z, Kaharaman N, Veziroglu TN (2004) Internal combustion engines fuelled by natural gas–hydrogen mixtures. Int J Hydrogen Energy 29:1527–1539
18. Ortenzi F, Chiesa M, Scarcelli R, Pede G (2008) Experimental tests of blends of hydrogen and natural gas in light-duty vehicles. Int J Hydrogen Energy 33:3225–3229

Methane/Hydrogen Mixtures from Concentrated Solar Energy: The METISOL Project

Giampaolo Caputo, Domenico Mazzei and Mauro Francesco Sgroi

Abstract The present chapter summarizes the results of the METISOL project, an initiative funded by the Italian Government and devoted to the production and storage in solid state adsorbers of methane/hydrogen mixtures. Two main routes were investigated for the production: steam reforming associated with Concentrated Solar Power (CSP) and biological production based on optimized two steps methane and hydrogen production. The storage of the gas mixture was focused on automotive applications and was based on solid state high specific surface adsorbers such as activated carbons and Metal Organic Frameworks (MOFs). The most interesting results of the project were related to the possibility to build a methane/hydrogen automotive filling station energetically coupled with the CSP/reforming plant. The following pages contain a detailed overview of the CSP plant.

Keywords Enriched methane production · CSP · Solar radiation concentration efficiency

List of Symbols

ANI	Aperture Normal Irradiance (W/m^2)
A_{SCA}	Area of solar collector (m^2)
CNG	Compressed Natural Gas
CSP	Concentrated Solar Power
DNI	Direct Normal Irradiance (W/m^2)
EL	End Losses
ENEA	Agenzia nazionale per le nuove tecnologie, l'energia e lo sviluppo economico sostenibile
HCE	Heat Collecting Element
HTF	Heat Transfer Fluid
IAM	Incidence Angle Modifier

G. Caputo (✉) · D. Mazzei
ENEA Renewable Sources Unit, ENEA Research Centre Casaccia, Rome, Italy
e-mail: giampaolo.caputo@enea.it

M.F. Sgroi
Centro Ricerche FIAT, Strada Torino 50, 10043 Orbassano, Italy

M. De Falco and A. Basile (eds.), *Enriched Methane*,
Green Energy and Technology, DOI 10.1007/978-3-319-22192-2_3

METISOL	Metano-Idrogeno da energia SOLare (methane–hydrogen from solar energy)
MOF	Metal Organic Frameworks
P_{SUN}	Solar thermal power (kWh/year)
P_{HCE}	Power concentrated on collecting element (kWh/year)
P_{HTF}	Power transferred to thermal fluid (kWh/year)
P_{TLoss}	Power lost due to the irradiation by the heat collecting element (HCE)
RS	Row Shadow
TES	Thermal Energy Storage
VTES	Volume of thermal energy storage (m^3)
θ	Angle of incidence of solar radiation on the collector (rad)
η_{opt}	Optical efficiency of the collector
η_{th}	Thermal efficiency of the heat collecting element
η	Total efficiency of the collection system

1 Introduction

The use of methane as an automotive fuel has the theoretical potential to reduce the CO_2 tailpipe emissions to 29 % when compared to gasoline. In real conditions, engine efficiencies on different test cycles will be different and vehicles using Compressed Natural Gas (CNG) cylinders normally have a slight weight penalty compared to similar gasoline powered vehicles. State-of-the-art Natural Gas Vehicles (NGVs) achieve a 25 % CO_2 benefit if compared to similar gasoline powered vehicles [1–3].

One of the main drawbacks of NGVs is the limited kilometric range associated to the low density of methane and to the low gravimetric and volumetric energy density of high-pressure automotive storage systems.

The METISOL Italian research project was funded by the Italian Ministry of Environment to promote the technologies related to the production, storage and use of methane and hydrogen enriched methane blends for automotive applications.

Part of the activity project was devoted to investigate the storage capacity of state of the art solid sorbents for natural gas and hydrogen. Metal organic frameworks are considered as potential candidates for effective methane storage for automotive applications [4, 5]. During the project, a full-scale automotive demonstrator was developed employing commercial zinc-based MOF. The prototype car comprising a storage system based on MOF was able to cover a kilometric range of 5000 km showing no performance losses with respect to the corresponding standard CNG vehicle. The details of the results of the experimental campaign cannot be reported here due to confidentiality reasons.

Hydrogen is considered one of the most promising future energy carriers and transportation fuel; but, because of the lack of a distribution infrastructure, widespread introduction of vehicles powered by pure hydrogen is not likely in the near future [6–9] (refer to chapter "Enriched Methane: A Ready Solution for the Transition Toward the Hydrogen Economy"). Blending hydrogen with methane could be one solution to pave the way for hydrogen economy [10, 11]. Only minor adjustments in spark timing and injection duration are necessary for an engine calibrated and tuned for operation on pure methane to run on hydrogen/methane blends (see chapters "Emissions and Efficiency of Turbocharged Lean-Burn Hydrogen-Supplemented Natural Gas Fueled Engines" and "Using Natural Gas/Hydrogen Mixture as a Fuel in a 6-Cylinder Stoichiometric Spark Ignition Engine" for further information).

One approach to produce methane/hydrogen blends consists of the anaerobic digestion of organic waste substrates [12–14]. The METISOL consortium worked in particular on two stage methane and hydrogen production process starting from dairy industry wastes. That particular substrate allowed producing a biogas with reduced hydrogen sulphide content, an important prerequisite for automotive applications.

Another effective way to produce hydrogen/methane blends is to perform a low-temperature steam reforming reaction of natural gas converting partially methane to hydrogen (see chapter "Biological Hydrogen Production from Lignocellulosic Biomass" for detailed information on processes and catalytic materials for low-temperature steam reforming). The obtained gas stream is then purified to reach the required specifications (see chapter "Purification of Hydrogen-Methane Mixtures Using PSA Technology" for details on gas purification processes). The steam reforming reaction is highly endothermic; so, an environmental and economic feasible approach is to use Concentrated Solar Power (CSP) to supply the required process heat.

A CSP plant is an energy conversion system that makes use of solar radiation as main or exclusive source of energy instead of conventional fossil fuels [14–19]. See Fig. 1 for a general scheme of the CSP plant. To reach high temperature, comparable to that associated with combustion processes, it is therefore necessary to concentrate the solar light. CSP plants use optical systems: "concentrators", to collect and focus the electromagnetic radiation on a specific component; and "receiver", which has the scope to transfer the energy to a diathermic fluid. In this way, the solar heat is stored and used to produce electrical energy or process heat to perform selected chemical reactions.

CSP plants can use only the direct component of the solar radiation, Direct Normal Irradiance (DNI) and for this reason they can be installed in areas where the DNI reaches high medium values during the year (typically about 230 W/m^2). In case of lower DNI, the integration with an external fossil or, better, other renewable energy source, as biomass, is necessary.

The present chapter describes the CSP technology developed by ENEA, which makes use of linear parabolic solar concentrators and a mixture of sodium and potassium nitrates as heat transfer and accumulation fluid. In standard applications, the accumulated heat is used to power a steam production plant coupled with a

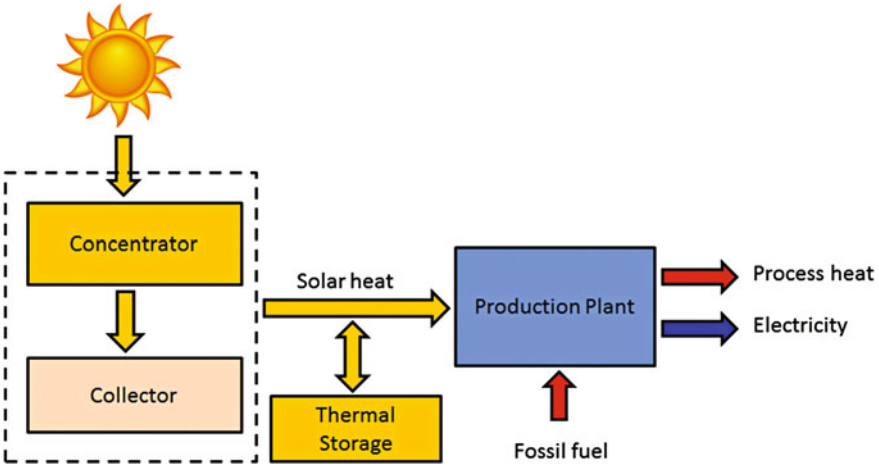

Fig. 1 Scheme of the CSP plant

Rankine cycle for the production of electric energy. During the METISOL project, the heat produced by the CSP plant was used to feed a steam reforming reactor converting natural gas in hydrogen/methane blends for automotive applications.

2 Concentrating Solar Power: General Principles

The availability of solar radiation is one of the basic requirements for the technical and economic feasibility of systems using solar energy as the main energy source. In particular, for concentrating technologies, which are able to collect only the direct radiation from the sun disc, the fundamental parameter for the project is the annual profile of the direct radiation in the area. For example, the global radiation on the horizontal plane ranges between 3.4 and 4.8 kWh/m^2/day, passing from the northern to southern regions. In addition to latitude, other factors have to be considered for the selection of the proper installation site:

- an orographic configuration, far away from mountains, produces a positive atmospheric stability that improves the direct component of the radiation;
- absence of abrupt and sudden changes of wheatear, cloudiness and rainfall;
- absence of fog, phenomena of retention of water vapour and other gaseous substances into the atmosphere;
- constancy of the climatic conditions over the years with a relatively easy and stable prediction of solar irradiation energetic data;
- flat installation surface, facing south, resulting in easy and effective installation of the field mirrors;
- low intensity of the prevailing winds, with the benefit on the operation of mirrors and little risk of damages.

The main elements of the high-temperature CSP plant developed by ENEA are

- the solar field;
- the storage system;
- the steam generator;
- the auxiliary systems for starting and controlling the plant.

The solar field is the heart of the system: it collects, focuses and absorbs the solar radiation that replaces the fuel and the generator of thermal energy in conventional industrial plants. It consists of linear parabolic collectors arranged in parallel rows, each of which is formed by several elements connected in series to constitute the single module or string. The solar field, therefore, has a modular structure: the number of modules determines the thermal energy collected, and then the system power. The solar collectors are the basic element of the solar field and are constituted by a reflector of parabolic section that collects and focuses continuously, via an appropriate control system, the direct radiation of the sun on a linear receiver arranged on the focus of the parabola, inside which a fluid circulates for the removal of solar energy (see Fig. 2).

The ENEA's CSP plant is based on a thermal fluid constituted by a binary mixture of sodium and potassium nitrates (composition 40/60 % by weight).

The use of this fluid allows increasing the operating temperature of the solar field up to 550 °C, while standard oil-based systems can reach the maximum temperature of 390 °C.

To increase the collection efficiency of the solar radiation, it was necessary to develop a new selective coating of the receiver tube that enables to operate at high temperature with better absorption factors and reduced thermal losses.

The choice of the molten salt as heat transfer fluid in the primary circuit and as a means of storing heat is a major technological innovation introduced by ENEA in the design of solar parabolic collectors. The use of molten salt presents undoubted

Fig. 2 String of solar collectors (Archimede 5 MW plant located in Priolo Gargallo, Sicily)

advantages compared to the use of oil: the high operating temperature, which implies a better efficiency of conversion and accumulation and in turn allows designing a more compact system, the absence of vapour pressure (storage tanks at atmospheric pressure), the fact that the mixture is not toxic and harmful for the environment (it is the basis of the common agricultural fertilizers). On the other hand, the management of the plant is more complex. In fact, molten salt has a high solidification temperature (about 240 °C), in the absence of solar radiation which is necessary to have a minimum flow through the solar field, to maintain the temperature above the solidification point. The energy to compensate thermal losses is taken from the storage system and if necessary, by use of an external source of energy.

Finally, the large amount of thermal fluid involved requires a careful study of the procurement processes, fusion, storage, maintenance and disposal.

The heat storage system has the task of storing the thermal energy absorbed by the solar field and making it available continuously regardless of the variability of the solar irradiation. This system therefore allows not only to stabilize the production but also to increase the load factor and to improve the flexibility of the plant allowing shifting the production in the hours of peak demand.

The system consists of two tanks which operate at two different temperatures and is connected to the solar field through a network of distribution that allows the transport of thermal energy from solar collectors to the storage tanks. In the presence of solar radiation, the thermal fluid, taken from the cold tank to a temperature of about 290 °C, is circulated through the network of collectors where it is heated to a temperature of 550 °C and then sent to the hot tank. The flow rate of the salts in the distribution network is adjusted according to the intensity of the solar radiation, so as to maintain constant the temperature of the salts in input to the hot tank. Figure 3 shows the heat storage vessels installed in the Archimede plant in the Priolo Gargallo site.

The steam generator (Fig. 4) is the system used to convert the thermal energy accumulated in the storage and is composed of a series of heat exchangers in which

Fig. 3 Heat storage system installed in the Archimede plant

Fig. 4 Steam generator of the Archimede plant

the sensible heat of the process fluid is transferred to the water to produce superheated steam to power a turbine of a conventional cycle Rankine and produce electricity. The thermal energy accumulated may also be used to power endothermic industrial processes. In particular, during the METISOL project, it was used for the heating of the reactants in a chemical plant for the production of mixtures methane/hydrogen on the basis of steam reforming of natural gas.

Finally, the solar plant comprises also auxiliary systems devoted to the preparation of the process fluid, its circulation in the plant, to the heating of the pipes and components and to the movement of the solar collectors.

3 Selection of Installation Site for the CSP Plant

The feasibility study for the installation of a CSP plant on a given site, has to be based on the evaluation of the meteorological characteristic of the site itself, not only from the point of view of the solar radiation but also from other properties such as medium temperature, speed and direction of dominant wind, which may affect the operability of the main components of the solar system, in particular the solar collector and the receiver tube. The design of the system on the basis of the expected thermal power and performances requires the direct solar radiation profile over the year. For METISOL project, the Archimede plant installed at Priolo Gargallo (Italy) was considered. The data of the hourly direct solar radiation were

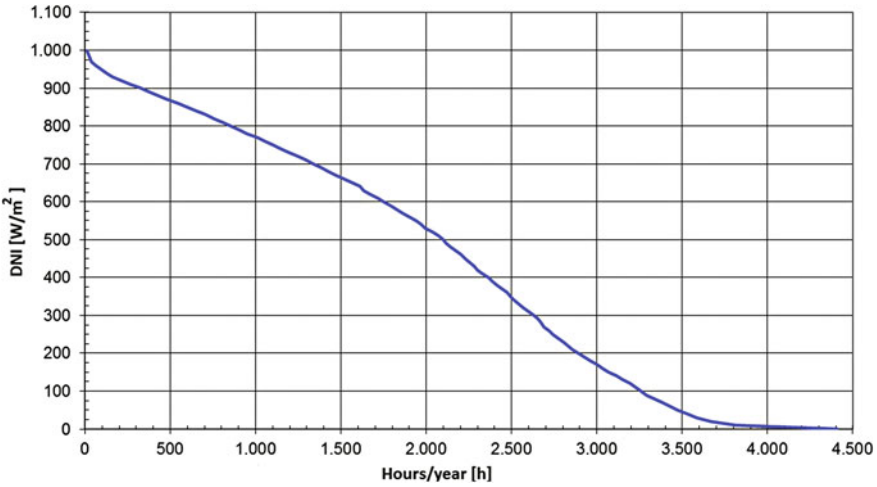

Fig. 5 Yearly distribution of direct normal irradiation on the Priolo Gargallo solar field

obtained by the weather station installed in the site. According to the measurements collected during the last 10 years, the integral annual value of the annual DNI is 221 W/m^2. The maximum value of the radiation is of 1042 W/m^2 with an average value over the year of 220 W/m^2. The distribution of the solar radiation is shown in Fig. 5. The radiation is present for about 4000 h/year, for 2100 h it is >500 W/m^2, while only for 856 h it exceeds 800 W/m^2.

4 Solar Radiation Concentration Efficiency

To evaluate the energy that can be actually collected and stored by the CSP plant, it is necessary to consider the characteristics of the system used for the collection and concentration of solar radiation. For the project METISOL, linear parabolic collectors were used as concentration system and then, the dimensioning of the plant has to take into account the fact that the tracking of solar radiation occurs only on one axis. To calculate the solar radiation falling on the opening of the collector is necessary to consider the effect of incidence angle formed between the solar radiation and the normal to the surface of the collector (see Fig. 6). So, the radiation normal to the opening of the collector, Aperture Normal Irradiance (ANI), can be calculated by multiplying the DNI by the cosine of the angle of incidence

$$\mathrm{ANI} = \mathrm{DNI} \times \cos\theta \tag{1}$$

The angle of incidence varies during the day and the year, and greatly influences the performance of the collectors. The effect of the angle of incidence reduces the

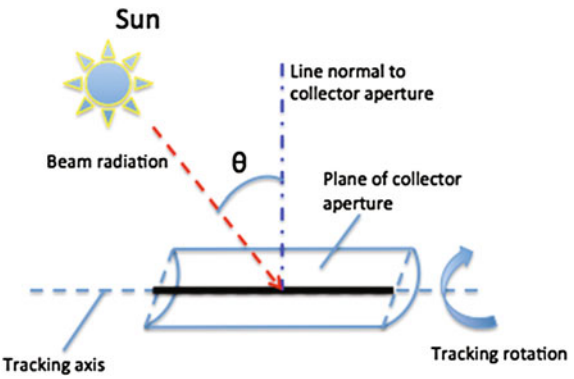

Fig. 6 Incidence angle of the solar radiation

solar radiation of about 12 % with a minimum value of 2 % during summer months and a maximum value of 40 % during the winter months.

Moreover, several other factors, which depend on the angle of incidence, further reduce the effective radiation on the opening of the collector. The aperture normal irradiance can be calculated as follows:

$$\text{ANI} = \text{DNI} \times \cos\theta \cdot \text{IAM} \cdot \text{RS} \cdot \text{EL} \tag{2}$$

where

- IAM: Incidence Angle Modifier—it is a correction factor to be applied to the efficiency optics to take into account the influence of the angle of incidence of solar radiation on the energy performance of the collector.
- RS: Row Shadow—adimensional parameter taking into account the losses related to the shadows between different rows of collectors.
- EL: End Loss—adimensional parameter taking into consideration the losses related to the end sections of collectors when they are not irradiated by the solar radiation.

Considering all these effects, the solar radiation that actually can be collected is reduced to a mean value of 176 W/m^2 with a maximum peak value of 967 W/m^2. The reduction is about 20 % compared to the DNI with a maximum value of 57 % in December.

The ANI determines the solar radiation that potentially reaches the solar collector. To evaluate the energy that can be effectively collected and transferred to the thermal fluid where it is necessary to take into account the optical and thermal efficiency of the collector. In fact, with reference to Fig. 7, it is possible to calculate the solar thermal power P_{SUN} from the ANI and the area of the collector A_{SCA}

$$P_{\text{SUN}} = \text{ANI} \cdot A_{\text{SCA}} \tag{3}$$

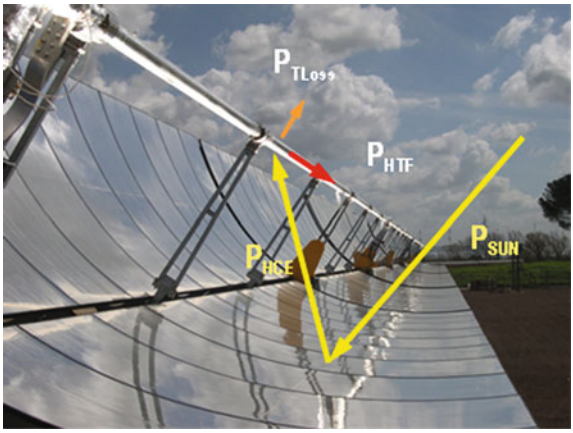

Fig. 7 Energy fluxes on the solar collector

The thermal power concentrated on the receiving tube, Heat Collecting Element (HCE), depends on the optical efficiency of the collector

$$P_{\mathrm{HCE}} = P_{\mathrm{SUN}} \times \eta_{\mathrm{opt}}, \tag{4}$$

where η_{opt} depends on several parameters such as the constructive quality and the nominal reflectivity of the mirror and the cleanliness of the reflecting surface.

The thermal energy that can be transferred to the thermal fluid, Heat Transfer Fluid (HTF), depends on the thermal efficiency of the receiving tubes

$$P_{\mathrm{HTF}} = P_{\mathrm{HCE}} \cdot \eta_{\mathrm{th}}, \tag{5}$$

where η_{th} accounts for the power irradiated by the HCE and indicated as P_{TLoss} in Fig. 7. The total efficiency of the collector is given by the product of thermal and optical efficiencies

$$\eta = \frac{P_{\mathrm{HTF}}}{P_{\mathrm{SUN}}} = \eta_{\mathrm{opt}} \cdot \eta_{\mathrm{th}} \tag{6}$$

The value of η reached on the Archimede plant was about 0.76.

5 Methane/Hydrogen Production Plant

The METISOL project was devoted to the construction of a solar energy system capable of providing thermal energy to both steam plant for the production of electricity and to chemical plant for the production of mixtures of methane/hydrogen, to be integrated in a filling station for cars and industrial vehicles powered by natural gas.

The specifications for the METISOL project can be summarized as follows:

- CH_4/H_2 ratio: 25 % molar ratio corresponding to 4 % mass fraction;
- Methane/hydrogen mixture flow rate: 350 kg/h (600 Nm^3/h).

The filling station will be able to guarantee the daily fuel supply for

- a fleet of 42 bus or industrial vehicles for the urban waste collection;
- 150 cars or light duty vehicles.

The solar plant was therefore dimensioned to produce steam as a reactant for the chemical plant and to preheat the natural gas at a temperature of 550 °C. Steam and natural gas are then mixed and sent to an adiabatic catalytic reactor for the partial steam reforming. The solar plant was over-dimensioned to generate steam for a Rankine cycle used to produce electricity for the auxiliary components of the plant and for the electric consumption of the filling station (the Rankine cycle was dimensioned to produce 700 kW of electric power).

The required natural gas flow rate to be sent to the steam reformer is 160 kg/h whereas the steam quantity was fixed to 480 kg/h (steam to carbon ratio 3). The design of the plant was done using the *GateCycle* program by General Electric. The simplified diagram of the METISOL plant is reported in Fig. 8. The molten salts are circulated in the concentration and accumulation circuit comprising the two heat storage vessels and the solar field integrating the solar collectors. Then, the thermal fluid is sent to heat exchangers to preheat the natural gas and produce steam at 550 °C for the low-temperature partial steam reforming reactor and for the Rankine cycle.

The thermal power required to fulfil the specifications is of 3175 kW.

So, a solar field with at least two strings composed of six collectors is required (see Fig. 9). Moreover, since the excess of thermal energy must be stored to be used during periods of low insolation, it was necessary to further increase the solar field foreseeing three strings of collectors.

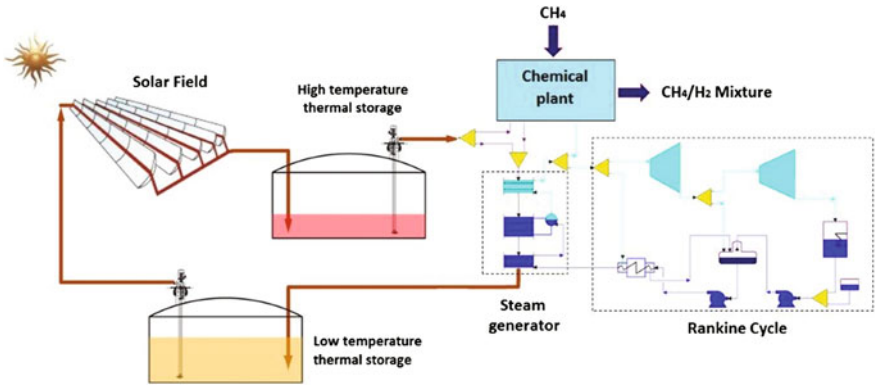

Fig. 8 Simplified scheme of the METISOL plant. The low- and high-temperature storage vessels work, respectively, at 290 and 550 °C

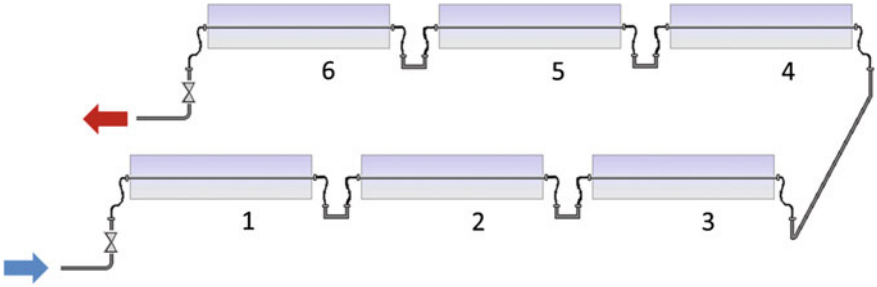

Fig. 9 String of six solar collectors connected in series

The thermal power collected from the solar field, with an average radiation of 800 W/m^2, is about 5400 kW, of this, approximately 60 % is used by the system of production, while the remaining 40 % is accumulated to extend the production during periods of insufficient solar radiation. If the production of the plant should be kept constant, it could be necessary to integrate the thermal power required during periods of low solar irradiation (e.g. using the natural gas as an energy source). The maximum thermal energy that can be collected by the solar field is limited by the capacity of the storage system. If the solar field collects an excess energy that cannot be used or stored, the control system of the plant has to discard a part of the available solar energy defocusing the collectors.

The capacity of a thermal storage system, Thermal Energy Storage (TES), is normally defined as the hours of operation of the plant at the nominal power without sunshine. For the METISOL project, the nominal thermal input required by the filling station is of 3175 kW and autonomy of 6.5 h was fixed as a reasonable requirement. This corresponds to a maximum accumulated energy of 20,637 kWh.

The energy is accumulated as sensible heat in the molten salts. To calculate the required mass of nitrates, it is necessary to consider the temperature operating range of the storage system, limited between 550 °C (high temperature storage) and 290 °C (vessel collecting the thermal fluid arriving from the steam generator). The specific heat capacity of the fluid, taking into account a temperature variation of 260 °C, is 190.4 kWh/m^3, hence the required volume of molten salts is V_{TES} = 18.4 m^3, corresponding to a mass of 188,616 kg. Figure 10 shows a schematic view of the heat storage system.

6 Analysis of Solar Collection During the Year

The collection and storage of solar energy during the year were analysed supposing that at the beginning of each day, all the molten salts are in the low-temperature storage at 290 °C (the storage system is "discharged") and that the plant is running continuously with constant thermal energy power of 3175 kW.

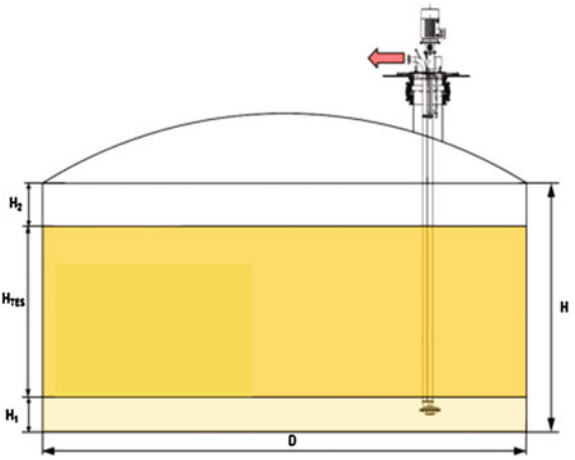

Fig. 10 Heat storage vessel containing the molten salts

The first case considered is represented by the July month: the daily medium solar energy was about 9.5 kWh/m^2 and the energy collected by the plant was about 62 kWh. Because of the saturation of the accumulation system, it was necessary to defocus the solar collector; so, about 6 % of the available solar energy was lost. The energy supplied to the reforming plant and to the filling station was 74 % solar with an integration of 26 % coming by external sources.

An accumulation system designed for a higher thermal capacity would allow using also the amount of energy lost due to defocusing the solar collectors and would permit to reduce the percentage of required external energy. On the other hand, this consideration is valid during a limited period of the year characterized by a high solar irradiation. In fact, considering the data collected in October, the maximum solar energy that is possible to collect daily is <24 kWh, so defocusing of collectors is not required and there is no energy loss. For this reason, to design a heat storage vessel with higher capacity would add extra cost to the plant with no substantial energetic benefits during the year. The fraction of solar energy used by the plant in October was 28 % with an external integration of the remaining part.

A more extended analysis of yearly data shows that the integration with external energy ranges between 100 and 25 % according to the normal variation of solar irradiation during the year.

7 Conclusions

The METISOL project had the aim of developing technological solutions for the production of methane–hydrogen mixtures, for use as motor fuel, through the process of steam reforming of natural gas, using the heat supplied by a concentrating solar plant at high temperature. On the basis of the required production of

hydrogen/methane mixture and of the electrical consumption of the components of the filling station, the thermal power that has to be supplied by the solar system was defined. The energy balances of the system were calculated using as a reference the solar irradiation data of the Priolo Gargallo (Italy) site.

With this selection of boundary conditions and specifications it was possible to design the solar field fixing the capacity of the storage system. In particular, the solar field is constituted by a total of 18 collectors arranged in three strings containing six elements each, while the thermal storage system is dimensioned for a capacity of 6.5 h (operation at rated power in the absence of solar radiation).

The experimental campaign on the solar plant demonstrated that the maximum solar fraction (proportion of the thermal energy which is supplied by the solar system), was about 75 %. Thus, for a continuous operation of the plant it would be necessary to integrate part of the energy required with an external source of energy.

In conclusion, the METISOL project gave the opportunity to design and test a real full-scale solar reformer for the production of methane/hydrogen blends. The plant became a testing bench where new technologies and concepts were tested, such as news materials for the catalysis of steam reforming reaction, new coatings for the mirrors and heat collecting elements and new gas purification strategies.

The authors acknowledge the Italian Ministry of Environment, Land Protection and Sea for having supported the activities of the METISOL project.

References

1. Saad A, Wan Mohd F, Shahrir A, Yusoff A (2014) Comparison of performance and emission of a gasoline engine fuelled by gasoline and CNG under various throttle positions. J App Sci 14:386–390
2. How HG, Taib IM, Shahrir A, Yusoff A, Azhari S, Elvis A (2009) Experimental investigation of performance and emission of a sequential port injection natural gas engine. Eur J Sci Res 30:204–214
3. Munde GG, Dalu RS (2012) Compressed natural gas as an alternative fuel for spark ignition engine: a review. Int J Eng Innovative Technol 2 92–96
4. Ma S, Zhou HC (2010) Gas storage in porous metal–organic frameworks for clean energy applications. Chem Commun 46:44–53
5. Li JR, Kuppler RJ, Zhou HK (2009) Selective gas adsorption and separation in metal–organic frameworks. Chem Soc Rev 1477–1504
6. Stolten D (ed) (2010) Hydrogen and fuel cells fundamentals, technologies and applications. Wiley-VCH, New York
7. Godula-Jopek A, Jehle W, Wellnitz J (2012) Hydrogen storage technologies: new materials, transport, and infrastructure. Wiley-VCH, New York
8. Sorensen B (2011) Hydrogen and fuel cells: emerging technologies and applications, 2nd edn. Academic Press, New York
9. Gandia LM, Arzamendi G, Dieguez PM (2013) Renewable hydrogen technologies—production purification storage, applications and safety. Elsevier, Amsterdam
10. Nitnaware PT, Suryawanshi JG (2014) Investigation on multi-cylinder S.I engine using blends of hydrogen and CNG. Int J Res Eng Technol 03:976–981
11. Akansu SO, Dulger Z, Kahraman N, Veziroğlu TN (2004) Internal combustion engines fueled by natural gas—hydrogen mixtures. Int J Hydrogen Energy 29:1527–1539

12. Das D, Veziroglu TN (2001) H_2 production by biological processes: a survey of literature. Int J Hydrogen Energy 26:13–28
13. Davila-Vazquez G, Arriaga S, Alatriste-Mondragòn F, Leon-Rodriguez A, Rosales-Colunga LM, Razo-Flores E (2008) Fermentative biohydrogen production: trends and perspectives. Environ Sci Biotechnol 7:27–45
14. Hallenbeck PC (2009) Fermentative hydrogen production: principles, progress, and prognosis. Int J Hydrogen Energy 34:7379–7389
15. Lovegrove K, Stein W (2012) Concentrating solar power technology principles, developments and applications. IT Power Group, UK
16. Concentrating Solar Power, Renewable Energy Technologies: Cost Analysis Series (2012) International Renewable Energy Agency (IRENA)
17. Giaconia A, De Falco M, Caputo G, Grena R, Tarquini P, Marrelli L (2008) Solarsteam reforming of natural gas for hydrogen production using molten salt heat carriers. AIChE J 54:1932–1944
18. De Falco M, Giaconia A, Marrelli L, Tarquini P, Grena R, Caputo G (2009) Enriched methane production using solar energy: an assessment of plant performance. Int J Hydrogen Energy 34:98–109
19. NREL (2012) Concentrating solar power projects database, US Department of Energy. http://www.nrel.gov/csp/solarpaces/by_country.cfm

Low Temperature Steam Reforming Catalysts for Enriched Methane Production

Gloria Berlier

Abstract Methane steam reforming (MSR) is still the most competitive process for the production of hydrogen due to the available technology and low cost. A possible shortcut to the "hydrogen economy" is based on enriched methane (EM), a gas mixture composed of hydrogen and methane, which could be employed as a fuel by exploiting existing technologies and infrastructures, with great improvement in emissions reduction. EM can be directly obtained by low temperature MSR, due to the endothermic character of the reaction, which is usually carried out at high temperature to obtain high methane conversion. An important aspect of this process is the choice of the catalyst, which should ensure the required activity, together with stability toward deactivation. A short review of the state-of-the-art catalysts for MSR is provided, with focus on both the active phase (mainly supported Ni particles) and the oxidic support properties. Attention is then focused on the current research on low temperature catalysts, including some hints to SR of oxygenated feedstocks (ethanol, glycerol, etc.), where Ru and Rh are often employed. In this context, the importance of the support is underlined, especially to improve the stability toward deactivation. Attention is focused on the most studied low temperature MSR catalyst $Ni/CeZrO_2$, with particular attention to the structural and surface properties of both active phase and support, which strongly influence the catalyst performances.

Keywords Low temperature steam reforming catalyst · $Ni/CeZrO_2$ catalyst · Catalyst performance and structure

List of Acronyms

APPES	Ambient pressure photoemission spectroscopy
CSP	Concentrating solar plant
CCS	Carbon capture and sequestration
EM	Enriched methane

G. Berlier (✉)
Dipartimento di Chimica and NIS Centre (Nanostructured Interfaces and Surfaces), Università di Torino, Via Giuria 7, 10125 Torino, Italy
e-mail: gloria.berlier@unito.it

M. De Falco and A. Basile (eds.), *Enriched Methane*,
Green Energy and Technology, DOI 10.1007/978-3-319-22192-2_4

FC	Fuel cells
ICE	Internal combustion engines
LNG	Liquefied natural gas
MS	Molten salt
MSR	Methane steam reforming
NG	Natural gas
OSC	Oxygen storage capability
SMSI	Strong metal-support interaction
SR	Steam reforming
TEM	Transmission electron microscopy
TOF	Turnover frequency
TPO	Temperature programmed oxidation
TPR	Temperature programmed reduction
WGS	Water-gas shift
XRD	X-ray diffraction
XPS	X-ray photoelectron spectroscopy
XAS	X-ray absorption spectroscopy

1 Introduction

1.1 Enriched Methane as a Possible Shortcut Toward the Hydrogen Economy

Enriched methane (EM) is a gas mixture composed of hydrogen and methane, also known as hydromethane. Among the many H_2 mixtures employed as fuels or in the chemical industry (such as "syngas" or "coal gas") EM and H_2-enriched natural gas (H_2–NG) have gained increasing importance, as testified by the commercialization in the USA of Hythane®, a mixture of 20 % H_2 and 80 % NG. The reasons for the growing attention to EM are related to the possibility to employ it as fuel in traditional NG internal combustion engines (ICE), without the need of expensive technological modifications.

In fact, the last decade enthusiasm for the development and potentialities of hydrogen-based fuel cells (FC) has dwindled, due to the technological issues related to the managing and reliability for onboard applications. Since these aspects are still challenges for the scientific community, the technological maturity of FC is unfortunately still far from being reached. Another possibility to pursue the so-called "hydrogen-based economy" (a societal model based on the use of pure hydrogen as energy vector) is to employ it as fuel in ICE. However, the use of pure hydrogen in ICE, though fascinating, is limited by several drawbacks. These include the low energy density of hydrogen, which would result in a low mileage, and the intrinsic high-flame temperature, which could improve the engine efficiency

but also NO_x emissions. From the technological point of view, important aspects are the necessity to design ad hoc engines (in relation to high pressure and temperature) and the still open question of onboard hydrogen storage, with related safety issues.

Most of the described issues could be overcome by the employment of hydrogen-enriched mixtures in NG ICE vehicles. From the environmental point of view NG vehicles are up to now one of the best solutions, thanks to reduced emissions of particulate matter and gaseous products. NG, which is mostly composed by methane (from 85 to 98 %) is characterized by a H/C ratio of 3.5–4.0, which is much higher with respect to diesel (2.1–2.2) and gasoline (2.2–2.4). This is important, in relation to the increasing urgency in the need to reduce CO_2 emissions. A further improvement in this line is the use of hydrogen (10–30 %) as an additive to NG, resulting in H/C ratios higher than 4.2. This could result in an improvement of the engine efficiency with the simultaneous reduction of CO, CO_2, NO_x, and unburned emissions [1–8]. Another important aspect is the possibility to use existing NG ICE technologies and NG pipeline for mixture supply. Thus, among the commercial claims of Hythane® Company LLC for the use of their H_2–NG mixture (5–7 % hydrogen) we can mention: (i) a reduction of CO and NO_x by 50 %; (ii) low capital and operating costs; (iii) cheapest way to meet new emission standards.

It is thus not surprising that the feasibility of the EM approach has been proved in several international research centers by on-road tests [2, 7, 10, 11]. On the basis of an energy and environmental sustainability analysis, Villante and Genovese [2] pointed out the gain in energy efficiency and CO_2 emission reduction when passing from NG to EM blends with H_2 concentrations ranging from 5 to 25 %. However, the process efficiency (and global CO_2 emission) is strongly dependent on the method employed for hydrogen production [2]. Accordingly, De Falco et al. [12] recently discussed a solar low temperature steam reforming (SR) process for the production of EM, by exploiting the solar energy stored in a molten salt stream heated up by a concentrating solar plant (Fig. 1) (MS-CSP). The work demonstrated the technological feasibility and the good match between a solar plant and an endothermic chemical process, which would be able to exploit solar energy to produce hydrogen.

1.2 Low Temperature Steam Reforming for Enriched Methane Production

One of the most extensively employed processes for hydrogen generation (together with NG gasification) is SR, in that about 95 % of worldwide hydrogen is currently estimated to be produced through these processes from fossil fuels [13–16]. The process mainly employs NG (85–98 % of methane), even if other hydrocarbons could be employed, such as propane [17], butane [18], gasoline [19], naphta [20],

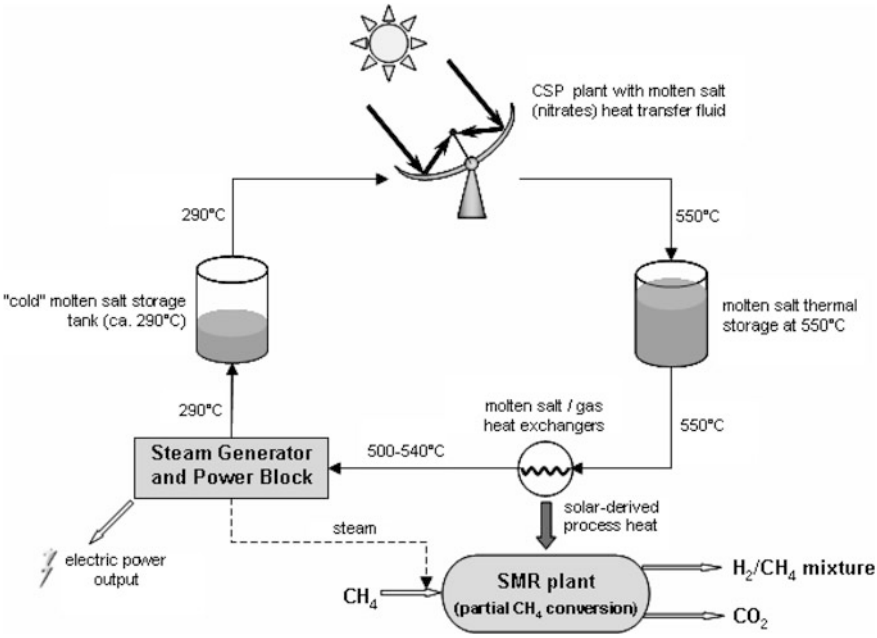

Fig. 1 Simplified scheme of CSP plant and molten salt loop, coupled to SR and electrical power generation plants. Reproduced from Ref. [9] with permission from the International Association of Hydrogen Energy

and liquefied natural gas (LNG) [21, 22]. More recently many SR processes of oxygenated feedstocks such as methanol, ethanol, and glycerol are being investigated [23–30]. The competitiveness of NG SR is clearly related to costs and availability of existing technologies with respect to more environmentally friendly alternatives for "renewable hydrogen" [31, 32].

Methane steam reforming (MSR) is based on the following reactions:

$$CH_4 + H_2O \rightleftarrows CO + 3H_2 \quad \Delta H^0 = 206 \text{ kJ/mol} \tag{1}$$

$$CO + H_2O \rightleftarrows CO_2 + H_2 \quad \Delta H^0 = -41 \text{ kJ/mol} \tag{2}$$

where the SR step is the first, highly endothermic, while the second exothermic step is water-gas shift (WGS), producing further amount of hydrogen in the conversion of CO to CO_2. Due to endothermic character of the SR step, the process is usually carried out at 1073–1273 K, in order to achieve high hydrogen yield (methane conversion >90 %) [33, 34]. The gas produced in this process usually contains 70–80 % of hydrogen, with a mixture of CO, CO_2, H_2O and CH_4, so that purification processes are necessary. One of the main issues is CO_2 sequestration, which is usually carried out by CCS (Carbon Capture and Sequestration) techniques, with an important energy consumption and environmental impact [2]. This implies that

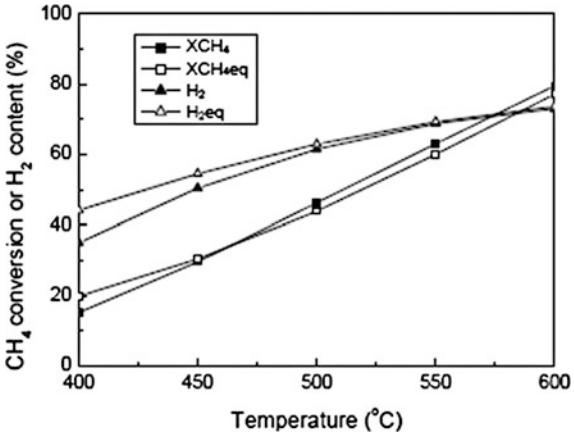

Fig. 2 Equilibrium values for CH_4 conversion and H_2 content in low temperature MSR (*hollow symbols*). Experimental values (*solid symbols*) were obtained at GHSV = 20,000 mL/g_{cat}· h with Ni/$CeZrO_2$/θ-Al_2O_3 catalysts. Reproduced from Ref. [35] with permission from the Korean Chemical Society

there is a large room for maneuver to improve both the energy efficiency and the environmental impact of SR processes.

One main parameter for improving the energetic sustainability of SR processes is the reaction temperature. Roh and Jun [35] showed that low temperature MSR is thermodynamically and experimentally possible for the generation of H_2 for fuel cells. As pointed out by De Falco et al. [9, 12], reduction of the process temperature around 773–873 K would allow the coupling to MS-CSP technologies, resulting in an important improvement of the process energetic and environmental sustainability.

Clearly, due to the endothermic character of the process, a low reaction temperature causes a decrease in methane conversion, as directed by thermodynamics (Fig. 2). This implies the direct formation of a hydrogen-enriched methane mixture (EM) (Fig. 3). An additional advantage of this approach is due to the fact that it is not necessary to separate the produced hydrogen from methane, avoiding the installation of expensive separation units. However, a separation unit for CO_2 removal cannot be avoided.

2 Catalysts for Steam Reforming Processes

2.1 Active Phases and Promoters

MSR process is traditionally carried out by employing catalysts based on Ni particles supported on ceramic oxides such as Al_2O_3, MgO, $MgAl_2O_4$ spinels, or

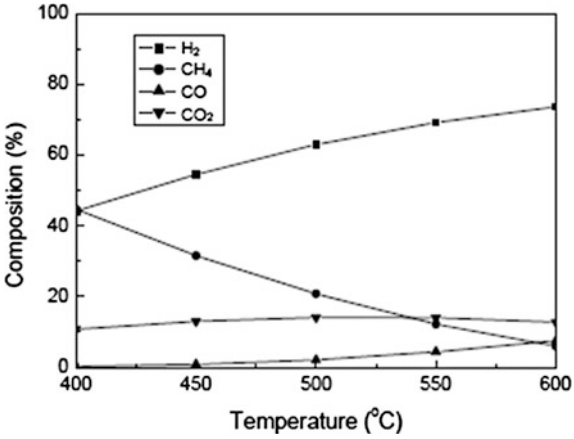

Fig. 3 Product gas composition (*dry basis*) as a function of reaction temperature for MSR on $Ni/CeZrO_2/\theta\text{-}Al_2O_3$ catalysts. Reproduced from Ref. [35] with permission from the Korean Chemical Society

mixtures of these oxides [16, 20, 33, 36–38]. The choice of the support is very important since it has been reported that the metal could be inactive on inert supports [34, 39]. Other active metals were tested, including transition metal ions (Fe and Co) [40, 41] and noble metals (Ru, Rh, Pd, Pt, and Ir) (Fig. 4) [42–46]. Usually, Ni and noble metals-based catalysts (particularly Ru and Rh) show good activity also at relatively low temperature [34, 46, 47], and they are often employed as catalysts for SR of oxygenated feedstocks [44, 45, 48–50]. The main drawbacks, especially when Ni catalysts are employed, are related to deactivation processes due to sintering of Ni particles and/or carbon deposition [17, 51–56].

The problem of Ni particle sintering is often related to the severe conditions of the "classical" SR process (temperature around 1073–1273 K and vapor pressure up to 30 bar), which are required to shift the reaction toward product formation [34, 57]. These conditions lead to the formation on the industrial catalysts of relatively large Ni particles (20–100 nm), with related loss in surface area and activity. Direct information on the mechanism of Ni sintering could be provided by in situ transmission electron microscopy (TEM) (Fig. 5) [58, 59]. In Ref. [59] the authors tried to explain the different conclusions obtained in the literature with the same in situ technique. By studying $Ni/MgAl_2O_4$ catalysts very similar to the industrial one they pointed out that very fast Ostwald ripening of the smallest Ni particles is observed at the early stages, while migration and coalescence most clearly appear at later stages of sintering, when the smallest particles had disappeared [59].

The formation of carbon deposits could instead cause blocking of the reactor and disruption of the catalyst. Deposited carbon could have different structures depending on the catalyst and the reaction conditions, embedding or encapsulating Ni particles (Fig. 6) [60, 61]. This could be explained by the diffusion of surface carbon atoms (selectively adsorbed on reactive step sites) to subsurface octahedral sites forming graphene islands [62].

The high mechanical strength of carbon filaments ("whiskers") can cause the removal of active phase particles from the support. This drawback could be

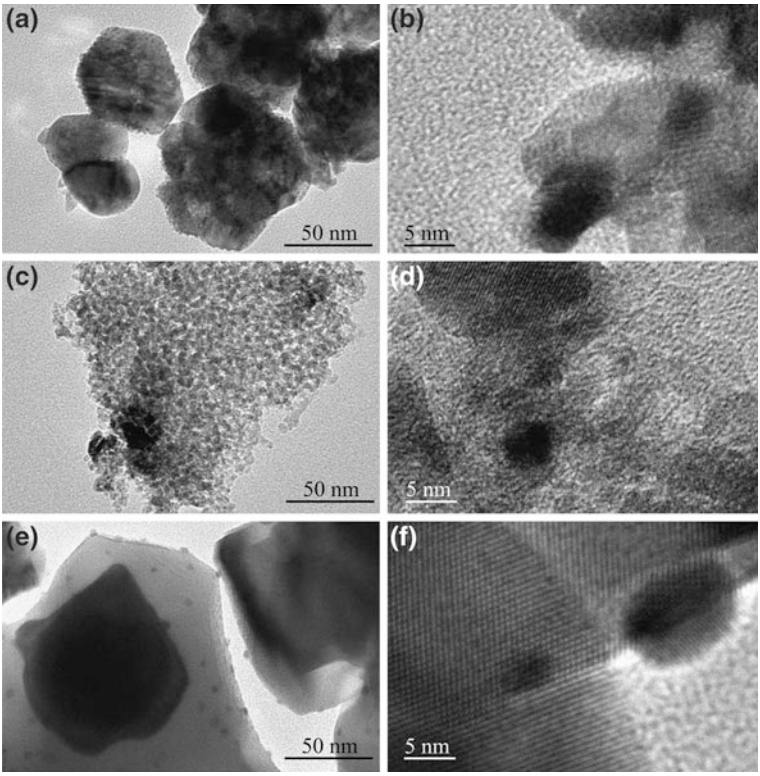

Fig. 4 TEM images at various magnifications of 1.5 % Rh/CeO_2 (**A** and **B**), 1.5 % Ru/Al_2O_3 (**C** and **D**), and 1.1 % Pt/CeO_2 (**E** and **F**) catalysts. Reprinted with permission from Ref. [42]. Copyright (2013) American Chemical Society

minimized by modifying the steam-to-carbon (S/C) ratio of the reaction mixture. This, however, leads to a restriction in the process parameters and a lower H_2/CO ratio in the products [34, 57].

Different promoters were proposed to improve the catalyst stability toward deactivation [63]. These include alkali and alkali-earth metal ions (potassium and/or calcium) [48, 64, 65], or metallic/bimetallic precursors (Ag, Au, Cu, Sn, W, Re, etc.) [19]. The positive effect of additives such as potassium, sulfur, or gold toward carbonization was explained by their binding to reactive step surface sites, thus removing the nucleation sites for the growth of graphitic filaments [36]. As for metallic systems, the promoters could also form alloys with Ni, and the change in reactivity could be related to electronic and/or "ensemble" (distribution and type of reaction sites) effects (Fig. 7) [1, 66].

A similar mechanism was proposed for boron as a promoter, showing positive effects on both coke formation and activity [62]. This was explained on the basis of a similar chemisorption preference of boron and carbon for Ni, so that boron can

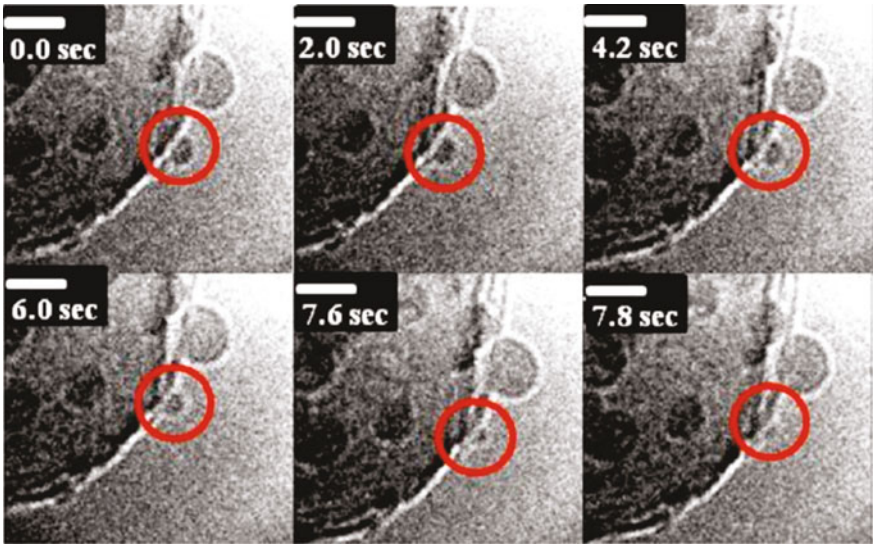

Fig. 5 TEM time-lapse image series of a $Ni/MgAl_2O_4$ catalyst imaged in a H_2/H_2O (3.6 mbar) atmosphere at 1023 K, showing the disappearance of small particles of Ni and the growth of larger ones (*scale bar* 5 nm). These observations are characteristic of Ostwald ripening. Reprinted with permission from Ref. [58]. Copyright (2011) American Chemical Society

selectively block step and subsurface Ni octahedral sites. This would reduce the diffusion of carbon to the subsurface sites and subsequently to the Ni bulk (Fig. 8) [62, 67].

3 Influence of the Support on the Performance of the Active Phase

Apart from the use of promoters, the choice of the support and the methodology employed for the deposition or growth of Ni particles are of fundamental importance to improve stability and performances of SR catalysts. Many aspects of the support surface chemistry can influence at the same time reaction temperature and stability, both in terms of Ni particles aggregation and carbon deposition. For instance, Matsumura and Nakamori [33] compared the performances of Ni supported on Al_2O_3, SiO_2 and ZrO_2 for MSR at low temperature, and proposed the important role of surface hydroxyl group in the activity of the Ni/ZrO_2 catalyst. The surface acidity of TiO_2, ZrO_2, and SiO_2 supports (Lewis or Brønsted as silanols and titanols) was also taken into consideration for the low temperature steam reforming of glycerol [68]. Moreover, the same authors explained the difference in reactivity on the basis of the metal-support interaction [68], which strongly depends on the support nature and on the preparation procedure [69–72]. In particular, the stronger

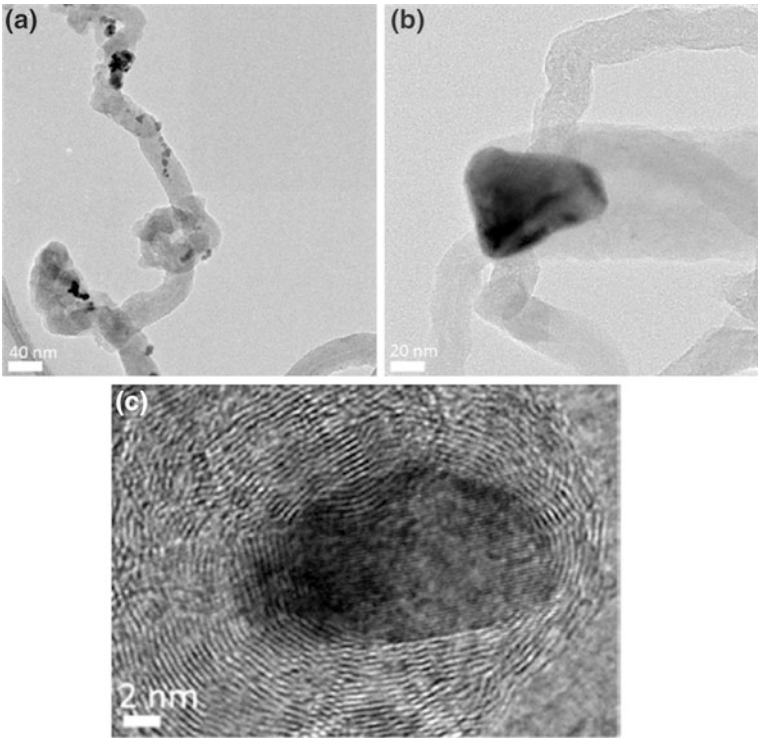

Fig. 6 TEM micrographs of a Ni/CeO_2 catalyst showing (**a**, **b**) carbon fibers embedding Ni particles and **c** a Ni or NiO particle encased in graphitic carbon. Adapted with permission from Ref. [61]. Copyright (2013) American Chemical Society

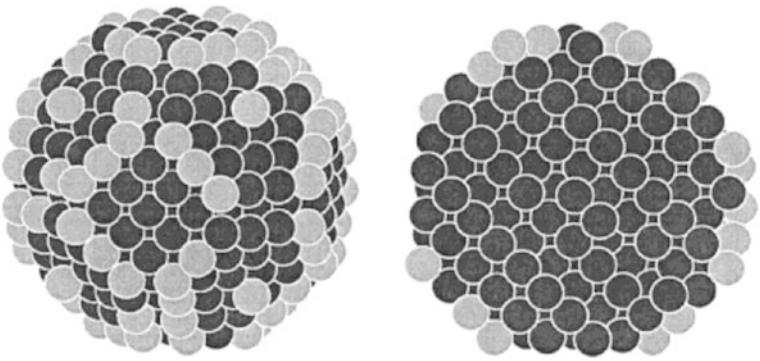

Fig. 7 Snapshot from a Monte Carlo simulation of a Au/Ni nanoparticle consisting of 100 Au atoms (*light*) and 583 Ni atoms (*dark*), with an outer diameter of 2.6 nm. Projected (*left*) and sliced through the center of the particle (*right*) snapshots show the formation of Au as a surface alloy at the surface of Ni cluster, with preferential binding to step sites. Reprinted with permission from Ref. [66]. Copyright (2001) American Chemical Society

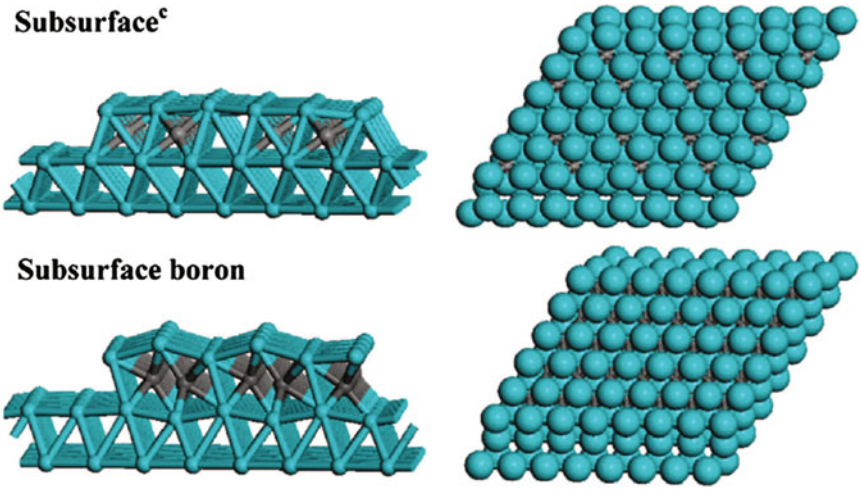

Fig. 8 Structure of a Ni (111) surface with subsurface carbon (*top*) or boron atoms. Small *gray balls* indicate carbon and boron atoms. Adapted with permission from Ref. [67]. Copyright (2009) American Chemical Society

the interaction, the more stable the metallic Ni clusters, which in turn lead to a higher catalytic activity and stability [68] A strong metal-support interaction (SMSI) was also proposed for $Ni/CeZrO_2$ catalysts, where some parts of NiO were proposed to incorporate in the $CeZrO_2$ support, thus suppressing Ni clustering and deactivation [73].

Besides chemical composition and structure, textural properties could also play an important role in improving the performances of SR catalysts. Namely, the employment of mesoporous materials as supports is steadily growing, thanks to the intrinsic advantages of this class of materials, such as large specific surface area and available volume, improving reactants and products diffusion. For instance, many papers were recently reported by Seo et al. [21, 22, 74–80] about the use of mesoporous Al_2O_3 as support for Ni particles in LNG SR. The authors studied the performances of different Ni/Al_2O_3 mesoporous catalysts, including aerogels [22, 76] and xerogels [81]. They focused on the preparation procedures to obtain high surface area porous alumina by precipitation/coprecipitation [77, 79], sol–gel [81, 82], and surfactant-assisted synthesis [21, 78, 80]. For instance, Ni/Al_2O_3 catalysts prepared by a nonionic surfactant templating method showed higher activity and stability with respect to a reference material based on commercial Al_2O_3 (Fig. 9) [21]. This was explained with SMSI and greatly enhanced Ni dispersion and surface area, thanks to the formation of a surface nickel aluminate.

With a similar philosophy (aimed at increasing of Ni dispersion and surface area) Ni-based catalysts on mesoporous zirconia were developed and tested in methane dry reforming [83–86]. In this case the obtained specific surface areas were high (around 150 cm^2/g) with respect to classical ZrO_2 supports, but sensibly lower with

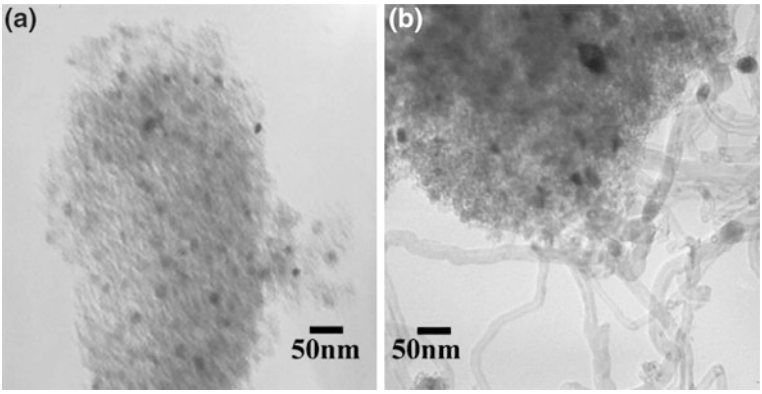

Fig. 9 TEM images of two Ni/Al_2O_3 catalysts prepared by impregnation on **a** mesoporous alumina prepared with nonionic surfactants and **b** commercial Al_2O_3 (Degussa). The images were taken on catalysts after 1000 min reaction in LNG SR at 873 K. In the sample prepared with commercial support, nickel was highly sintered and filamentous carbon was formed during the reaction. Reprinted from Ref. [21] with permission from the International Association of Hydrogen Energy

respect to what obtained with Al_2O_3 (around 300 cm^2/g) and with the mesoporous material "par excellence," that is SiO_2 (typically around 1000 cm^2/g). This is probably the reason why many reports are found about the use of mesoporous silica (mainly SBA-15) as support or additive for Ni-based catalysts [65, 87, 88]. In particular, in some of these reports the intrinsic properties of the porous (inert) support are coupled to that of the $CeZrO_2$ one [87, 88]. A positive effect toward sintering was reported, suggesting that the silica pores could prevent the aggregation of nickel [88].

4 Catalysts for Low Temperature Steam Reforming

4.1 General Concepts

A comprehensive review about the most studied catalysts for low temperature MSR was recently reported by Angeli et al. [89]. The authors considered three major groups of materials: nickel-based, noble metal-based and bimetallic catalysts, concentrating on their catalytic performances and related kinetic models. When Ni-based catalysts are reviewed, a large variety of oxide supports were compared. Among these, CeO_2 or $CeZrO_2$ based catalysts showed interesting performances [70]. Noticeably, these same supports were widely employed for low temperature SR catalysts based on Rh, Ru, Pt or Pd, while "classical" supports (mainly γ-Al_2O_3 and $MgAl_2O_4$) were explored for bimetallic active phases [70].

The point of view of this contribution is not focused on the catalytic performance itself, but on the structural and surface properties of active phases and supports, with particular attention to the influence on the catalysts activity and stability. Some of these properties were already mentioned and discussed in the previous paragraphs, since the issues are similar when dealing with high or low temperature processes. In both cases the percentage of hydrogen in the product mixture is governed by thermodynamics, but the catalyst can affect methane conversion and obviously influence the reaction kinetics, with its turnover frequency (TOF), diffusion issues, etc. [89]. The other important aspect is catalyst stability, especially when Ni-based catalysts are employed. Even if both nickel sintering and carbon deposition are usually explained with the harsh conditions of the industrial process, both phenomena can take place at relatively low temperature, and the choice of the support can be fundamental to avoid or limit these problems [79, 85, 90].

5 Structure, Active Sites, and Mechanisms

With the above considerations in mind, this paragraph will be mainly focused on the surface and structural properties of Ni-based catalysts, especially when CeO_2 or $CeZrO_2$ supports are employed. This choice is based on interesting properties of this support, largely investigated also in the low temperature SR reaction with noble metals [47, 70].

Among the other employed supports, the interesting paper from Matsumura et al. [33] reported the comparison among Ni (20 wt%) supported on SiO_2, γ-Al_2O_3, and ZrO_2. The reaction was carried out at 773 K, with S/C = 2. The silica-based catalysts were shown to deactivate quickly, while the employment of ZrO_2 as support showed the highest activity and stability, also at 5 % Ni wt. The authors interpreted the results in terms of the support surface properties, by feeding separately methane and carbon to the catalysts. Their interpretation was in terms of the formation of hydroxyl groups on the surface of zirconia as a consequence of water accumulation. The in situ formed mildly acidic hydroxyl groups were proposed to play an important role in low temperature methane conversion to H_2, following the reaction:

$$CH_x - S_n^* + HO - S^* \rightarrow CO_2 + \left(\frac{1}{2}x + 1\right)H_2 + (n+2)S^*$$

where S^* are the surface active sites, CH_x is supposed to be formed by adsorption on a partially reduced surface and HO–S^* are the hydroxyl groups formed upon water accumulation [33].

As mentioned above, apart from this interesting report, most studies proposing correlations between structural/surface properties and performances are based on CeO_2, or $CeZrO_2$ supports. CeO_2 is an active support, widely employed in catalysis, thanks to the reported enhancement of metal dispersion and SMSI [43, 69, 91–93].

Moreover, CeO_2 has a high "oxygen storage capability" (OSC), related to the presence of oxygen vacancies in defective sites that can be quickly formed and destroyed [94–96]. This feature could be useful to avoid deactivation as a consequence of coke formation. At high reaction temperature, however, CeO_2 is readily sintered, which results in catalyst deactivation. It has been reported that the addition of ZrO_2 leads to improvement in thermal resistance and OCS of CeO_2 [97–101]. This was found to be due to the partial substitution of Ce^{4+} with Zr^{4+} in the lattice of CeO_2, which results in a solid solution formation [102–104].

Ni/CeO_2 and $Ni/CeZrO_2$ catalysts, often prepared by quite simple coprecipitation reaction procedures, were reported to be active and stable in the low temperature SR process [35, 53, 88, 93, 105]. The reasons for this performance could be related to the support potential for SMSI with Ni particles and to the well-known oxygen storage and exchange properties, favoring reaction of surface carbon deposits with mobile surface or lattice oxygen [53, 92, 93, 106, 107]. The intrinsic properties of ceria were further enhanced by the formation of thermally stable solid solutions with zirconia, resulting in easier reduction of ceria, as shown by temperature programmed reduction (TPR) experiments and high catalyst stability even at S/C = 1 [106].

Roh et al. [108] proposed that the enhanced catalytic activity and stability of the coprecipitated $Ni/CeZrO_2$ catalysts (0.8 Ce and 0.2 Zr in atomic ratio) are related to the combination of the nanocrystalline nature of cubic $Ce_{0.8}Zr_{0.2}O_2$ support and finely dispersed nano-sized NiO_x crystallites. This would result in intimate contact between Ni and support, better Ni dispersion, higher Ni surface area, and enhanced oxygen transfer during the reaction. This interpretation was mainly based on the correlation between catalytic results and powder X-ray diffraction (XRD) results. Xu and Wang [107] pointed out that higher surface area and small particle size of Ni could be obtained by one-pot coprecipitation method with respect to impregnation. This also favored a strong interaction of Ni with the support, in turn suppressing carbon deposition. This was also shown in Ref. [73], suggesting the incorporation of NiO in the surface of $CeZrO_2$, with consequent modifications of the chemical environment of nickel particles. The resulting lower reducibility of NiO could be exploited in providing oxygen atoms for carbon removal, thus enhancing the catalyst activity and stability [73].

Many schemes were proposed to explain the unusual properties of Ni/CeO_2 and $Ni/CeZrO_2$ catalysts. This is easily understood since the structural and surface properties of the active phase, support, and interface can be characterized by many complementary techniques. As already mentioned, TPR is typically employed to study the reducibility of both Ni particles and support. These information could be combined with those obtained by X-ray photoelectron spectroscopy (XPS), which could provide details about the oxidation state and local environment of all surface atoms (Ni, Ce, Zr, and O). This kind of analysis was carried out by Roh et al. [106], who also measured the amount of mobile oxygen in both supports and catalysts by pulse experiments. On this basis, the structure of catalysts surface could be proposed, as depicted in Fig. 10. The authors describe the catalyst as a composite of different layers. The top layer is composed by relatively free Ni particles, while an

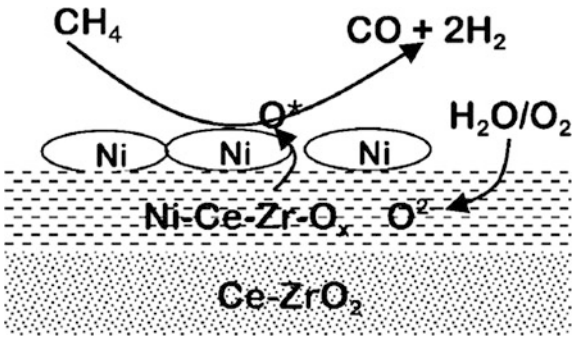

Fig. 10 Pictorial representation of the surface layers of Ni/$CeZrO_2$ catalyst, and proposed mechanism for syngas production. Reproduced from Ref. [106] with kind permission from Springer Science and Business Media

intermediate one with strongly interacting Ni and $CeZrO_2$ is sandwiched between top Ni and bottom $CeZrO_2$ support. The same authors pointed out the higher loading of mobile oxygen in $CeZrO_2$ and CeO_2 with respect to ZrO_2, thus supporting the hypothesis that the OSC of ceria is at the basis of the peculiar properties of the catalyst [106].

In another contribution, Kumar et al. [53] showed the importance of zirconia in stabilizing and optimizing ceria properties by solid solution formation. In fact, Ni particles supported on ZrO_2 and Ce-doped ZrO_2 catalyst were found to be less stable in low temperature methane dry reforming with respect to Ni on a $CeZrO_2$ solid solution. In this case the stability toward carbon deposition was studied by temperature programmed oxidation (TPO) experiments, coupled to TPR [53]. Another interesting report was instead focused on a new $Ni_{10}Ce_{90}$ mixed oxide, which coupled the usual claims about high stability toward coke formation and high activity to the unusual observation of an immediate activity without pre-activation (usually carried out to obtain Ni metal particles) [53]. This was explained by the important role of interfacial oxygen and by a balance between the rate of generation and supplement of oxygen vacancies.

Another unusual observation about Ni/NiO redox properties on $CeZrO_2$ was reported by Gopalakrishnan et al. [90]. The authors studied a Ni/$CeZrO_2$ catalyst prepared by coprecipitation in the low temperature methane SR, and tried to correlate its high stability (up to 250 h with S/C = 2 or 3) to structural and surface properties. The sample was characterized by well-defined crystalline $CeZrO_2$ particles (5–6 nm average size) with spherical/hexagonal morphology (Fig. 11). Nickel particles could not be directly observed by TEM, due to the low contrast between Ni and the support atoms, but Fourier transform analysis confirmed the presence of small NiO particles (5 nm as average size) in intimate contact with the support, as suggested by Roh et al. [108]. Interestingly, when the sample was reduced in hydrogen and then exposed to atmosphere, a rapid change in color from black to dark brown was observed, suggesting the transformation from Ni^0 to NiO, as

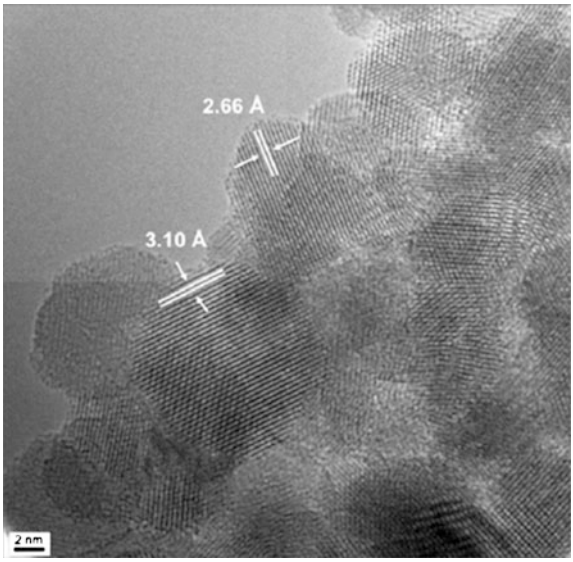

Fig. 11 TEM image of a $NiCeZrO_2$ catalyst prepared by coprecipitation. The particles are characterized by lattice distances compatible with a cubic $CeZrO_2$ phase. Adapted from Ref. [90] with permission from Elsevier

confirmed by both XRD and TEM measurements. This extreme reactivity of supported Ni^0 particles was related to the strong interaction with the support, displaying oxygen vacancies on the surface, as schematically represented in Fig. 12. Interestingly, a $NiCeZrO_2$ prepared at different pH did not show this phenomenon. The latter catalyst was characterized by larger Ni particles (10 nm) and showed deactivation due to carbon deposit formation and sintering [90].

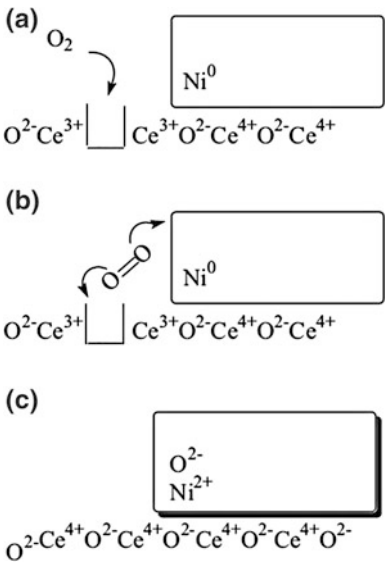

Fig. 12 Simplified representation of room temperature oxidation of a previously reduced Ni-$CeZrO_2$ surface as a result of contact with atmospheric oxygen. Reprinted from Ref. [90] with permission from Elsevier

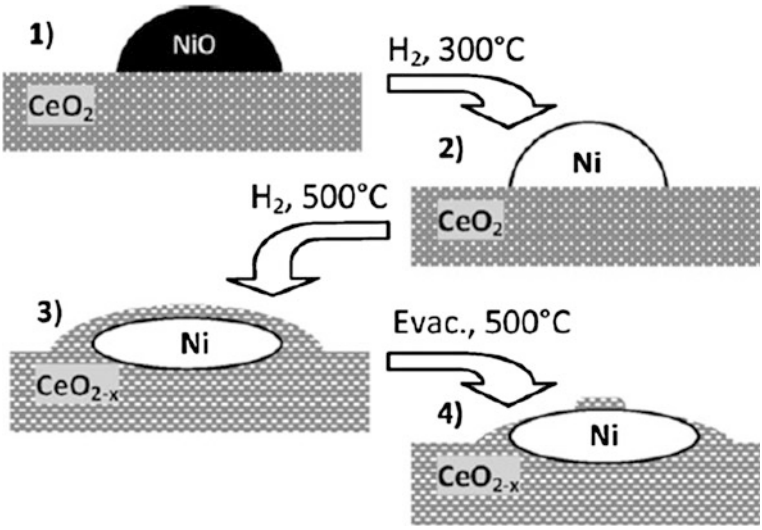

Fig. 13 Schematic evolution of Ni/CeO_2 system submitted to reduction and evacuation treatments. Reproduced from Ref. [69] with permission of The Royal Society of Chemistry

Other models and mechanisms were proposed by several authors to explain the intriguing properties of metal or oxidic particles supported on CeO_2-based catalysts by employing many characterization techniques. It is not possible in this context to review all the impressive literature on the subject. A mention is, however, made to the very interesting works reported by Caballero et al. [69, 70]. The authors studied Ni/CeO_2 systems by in situ X-ray absorption spectroscopy (XAS) and X-ray photoemission experiments under near-ambient pressure conditions (APPES). These techniques allowed following changes in morphology of Ni particles during reduction or SR reactions. More in detail, the burial and digging out of metallic nickel on the surface of ceria was monitored, as a consequence of SMSI and ceria moieties migration (Fig. 13) [69]. Finally, it is important to mention the fact that similar models and reaction mechanisms were proposed in the literature to explain the activity of noble metal supported on CeO_2 or $CeZrO_2$ for low temperature SR processes [47].

6 Conclusions

This contribution deals with the surface and structural properties of catalysts for low temperature MSR. The importance of this reaction from the energetic and environmental point of view was discussed by considering the direct synthesis of EM as a shortcut toward the "hydrogen economy." Then, the general requirements and issues of catalysts for SR were described, with particular attention to the

improvements obtained by promoters and a careful selection of the support. This discussion suggested that one of the main point for the development of low temperature SR catalysts is not the selection of the active phase (both Ni and noble metal particles are highly active in a large range of temperature) but of the support. The interaction of the active phase with the support is in fact essential to increase its dispersion, surface area, and to stabilize metal particles toward sintering during SR reaction. Hence, stability of the catalysts toward deactivation is crucial for the low temperature reaction as in classical process. This includes the ability of promoters, supports, or metal/support interfaces in suppressing carbon deposition mechanisms.

In this context, the attention is focused on Ni/CeO_2 or $NiCeZrO_2$ catalysts, since this class of materials (especially when prepared by one-pot coprecipitation) has shown interesting low temperature activity and many surface and structural studies were reported to explain their properties and catalytic behavior. This complex surface chemistry could be useful also to interpret the activity in the same reaction of noble metal catalysts (mainly Ru and Rh). Two main mechanisms are proposed for the low temperature SR activity and stability from the point of view of surface sites structure. One is based on the role of surface hydroxyl on ZrO_2 supports, while the other, investigated in deeper detail, focus the oxygen storage and exchange properties of ceria, stabilized by the formation of solid solutions with zirconia. The intimate contact of Ni (or noble metal) particles with the $CeO_2/CeZrO_2$ support, through SMSI and oxygen/vacancies exchange equilibria are the basis to interpret the high activity at low temperature coupled to stability toward sintering and carbon growth.

References

1. Larsen JH, Chorkendorff I (1999) From fundamental studies of reactivity on single crystals to the design of catalysts. Surf Sci Rep 35:165–222
2. Villante C, Genovese A (2012) Hydromethane: a bridge towards the hydrogen economy or an unsustainable promise? Int J Hydrogen Energy 37:11541–11548
3. Larsen JF, Wallace JS (1997) Comparison of emissions and efficiency of a turbocharged lean-burn natural gas and hythane-fueled engine. J Eng Gas Turbines Power-Trans ASME 119:218–226
4. Bauer CG, Forest TW (2001) Effect of hydrogen addition on the performance of methane-fueled vehicles. Part I: effect on SI engine performance. Int J Hydrogen Energy 26:55–70
5. Bauer CG, Forest TW (2001) Effect of hydrogen addition on the performance of methane-fueled vehicles. Part II: driving cycle simulations. Int J Hydrogen Energy 26:71–90
6. Akansu SO, Dulger Z, Kahraman N, Veziroglu TN (2004) Internal combustion engines fueled by natural gas - hydrogen mixtures. Int J Hydrogen Energy 29:1527–1539
7. Ortenzi F, Chiesa M, Scarcelli R, Pede G (2008) Experimental tests of blends of hydrogen and natural gas in light-duty vehicles. Int J Hydrogen Energy 33:3225–3229
8. Yon S, Sautet J-C (2012) Flame lift-off height, velocity flow and mixing of hythane in oxy-combustion in a burner with two separated jets. Appl Therm Eng 32:83–92

9. De Falco M, Giaconia A, Marrelli L, Tarquini P, Grena R, Caputo G (2009) Enriched methane production using solar energy: an assessment of plant performance. Int J Hydrogen Energy 34:98–109
10. Del Toro A, Railey M, Barrientos LF, Munshi S, Wayne S (2005) Development and demonstration of hydrogen and compressed natural gas blend transit buses. Nat Renew Energy Lab. http://www.nrel.gov/publications/ (NREL/TP-540–38707)
11. Riddel B, Bro C (2006) Malmö hydrogen and CNG/hydrogen filling station and hythane bus project. Lyon, France
12. De Falco M, Caputo G, Frattari S, Gironi F, Annesini MC (2014) Solar steam reforming for enriched methane production: reactor configurations modeling and comparison. Int J Hydrogen Energy 39:13979–13990
13. Rostrup-Nielsen JR (1993) Production of synthesis gas. Catal Today 18:305–324
14. Armor JN (1999) The multiple roles for catalysis in the production of H-2. Appl Catal A-Gen 176:159–176
15. Armor JN (2005) Catalysis and the hydrogen economy. Catal Lett 101:131–135
16. Rostrup-Nielsen J (2004) Steam reforming of hydrocarbons. A historical perspective. In: Bao X, Xu Y (eds) Natural Gas Conversion vol 7, pp 121–126
17. Takenaka S, Orita Y, Umebayashi H, Matsune H, Kishida M (2008) High resistance to carbon deposition of silica-coated Ni catalysts in propane stream reforming. Appl Catal A-Gen 351:189–194
18. Avci AK, Trimm DL, Aksoylu AE, Onsan ZI (2004) Hydrogen production by steam reforming of n-butane over supported Ni and Pt-Ni catalysts. Appl Catal A-Gen 258:235–240
19. Wang L, Murata K, Inaba M (2009) Highly efficient conversion of gasoline into hydrogen on Al_2O_3-supported Ni-based catalysts: catalyst stability enhancement by modification with W. Appl Catal A-Gen 358:264–268
20. Melo F, Morlanes N (2008) Synthesis, characterization and catalytic behaviour of NiMgAl mixed oxides as catalysts for hydrogen production by naphtha steam reforming. Catal Today 133:383–393
21. Seo JG, Youn MH, Song IK (2009) Hydrogen production by steam reforming of liquefied natural gas (LNG) over nickel catalyst supported on mesoporous alumina prepared by a non-ionic surfactant-templating method. Int J Hydrogen Energy 34:1809–1817
22. Seo JG, Youn MH, Bang Y, Song IK (2011) Hydrogen production by steam reforming of simulated liquefied natural gas (LNG) over mesoporous nickel-M-alumina (M = Ni, Ce, La, Y, Cs, Fe Co, and Mg) aerogel catalysts. Int J Hydrogen Energy 36:3505–3514
23. Patel S, Pant KK (2007) Experimental study and mechanistic kinetic modeling for selective production of hydrogen via catalytic steam reforming of methanol. Chem Eng Sci 62:5425–5435
24. Tesser R, Di Serio M, Santacesaria E (2009) Methanol steam reforming: a comparison of different kinetics in the simulation of a packed bed reactor. Chem Eng J 154:69–75
25. Nichele V, Signoretto M, Menegazzo F, Gallo A, Dal Santo V, Cruciani G, Cerrato G (2012) Glycerol steam reforming for hydrogen production: Design of Ni supported catalysts. Appl Catal B-Environ 111:225–232
26. Avila-Neto CN, Zanchet D, Hori CE, Ribeiro RU, Bueno JMC (2013) Interplay between particle size, composition, and structure of $MgAl_2O_4$-supported Co-Cu catalysts and their influence on carbon accumulation during steam reforming of ethanol. J Catal 307:222–237
27. Palma V, Castaldo F, Ciambelli P, Iaquaniello G, Capitani G (2013) On the activity of bimetallic catalysts for ethanol steam reforming. Int J Hydrogen Energy 38:6633–6645
28. Franchini CA, Aranzaez W, Duarte De Farias AM, Pecchi G, Fraga MA (2014) Ce-substituted $LaNiO_3$ mixed oxides as catalyst precursors for glycerol steam reforming. Appl Catal B-Environ 147:193–202
29. Palma V, Castaldo F, Ciambelli P, Iaquaniello G (2014) CeO_2-supported Pt/Ni catalyst for the renewable and clean H-2 production via ethanol steam reforming. Appl Catal B-Environ 145:73–84

30. Wu G, Li S, Zhang C, Wang T, Gong J (2014) Glycerol steam reforming over perovskite-derived nickel-based catalysts. Appl Catal B-Environ 144:277–285
31. Abbasi T, Abbasi SA (2011) 'Renewable' hydrogen: Prospects and challenges. Renew Sustain Energy Rev 15:3034–3040
32. Rostrup-Nielsen JR, Rostrup-Nielsen T (2002) Large-scale hydrogen production. Cattech 6:150–159
33. Matsumura Y, Nakamori T (2004) Steam reforming of methane over nickel catalysts at low reaction temperature. Appl Catal A-Gen 258:107–114
34. Rostrup-Nielsen JR, Sehested J, Nørskov JK (2002) Hydrogen and synthesis gas by steam- and CO_2 reforming. Adv Catal 47:65–139
35. Roh H-S, Jun K-W (2009) Low temperature methane steam reforming for hydrogen production for fuel cells. Bull Korean Chem Soc 30:153–156
36. Bengaard HS, Nørskov JK, Sehested J, Clausen BS, Nielsen LP, Molenbroek AM, Rostrup-Nielsen JR (2002) Steam reforming and graphite formation on Ni catalysts. J Catal 209:365–384
37. Miao Q, Xiong GX, Sheng SS, Cui W, Xu L, Guo XX (1997) Partial oxidation of methane to syngas over nickel-based catalysts modified by alkali metal oxide and rare earth metal oxide. Appl Catal A-Gen 154:17–27
38. Roh HS, Jun KW, Dong WS, Baek SC, Park SE (2002) Methane reforming reactions over stable Ni/theta-Al2O3 catalysts. J Ind Eng Chem 8:464–471
39. Wang X, Gorte RJ (2002) A study of steam reforming of hydrocarbon fuels on Pd/ceria. Appl Catal A-Gen 224:209–218
40. Profeti LPR, Ticianelli EA, Assaf EM (2008) Co/Al_2O_3 catalysts promoted with noble metals for production of hydrogen by methane steam reforming. Fuel 87:2076–2081
41. Gonzalez-Delacruz VM, Pereniguez R, Ternero F, Holgado JP, Caballero A (2011) In Situ XAS Study of Synergic Effects on Ni-Co/ZrO2 Methane Reforming Catalysts. J Phys Chem C 116:2919–2926
42. Amjad U-ES, Vita A, Galletti C, Pino L, Specchia S (2013) Comparative study on steam and oxidative steam reforming of methane with noble metal catalysts. Ind Eng Chem Res 52:15428–15436
43. Martinez-Arias A, Coronado JM, Cataluna R, Conesa JC, Soria J (1998) Influence of mutual platinum-dispersed ceria interactions on the promoting effect of ceria for the CO oxidation reaction in a $Pt/CeO_2/Al_2O_3$ catalyst. J Phys Chem B 102:4357–4365
44. Dal Santo V, Gallo A, Naldoni A, Guidotti M, Psaro R (2012) Bimetallic heterogeneous catalysts for hydrogen production. Catal Today 197:190–205
45. Gallo A, Pirovano C, Ferrini P, Marelli M, Psaro R, Santangelo S, Faggio G, Dal Santo V (2012) Influence of reaction parameters on the activity of ruthenium based catalysts for glycerol steam reforming. Appl Catal B-Environ 121:40–49
46. Jones G, Jakobsen JG, Shim SS, Kleis J, Andersson MP, Rossmeisl J, Abild-Pedersen F, Bligaard T, Helveg S, Hinnemann B, Rostrup-Nielsen JR, Chorkendorff I, Sehested J, Norskov JK (2008) First principles calculations and experimental insight into methane steam reforming over transition metal catalysts. J Catal 259:147–160
47. Halabi MH, De Croon MHJM, Van Der Schaaf J, Cobden PD, Schouten JC (2010) Low temperature catalytic methane steam reforming over ceria-zirconia supported rhodium. Appl Catal A-Gen 389:68–79
48. Rass-Hansen J, Christensen CH, Sehested J, Helveg S, Rostrup-Nielsen JR, Dahl S (2007) Renewable hydrogen: carbon formation on Ni and Ru catalysts during ethanol steam-reforming. Green Chem 9:1016–1021
49. Koh ACW, Leong WK, Chen L, Ang TP, Lin J, Johnson BFG, Khimyak T (2008) Highly efficient ruthenium and ruthenium-platinum cluster-derived nanocatalysts for hydrogen production via ethanol steam reforming. Catal Commun 9:170–175
50. Liguras DK, Kondarides DI, Verykios XE (2003) Production of hydrogen for fuel cells by steam reforming of ethanol over supported noble metal catalysts. Appl Catal B-Environ 43:345–354

51. Parmaliana A, Arena F, Frusteri F, Coluccia S, Marchese L, Martra G, Chuvilin AL (1993) Magnesia-supported nickel-catalysts. 2. Surface-properties and reactivity in methane steam reforming. J Catal 141:34–47
52. Martra G, Arena F, Baricco M, Coluccia S, Marchese L, Parmaliana A (1993) High loading Ni MgO catalysts—surface characterization by IR-spectra of adsorbed CO. Catal Today 17:449–458
53. Kumar P, Sun Y, Idem RO (2007) Nickel-based ceria, zirconia, and ceria-zirconia catalytic systems for low-temperature carbon dioxide reforming of methane. Energy Fuel 21:3113–3123
54. Liu ZW, Roh HS, Jun KW (2003) Important factors on carbon dioxide reforming of methane over nickel-based catalysts. J Ind Eng Chem 9:753–761
55. Wang SB, Lu GQ (1998) Thermogravimetric analysis of carbon deposition over Ni/gamma-Al2O3 catalysts in carbon dioxide reforming of methane. Energy Fuel 12:1235–1240
56. Koo KY, Roh H-S, Jung UH, Yoon WL (2009) CeO_2 promoted Ni/Al_2O_3 catalyst in combined steam and carbon dioxide reforming of methane for gas to liquid (GTL) process. Catal Lett 130:217–221
57. Liu ZW, Jun KW, Roh HS, Park SE (2002) Hydrogen production for fuel cells through methane reforming at low temperatures. J Power Sources 111:283–287
58. Challa SR, Delariva AT, Hansen TW, Helveg S, Sehested J, Hansen PL, Garzon F, Datye AK (2011) Relating rates of catalyst sintering to the disappearance of individual nanoparticles during ostwald ripening. J Am Chem Soc 133:20672–20675
59. Delariva AT, Hansen TW, Challa SR, Datye AK (2013) In situ transmission electron microscopy of catalyst sintering. J Catal 308:291–305
60. Serrano-Lotina A, Daza L (2014) Long-term stability test of Ni-based catalyst in carbon dioxide reforming of methane. Appl Catal A-Gen 474:107–113
61. Xu W, Liu Z, Johnston-Peck AC, Senanayake SD, Zhou G, Stacchiola D, Stach EA, Rodriguez JA (2013) Steam reforming of ethanol on Ni/CeO_2: reaction pathway and interaction between Ni and the CeO_2 support. ACS Catal 3:975–984
62. Xu J, Chen L, Tan KF, Borgna A, Saeys M (2009) Effect of boron on the stability of Ni catalysts during steam methane reforming. J Catal 261:158–165
63. Ligthart DAJM, Pieterse JAZ, Hensen EJM (2011) The role of promoters for Ni catalysts in low temperature (membrane) steam methane reforming. Appl Catal A-Gen 405:108–119
64. Borowiecki T, Denis A, Rawski M, Golebiowski A, Stolecki K, Dmytrzyk J, Kotarba A (2014) Studies of potassium-promoted nickel catalysts for methane steam reforming: Effect of surface potassium location. Appl Surf Sci 300:191–200
65. Calles JA, Carrero A, Vizcaino AJ, Garcia-Moreno L (2014) Hydrogen production by glycerol steam reforming over SBA-15-supported nickel catalysts: Effect of alkaline earth promoters on activity and stability. Catal Today 227:198–206
66. Molenbroek AM, Norskov JK, Clausen BS (2001) Structure and reactivity of Ni-Au nanoparticle catalysts. J Phys Chem B 105:5450–5458
67. Xu J, Saeys M (2009) First principles study of the effect of carbon and boron on the activity of a Ni catalyst. J Phys Chem C 113:4099–4106
68. Rossetti I, Gallo A, Dal Santo V, Bianchi CL, Nichele V, Signoretto M, Finocchio E, Ramis G, Di Michele A (2013) Nickel catalysts supported over TiO_2, SiO_2 and ZrO_2 for the steam reforming of glycerol. Chemcatchem 5:294–306
69. Caballero A, Holgado JP, Gonzalez-Delacruz VM, Habas SE, Herranz T, Salmeron M (2010) In situ spectroscopic detection of SMSI effect in a Ni/CeO_2 system: hydrogen-induced burial and dig out of metallic nickel. Chem Commun 46:1097–1099
70. Gonzalez-Delacruz VM, Holgado JP, Pereniguez R, Caballero A (2008) Morphology changes induced by strong metal-support interaction on a Ni-ceria catalytic system. J Catal 257:307–314

71. Hadjiivanov K, Mihaylov M, Abadjieva N, Klissurski D (1998) Characterization of Ni/TiO_2 catalysts prepared by successive adsorption-reduction of Ni^{2+} ions. J Chem Soc, Faraday Trans 94:3711–3716
72. Jun K-W, Roh H-S, Chary KVR (2007) Structure and catalytic properties of ceria-based nickel catalysts for CO_2 reforming of methane. Catal Surv Asia 11:97–113
73. Dong WS, Roh HS, Jun KW, Park SE, Oh YS (2002) Methane reforming over Ni/Ce-ZrO_2 catalysts: effect of nickel content. Appl Catal A-Gen 226:63–72
74. Seo JG, Youn MH, Bang Y, Song IK (2010) Effect of Ni/Al atomic ratio of mesoporous Ni-Al_2O_3 aerogel catalysts on their catalytic activity for hydrogen production by steam reforming of liquefied natural gas (LNG). Int J Hydrogen Energy 35:12174–12181
75. Seo JG, Youn MH, Chung JS, Song IK (2010) Effect of calcination temperature of mesoporous nickel-alumina catalysts on their catalytic performance in hydrogen production by steam reforming of liquefied natural gas (LNG). J Ind Eng Chem 16:795–799
76. Seo JG, Youn MH, Jung JC, Song IK (2010) Hydrogen production by steam reforming of liquefied natural gas (LNG) over mesoporous nickel-alumina aerogel catalyst. Int J Hydrogen Energy 35:6738–6746
77. Seo JG, Youn MH, Nam I, Hwang S, Chung JS, Song IK (2009) Hydrogen Production by Steam Reforming of Liquefied Natural Gas over Mesoporous Ni-Al_2O_3 Catalysts Prepared by a Co-Precipitation Method: Effect of Ni/Al Atomic Ratio. Catal Lett 130:410–416
78. Seo JG, Youn MH, Park DR, Jung JC, Song IK (2009) Hydrogen production by steam reforming of liquefied natural gas over mesoporous Ni-Al2O3 composite catalyst prepared by a single-step non-ionic surfactant-templating method. Catal Lett 132:395–401
79. Seo JG, Youn MH, Park DR, Nam I, Song IK (2009) Hydrogen production by steam reforming of liquefied natural gas (LNG) over Ni-Al_2O_3 catalysts prepared by a sequential precipitation method: Effect of precipitation agent. Int J Hydrogen Energy 34:8053–8060
80. Seo JG, Youn MH, Park S, Park DR, Jung JC, Chung JS, Song IK (2009) Hydrogen production by steam reforming of liquefied natural gas (LNG) over mesoporous nickel-alumina composite catalyst prepared by an anionic surfactant-templating method. Catal Today 146:44–49
81. Bang Y, Lee J, Han SJ, Seo JG, Youn MH, Song JH, Song IK (2012) Hydrogen production by steam reforming of liquefied natural gas (LNG) over mesoporous nickel-alumina xerogel catalysts prepared by a single-step carbon-templating sol-gel method. Int J Hydrogen Energy 37:11208–11217
82. Bang Y, Seo JG, Youn MH, Song IK (2012) Hydrogen production by steam reforming of liquefied natural gas (LNG) over mesoporous Ni-Al_2O_3 aerogel catalyst prepared by a single-step epoxide-driven sol-gel method. Int J Hydrogen Energy 37:1436–1443
83. Rezaei A, Alavi SM, Sahebdelfar S, Yan Z-F (2007) Mesoporous nanocrystalline zirconia powders: A promising support for nickel catalyst in CH_4 reforming with CO_2. Mater Lett 61:2628–2631
84. Rezaei M, Alavi SM, Sahebdelfar S, Bai P, Liu X, Yan Z-F (2008) CO_2 reforming of CH_4 over nanocrystalline zirconia-supported nickel catalysts. Appl Catal B-Environ 77:346–354
85. Rezaei M, Alavi SM, Sahebdelfar S, Liu X, Qian L, Yan Z-F (2007) CO_2-CH_4 reforming over nickel catalysts supported on mesoporous nanocrystalline zirconia with high surface area. Energy Fuel 21:581–589
86. Rezaei M, Alavi SM, Sahebdelfar S, Yan Z-F (2008) Effects of K_2O promoter on the activity and stability of nickel catalysts supported on mesoporous nanocrystalline zirconia in CH_4 reforming with CO_2. Energy Fuel 22:2195–2202
87. Burri DR, Choi K-M, Lee J-H, Han D-S, Park S-E (2007) Influence of SBA-15 support on CeO_2-ZrO_2 catalyst for the dehydrogenation of ethylbenzene to styrene with CO_2. Catal Commun 8:43–48
88. Wang K, Li X, Ji S, Shi X, Tang J (2009) Effect of $Ce_xZr_{1-x}O_2$ promoter on Ni-Based SBA-15 catalyst for steam reforming of methane. Energy Fuel 23:25–31
89. Angeli SD, Monteleone G, Giaconia A, Lemonidou AA (2014) State-of-the-art catalysts for CH_4 steam reforming at low temperature. Int J Hydrogen Energy 39:1979–1997

90. Gopalakrishnan S, Faga MG, Miletto I, Coluccia S, Caputo G, Sau S, Giaconia A, Berlier G (2013) Unravelling the structure and reactivity of supported Ni particles in Ni-$CeZrO_2$ catalysts. Appl Catal B-Environ 138:353–361
91. Bera P, Mitra S, Sampath S, Hegde MS (2001) Promoting effect of CeO_2 in a Cu/CeO_2 catalyst: lowering of redox potentials of Cu species in the CeO_2 matrix. Chem Commun 927–928
92. Kim DK, Stoewe K, Mueller F, Maier WF (2007) Mechanistic study of the unusual catalytic properties of a new Ni-Ce mixed oxide for the CO_2 reforming of methane. J Catal 247:101–111
93. Xu S, Yan X, Wang X (2006) Catalytic performances of NiO-CeO_2 for the reforming of methane with CO_2 and O_2. Fuel 85:2243–2247
94. Trovarelli A (1996) Catalytic properties of ceria and CeO_2-containing materials. Catal Rev-Sci Eng 38:439–520
95. Campbell CT, Peden CHF (2005) Oxygen vacancies and catalysis on ceria surfaces. Science 309:713–714
96. Esch F, Fabris S, Zhou L, Montini T, Africh C, Fornasiero P, Comelli G, Rosei R (2005) Electron localization determines defect formation on ceria substrates. Science 309:752–755
97. Trovarelli A, Zamar F, Llorca J, Deleitenburg C, Dolcetti G, Kiss JT (1997) Nanophase fluorite-structured CeO_2-ZrO_2 catalysts prepared by high-energy mechanical milling—Analysis of low-temperature redox activity and oxygen storage capacity. J Catal 169:490–502
98. Kaspar J, Fornasiero P, Graziani M (1999) Use of CeO_2-based oxides in the three-way catalysis. Catal Today 50:285–298
99. Daturi M, Finocchio E, Binet C, Lavalley JC, Fally F, Perrichon V, Vidal H, Hickey N, Kaspar J (2000) Reduction of high surface area CeO_2-ZrO_2 mixed oxides. J Phys Chem B 104:9186–9194
100. Thammachart M, Meeyoo V, Risksomboon T, Osuwan S (2001) Catalytic activity of CeO_2-ZrO_2 mixed oxide catalysts prepared via sol-gel technique: CO oxidation. Catal Today 68:53–61
101. Damyanova S, Pawelec B, Arishtirova K, Huerta MVM, Fierro JLG (2008) Study of the surface and redox properties of ceria-zirconia oxides. Appl Catal A-Gen 337:86–96
102. Colon G, Pijolat M, Valdivieso F, Vidal H, Kaspar J, Finocchio E, Daturi M, Binet C, Lavalley JC, Baker RT, Bernal S (1998) Surface and structural characterization of $Ce_xZr_{1-x}O_2$ CEZIRENCAT mixed oxides as potential three-way catalyst promoters. J Chem Soc, Faraday Trans 94:3717–3726
103. Balducci G, Islam MS, Kaspar J, Fornasiero P, Graziani M (2000) Bulk reduction and oxygen migration in the ceria-based oxides. Chem Mater 12:677–681
104. Escribano VS, Lopez EF, Panizza M, Resini C, Amores JMG, Busca G (2003) Characterization of cubic ceria-zirconia powders by X-ray diffraction and vibrational and electronic spectroscopy. Solid State Sci 5:1369–1376
105. Roh HS, Potdar HS, Jun KW, Kim JW, Oh YS (2004) Carbon dioxide reforming of methane over Ni incorporated into Ce-ZrO_2 catalysts. Appl Catal A-Gen 276:231–239
106. Roh HS, Jun KW, Dong WS, Park SE, Baek YS (2001) Highly stable Ni catalyst supported on Ce-ZrO_2 for oxy-steam reforming of methane. Catal Lett 74:31–36
107. Xu S, Wang XL (2005) Highly active and coking resistant Ni/CeO_2-ZrO_2 catalyst for partial oxidation of methane. Fuel 84:563–567
108. Roh HS, Potdar HS, Jun KW (2004) Carbon dioxide reforming of methane over co-precipitated Ni-CeO_2, Ni-ZrO_2 and Ni-Ce-ZrO_2 catalysts. Catal Today 93–5:39–44

Two-Phase Anaerobic Digestion of Food Wastes for Hydrogen and Methane Production

Cristina Cavinato, David Bolzonella, Paolo Pavan and Franco Cecchi

Abstract Food waste is successfully treated by anaerobic digestion process, where the organic matter is converted into methane. On the other hand, food waste bio-processing to produce hydrogen has been only recently implemented, wherein a number of expensive pretreatment techniques have been proven. This chapter describes the recent studies on hydrogen and methane production from food waste using a dark fermentation reactor coupled with anaerobic digestion at thermophilic temperature. The use of external chemicals to control the pH was avoided, but sludge recirculation from the methanogenic reactor to the dark fermentation was exploited to maintain the system in an optimal pH range for production of a gas mixture with the typical composition of enriched methane. Ammonia accumulation and variation was observed during 1 year of process monitoring and was finally elaborated with a chemometric analysis tool, giving back useful results to be implemented in an automatic process control based on correlation between ammonia, conductivity and alkalinity.

Keywords Anaerobic digestion · Food waste valorisation · Sludge recirculation · Fermentation process control

List of Acronyms

ATP	Adenosin triphosphate
COD	Chemical oxygen demand
CSTR	Continuous stirred tank reactor
D	Dilution rate
EM	Enriched methane
FW	Food waste

C. Cavinato (✉) · P. Pavan
Department of Environmental Sciences, Informatics and Statistics,
University Ca' Foscari of Venice, Calle Larga Santa Marta, 30127 Venice, Italy
e-mail: cavinato@unive.it

D. Bolzonella · F. Cecchi
Department of Biotechnology, University of Verona, Strada Le Grazie 15,
37134 Verona, Italy

M. De Falco and A. Basile (eds.), *Enriched Methane*,
Green Energy and Technology, DOI 10.1007/978-3-319-22192-2_5

GHG	Greenhouse gas
GPR	Gas production rate
HRT	Hydraulic retention time
LAB	Lactic acid bacteria
NADH	Nicotinammide adenina dinucleotide
OFMSW	Organic fraction of municipal solid waste
OLR	Organic loading rate
SGP	Specific gas production
SHP	Specific hydrogen production
SMP	Specific methane production
TS	Total solids
TVS	Total volatile solids
VFA	Volatile fatty acid

1 Introduction

Methane and hydrogen are considered as the most important gaseous energy carriers; they have independent commercial interest, but mixed together as enriched methane (EM), they could be better exploited. EM (methane gas with 10–25 % of hydrogen) has been used commercially as vehicle fuel in the USA and India [1, 2] and applied as fuel in some prototype of many companies such as Volvo, Fiat and others. The advantage of this gas mixture is that hydrogen promotes better exploitation of methane during combustion. In fact, it has proprieties that perfectly complement the weak points of methane: with the addition of hydrogen the H/C ratio is increased, and the effect is a reduction of GHG emissions; the narrow range of flammability of methane can be extended by adding hydrogen, thus improving the fuel efficiency; hydrogen greatly increases the flame speed of methane, eventually reducing combustion duration and improving heat efficiency; the quenching distance of methane can be reduced by addition of hydrogen, making the engine easy to ignite with less input energy. In spite of the benefits, the addition of hydrogen to methane still has problems that must be overcome: usually hydrogen is produced in an energy intensive way, for example by means of syngas production or methane reforming. The biological hydrogen production by photosynthetic bacteria, algae or fermentative microorganism or via water hydrolysis using extra load power from wind and photovoltaic appears to be a promising alternative. The emerging challenge, among the biological technologies, is the biological hydrogen and methane production via a two-phase process composed of dark fermentation and anaerobic digestion, exploiting a number of residual substrates. Among the suitable substrates evaluated during about 10 years of researches, food waste (FW) and the mixture of food waste and other organic residues, such as the organic fraction of municipal solid waste (OFMSW), represent a great opportunity matching together three fundamental characteristics: wide availability, high carbohydrate content and a renewable source.

2 General Process Description

In the anaerobic digestion process different microorganisms are involved in a synergic way to produce methane from complex biomass through four steps: hydrolysis, acidogenesis, acetogenesis and methanogenesis. Three major groups of microorganisms have been identified with different functions in the overall degradation process: the hydrolyzing and fermenting microorganisms, the obligate hydrogen-producing acetogenic bacteria and two groups of methanogenic archaea. The latter groups drive two specific pathways for methane formation: acetoclastic (acetate degrading microorganisms) that produces CH_4 and CO_2 using acetate, hydrogenotrophic (hydrogen utilizing microorganism) that produces CH_4 using hydrogen and carbon dioxide. So it is easy to understand why, if hydrogen must be recovered, it is necessary to avoid the second pathway.

Two-phase processes for biological hydrogen and methane production operate with an appropriate separation of acidogenic and methanogenic phases; this separation allows to convert the complex organic material into hydrogen, carbon dioxide and volatile fatty acids (VFAs) during the acidogenic stage, and a subsequent conversion of these easily biodegradable compounds into methane and carbon dioxide during the methanogenic stage.

The microbiological "appropriate separation" concept is actually a hot issue, because the adopted operating condition could influence (inhibiting or promoting) various metabolic pathways and consequently the bio-H_2 production.

Especially if treating complex substrates, it must be taken into account the conversion efficiency: in fact, theoretically from 1 mol of glucose, 12 mol of hydrogen can be obtained, but this reaction is energetically unfavourable with respect to biomass growth, and real conversion is usually lower than this. It is possible to assume, in biochemistry terms, that in the acidogenic fermentation, pyruvate produced from fermentation of hexose and pentose sugars is oxidized in the presence of coenzyme A (CoA) to acetyl—CoA, while CO_2 and reduced ferredoxin are generated. The acetyl—CoA can be phosphorylated to generate acetate or butyrate and ATP, and the reduced ferredoxin can transfer electrons to hydrogenase enzyme and molecular H_2 is released from the cell. As reported in Eqs. (1) and (2), the maximum theoretical yield of hydrogen, when the acetic acid is the final product of fermentation, is 4 mol per mole of glucose consumed; when butyric acid is the final product of fermentation, the maximum theoretical yield of hydrogen is 2 mol per mole of glucose consumed [3, 4].

$$C_6H_{12}O_6 + 2H_2O \rightarrow 4H_2 + 2CO_2 + 2CH_3COOH \quad (1)$$

$$C_6H_{12}O_6 \rightarrow 2H_2O + 2CO_2 + CH_3CH_2CH_2COOH \quad (2)$$

Besides acetate (1) and butyrate (2) pathways, in a mixed culture other reduced compounds could be produced such as propionate, ethanol and lactic acid, in order to sustain microbial growth but causing a decreased hydrogen yield, with a

conversion efficiency (under optimal condition) of less than 15 % of the electrons in the substrate [3] (or less than 33 % of the energy content of substrate into H_2). Basically, when the hydrogenase enzyme is inhibited, the reduced ferredoxin is oxidized by nicotinamide adenine dinucleotide (NAD+), and the NADH generated reduces the acetyl-CoA and butyryl-CoA to ethanol and butanol, respectively. For these reasons when lactic acid, ethanol and butanol are produced, they are not related to hydrogen production; furthermore, the formation of propionate and formate indicates the consumption of hydrogen.

It was widely demonstrated that pH condition and temperature condition affect the activity of hydrogenase enzyme in the H_2 production process. The optimal condition reported for best enzyme activity was observed to be between pH 5 and 6 with an optimum value at 5.5, and at 55 °C of working temperature [5, 6]. During fermentative metabolism the organic acids accumulate, decreasing both pH value and H_2 production as a consequence. The study of pH control in dark fermentation was carried out by a number of researchers during the past 10 years, developing several strategies, for example the addition of chemicals [7–9] or the use of protein-containing substrates. These approaches are often expensive or environmentally not sustainable, so some simple strategy was developed just adapting some process parameters favouring the proliferation of hydrogen-producing microorganisms.

3 Fermentative Hydrogen Production Process Parameters: Inhibition of Hydrogenotrophic Activity Treating Food Wastes

The most important challenge for sustaining hydrogen production in a reactor optimized for dark fermentation is to avoid the growth of hydrogen consuming bacteria [10]. Due to the daily addition of mixed culture through food waste fed there is always the risk that unwanted archaea such as H_2-consuming methanogens could grow and deplete the hydrogen already produced. The strategies that can be adopted to select the H_2-producing bacteria in a mixed culture approach are:

- Inoculum and/or substrate treatments;
- Hydraulic Retention Time (HRT);
- Organic Loading Rate (OLR);
- Temperature.

3.1 Inoculum and/or Substrate Treatments

Mixed cultures from anaerobic digestion process have a dominance of non-H_2 producing acidogens and/or H_2 consuming microorganism and, besides, the organic solid waste itself contains many types of indigenous microorganisms. The microorganism could prevail easily in the start-up period when the H_2 producing bacteria have not been fully acclimated to waste [11]. To reduce the risk and provide a favourable environment for H_2 producing bacteria it is possible to select them by treating the inoculum or food waste physically or chemically.

Inoculum from anaerobic digestion could be treated by acid, basic or heat shock treatment. Among these treatments heat shock gives better yields compared to others. Some authors use a 90 °C temperature for 10–30 min [9, 12], but Valdez-Vazquez et al. [5] reviewed the effectiveness of heat treatment with 100 °C for 15 min or 80 °C for 3 h, suggesting the necessity to repeat the treatment during long working periods in order to avoid the formation of H_2 consuming microorganism, especially when using complex substrate. As an alternative to inoculum treatment some authors treat the organic waste directly. Kim et al. [13] found that in food waste there are 11 types of lactic acid bacteria (LAB); Noike et al. [14] studied the inhibition of hydrogen production using organic waste at low pH value of 4.5 by lactic acid bacteria. Kim et al. [13] studied the hydrogen fermentation of food waste without inoculum addition in batch test, using acid, basic and heat shock treatment and they found that heat shock was the best treatment associated with the highest hydrogen yield and with depletion of the LAB. Heat shock treatment effectiveness was even confirmed by Noike et al. [15], who treated waste at 70 °C for 30 min. Also, Wang et al. [16] used the organic waste directly in a semi-continuous rotating drum reactor, but in this case they obtained good yields without any treatment.

It is also possible to use different types of inoculum, not from anaerobic digestion: Chou et al. [17] used the supernatant liquid of grass composting mixture heated at 85 °C for 3 h; Alzate-Gaviria et al. [18] prepared a mixture of non-anaerobic inoculum composed of deep soil, pig manure, sodium carbonate and water; Fan et al. [19] used a composted sludge treated at 103° for 24 h, then re-suspended and filtrated; Li et al. [20] used acidogenic sludge from a kitchen waste composting plant.

Another technique used by some authors is acclimatization of the inoculum, for example Shin et al. [21] used an inoculum from anaerobic digestion and fed it with organic waste for 3 months using a CSTR (55 °C, HRT 3d, OLR 2 kgVS m^{-3} d^{-1}), or Zhu et al. [22] that fed the inoculum with a sugar solution, obtaining the depletion of H_2-consuming microorganism.

3.2 Hydraulic Retention Time

Hydraulic retention time (HRT) is defined as the volume of the reactor divided by the volumetric flow and is also known as the inverse of the dilution rate (D). The continuous stirred tank reactors (CSTR) or chemostat could be used to select microbial populations whose growth rates are able to catch up to the dilution caused by continuous volumetric flow. In this way, only microbial populations with growth rates larger than the dilution rate can remain in the reactor ($\mu_{max} > D$) [23]. Based on this, high dilution rates (short HRT) could be used to cause the complete washout of methanogens since the specific growth rates of methanogens are much shorter than those of H_2-producing bacteria (0.0167 and 0.083 h^{-1} respectively) [5].

The H_2 fermentation pattern may shift to methanogenic fermentation if the HRT is increased but with complex substrate like organic waste it is necessary to apply higher HRT in order to give the time to decompose carbohydrates. The typical HRT applied in a CSTR treating solid organic waste ranged from 5 to 2 days [24], while with other reactor configurations it is possible to use lower HRT (until 6 h).

There is not an optimum HRT because the optimization of the process depends also on other process parameters such as the organic loading rate, characteristics of organic substrate and pH control, but considering the literature data the higher hydrogen production rate (HPR) is observed at HRT < 3d (Fig. 1).

3.3 Organic Loading Rate (OLR)

The same objective of H_2-producing bacteria selection could be achieved using the organic loading rate (OLR). With HRT it is possible to cause a washout of methanogenic archaea avoiding the use of H_2 produced to form methane, while with OLR it is possible to cause a decrease of pH as consequence of the overloading of the reactor that leads to an overproduction of organic acids and other metabolites from the degradation of incoming substrate. In this condition it is necessary to

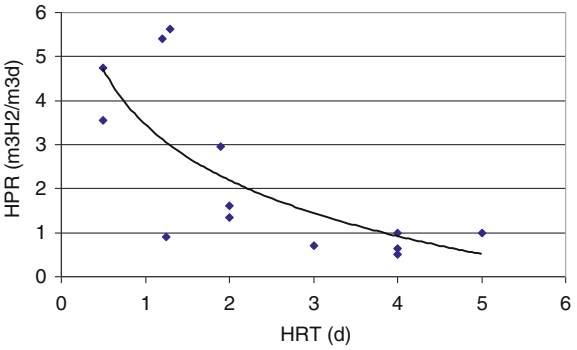

Fig. 1 Relation between hydraulic retention time (d) and hydrogen production rate (m^3/m^3d) considering the literature data

exercise a pH control in order to keep the pH in a range favourable for hydrogen accumulation [5].

Lee and co-workers [9] observed the variation in H_2 production maintaining HRT at 4 d, in a CSTR reactor, changing the OLR from 19 to 28 kgCOD m^{-3} d^{-1}, controlling the pH at 6. They found an increase in H_2 % from 35 to 48 and an SHP from 20.2 to 38.8 LH_2 $kg^{-1}COD_{fed}$.

Usually the OLR applied varies significantly between 14 and 38.5 kgVS m^{-3} d^{-1}. Basically, assuming no pH control, the higher the organic load applied the lower specific hydrogen production was observed. Along with pH, high organic acid concentrations could result in detrimental effects to H_2 fermentation. Undissociated acids act as uncouplers that allow protons to enter the cell; sufficiently high concentrations of undissociated acids could generate a collapse in the pH gradient across the membrane. Thus, the shift to solventogenesis has been related to a detoxification mechanism of the cell to avoid inhibitory effects [5].

3.4 Temperature

The temperature range is another process parameter but it is not linked to the selection of the H_2 producing microflora. It is important mainly from the kinetic point of view because, as in anaerobic digestion, higher temperature increases the degradation velocity improving the gas yields. Valdez-Vazquez et al. [25] compared mesophilic and thermophilic temperature in a CSTR reactor fed with organic waste (11 kgVS m^{-3} d^{-1}) and they observed an increase in the specific hydrogen production from 94 to 198 NL kg^{-1}VS. Lee et al. [9] and Li et al. [20] used a similar condition: 4 days of HRT, 26–28 kgCOD m^{-3} d^{-1} of OLR and a pH control, but they applied different temperature ranges. Changing from mesophilic to thermophilic range, the hydrogen production rate increased from 0.63 to 1 m^3/m^3d and the specific hydrogen production from 22.4 to 38.1 LH_2 $kg^{-1}COD_{fed}$.

Considering all the parameters mentioned above, it is evident that HRT, OLR and pH are dependent among each other, since the higher the OLR, the higher the production of VFAs will be with consequent dropping in pH. Low HRT itself can cause a washout of the acid-consumers bacteria, lead to an accumulation of organic acids and a drop in pH. pH is definitely the most important parameter if we want to maximize hydrogen production in dark fermentation reactor, because it influences the functionality of hydrogenase enzyme and H_2 production.

4 Biohydrogen Production from Food Waste

When choosing the type of substrate among several types of substrates available, it must be considered a huge necessity to recover energy and material from wastes. Food industry wastes constitute a major fraction of the municipal solid wastes.

Composting, incineration and anaerobic digestion are the conventional approaches for solid waste management. However, high carbohydrate content in the form of simple sugars, starch and cellulose makes solid food wastes a potential feedstock for biological hydrogen production. The problem with food waste is mainly the variations in carbohydrate and protein types and concentrations in the mixture; in fact each component requires different environmental and process conditions for hydrogen gas production. This favourable condition could be achieved in a mixed culture system under specific operation parameters.

Several studies were carried out in the past years on the hydrogen production potential of proteins, carbohydrates and lipids, showing that carbohydrates were the most suitable categories with the highest H_2 conversion yields [26]. Lay et al. [27] studied the hydrolysis rate as the limiting step for hydrogen production, and found that H_2 production treating carbohydrate-rich substrate was 20 times greater than the production treating protein and fat rich substrates. On the other hand, there are disadvantages such as conversion of carbohydrates into acids during storage [20] and the existence of indigenous micro flora that could convert carbohydrate into lactic acid.

Currently, dark fermentation is of particularly high interest because it can be coupled with the anaerobic digestion process in order to produce biohydrogen and biogas (or to obtain, after upgrade, the enriched methane), exploiting most of the energy content of complex substrate fed in the process. Biohydrogen production via dark fermentation of carbohydrate-rich substrates is carried out by various anaerobic bacteria, particularly *Clostridium spp., Thermoanaerobacterium spp., Enterobacter* and *Bacillus* [26], as a result of a chain of microbial activities and provided that environmental conditions such as pH and temperature are favourable.

The pH is a key parameter to be controlled, especially if treating heterogeneous substrates such as food waste; in fact, in order to obtain the best performances of hydrogenase enzyme activity, the pH must range between 5 and 6 (optimum value at 5.5). There are several strategies available to control the pH, for example the addition of chemicals or the use of protein-containing substrates [5].

An advanced strategy is the pH control coupling in series the dark fermentation together with the anaerobic digestion process and using the recirculation of the digested effluent, rich in buffer agents, to control the dark fermentation pH. The recirculation flow from a methanogenic reactor to a hydrogen-producing reactor allows to exploit the residual buffer capacity (ammonium, bicarbonate) of digestate [28], to supply nutrients and dilute the feedstock used [9, 29, 30]. Moreover, it is possible to produce EM, resulting in a highly efficient biological process for waste treatment [28, 31–33].

4.1 Two-Phase Anaerobic Digestion: Lab-Scale Tests on Effluent Recirculation for Hydrogen Production

Among the strategies for pH control, the recirculation of the anaerobic digestion effluent, rich in buffer agents, to control the dark fermentation pH is a promising approach, both in economics and in technical terms.

Kataoka et al. [29] compared two operations with and without recirculation of the sludge, and observed how the process yields were influenced by the pH: without the recirculation the pH values were about 4.0–4.5 and the specific hydrogen production was less than 5 LH_2 kg^{-1} TVS d^{-1}, while with a recirculation the pH was between 5 and 6 and the SHP reached the highest values of 20–30 LH_2 kg^{-1} TVS d^{-1}. This means that the alkalinity of the anaerobic digestion sludge allows a pH control without external chemicals addition.

The best yields, obtained using the recirculation approach, were achieved by Chu et al. [30]. They used two CSTR reactors (one was a rotating drum), with a recirculation rate of two and obtained the 42 % of H_2 content in the biogas and 205 LH_2 kg^{-1} TVS_{fed}. In this experimental work the digested sludge was settled before and only the thickened sludge was recirculated; pH was maintained at 5.5 and no methane was detected.

In these experiences, and others in the literature, the digested sludge was recirculated in different ways (i.e. solid part or liquid part after separation, different recirculation ratios, etc.), giving different results and bringing researchers to ask themselves if it was better to use the supernatant, recirculating the alkalinity, or the whole sludge in order to recirculate the biomass.

Some tests were done on lab scale on recirculation of second phase effluent, in order to understand if it was just a matter of alkalinity supply or the necessity of new hydrogen-producing biomass. Chinellato et al. [32] tested in a two-phase system, the two conditions, applying four organic loading rates (15, 20, 25 and 30 kg TVS m^{-3} d^{-1}) to the dark fermentation reactor, with 3 days of HRT, and comparing the process yields among supernatant and whole digestate recirculation. The substrate used was only food waste and the reactors were maintained at 55 °C.

The trials carried out with supernatant recirculation showed no positive results in terms of hydrogen production; in fact at higher OLR (25 and 30 kg TVS m^{-3} d^{-1}) the first phase immediately fell into acidic conditions leading quickly to failure in the methanogenic phase. At OLR 15 and 20 kg TVS m^{-3} d^{-1} the first phase was basically producing VFA without hydrogen production, due to a pH lower than 5, but methanogenic reactor was not inhibited.

At the organic loading rate of 20 kg TVS m^{-3} d^{-1} the tests carried out with recirculation of the whole digestate gave much more interesting results, with a stable hydrogen concentration of 47.7 % in the first phase and 60 % methane in the second phase. During the experimental test the first phase pH was self-controlled at a value of 5.22 and an SHP of 0.117 Nm^3 kg^{-1} TVS was observed. Hydrogen concentration in the biogas was 47.7 %. SGP in the second phase was 0.512 Nm^3 kg^{-1} TVS while the total SGP was 0.752 Nm^3 kg^{-1} TVS. The final gas

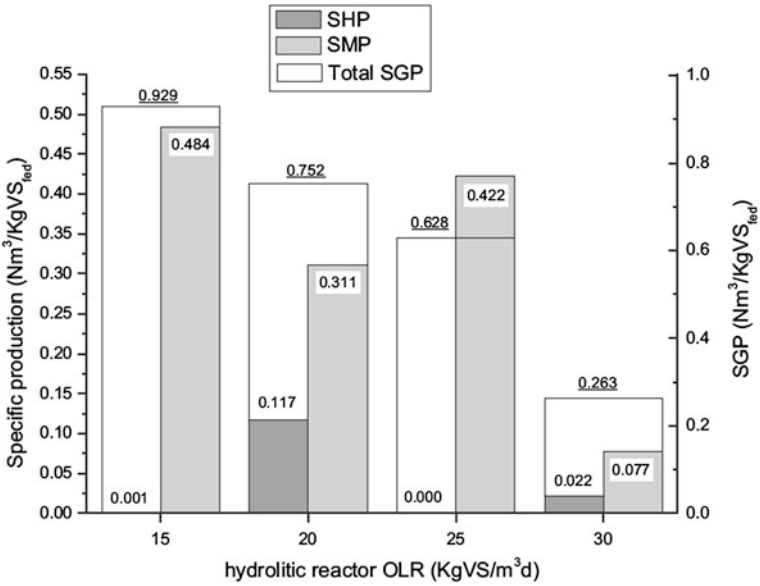

Fig. 2 Specific gas productions for all loadings tested with whole digestate recirculation [32]

composition was 18 % H_2, 39 % CH_4 and 43 % CO_2 which does not match the ideal bio-EM profile as the percentage of hydrogen is too high, but it is possible to regulate the right percentage after gas collection.

In Fig. 2 the gas yields of fermentation reactor with whole digestate recirculation are reported.

Not all of the conditions tested were suitable for combined hydrogen and methane production. In fact at all of the loadings tested, recirculation of supernatant alone did not lead to adequate pH control and was not sufficient to sustain hydrogen production in the first phase [32].

Recirculation of whole digestate returned not only alkalinity but also biomass, providing a continual inoculum of fermentative organisms to the first phase.

The main problem seen in the operation of this system was the accumulation of ammonia: this in turn may be associated with population changes in the anaerobic consortium and with VFA accumulation.

4.2 Two-Phase Anaerobic Digestion: Pilot-Scale Tests on Effluent Recirculation for Hydrogen Production

Moving from lab to pilot scale, Cavinato et al. [31] tested the process parameters applied by Chinellato and co-workers [32] in order to verify and optimize the best results obtained. The test was carried out on two thermophilic pilot-scale CSTR of

0.2 and 0.76 m^3 using real organic fraction of municipal solid waste as substrate and adopting the same process parameters (first phase HRT was 3.3 days, OLR about 16.3 kg TVS m^{-3} d^{-1}). The recirculated sludge was previously physically pretreated with a mild solid/liquid separation in order to remove inert materials. Thanks to sludge recirculation, dark fermentation pH was always in the optimal range of hydrogenase enzyme with an average value of 5.7. The gas yields were comparable with those found in the literature: the biogas produced were 0.17 m^3 kg^{-1} TVS and 0.72 m^3 kg^{-1} TVS for the first and second phase, respectively, with an average percentage of H_2 in dark fermentation and CH_4 in anaerobic digestion being 39 and 67 % respectively. After 90 days of operation the gas production was almost stable and the verified bio-EM composition met the typical values (CH_4 58 %, H_2 6.9 % and CO_2 36 %) with a specific hydrogen production of 66.7 LH_2 kg^{-1} TVS.

The stability of two-phase systems in a long-term approach with sludge recirculation was influenced by ammonia accumulation. The ammonia in fact accumulates for a long time due to the continuous ammonia flow back to the first phase. High ammonia concentration restrains the good performance of anaerobic microflora specialized for both hydrogen and methane production, and it is mainly due to the decompositions of proteins contained in food waste during anaerobic digestion.

In order to avoid ammonia inhibition, another long-term pilot scale test was carried out and elaborated by Micolucci et al. [34], adopting a dynamic recirculation of anaerobic digestion effluent. So ammonia removal was dynamically controlled depending on daily stability behaviour observed through pH, volatile fatty acids (VFAs) and alkalinity values. The recirculation flow was daily changed in order to maintain NH_3 concentration below the critical value observed (600–700 mg l^{-1}) in the methanogenic reactor: in this way a sufficient alkalinity supply was ensured for the fermentative reactor so as to buffer the high VFA content and to optimize H_2 production. The specific biogas production average was 0.240 Nm^3 kg^{-1} TVS with an H_2 content of 25 %.

Table 1 summarizes the results obtained in the above-mentioned similar two-phase anaerobic digestion experiences for food waste treatment, in order to produce hydrogen and methane.

The EM mixture produced in the pilot experimental trials matches the typical composition values: in the first reported test the bio-EM was composed of 6.9 % H_2 57.6 % CH_4 and 35.5 % CO_2; during dynamically controlled process the bio-EM has an average composition percentage of H_2, CH_4 and CO_2 respectively 7, 58 and 35 %.

4.3 Ammonia/Recirculation Control

The feasibility of bio-EM production using two-phase anaerobic approach was assessed, but the new challenges are nowadays related to scale-up of the process

Table 1 Process parameters and yields obtained, in similar operating condition

	[32]	[31]	[34]
Temperature (°C)	55	55	55
OLR 1° phase (kg TVS m^{-3} d^{-1})	20.0	16.3	18.4
OLR 2° phase (kg TVS m^{-3} d^{-1})	4.0	4.8	4.8
HRT 1° phase (d)	3.0	3.3	3.3
HRT 2° phase (d)	12.0	12.6	12.6
SGP 1° phase (m^3 kg^{-1} TVS)	0.240[a] ± 0.032	0.170 ± 0.1	0.220 ± 0.14
H_2 (%)	47.7 ± 1.1	38.5 ± 9.7	25.0 ± 9.0
SGP 2° phase (Nm^3 kg^{-1} TVS)	0.512[a] ± 0.031	0.720 ± 0.1	0.710 ± 0.09
CH_4 (%)	61.2 ± 2.4	67.0 ± 3.7	67.0 ± 3.0

[a]Nm^3 kg^{-1} TVS

and automatic control, taking into account the economic aspect and the long-term feasibility of the process.

As discussed previously, in a two-phase system for hydrogen and methane production without any chemical or physical pretreatment, not even with external pH control, the strategic approach is the right recirculation of digested sludge to control pH and avoid ammonia accumulation. But how to control the system equilibrium if a process control based on ammonia monitoring is not feasible at full scale, yet? In fact ammonia probes applied in such a heterogeneous media could be difficult to use and may not be reliable in the long term. Taking into account the data of the long-term tests carried out by Giuliano et al. [35], Micolucci and co-workers [34] developed a statistical model to predict ammonia concentration in a two-phase anaerobic digestion system using the measure of electrical conductivity and alkalinity. According to this strategy the decisive step was to define the set-points of these stability parameters in order to maintain the right amount of recycled effluent according to the change in stability parameters of the reactors in real-time mode. In Fig. 3 is reported the process control flow scheme.

The main problem linked to this approach regards the choice of control parameters to be measured online. In fact, ammonia concentration probe is difficult to use and may prove to be reliable as a long-term effect. In order to predict the ammonia concentration through other simple parameters, the correlation among ammonia concentration and electrical conductivity was verified and they were linearly correlated in both reactors (dark fermentation and anaerobic digestion). Therefore, conductivity is a good candidate for real-time control, in fact it is a non specific measure, measurable with strong and reliable probes with relatively low maintenance procedures, and has good correlation even with alkalinity. Through chemometric studies all the experimental data collected were modelled for the anaerobic digestion reactor. Chemometric analysis was used to predict the ammonia–nitrogen concentration in the recirculation flow. Micolucci et al. [34] calculated an equation of the multivariate model to predict ammonia concentration, with conductivity and alkalinity as predictor variables.

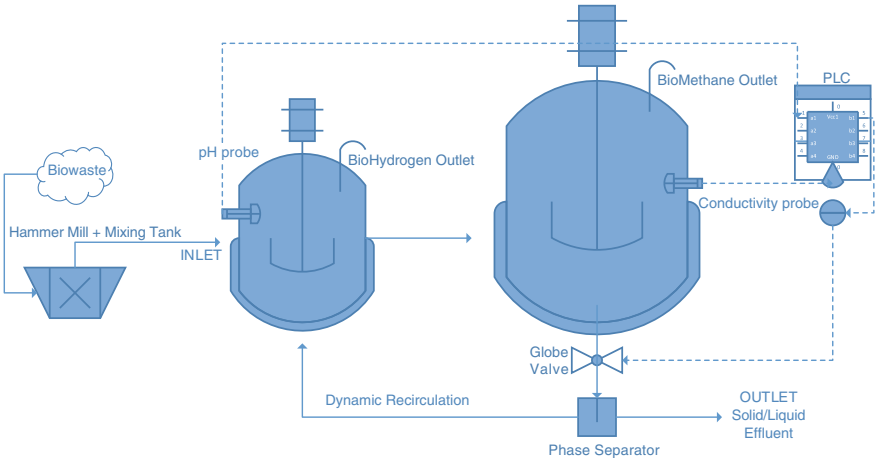

Fig. 3 Flow scheme of the two-phase process control

The equation of the multivariate model, using the predictor variables alkalinity and conductivity, to predict the concentration of ammonia is

$$NH_4^+ - N = -733 + 95.4 \times (\text{Conductivity}) - 0.138 \times (\text{Total Alkalinity}) \quad (3)$$

The stability of the model was validated as giving good prediction with an uncertainty of 121 (or 121 mg $l^{-1}NH_4^+ - N$).

The implementation of real-time monitoring and the development of automatic control of the process allow to verify process sustainability through a control logic based on set-point, automatically maintaining the best conditions for microorganisms and consequently maximizing the biohydrogen and biomethane yields.

5 Conclusions

In general, food waste is a good candidate feedstock for bio-EM production. In fact, pilot scale tests demonstrated optimal ranges for operational parameters for biohydrogen production (T 55 °C, OLR 16–20 kg TVS m^{-3} d^{-1}, HRT 3 days) to reach yields as high as 65 LH_2 $kg^{-1}TVS_{fed}$. Anaerobic digestion yields are even optimized giving a specific biogas production of 0.72 kg TVS m^{-3} d^{-1} with average methane content of 67 %. The bio-EM gas mixture reached the optimal and stable composition (H_2, CH_4 and CO_2 respectively 7, 58 and 35 %).

It is clear that in order to obtain biohydrogen and biogas treating food waste in a mixed culture system without pH control, sludge recirculation must be adopted to buffer the dark fermentation system and to maintain the pH at 5.5–6.

The increasing of ammonia observed while adopting sludge recirculation could be conveniently automatically controlled using strong and reliable conductivity probe and controlling the sludge amount, thus limiting inhibition effects.

Acknowledgements The authors wish to thank the European Union, 7° Framework program 2007–2013, Valorgas Project (ENERGY.2009.3.2.2, Valorization of food waste to biogas), PRIN-MIUR 2007. (Produzione di bio-hythane attraverso processo di digestione anaerobica a due stadi di biomasse primarie (energy crops) e secondarie (rifiuti)), and Industria 2015, (Ministero per lo Sviluppo Economico, "Produzione di energia rinnovabile con impatto minimo da un mix di biomasse e rifiuti speciali non pericolosi attraverso processi innovative") for the financial support of these studies.

References

1. Das LM, Gulati R, Gupta PK (2000) A comparative evaluation of the performance characteristics of a spark ignition engine using hydrogen and compressed natural gas as alternative fuels. Int J Hydrogen Energy 25:783–793
2. Eden (2010) Eden Annual Report. www.edenenergy.com.au
3. Angenent LT, Karim K, Al-Dahhan MH, Wrenn BA, Domìguez-Espinosa R (2004) Production of bioenergy and biochemicals from industrial and agricultural wastewater. Trends Biotechnol 22(9):477–485
4. Levin DB, Pitt L, Love M (2004) Biohydrogen production: prospects and limitations to practical application. Int J Hydrogen Energy 29:173–185
5. Valdez-Vazquez I, Poggi-Varaldo HM (2009) Hydrogen production by fermentative consortia. Renew Sustain Energy Rev 13:1000–1113
6. Hallenbeck P, Ghosh D, Skonieczny M, Yargeau V (2009) Microbiological and engineering aspects of biohydrogen production. Indian J Microbiol 49:48–59
7. Shin HS, Youn JH (2005) Conversion of food waste into hydrogen by thermophilic acidogenesis. Biodegradation 16:33–44
8. Gómez X, Morán A, Cuetos MJ, Sanchez ME (2006) The production of hydrogen by dark fermentation of municipal solid wastes and slaughterhouse waste: a two-phase process. J Power Sources 157:727–732
9. Lee DY, Ebie Y, Xu KQ, Li YY, Inamori Y (2010) Continuous H2 and CH4 production from high-solid food waste in the two-stage thermophilic fermentation process with the recirculation of digester sludge. Bioresour Technol 101:S42–S47
10. Cooney M, Maynard N, Canizzaro C, Benemann J (2007) Two phase anaerobic digestion for production of hydrogen-methane mixtures. Bioresour Technol 98:2641–2651
11. Hawkes FR, Dinsdale R, Hawkes DL, Hussy I (2002) Sustainablefermentative hydrogenproduction:challengesforprocessoptimization. Int J Hydrogen Energy 27:1339–1347
12. Kim SH, Shin HS (2008) Effects of base-pretreatment on continuous enriched culture for hydrogen production from food waste. Int J Hydrogen Energy 33:5266–5274
13. Kim DH, Kim SH, Shin HS (2009) Hydrogen fermentation of food waste without inoculum addition. Enzyme Microbiol Technol 45:181–187
14. Noike T, Takabatake H, Mizuno O, Ohba M (2002) Inhibition of hydrogen fermentation of organic waste by lactic acid bacteria. Int J Hydrogen Energy 27(11–12):1367–1371
15. Noike T, Yokoyama IB, Kohno Y, Li YY (2005) Continuous hydrogen production from organic waste. Water Sci Technol 52(1–2):145–151

16. Wang X, Zhao YC (2009) A bench scale study of fermentative hydrogen and methane production from food waste in integrated two-stage process. Int J Hydrogen Energy 43: 245–254
17. Chou CH, Wang CW, Huang CC, Lay JJ (2008) Pilot study on the influence of stirring and pH on anaerobes converting high-solid organic wastes to hydrogen. Int J Hydrogen Energy 33:1550–1558
18. Alzate-Gaviria LM, Sebastián PJ, Perez-Hernandez A, Eapen D (2007) Comparison o two anaerobic system for hydrogen production from organic fraction of municipal solid waste and synthetic wastewater. Int J Hydrogen Energy 32:3141–3146
19. Fan KS, Kan NK., Lay JJ (2006) Effect of hydraulic retention time on anaerobic hydrogenesis in CSTR Bioresources technology.97:84–89
20. Li SL, Kuo SC, Lin JS, Lee ZK, Wang YH, Cheng SS (2008) Process performance evaluation of intermittent-continuous stirred tank reactor for anaerobic hydrogen fermentation with kitchen waste. Int J Hydrogen Energy 33:1522–1531
21. Shin HS, Youn JH (2005) Conversion into hydrogen by thermophilic acidogenesis. Biodegradation 16:33–44
22. Zhu H, Stadnyk A, Bèland M, Seto P (2008) Co-production of hydrogen and methane from potato waste using a two-stage anaerobic digestion process. Bioresour Technol 99(11): 5078–5084
23. Kongjan P, Angelidaki I (2010) Extreme thermophilic biohydrogen production from wheat straw hydrolysate using mixed culture fermentation: effect of reactor configuration. Biores Technol 101(20):7789–7796
24. Hawkes FR, Hussy I, Kyazze G, Dinsdale R, Hawkes DL (2007) Continuousdark fermentative hydrogen production by mesophilic microflora: principles and progress. Int J Hydrogen Energy 32:172–184
25. Valdez-Vazquez I, Rios-Leal E, Esparza-Garcia F, Cecchi F, Poggi-Varaldo H (2005) Semi-continuous solid substrate anaerobic reactors for H2 production from organic waste: mesophilic versus thermophilic regime. Int J Hydrogen Energy 30:1383–1391
26. Reith JH, Wijffels RH, Barten H (2003) Bio-methane & bio-hydrogen, status and perspectives of biological methane and hydrogen production. Dutch Biological Hydrogen Foundation,
27. Lay JJ, Fan KS, Chang J, Ku CH (2003) Influence of chemical nature of organic wastes on their conversion to hydrogen by heat-shock digested sludge. Int J Hydrogen Energy 28: 1361–1367
28. Cavinato C, Bolzanella D, Fatone F, Cecchi F, Pavan P (2011) Optimization of two-phase thermophilic anaerobic digestion of biowaste for hydrogen and methane production through reject water recirculation. Bioresour Technol 102:8605–8611
29. Kataoka, N., Ayame, S., Miya, A., Ueno, Y., Oshita, N., Tsukahara, K., Sawayama, S., Yokota, N. (2005) Studies on hydrogen-methane fermentation process for treating garbage and waste paper. In: ADSW 2005 Conference proceedings, 2, process engineering
30. Chu CF, Li YY, Xu KQ, Ebie Y, Inamori Y, Kong HN (2008) A pH-temperature-phased two-stage process for hydrogen and methane production from food waste. Int J Hydrogen Energy 33:4739–4746
31. Cavinato C, Giuliano A, Bolzonella D, Pavan P, Cecchi F (2012) Bio-hythane production from food waste by dark fermentation coupled with anaerobic digestion process: a long-term pilot scale experience. Int J Hydrogen Energy 37:11549–11555
32. Chinellato G, Cavinato C, Bolzonella D, Heaven S, Banks CJ (2013) Biohydrogen production from food waste in batch and semi-continuous conditions: Evaluation of a two-phase approach with digestate recirculation for pH control. Int J Hydrogen Energy 38:4351–4360. http://dx.doi.org/10.1016/j.ijhydene.2013.01.078 (Copyright 2013, Hydrogen Energy Publications, LLC. Published by Elsevier Ltd. All rights reserved)
33. Gottardo M, Cavinato C, Bolzonella D, Pavan P (2013) Dark fermentation optimization by anaerobic digested sludge recirculation: effects on hydrogen production. Chem Eng Trans 32:997–1002

34. Micolucci F, Gottardo M, Bolzonella D, Pavan P (2014) Automatic process control for stable bio-hythane production in two-phase thermophilic anaerobic digestion of food waste. Int J Hydrogen Energy 39(31):17563–17572 ISSN 0360-3199
35. Giuliano A, Zanetti L, Micolucci F, Cavinato C (2014) Thermophilic two-phase anaerobic digestion of SS-OFMSW for bio-hythane production: effect of recirculation sludge on process stability and microbiology over a long-term pilot scale experience. Water Sci Technol 69 (11):2200–2009

Bio-production of Hydrogen and Methane Through Anaerobic Digestion Stages

Chiara Patriarca, Elena De Luca, Claudio Felici, Luigia Lona, Valentina Mazzurco Miritana and Giulia Massini

Abstract The anaerobic digestion (AD) is a widespread technology for the energetic valorization of organic wastes and the plants number is increasing both in industrialized and emerging countries. On the other hand, a low efficiency of the biogas production is still observed mainly due to the limited knowledge on the microorganism interactions and the lack of microbiological monitoring in the AD process. The energetic valorization of organic waste, producing both methane and hydrogen, can be increased by applying microbial ecology principles and exploiting the potential offered by functional microbial biodiversity.

Keywords Anaerobic digestion · Organic wastes · Microbial ecology

List of Symbols

ADP	Adenosine DiPhosphate
ATP	Adenosine TriPhosphate
AD	Anaerobic Digestion
BChl	BacterioChlorophyll
GSB	Green Sulphur Bacteria
LED	Light-Emitting Diodes
NADH	Nicotinamide Adenine Dinucleotide
VFA	Volatile Fatty Acids

C. Patriarca (✉) · E. De Luca · C. Felici · L. Lona · V.M. Miritana · G. Massini
ENEA, Italian National Agency for New Technologies, Energies and Sustainable Economic Development, Via Anguillarese, 301, 00123 Rome, Italy
e-mail: chiara.patriarca@enea.it

L. Lona · V.M. Miritana
Department of Ecology and Economic Development, Università della Tuscia, Largo dell'Università, 01100 Viterbo, Italy

M. De Falco and A. Basile (eds.), *Enriched Methane*,
Green Energy and Technology, DOI 10.1007/978-3-319-22192-2_6

1 Introduction

The consumption of energy resources, with a flow rate higher than their regeneration capacity, and the incomplete cyclization of industrial processes, has meant that within a few decades huge amounts of by-products and wastes arising from human activities have been produced: combustion gases, liquid pollutants, artefacts and solid compounds. The excess of waste materials and their irregular distribution in the geological compartments change the flow rate and the turnover by which the fundamental elements circulate, altering biogeochemical cycles and causing the phenomenon of pollution. It should also be added that the energy used by human activities is, in the end, lost to the environment as heat at a low temperature (entropy), contributing to the rapid change of the natural balances.

To counteract the current energy and environmental crisis as well as the acceleration of climate change caused by the use of fossil fuels, the scientific community is addressing the research on the diversification of the energy sources, focusing on sustainable alternative solutions, in particular bioenergy.

Within bioenergy, the production of biogas by anaerobic digestion (AD) of organic waste has emerged as one of the most promising process. It allows to produce bioenergy in form of methane, fulfilling the double goal of producing energy and valorizing organic wastes (agrozootechnical, agroindustrial and municipal organic materials) reducing its disposal costs. Moreover, the technology of the AD process is enough, simple and not very expensive.

In such a scenario it has also opened a lively debate on biohydrogen production. Hydrogen (H_2), in fact, is produced and consumed during AD process, but new reactor configuration can allow to separate it before its consumption. Then it can be added to the biogas in order to increase its energetic value or it can be used alone. H_2, in fact, is considered the fuel of the future as its combustion produces more than three times the heat developed from fossil oil, while in terms of environmental sustainability the combustion process leads to the formation of only water vapour [13]. Therefore increasing the efficiency of H_2 production within the dark fermentation stage may enhance methane production and the overall AD process. Recent research has been addressed towards a double-stage AD process consisting of a first fermentation stage for the H_2 production and a second stage, feed with the effluent of the first one for the methane production. The use of a two-stage system should enhance the efficiency of the process, due to the fact that in the first reactor the fermentation allows the rapid production of organic acids and alcohols, which when released into the second stage would increase the production of methane.

2 Anaerobic Digestion Process

The AD process consists of a sequence of biochemical reactions carried out by various microorganisms that, in the absence of oxygen, transform organic substrates into simpler molecules, mainly acetic acid, H_2, methane (CH_4) and carbon dioxide

(CO_2). The content of CH_4 in the biogas varies depending on the characteristics of the organic matter, as well as by the process conditions and the reactor configuration. Although the methanogenic bacteria perform only the last step of the whole process, AD works as *an unicum* because the different groups of microorganism have evolved very close relationships of cooperation and the members of the food chain always depend on the earlier ones for their substrates.

Within AD, primary fermentation with H_2 production is due to an incomplete digestion process stopped before the methanogenic phase. The methanogenesis, in fact, consumes the amount of H_2 produced in the previous stages [45].

The techniques of AD can be divided into two main groups:

- Dry digestion when the substrate has a dry matter content higher than 20 %;
- Wet digestion when the substrate has a dry matter content lesser than 10 %, this is the most common technique, especially with the slurry.

The production of H_2 by dark fermentation is a natural biological process characteristic of the first two phases of AD (hydrolysis-acidogenesis) where bacteria hydrolyze the macromolecules involved and partially oxidize the organic substrates with the production of H_2 and CO_2. The next two stages of AD (acetogenesis–methanogenesis) lead to the production of biogas, a mixture of 50–70 % CH_4 and 50–30 % for CO_2.

2.1 Hydrolysis

The hydrolysis is the first phase of AD, during which complex organic molecules like polysaccharides, proteins, nucleic acids and lipids are split in their respective constituent oligomers and monomers. This phase is one of the most important processes: it may constitute a “bottleneck” for the entire process mainly when lignocellulosic substrates are used. In fact, not all the fermenting bacteria have high hydrolytic capacity and, on the other hand, the amount of substrate hydrolyzed contributes to determining the efficiency of the process.

2.2 Acidogenesis

It is considered the second phase of AD, during which the monomers that constitute the macromolecules are reduced into low molecular weight acids, the volatile fatty acids (VFA). Hydrolysis and acidogenesis perform the primary fermentation.

2.3 The Fermentation

In the absence of electron acceptors supplied from the environment, many organisms perform oxidation-reduction reactions of organic compounds internally balanced, with release of energy: this process is called fermentation.

The fermentation is an anaerobic metabolic process in which the donor and acceptor of electrons (e^-) are organic molecules. In the course of the fermentation, an organic compound acts as a donor and oxidizes, while generating nicotinamide adenine dinucleotide (NADH) (i.e. NAD^+ oxidaze form). The NADH cannot unload its electrons in the transport chain; therefore to regenerate the pool of NAD^+ necessary for the continuation of the process, the reoxidation of NADH occurs at the expense of an intermediate compounds of the process, which acts as acceptor and the fermentation process is therefore a redox balanced in its interior.

When an organism degrade,s organic compounds have to face two main energetic metabolic issues:

- Eliminate the electrons removed from the electron donor;
- Store into adenosine triphosphate (ATP) part of the energy released during the process.

During the fermentation there is not the complete demolition of the starting compound, which is only partially fermented in one or more end products still mostly organic and which still retain part of the energy of the initial compound. Therefore, the energy yield of the fermentation is not comparable to that of respiratory processes and ATP, a phosphate compound of high energy, is generated only for the transfer of a phosphate group bonded to an intermediate of the process with a bond to adenosine diphosphate (ADP) (substrate-level phosphorylation).

During the fermentation the redox balance is maintained producing molecular H_2. Generally the production of H_2 is associated with the presence in the organism of a protein called iron-sulphur ferredoxin, an electron carrier at low redox potential. The transfer of electrons from ferredoxin to H^+ is catalyzed by the enzyme H_2ase. The diversity of fermentation and the metabolic pathways used by the bacteria lead to the formation of an alternative set of metabolic products and since H_2 has the task of maintaining the redox balance, if the final products are more reduced, they result in a lower production of H_2. For example, when the ethanol, more reduced than acetate, is produced then H_2 production will be less. Several bacteria produce acetate among the fermentation products. The production of acetate is energetically advantageous, because it allows the organism to produce additional ATP, always by substrate-level phosphorylation. The intermediate generated during the production of acetate is the acetyl-CoA, an intermediate high energy, which can be converted into acetylphosphate, where the phosphate group is transferred to ADP with the formation of ATP and acetate.

2.4 Acetogenesis

The third stage of the AD is represented by acetogenesis. In this phase, the volatile fatty acids previously produced are converted into acetic acid, CO_2 and H_2. Acetogenesis is an interesting step, as it is performed by microorganisms that have evolved a syntrophic relationship with methanogenic bacteria so that that neither partner can operate without the other.

2.5 Methanogenesis

The production of CH_4 is the conclusion of the AD process. Its production can take place essentially through two different pathways of reactions: a path provides CH_4 by hydrogenotrophic bacteria that operate under the anaerobic oxidation of H_2, while the second pathway, the so-called acetoclastic, provides the dismutation of anaerobic acetic acid with formation of methane and carbon monoxide. In mesophylic condition, most of the CH_4 production occurs through this second pathway. The quantity and composition of the biogas (at least in terms of CH_4 and CO_2) are of fundamental importance for the stability control of the AD process. If the reactor is operating under stable conditions, the production and composition of the biogas are constants. A decrease in the overall production of biogas and an increase in CO_2 percentage may indicate phenomenal inhibition of the process. It follows that the production analysis and percentage composition of the biogas should always be associated with the control of parameters such as the concentration of volatile fatty acids.

3 Dark Fermentation and Its Limiting Factors

The production of H_2 by dark fermentation is one of the oldest life processes; it is produced by many different microorganisms that are able to derive energy from organic substrates (heterotrophic). This means that heterotrophic organisms can also produce H_2 from renewable sources, such as waste biomass from agricultural industry, the organic fraction of municipal waste, the wastewater from industrial and agricultural activities, offering the possibility of obtaining energy in an economically and ecologically even more sustainable way. In addition to reducing the cost of waste disposal, turning them into a resource, agricultural and food production processes or industrial processes are directed to closed circuits, which maximize the recycling of materials. It is a process that can take place at room temperature and pressure, without external energy input addition, so it is a process at positive energy balance.

Depending on the bacterial species, the organic substrates are employed and therefore the conditions of fermentation, the process leads to the formation of an

abundance of small organic molecules, VFA (butyrate, acetate, lactate, malate) and alcohols (ethanol, propanediol, butanediol) [44]. The theoretical yield (moles of H_2 produced per mole of substrate consumed) varies in function of the metabolic pathway, namely the organic acid/alcohol predominantly accumulated in the course of the fermentation, and is in turn the expression of the adaptations of the organisms themselves to "ecological factors" of the fermentation [20, 36].

The accumulation of these metabolites, on the one hand, constitutes a limiting factor for the production of H_2 but, on the other hand, they may confer an added value to the whole process as they have still a lot of energy in the form of chemical bonds. Depending on their nature, these molecules can be used as a substrate for further production of energy. Addressing this second step towards the H_2 production, the alternative possible solutions are:

(a) photo-bioreactors in which purple non-sulphur bacteria produce H_2 in ambient light near infrared;
(b) adoption of recent organic hydrolysis technology in which an electrolytic cell, with constructive features advanced (with bacteria adherent to the anode and cathode), stimulated with a potential difference of about 0.4 V, develops H_2.

A more feasible alternative is given by the transfer of metabolites in reactors for the production of bio-methane, which is indicated by the EU as renewable energy sources and environmentally friendly energy that contributes to autonomy. This technology, which is consolidated and is now known on a large scale, was initially used with the objective of reducing the environmental impacts on air and soil originating from animal manure [58].

The maximum theoretical yield per mole of hexose by a complete conversion of glucose is 12 mol of H_2 [14]:

$$C_6H_{12}O_6 + 6H_2O \rightarrow 6CO_2 + 12H_2 \quad (1)$$

This would not, however, produce energy necessary for the growth of bacteria [19]. The yield of the process of production from glucose (moles of H_2/moles substrate) varies depending of the final products that are formed, in fact, as previously mentioned, the H_2 is produced exclusively to balance the redox reaction, when the substrate is more or less reduced the formation of H_2 is less or more, respectively.

In the fermentation process acetic and butyric acid together with the production of acetone ensures the greatest accumulation of NADH corresponding to the increased productivity of the H_2.

$$C_6H_{12}O_6 + 2H_2O + 2CO_2 + 4H_2 \rightarrow 2CH_3COOH \text{ acetic} \quad (2)$$

$$CH_3COCH_3 + H_2O \rightarrow C_6H_{12}O_6 + 3CO_2 + 4H_2 \text{ acetone} \quad (3)$$

$$CH_3CH_2CH_2COOH \rightarrow C_6H_{12}O_6 + 2CO_2 + 2H_2 \text{ butyric} \quad (4)$$

H_2 is also produced by the decomposition of formic acid, a by-product of acetic acid and alcoholic fermentation. Therefore the acetic acid fermentation appears to be the most promising for the synthesis of H_2 and ensures a potential productivity of 4 mol of H_2 per mole of glucose, while the butyric reaches a maximum of 2 mol.

$$HCOOH \rightarrow H_2 + CO_2 \text{ decomposition of formic} \quad (5)$$

3.1 Main Process Parameters and Inhibition Factors

In a mixed natural bacterial community the microorganisms have different enzyme complexes and may follow more than one metabolic pathway. Different parameters discriminate which becomes prevalent:

- pH
- Temperature
- H_2 partial pressure
- HRT (hydraulic retention time)
- VFA (volatile organic acids)
- resource mapping (quantity and type of fermentation substrate)
- concentration of metal ions.

3.2 pH

The fermentation medium acidity influences not only the biomass vitality conditions but also the type of products. The variation of the pH results in a variation of the electrostatic conditions (H^+ ions) which leads to a change in the conformation of the enzyme and the enzymatic activity responsible for the metabolic processes by reducing the catalytic action. It can lead to the transformation of nutrient substrates turning them into toxic substances.

Between pH 6–5.5 the proliferation of methanogenic bacteria (responsible for the consumption of H_2) is prevented, but below pH 5 the productivity of H_2 is reduced causing a metabolic shift in favour of lactic acid. Furthermore, pH less than 4.6 converts the butyric fermentation in ethanolic reducing production yields [36].

Some studies have shown that a low initial pH (4–4.5) can cause a longer stationary phase compared to an initial high pH value [5]. However, the H_2 yield is lower with a high initial pH: in fact it causes a rapid production of H_2 and VFA that inhibit the buffering capacity and the bacteria cannot adapt to sudden environmental change [28].

3.3 Temperature

Temperature affects all physiological activities of microorganisms and the conversion rates of the fermentation products. The H_2 producing bacteria are very sensitive to temperature changing and the production rate undergoes various fluctuations before stabilizing at a given temperature [36].

All fermentation reactions can take place at mesophilic temperatures (25–40 °C), thermophilic (40–65 °C) or hyperthermophilic (>80 °C). In many studies the H_2 production is supported by mesophilic conditions and also in some thermophilic.

The effect of temperature on H_2 production can be explained thermodynamically by Van't Hoff equation

$$\ln K1/K2 = -\Delta H^{\circ}/R(1/T1 - T2) \tag{6}$$

Considering the Gibbs free energy and enthalpy of the glucose conversion to acetate

$$\begin{aligned} &C_6H_{12}O_6 + 2H_2O \rightarrow 2CH_3COOH + 4H_2 + 2CO_2 \\ &\Delta G^{\circ} = -176.1 \text{ kJ/mol} \\ &\Delta H^{\circ} = +90.69 \text{ kJ/mol} \end{aligned} \tag{7}$$

With increasing temperature the equilibrium constant kinetic increases, because the reaction is endothermic and thereby increases the concentration of H_2.

In other studies it has been reported that the volumetric rate of H_2 production in thermophilic conditions was 60 % more compared to mesophilic conditions. Already at 37 °C, for example, it not only inhibits the activity of H_2 consumers, but also suppresses the growth of lactic acid bacteria [50].

However, high temperatures can cause thermic denaturation of proteins by damaging microbial activity and also with respect to the ambient temperature is higher than the energy cost.

3.4 Hydrogen Partial Pressure

Theoretical studies show that an increase of the H_2 partial pressure inhibits the same yield of H_2 production [20]. The H_2 partial pressure significantly influences its own production, especially when considering the continuous production, because when its concentration increases, the synthesis decreases. This is due to a mechanism of negative feedback inhibition, which produces other alternative metabolic pathways, leading to the synthesis of smaller substrates, such as lactate, ethanol, butanol or alanine. An increase of about 50 % of the production of H_2 was obtained in fact by removing the product from the headspace of the bioreactor through "sparge" nitrogen [32].

The H_2 partial pressure has influence in the conversion rate of ethanol. It is well-known that ethanol can be accumulated only if the H_2 partial pressure is greater than 104 Pa. However, when the H_2 partial pressure is less than 104 Pa ethanol is converted into acetic acid.

The hydraulic retention time (HRT) retention time of the H_2 phase is relatively short (24–72 h) with respect to that of the classic methanogenic reactors (15–40 d). This allows a significant reduction of the fermenter size among the methane one.

Some studies have shown that the degree of acidification during the fermentation process increases together with the HRT going from 28.2 to 59.1 % from 4 to 24 h. Moreover, the prolongation of HRT favours the biodegradability of some compounds; following the order of degradation carbohydrates > proteins > lipids [18].

The HRT also has significant effects on the metabolites distribution produced during the fermentation process as reported by Elefsiniotis and Oldham [17] and Henry et al. [21]. Indeed shorter retention times favour the production of propionate, but in general the total production of VFA/alcohol doubling from a hydraulic retention time of 4–12 h.

3.5 Volatile Fatty Acids

Volatile Fatty Acids are closely related to the pH of the system, able to select the fermentation process and also the production of H_2 connected to the production of acids (particularly acetate and butyrate) by precise stoichiometric ratios. The same H_2 formation matches with the formation of organic acids, the accumulation of which not only influences the rate of H_2 production but may also change the fermentation pathways [41].

The anaerobic fermentation leads to the production of VFA and also to the formation of alcohols and reduced end products (involving the oxidation of NADH), such as ethanol, butanol and lactate containing H_2 atoms withheld and not contributing to the H_2 yield.

3.6 Resource Mapping

The type of substrate promotes the interspecific competition between the H_2-producing microorganisms, while the amount of substrate mainly determines intraspecific competition and helps to modify the enzymatic activity of bacteria causing a metabolic shift towards the production of lactic acid with a decrease of production yields.

The number of dominant populations at steady state depends on the number of types of substrates, however, this does not mean that the anaerobic fermentation of a particular substrate belong to just one type of fermentation. The metabolic

pathways may shift during fermentation with the self-metabolic activity of microorganisms that are adapted to the changes "ecosystem" [36].

3.7 Concentration of Metal Ions

Metal ions (Na, Mg, Zn, Fe) are essential micronutrients for bacterial metabolism, as they are required in the transport processes and enzymatic metabolism. For example, the Fe is involved in pyruvate oxidation to acetyl-CoA and in the proper action of the enzyme hydrogenase. Suboptimal concentrations of Fe ion can lead to shifts in metabolic pathways. When the concentration of Fe ions is very low in the fermentation medium of the enzymatic activity favours the production of lactic acid to ethanol by reducing the production of H_2. Recent studies in the literature have shown that iron and nickel are elements essential for the production of gas by anaerobic microorganisms, since they are indispensable constituents of hydrogenase enzyme, which catalyzes the oxidation reaction of H_2 and reduction of protons during the fermentation process of degradation [6]. The results of different studies [34, 37, 64, 65, 68] have confirmed that the optimal dosage of nickel and iron to interior of the anaerobic system, as well as that inhibiting the production of H_2, are closely dependent on the substrate, after inoculation and the operating conditions used in the digestion process.

4 Microbial Ecology and Syntrophic Cooperation Between Microorganism

Methanogenesis is a widespread process occurring mainly where primordial environment of Earth is retained. All the conditions are characterized by rich organic matter content and limited supply, not only of oxygen, but also of nitrate, sulphate, or oxidized iron or manganese species [38]. So when the electron acceptors with a decreasing energy yield are depleted [48], the degradation process becomes predominant. It is the least exergonic process in the degradation of organic matter and it is realized by complex networks of microorganisms that, operating subsequent reactions of oxidation and reduction, convert complex matter to its most oxidized state CO_2, and its most reduced states CH_4 [47].

Compared with aerobic degradation or the alternative anaerobic respirations, methanogenic degradation is very poor in energy release; Shink stated that it gets back only 15 % of the energy that would be available in aerobic degradation, methane still having a high content of chemical energy.

From a metabolic point of view all methanogenic *Archaea* can be considered physiologically specialized as they produce methane using only a limited range of substrates, however simple, such as H_2/CO_2, formate and some methyl acetate compounds [38] relying on other organisms, belonging to the *Eubacteria* domain,

for the supply of this simple substrates. So the sequences of reactions that make possible the conversion of biomasses highly refractory to degradation like cellulose into CH_4 and CO_2, is operated by the concerted action of major metabolic groups of bacteria that break down complex organic compounds in simple substrates available to methanogen [26]: the trophic chain comprises primary fermenting bacteria (hydrolitic and acidogen), secondary fermenting bacteria (proton-reducing acetogenic bacteria), and only at least, alternatively, two functional types of methanogens (hydrogenotrophic and acetoclastic) [2, 16, 38]. Moreover another functional group co-occurred to build up the complexity of the trophic web, the homoagetogenic bacteria [42]; they connect, in reversible way, the pool of one-carbon compounds and H_2 to that of acetate. So, it can be said that the energetic constrains together with the metabolic limits of the *Archaea* have pushed different kinds of microorganisms in a very efficient cooperation evolving the very complex process of the AD.

From an ecological point of view the main groups of bacteria are associated to functional guilds [62], i.e. strains of microorganisms generally taxonomical related that perform similar functions, often in a similar way. Inside each guild, single microbial strain can be replaced by another, as a consequence of ecological constrains, but every functional role must be present in order to complete the whole AD process. This means that it is not possible to achieve a complete AD process with a single bacterial strain or, conversely, even if a single kind of substrate is provided or is available, the AD process is still carried on by many microorganism strains that interact together. The cooperation relationships evolved in methanogen community are of different kind of strength and some of them evolved even in mutualistic way, and therefore obliged relationships. The most extreme case is a special symbiotic cooperation termed *syntrophism*: it refers to a kind of relationship evolved between metabolically different types of bacteria which depend on each other for substrate degradation for energetic reasons. Shink [47] underlines that the mutual dependence comprises the fact that neither partner can operate without the other and that together they exhibit a metabolic activity that neither one could accomplish on its own. This means that in natural environment the mutual dependence cannot be overcome by simply adding a co-substrate or any type of nutrient.

Relatively to AD the relationship was already identified in 1979 by McInerney et al. [39] describing the mutual cooperation of fatty acid-oxidizing fermenting bacteria or secondary fermenting bacteria, with H_2-oxidizing methanogens. During microbiological researches related to AD, it happens that some isolated culture, initially considered pure, shown to be cocultures of two partner organisms: *Archaea* populations thrive using H_2 that is produced by other microorganism, the syntrophic ones, which in turn need someone else that is an H_2 scavenging, i.e. the *Archaea*. *Archaea* and *Eubacteria* have coevolved their ecological niche in order to share an interspecific transfer of H_2 [9], mainly to overcome thermodynamic thresholds, as we shall see below [2, 25]. More particulary, syntrophic bacteria, most belonging to *Syntrophobacter* genus from *Proteobacteria*, oxidize intermediate product during AD, like propionate or butyrate and thereby obligatorily use H_2 as electron acceptor. In order to be energetically favourable, these reactions may

occur only when low pressure of H_2 is maintained, which means below 10–4 atm [16, 47].

The main thermodynamic aspects of syntrophic relationship are very well reported from [26] on their study on the bacterium strain, the syntrophic specialist *Pelotomaculum thermopropionicum.*

They report the example of syntrophic propionate-oxidizing bacteria that oxidize propionate into acetate, and synthesize ATP through substrate-level phosphorylation. In this reaction the reducing equivalents generated through the oxidation process are consumed by H_2 (or formate) production. The interesting thing is that the Gibbs's free energy change of this reaction is positive, and the reaction is unfavorable for bacteria under standard conditions.

$$\begin{gathered} CH_3CH_2COO- + 3H_2O \rightarrow CH_3COO + HCO_3 + H + 3H_2 \\ \Delta G^{\circ\prime} = +76.1 \text{ kJ(per mol of propionate)} \end{gathered} \tag{8}$$

But the reaction becomes energetically favourable, if the H_2 partial pressure is below 10–4 atm. In methanogenic environments, hydrogenotrophic methanogens play the role of H_2 subtractors, conserving energy by producing methane from H_2/CO_2.

$$\begin{gathered} 3H_2 + 3/4HCO_3- + 3/4H+ \rightarrow 3/4CH_4 + 9/4H_2O \\ \Delta G^{\circ\prime} = -101.7 \text{ kJ (per 3 mol of } H_2) \end{gathered} \tag{9}$$

When the two reactions (Eqs. 8 and 9) concomitantly occur as if it were an *unicum*, the syntrophic degradation of propionate becomes energetically feasible (10)

$$\begin{gathered} CH_3CH_2COO- + 3/4H_2O \rightarrow 3/4CH_4 + CH_3COO + 1/4HCO_3 + 1/4H \\ \Delta G^{\circ\prime} = -25.6 \text{ kJ (per mol of propionate)} \end{gathered} \tag{10}$$

It is important to note that in this case the Gibbs free energy change of the overall reaction is very low, less than the energy required for the synthesis of ATP (40–70 kJ/mol of ATP). This means that syntrophic bacteria and hydrogenotrophic methanogens thrive by sharing very little energy and were forced to coevolve into an extremely efficient and complex catabolic systems enabling them to survive under such thermodynamically extreme conditions [25].

In this contest, a really interesting scientific challenge is to understand the evolutionary steps that led to the syntrophic relationships.

It is well-known that methanogen *Archaea* are among the oldest organisms on earth: because they evolved in primordial environments, at the present they are considered extremophiles, mainly in terms of temperature, pressure, composition of the atmosphere and pH value. *Archaea* produce methane using only a limited range of substrates, such as H_2/CO_2, formate and some methyl acetate compounds.

Probably, in ancient times, *Archaea* obtained the H_2 through a "geochemical route", nearby submarine hydrothermal vents, where H_2 is produced by the serpentinization process [27, 52].

Moreover, Amend et al. [3] states that submarine hydrothermal vents are highly reactive chemical environments with far-from-equilibrium conditions are rich in gradients of redox, pH and temperature and harbouring the potential for exergonic chemical reactions.

Along the time methanogen *Archaea* coevolved with other organisms belonging to a different evolutionary domain, the *Eubacteria,* in the way to use the H_2 they produce. Shifting from substrates of geochemical origin to those generated by biochemical pathway, methanogenesis became independent from the hydrothermal sites and the whole process of AD has evolved as we know it today, i.e. operated by a complex array of microorganisms in which the metabolic activities of some anticipate those of others.

It is the results of a long coevolutionary history that have metabolically linked different bacterial domains, *Eubacteria* and *Archaea*, to overcome the severity of the environmental and energetic conditions and, at the same time, have driven methanogen at the end of the AD process.

5 Biological Clean-up of Hydrogen Sulphide by Green Sulphur Bacteria Based Photobioreactor

The biogas produced from AD of manure and agroindustrial wastes can contain high amounts of hydrogen sulphide (H_2S) [46]. H_2S is also the principal odorous component in wastewater collection, treatment facilities and in the landfill biogas plants [12]. The H_2S amount depends on proteins and other sulphur-containing compounds that are reduced by sulphur reducer microorganisms during the decomposition of organic matters.

Even if the biogas production could contribute to the greenhouse gas reduction [1], the biogas cannot be used directly as a fuel because H_2S is very corrosive and it can cause damage to engines and gas pipelines. Furthermore, it brings to a less efficiency of energy production and sulphur dioxide (SO_2) in the exhaust gases after combustion.

Moreover, H_2S is highly toxic. Continuous exposure at low concentrations (15–50 ppm) generally causes irritation to mucous membranes whereas at high concentrations may result in respiratory arrest. Prolonged exposures (30 min) at concentrations greater than 600 ppm can cause death [40].

Physical and chemical H_2S removal processes from biogas streams are available on an industrial scale: scrubbing, carbon adsorption, chemical and thermal oxidation [7, 49]. The Claus process is used for H_2S removal with sulphur recovery [10]. These processes are expensive due to high chemical requirements, energy and disposal costs.

A biological H_2S removal method could be an eco-friendly and sustainable alternative. Chemotrophs bacteria are used in plants for biogas upgrading but they need oxygen supply and require careful control of growth condition to produce elemental sulphur instead of sulphate [56]. Among these, *Beggiatoa alba* forms characteristic encrustations on the apical part of digesters, but the clean-up process is not effective and the biogas produced needs further treatments.

Phototrophic bacteria from *Chlorobiaceae* family, indicated as green sulphur bacteria (GSB), oxidize H_2S to elemental sulphur during the photosynthetic process. Among this group, *Cholorobium limicola* has demonstrated to be the most suitable for sulphide removal and satisfies the criteria for desirable applications [11, 29–31, 54–56]. It has high tolerance to H_2S of which the inhibitory effect on growth starts at light saturation (100–300 μE m^{-2} s^{-1}) [60].

C. limicola lives in mud and stagnant water containing H_2S where the light irradiation is very low; it is characterized by non-motile rod-shaped cells (0.7–1.1 μm) that occur singly or in aggregates and spinae have been evidenced on the cell wall.

Special structures called chlorosomes contain the light-harvesting pigments and are connected to the photosynthetic reaction centre, located in the cytoplasmic membrane, by the baseplate protein complex containing small amounts of bacteriochlorophyll (BChl) *a*. The light-harvesting pigments are: BChl *c*, *d* and *e* and the carotenoid chlorobactene. The light absorption spectrum of *C. limicola* is between 350 and 850 nm; the main peak is due to BChl *c* (745–755 nm) that represents the principal harvesting pigment [24, 53].

C. limicola is strictly anaerobic in presence of light and grows with CO_2 as sole carbon source which is fixed exclusively through the reductive tricarboxylic acid cycle that is less energy demanding than Calvin cycle used by the other phototrophs [51]. Sulphide (S^{2-}) is used as electron donor in the first step of oxidation that produces elemental sulphur (S^0) globules deposited outside the cells. The S^0 is further oxidized to sulphate (SO_4^{2-}) in lack of sulphide and excess of light [33, 61]. The relationship between S^{2-} loading rate, light irradiance (W m^{-2}), S^0 or SO_4^{2-} formation is well described by the "van Niel curve" [11].

The complete oxidation of suphide is showed in (11):

$$n\mathrm{H_2S} + 2n\mathrm{CO_2} + 2n\mathrm{H_2O} + \mathrm{h}v \rightarrow n\mathrm{SO_4^{2-}} + 2n\mathrm{H^+} + 2n(\mathrm{CH_2O}) \qquad (11)$$

Some authors have found that S^{2-} pulsing is a key factor in the control of the spination process that seems to be a structural adaption of the cells to special environments with highly variable S^{2-} concentration. In fact, the number of spinae comes up with S^{2-} underloading. These observations indicate that the presence of spinae favours the retention of the external sulphur globules physically attached to the cell wall. Therefore, sulphur globules retained near the cells could easily be oxidized to SO_4^{2} [43].

Commonly the further elemental sulphur oxidation to SO_4^{2-} is considered not suitable for industrial applications, as the S^0 is easier to separate and recycle. Moreover, the SO_4^{2-} release in the environment could constitute a threat. Therefore,

it is very important to set both a proper light intensity and a sulphide-loading rate to have an efficient H_2S removal process avoiding the formation of SO_4^{2-} (12):

$$2nH_2S + nCO_2 + h\nu \rightarrow 2nS^0 + n(CH_2O) + nH_2O \quad (12)$$

So far photosynthetic bacteria have not yet reached the applicability to industrial gas cleaning-up processes; the main reason they have not been yet commercially used has to be related to the illumination costs. Most of the studies investigated bacteria growth by using common incandescent light bulbs [4] or infrared lamps [22]. Since light-emitting diodes (LED) technology came out, new possibilities to use photosynthetic bacteria with low energy demand became available. The employment of a photobioreactor equipped with LED with a wavelength peak near to the BChl *c* absorption range reported a high sulphide conversion compared to infrared or incandescent bulb light sources [29, 30, 54, 55]. However, a higher efficiency of infrared bulbs is still hypothesized [55]. These studies are carried out using liquid effluents or synthetic gas mixtures and are limited to short experimental time.

In order to consider the feasibility of a photobioreactor based on *C. limicola* culture further trials were performed with different goals:

- to analyze different light parameters (wavelength and intensity) that best fit the process;
- to test a photobioreactor directly fed with biogas produced by an AD pilot plant [15];
- to design an optimized photobioreactor focusing on best geometry allowing the light penetration through the system reaching the total removal of H_2S (patent deposit number RM2015A000082).

Future perspectives will be to scaled up to a photobioreactor operating on a large temporal scale testing the stability of bacterial inoculum.

Moreover, a simultaneous clean-up and H_2 (H_2) photoproduction process is under study by syntrophic coculture of GSB with sulphur-reducing bacteria like *Desulfuromonas acetoxidans* [66]. In these syntrophic cocultures H_2 is produced as acetate is produced by a light-driven sulphur cycle where acetate is used as electron donor by the sulphur-reducing bacteria which convert sulphur to sulphide while the GSB reoxidised sulphide to sulphur. In presence of a high reducing power the photoproduction of H_2 by nitrogenase comes up.

6 Conclusions

AD technologies are well-developed and the plant number is increasing in both industrialized and emerging countries but suboptimal biogas productions are often observed both in terms of quantity and quality. This is in part due to the fact that dynamics and interactions between microorganisms, the engine of the AD process, are not well-known.

The study of the microbial process in natural ecosystems, as well as the investigations on the potential offered by functional microbial biodiversity, can play a pivotal role for the resolution of technological issues related to the energetic valorisation of organic waste. The efficiency of biogas production can be increased if microbial ecological principles are applied, mainly to fulfil microbial requirements.

References

1. Abraham ER, Ramachandran S, Ramalingam V (2007) Biogas: can it be an important source of energy? Environ Sci Pollut Res 14(1):67–71
2. Ali Shah F, Mahmood Q, Maroof Shah M, Pervez A, Ahmad Asad S (2014) Microbial ecology of anaerobic digesters: the key players of anaerobiosis. Sci World J 2014:1–21
3. Amend JP, LaRowe DE, McCollom TM, Shock EL (2013) The energetics of organic synthesis inside and outside the cell. Philos Trans R Soc B: Biol Sci 368:1622
4. Ball AS, Nedwell DB, Perkins RG (2007) Oxidation of hydrogen sulphide in sour gas by *Chlorobium limicola*. Enzyme MicrobTechnol 41:702–705
5. Cai ML, Liu JX, Wei YS (2004) Enhanced biohydrogen production from sewage sludge with alkaline pretreatment. Environ Sci Biotechnol 38:3195–3202
6. Casalot L, Rousset M (2001) Maturation of the [NiFe] hydrogenases. Trends Microbiol 9:228–237
7. Cha JM, Cha WS, Lee JH (1999) Removal of organosulphur odour compounds by Thiobacillus novellas SRM, sulphur-oxidizing microorganisms. Process Biochem 34(6–7):659–665
8. Chung YC, Huang C, Tseng CP (2001) Biological elimination of H_2S and NH_3 from waste gases by biofilter packed with immobilized heterotrophic bacteria. Chemosphere 43:1043–1050
9. Conrad R (1999) Contribution of hydrogen to methane production and control of hydrogen concentrations in methanogenic soils and sediments. FEMS Microbiol Ecol 28(3):193–202
10. Cooper DC, Alley EC (1986) Air pollution control: a design approach (Chapter 14, 411–450). PWS Engineering, Boston
11. Cork D, Mather J, Maka A, Srnak A (1985) Control of oxidative sulphur metabolism of *Chlorobium limicola* forma *thiosulfatophilum*. Appl Environ Microbiol 49:269–272
12. Cox HHJ, Deshusses AM (2001) Co-treatment of H_2S and toluene in a biotrickling filter. Chem Eng J 3901:1–10
13. Das D, Veziroglu TN (2001) H_2 production by biological processes: a survey of literature. Int J Hydrogen Energy 26:13–28
14. Davila-Vazquez G, Arriaga S, Alatriste-Mondragòn F, Leon-Rodriguez A, Rosales-Colunga LM, Razo-Flores E (2008) Fermentative biohydrogen production: trends and perspectives. Environ Sci Biotechnol 7:27–45
15. De Luca E, Felici C, Corsaro N, Rosa S, Signorini A, Izzo G (2014) Hydrogen sulphide removal from gas stream by green sulphur bacteria under LED illumination. In: proceedings of the 22nd European biomass conference and exhibition, 23–26 June 2014, Hamburg, Germany
16. Demirel R, Scherer P (2008) The roles of acetotrophic and hydrogenotrophic methanogens during anaerobic conversion of biomass to methane: a review. Environ Sci Biotechnol 7:173–190
17. Elefsiniotis P, Oldham WK (1994) Effect of HRT on acidogenic digestion of primary sludge. J Environ Eng 120:645–660

18. Fang HHP, Yu HQ (2000) Effect of HRT on mesophilic acidogenesis of dairy wastewater. J Environ Eng 126:1145–1148
19. Hallenbeck PC (2005) Fundamentals of the fermentative production of hydrogen. Water Sci Technol 52:21–29
20. Hallenbeck (2009) Fermentative hydrogen production: principles, progress, and prognosis. Int J Hydrogen Energy 34:7379–7389
21. Henry MP, Sajjad A, Ghosh S (1987) The effects of environmental factors on acid-phase digestion of sewage sludge. In: Proceedings 42nd Purdue industrial waste conference, Indiana, pp 727–737
22. Henshaw PF, Bewtra JK, Biswas N (1998) Hydrogen sulphide conversion to elemental sulphur in a suspended-growth continuous stirred tank reactor using *Chlorobium limicola*. Water Res 32(6):1769–1778
23. http://rstb.royalsocietypublishing.org/content/368/1622/20120255.full.pdf+html
24. Imhoff JF (1995) Taxonomy and physiology of phototrophic purple bacteria and green sulphur bacteria. Anoxygenic photosynthetic bacteria. Kluwer Academic Publishers, The Netherlands. Chap. 1, pp 1–15
25. Jackson BE, McInerney MJ (2002) Anaerobic microbial metabolism can proceed close to thermodynamic limits. Nature 415:454–456
26. Kato S, Watanabe K (2010) Ecological and evolutionary interactions in syntrophic methanogenic consortia. Microbes Environ 25(3):145–151
27. Kelley DS, Baross JA, Delaney JR (2002) Volcanoes, fluids, and life at mid-ocean ridge spreading centers. Annu Rev Earth Planet Sci 30:385–491
28. Khanal SK, Chen WH, Li L, Sung S (2004) Biological hydrogen production: effects of pH and intermediate products. Int J Hydrogen Energy 29:1123–1131
29. Kim BW, Kim EH, Chang HN (1991) Application of light emitting diodes as a light source to a photosynthetic culture of *Chlorobium thiosulfatophilum*. Biotechnol Tech 5(5):343–348
30. Kim JY, Kim BW, Chang HN (1996) Desulfurization in a plate type gas-lift photobioreactor using light emitting diodes. Korean J Chem Eng 13(6):606–611
31. Kim BW, Chang KP, Chang HN (1997) Effect of light on the microbiological desulfurisation in a photobioreactor. Bioprocess Bioeng 17:343–348
32. Kraemer J, Bagley D (2006) Supersaturation of dissolved H_2 and CO_2 during fermentative hydrogen production with N_2 sparging. Biotechnol Lett 28:1485–1491
33. Larsen H (1952) On the culture and general physiology of the green sulphur bacteria. J Bacteriol 64:187–196
34. Lee YJ, Miyahara T, Noike T (2001) Effect of iron concentration on hydrogen fermentation. Bioresour Technol 80:227–231
35. Li D, Chen H (2007) Biological hydrogen production from steam-exploded straw by simultaneous saccharification and fermentation. Int J Hydrogen Energy 32:1742–1748
36. Li YF, Ren NQ, Chen Y, Zheng GX (2007) Ecological mechanism of fermentative H_2 production by bacteria. Int J Hydrogen Energy 32:755–760
37. Liu G, Shen J (2004) Effects of culture and medium conditions on hydrogen. J Biosci Bioeng 98(4):251–256
38. Liu Y, Whitman WB (2008) Metabolic, phylogenetic, and ecological diversity of the methanogenic archaea. Ann New York Accad Sci 1125:171–189
39. McInerney MJ, Bryant MP, Pfennig N (1979) Anaerobic bacterium that degrades fatty acids in syntrophic association with methanogens. Arch Microbiol 122:129–135
40. MSDS (1996) Material safety data sheet for hydrogen sulphide. Murray Hill, NJ: BOC Gases. http://www.vngas.com/pdf/g94.pdf. Accessed 20 Feb 2006
41. Nath K, Das D (2004) Improvement of fermentative hydrogen production: various approaches. Appl Microbiol Biotechnol 65:520–529
42. Noory M, Saady Cata (2013) Homoacetogenesis during hydrogen production by mixed cultures dark fermentation: unresolved challenge. Int J Hydrogen Energy 38:13172–13191

43. Pibernat IV, Abella CA (1996) Sulfide pulsing as the controlling factor of spinae production in *Chlorobium limicola* strain UDG 6038. Arch Microbiol 165:272–278
44. Redwood MD, Paterson-Beedle M, Macaskie LE (2009) Integrating dark and light bio-hydrogen production strategies: towards the hydrogen economy. Environ Sci Biotechnol 8:149–185
45. Ruggeri B, Zitella P, Goretti M, Scaletta A (2008) hydrogen da fermentazione di biomasse con popolazioni batteriche miste. La Termotecnica
46. Schieder D, Quicker P, Schneider R, Winter H, Prechtl S, Faulstich M (2003) Microbiological removal of hydrogen sulphide from biogas by means of a separate biofilter system: experience with technical operation. Water Sci Technol 48(4):209–212
47. Schink B (1997) Energetics of syntrophic cooperation in methanogenic degradation. Microbiol Mol Biol Rev 61(2):262–280
48. Schlesinger WH (1991) Biogeochemistry. An analysis of global change. Academic Press, Inc., San Diego. ISBN 0-12-625157-6
49. Shareefdeen Z, Herner B, Wilson S (2002) Biofiltration of nuisance sulphur gaseous odors from a meat rendering plant. J Chem Technol Biotechnol 77:1296–1299
50. Sinha P, Pandey A (2011) An evaluative report and challenges for fermentative biohydrogen production. Int J Hydrogen Energy 36:7460–7478
51. Sirevåg R (1995) Carbon metabolism in green bacteria. In: Blankeship RE, Madigan MT, Bauer CE (eds) Anoxygenic photosynthetic bacteria. The Netherlands, pp 871–883
52. Sousa FL, Thiergart T, Landan G, Nelson-Sathi S, Pereira IAC, Allen JF, Lane N, Martin WF (2013) Early bioenergetic evolution. Philos Trans R Soc B: Biol Sci 368:1622
53. Stanier RY, Ingraham JL, Wheelis ML, Painter PR (1986) The microbial world, 5th edn. Prentice-Hall Inc, Englewood Cliffs
54. Syed MA, Henshaw PF (2003) Effect of tube size on performance of a fixed-film tubular bioreactor for conversion of hydrogen sulphide to elemental sulphur. Water Res 37(8):1932–1938
55. Syed MA, Henshaw PF (2005) Light emitting diodes and an infrared bulb as light sources of a fixed-film tubular photobioreactor for conversion of hydrogensulphide to elemental sulphur. J Chem Technol Biotechnol 80:119–123
56. Syed MA, Henshaw PF (2006) Modelling of a fixed-film tubular photobioreactor for conversion of hydrogen sulphide to elemental sulphur. Indian J Chem Technol 13:226–232
57. Syed MA, Soreanu G, Falletta P, Béland M (2006) Removal of hydrogen sulphide from gas streams using biological processes−a review
58. Tricase C, Lombardi M (2009) State of the art and prospects of Italian biogas production from animal sewage: technical-economic considerations. Renew Energy 34:477–485
59. Trüper HG, Schlegel HG (1964) Sulphur metabolism in Thiorhodaceae, I. Quantitative measurements on growing cells of *Chromatium okenii*. Antonie Van Leeuwenhoek 30:225–238
60. Van Gemerden H (1984) The sulphide affinity of phototrophic bacteria in relation to the location of elemental sulphur. Arch Microbiol 139:289–294
61. Van Niel CB (1931) On the morphology and physiology of the purple and green sulphur bacteria. Archiv fur Mikrobiologie 3:1–112
62. Vanwonterghem I, Jensen PD, Dennis PG, Hugenholtz P, Rabaey K, Tyson GW (2014) Deterministic processes guide long-term synchronised population dynamics in replicate anaerobic digesters. Int Soc Microbial Ecol 8:2015–2028
63. Volume 2014, Article ID 183752. http://dx.doi.org/10.1155/2014/183752
64. Wang J, Wan W (2008) Effect of Fe_2+ concentration on fermentative hydrogen production by mixed cultures. Int J Hydrogen Energy 33:1215–1220
65. Wang J, Wan W (2008) Effect of Ni_2+ concentration on biohydrogen production. Bioresour Technol 99:8864–8868

66. Warthmann R, Cypionka H, Pfennig N (1992) Photoproduction of H_2 from acetate by syntrophic cocultures of green sulphur bacteria and sulphur reducing bacteria. Arch Microbiol 157:343–348
67. Wei-Chih L, Yu-Pei C, Ching-Ping T (2013) Pilot-scale chemical–biological system for efficient H_2S removal from biogas. Bioresour Technol 135:283–291
68. Zhang ML, Fan Y, Xing Y, Pan C, Zhang G, Lay I (2007) Enhanced biohydrogen production from cornstalk wastes with acidification pretreatment by mixed anaerobic cultures. Int J Hydrogen Energy 31:250–254

Biological Hydrogen Production from Lignocellulosic Biomass

Sudhanshu S. Pawar, Eoin Byrne and Ed.W.J. van Niel

Abstract Biologically derived hydrogen (biohydrogen) from lignocellulosic biomass has the potential to be an ideal renewable fuel as its combustion does not produce carbon-based emissions and it can be derived from sources which do not affect food production. Moreover, the by-products of biohydrogen production can be fed to an anaerobic digester producing biogas. Thus, a two-step process involving biohydrogen production followed by biogas production is emerging as a viable option for conversion of lignocellulosic biomass. Essential aspects of designing a viable hydrogen production system such as biomass selection, inhibitory compounds in the biomass, removal and salvage of hydrogen and the desirable qualities in any hydrogen producing organism are discussed in this chapter.

Keywords Lignocellulosic biomass · Biohydrogen production · Biogas production · Two-step biological process

List of Acronyms

ABC	ATP-binding cassette
ATP	Adenosine triphosphate
CCR	Carbon catabolite repression
CSTR	Continuous stirred-tank reactor
DF	Dark fermentation
HMF	Hydroxymethylfurfural
MEC	Microbial electrolysis cells
NADH	Nicotinamide adenine dinucleotide (reduced form)
UA	Upflow anaerobic (reactor)
UASB	Upflow anaerobic sludge blanket

S.S. Pawar (✉)
Department of Chemical Engineering, Lund University, P.O. Box 124, 221 00 Lund, Sweden
e-mail: sudhanshu.pawar@tmb.lth.se

E. Byrne · Ed.W.J. van Niel
Division of Applied Microbiology, Lund University, P.O. Box 124, 221 00 Lund, Sweden

M. De Falco and A. Basile (eds.), *Enriched Methane*,
Green Energy and Technology, DOI 10.1007/978-3-319-22192-2_7

List of Symbols

Amp^r	Ampicillin resistance
ColEH1	*E. coli* origin of replication
hcr	HMG-CoA reductase (gene)
kan	Aminoglycoside 3-N-acetyltransferase (gene)
Kan^r	Kanamycin resistance
ldh	Lactate dehydrogenase (gene)
manA	Mannose-6-phosphate isomerase (gene)
MLS^r	Macrolidelincosamide-streptogramin Resistance
P_{H2}	Partial pressure of H_2
pyrBCF	Aspartate carbamoyltransferase, Dihydro-orotase, Orotate phosphoribosyltransferase (genes)
pyrF	Orotidine 5′-phosphate decarboxylase (gene)
Q_{H2}	Volumetric H_2 productivity
trpE	Component I of anthranilate synthase (gene)
Y_{H2}	Yield of H_2, H_2 obtained per unit of substrate consumed
Δ	Gene deletion

1 Introduction

The dependence on carbon-based non-renewable fossil fuels is unsustainable in the future both environmentally and economically. In order to secure both the environment and energy supply, alternative fuels must be fully developed, commercialized and become the fuels of choice. One potential fuel which is currently under research is hydrogen gas (H_2). H_2 can be seen as an ideal fuel from an environmental viewpoint as the combustion of hydrogen produces only water as a by-product and hydrogen has a high heat unit per mass unit (142 MJ/kg) [1].

In 2009, 96 % of H_2 was derived from fossil fuels while 4 % originated through water hydrolysis [2]. Unquestionably, these methods are environmentally unfriendly. Therefore, the fate of H_2 as a fuel of the future will depend on developing technologies of H_2 production through environmentally safe and sustainable means.

2 Sustainable Methods of Hydrogen Production

The sustainable methods of H_2 production can be divided into biological and non-biological methods. Non-biological methods mainly involve the application of existing renewable energy sources such as, solar, wind or geothermal to perform electrolytic splitting of water [3, 4]. However, further research and development is

needed before a complete potential of these methods can be tested on a large scale [4].

Alternatively, biological means of H_2 production may also provide viable alternatives. Biological hydrogen production mainly involves—(i) biophotolysis, (ii) microbial electrolysis cells (MEC) and (iii) (photo)fermentation [5]. In general terms, biophotolysis is a photosynthetic process wherein light energy drives the machinery of H_2 generation from water splitting [6]. On the other hand, MEC uses a combination of bacterial metabolism and electrochemistry [7].

Fermentative H_2 production can be performed with the aid of light energy, i.e. photo-fermentation or not, i.e. dark fermentation. Photo-fermentation is a process wherein photosynthetic bacteria use light energy to produce H_2 with the help of the enzyme nitrogenase [5]. Conversely, in dark fermentation microorganisms obtain energy from fermenting organic substrates for H_2 synthesis catalyzed by hydrogenases. Microorganisms performing dark fermentation can utilize a variety of renewable biomass, such as municipal, agricultural or forest waste, making dark fermentation more eco-friendly [8]. All these methods of biological H_2 production have their advantages and disadvantages, and each is in need of further research before their commercial realization is possible [5, 6, 9–11].

Dark fermentation performed at elevated temperature ($\sim$70 °C) termed frequently as 'thermophilic biohydrogen' has the potential to become commercially viable due to its higher H_2 productivity compared to (photo)fermentation [12]. Moreover, as dark fermentation is based on carbohydrate as a substrate, availability of carbohydrate-rich lignocellulosic biomass is of particular interest in biohydrogen production.

3 Lignocellulosic Biomass as a Feedstock for H_2 Production

Lignocellulosic or plant biomass has been described as 'the most abundant organic component of the biosphere' with an annual production of 1–5 × 10^{13} kg [13]. Due to the sheer volume available it is an attractive substrate for biofuel development. Lignocellulosic biomass primarily consists of cellulose (40–60 %), hemicellulose (20–40 %) and lignin (10–25 %) [14]. Cellulose and hemicellulose can be reduced into smaller sugar molecules by enzymatic hydrolysis or can be used directly by organisms producing various glycosyl hydrolases.

Biohydrogen can be divided into first and second generation based on the origin of the substrate. First-generation biofuels refer to biofuels which are generated from arable crops and thus affect food supply and food prices. This limits their long-term viability as a sustainable fuel source. In 2015, the European Parliament voted to limit the use of first-generation biofuels to 7 % of energy generation. In contrast, second-generation biofuels refers to fuel derived from non-food feedstock, i.e. lignocellulosic biomass such as agricultural residues and forestry residues [15].

Table 1 Biohydrogen from lignocellulosic biomass grown in various regions

Lignocellulosic biomass	Major cultivation regions	H_2 producing organism	T °C (mode of cultivation)	H_2 Productivity[a]	Refs.
Wheat straw	Europe, North America, India, China, Australia, South America	*Caldicellulosiruptor saccharolyticus*	70 (Continuous)	5.2	[19]
Rice straw	Asia	*Clostridium butyricum*	37 (Batch)	0.62	[20]
Corn stalks	North America, China, South America	Enriched microflora from cow dung	36 °C (Batch)	1.21	[21]
Napier grass	Sub-Saharan Africa	*Clostridium butyricum* CGS5	37 °C (Batch)	0.08–0.13	[22]
Switchgrass	North America	*Caldicellulosiruptor saccharolyticus*	70 °C (Batch)	0.05	[23]
Water hyacinth	Brazil (invasive species elsewhere)	Activated sludge/ *Rhodopseudomonas palustris*	30 °C (Batch)	0.20–0.21	[24]
Sugar cane bagasse	Brazil, India, China, Thailand	*Clostridium butyricum*	37 °C (Batch)	1.61	[25]

[a]Productivity unit is litres of H_2 produced per litre of medium in the reactor per day (L/L/day)

Agricultural waste is an ideal source of lignocellulose as it is readily available, low cost and does not affect land usage. Corn straw, wheat straw, rice straw and sugar cane bagasse are the most prevalent sources of lignocellulosic biomass available from agricultural waste as they are the mostly widely cultivated crops [16]. While biomasses such as wheat rice and corn straw do have alternative use as animal fodder, this is limited and thus biomass is often underutilized. For instance, in the USA 90 % of all corn straw is left in the fields [17].

Due to the bulky nature of lignocellulose the logistics of handling the feedstock is an essential part of designing such a process [18]. The cost and net energy yield from biohydrogen production would be badly affected by longer transportation distances. Therefore, the source of lignocellulosic biomass must be relatively close to the refinery. As the type of lignocellulose material varies between countries, the availability of local biomass (Table 1) must be integrated in the biohydrogen process design.

4 Biomass Recalcitration

The production of hydrogen through lignocellulosic biomass is a promising way of biofuel production, however, challenges exist which limit the utilization of the biomass. Plants have evolved to naturally resist microbial attack through a variety of mechanisms such as the presence of waxes, the amount of thick cell tissue and the quantity of lignin present. These prevent water penetration and enzymatic

access to the crystalline cellulose core [26], thereby greatly reducing the effect of hydrolysis of biomass to monomeric sugars. The direct utilization of cellulose is problematic for biohydrogen production as only certain hydrogen producing organisms (such as *Clostridia*) are capable of using cellulose as a substrate. Even then the H_2 yields tend to be lower than with mono- and disaccharides [27]. In addition, the availability of cellulose in untreated biomass tends to be less than 20 % [28]. One way of overcoming this limitation is through pretreatment of the biomass resulting in the degradation of cellulose and hemicellulose into smaller sugar units [29]. Such pretreatment can increase sugar availability up to 90 % [30] while also increasing the presence of inhibitory compounds.

Heat treatment of biomass involves heating the biomass to solubilize and degrade carbohydrates. However, use of heat treatment particularly over 160 °C result in the production of phenolic compounds from the degradation of lignin and products from sugar degradation such as hydroxymethyl-furfural (HMF) and furfural [31]. These compounds have a deleterious effect on microbial cells and are often toxic [32]

Acid treatment in particular increases monomer concentrations by hydrolysis of hemicellulose. The byproducts, however, include HMF and furfural [32]. In terms of hydrogen productivity HMF may have a stimulatory effect in low concentrations [33], while furfural and HMF concentrations above 1 g/L reduce H_2 production. The presence of both inhibitors' combination produces a higher synergistic inhibitory effect than when present individually [34].

One issue is that hemicellulose contains a pentose fraction comprising primarily of xylose, but not many H_2 producers are capable of fermenting xylose [27]. As xylose makes up 45 % the sugar content of organic wastes [35], it is a substantial energy source which could go unutilized. Therefore, selection of pentose consuming H_2 producers is essential to maximize productivity.

5 The Process

5.1 Complete Conversion of Biomass

According to one of the 12 principles of green chemistry, "synthetic methods should be designed to maximize the incorporation of all materials used in the process into final product" [36]. As stated above, the thermophilic biohydrogen production via dark fermentation can retrieve only up to 33 % (4 mol H_2/mol hexose) of the energy present in the substrate, with the remainder of it trapped in the by-products, mainly acetate. Hence, to make thermophilic biohydrogen production environmentally friendly and economical; it needs to be coupled with another process capable of converting its by-products into either H_2 or any other useful product. Currently, only two alternatives are available, which can convert the by-products of thermophilic biohydrogen production to H_2: (i) photo-fermentation and (ii) electro-hydrogenesis [37].

Photo-fermentation involves conversion of organic acids into hydrogen by purple photosynthetic bacteria such as *Rhodobacter sphaeroides* and *Rhodobacter capsulatus*, using the energy captured from sunlight. The potential of a two-stage process involving dark fermentation followed by photo-fermentation was evaluated in a European framework project—HYVOLUTION [38]. The project reported the overall efficiency of 57 % (6.9 mol H_2/mol of hexose)—the highest ever for microbial H_2 production [39]. However, the photo-fermentation was found to be the most expensive part of the process, accounting for more than 80 % of the total cost [38]. Among others, addition of buffers for pH control, large quantities of water requirements, lower H_2 productivities and cost of consumables contribute significantly to the production costs [40, 41].

Similarly, a promising, novel and elegant process of electro-hydrogenesis, which involves conversion of organic acids into H_2 using microbial fuel cells, has also been studied extensively [7]. However, owing to a number of technical issues, its practical potential still remains to be proven [37]. Alternatively, the organic acids present in the dark fermentation effluent can also be treated in an anaerobic digester to produce methane (CH_4), as discussed below.

Recently, a promising study focused on a two-stage un-coupled process termed as 'Biohythane' was evaluated (Fig. 1, [19]). In the first stage, wheat straw hydrolysate was subjected to dark fermentation (DF) by *Caldicellulosiruptor saccharolyticus* to produce H_2 along with effluent rich in organic acids in continuously stirred-tank reactors (CSTR) under controlled laboratory conditions. The effluent thus collected was then treated in an upflow anaerobic sludge blanket (UASB) reactor with the help of enriched microflora mainly consisting of acetoclastic methanogen producing methane (CH_4).

Furthermore, as discussed below, removal of H_2 from the DF reactor is essential for optimum growth and H_2 production by any H_2 producer, in particular *C. saccharolyticus*. Sparging with an inert gas would be a good option for H_2 removal, but

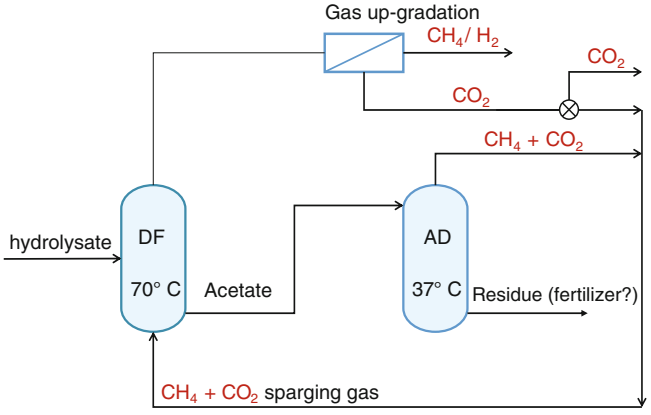

Fig. 1 Schematic representation of the biohythane process

N_2 is not an option as it is too costly to separate it afterwards from H_2. However, in the aforementioned biohythane process, methane produced in the second stage can be successfully used as a sparging gas, more so when it is purified from CO_2 (Fig. 1).

The overall biohythane process was able to convert about 57 % of the energy contained in wheat straw and about 67 % energy in its sugar fraction into H_2 and CH_4. A detailed study focused on the various individual aspects of the biohythane process highlighted many cost-related challenges, such as low H_2 productivity, the cost of nutrients and gas sparging for it to be practically applicable [42].

Thus for the biohythane process to be industrially viable, further research is needed to improve the thermophilic hydrogenogenic DF process. Interestingly, as described below, certain key metabolic features in the microorganisms performing DF may improve the feasibility process from technical as well as economic perspectives.

5.2 *Significance of Active H_2 Removal from the Bioreactor*

5.2.1 P_{H2} and Concentration of H_2 in Aqueous Phase ($H_{2,Aq}$)

Generally, due to practical difficulties in measuring the concentration of H_2 in the aqueous phase ($H_{2,aq}$), the partial pressure of H_2 (P_{H2}) in the gaseous phase of the reactor instead is considered as a parameter to monitor the behaviour of a microorganism when reactors are operating without employing any means of H_2 removal [43]. However, as there are liquid-to-gas mass transfer limitations of H_2, it can easily supersaturate in the aqueous phase. Therefore, the P_{H2} of the gas phase does not correlate with the corresponding $H_{2,aq}$ [43]. A previous study revealed that inhibition of H_2 production is mostly caused by $H_{2,aq}$ rather than the P_{H2}, and the former is dependent on the liquid-to-gas mass transfer rate of H_2 [44].

In the CSTR, the mass transfer rate, i.e. removal of H_2 from the aqueous phase, can be improved by two means—by sparging the reactor with an inert gas and/or by stirring the reactor. When a combination of sparging and stirring is applied in the continuous cultures of *C. saccharolyticus* in a CSTR, H_2 yields close to the theoretical maximum were obtained ([46], Fig. 2). However, consistent with a previous study [44], inhibition to H_2 production was more dependent on 'sparging' than on 'stirring' ([45, 47], Fig. 2).

5.2.2 Sparging and Choice of Reactor

For most studies with *C. saccharolyticus*, N_2 has been a popular choice as sparging gas for stripping the culture medium off $H_{2,aq}$ [48, 49]. Although N_2 is inexpensive and abundant, its inert nature makes it difficult to be separated from H_2 and is thus unsuitable on an industrial scale [50]. As discussed above, $H_{2,aq}$ influences the

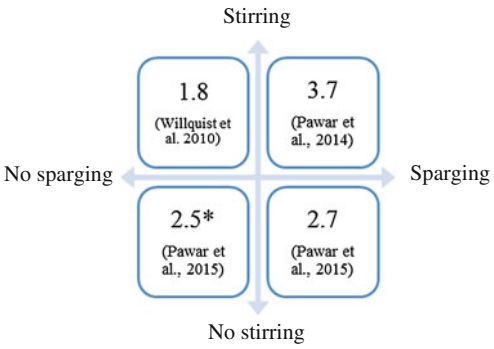

Fig. 2 H_2 yield in continuous cultures performed in a CSTR (*Note* the cultivation medium used for each condition was slightly different in its composition). *The experiment was performed with a co-culture of *C. saccharolyticus* and *C. owensensis* in upflow anaerobic reactor containing granular sludge (for details see [45])

growth and H_2 production in *C. saccharolyticus*. Therefore, various H_2 removal strategies were studied to evaluate their effect on the volumetric H_2 productivity (Q_{H2}, Table 2).

When a gas mixture mimicking the flue gas (CH_4 + CO_2) of the methanogenic anaerobic digester was used for sparging, the Q_{H2} was reduced by more than 50 % of the Q_{H2} obtained with N_2 or CH_4 as the sole sparging gas ([19], Table 2). This reduction in Q_{H2} was mainly due to the detrimental effect of CO_2 saturation on *C. saccharolyticus* in its culture medium [51]. Moreover, the use of 'CH_4 + CO_2' [19] had a similar effect on the Q_{H2} as when no sparging was applied in a CSTR [47]. Interestingly, the Q_{H2} obtained in the UA reactor in absence of sparging was almost twice that of the CSTR in similar conditions (Table 2). The reason for this was that the UA reactor allows re-circulation of culture medium which aids in improving

Table 2 The hydrogen productivity, Q_{H2}, (mmol/L/h) of *C. saccharolyticus* under various sparging conditions

Sparging gas/condition	Flow rate (L h^{-1})	Q_{H2} @ D = 0.05 h^{-1}	References
N_2	6	5.2	[47]
67 % CH_4 (N_2) + 33 % CO_2[a]	6	2.1	[19]
CH_4(N_2)[a]	6	5.2	[19]
No sparging, CSTR	–	2.4	[47]
No sparging, UA[b]	–	4.6	[45]

[a]This study revealed that CH_4 is as inert as N_2 to the growth of and H_2 production by *C. saccharolyticus*

[b]The experiment was performed with a co-culture of *C. saccharolyticus* and *C. owensensis* in a UA reactor containing granular sludge

substrate accessibility as well as increase in the turbulence in the reactor facilitating the removal of $H_{2,aq}$ [45]. Thus, a UA reactor can be used as an alternative to a CSTR for effective H_2 production.

6 Ideal Biohydrogen Producer: Desirable Metabolic Features

Over the past few decades a number of microorganisms with the natural ability of producing H_2 have been isolated [10, 52, 53]. However, the members belonging to the genus *Caldicellulosiruptor* appear to possess many interesting features desired in an ideal hydrogen producer (Fig. 3, [52]). Therefore, these properties will be discussed in reference to *C. saccharolyticus*.

6.1 Ability to Produce H_2 at High Yields

Numerous studies have reasoned that in comparison with the mesophilic H_2 producers, thermophilic ones such as *C. saccharolyticus* and *Thermotoga neapolitana* are better equipped to produce H_2 with yield approaching the theoretical maximum [10, 54]. The values of H_2 yield (Y_{H2}), i.e. the amount of H_2 obtained per unit of substrate consumed, signify the conversion efficiency of a process. Whereas the volumetric H_2 productivity (Q_{H2}) signifies the amount of H_2 produced per unit reactor volume per unit time. Unfortunately, the Y_{H2} and Q_{H2} have a reciprocal

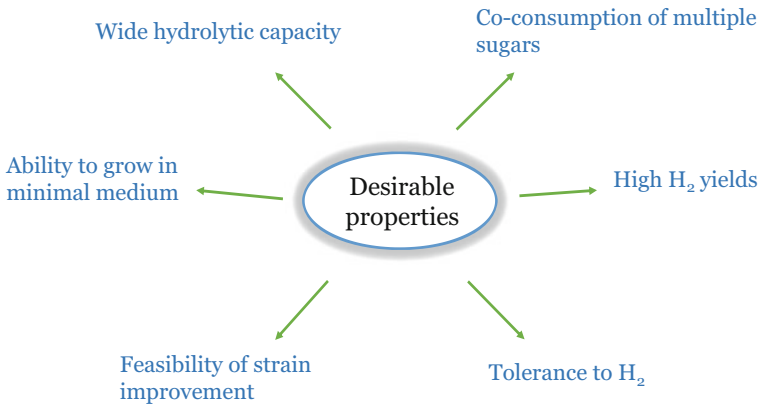

Fig. 3 Desirable metabolic features in an ideal biohydrogen producing microorganism

relationship, meaning that any attempt to improve either of them may result in diminution of the other [53]. Organism(s) capable of producing H_2 at higher yields will be desirable, especially when using costly feedstock such as energy crops.

6.2 Hydrolytic Capacity and Growth on Renewable Feedstock

Availability of lignocellulosic material varies with respect to geographical regions as well as with seasons (Table 1). Therefore, it is imperative that the microorganism (s) should have a wide range of hydrolytic capacity to hydrolyze various polymers derived from different lignocellulosic materials. This may enable the process to be flexible with respect to the availability of feedstock.

The natural habitats of the majority of thermophilic H_2 producers are low in simple sugars but abundant in complex polysaccharides [55]. Thus, these microorganisms usually possess a variety of hydrolases to breakdown these polysaccharides [56]. For instance, *C. saccharolyticus* has an extraordinary ability to hydrolyze a variety of naturally occurring polymers, such as lignocellulosic materials [55]. Interestingly, within the genus *Caldicellulosiruptor*, *C. kronotskyensis* followed closely by *C. saccharolyticus* has the best inventory of different *glycosyl hydrolases* [55]. Nonetheless, *C. saccharolyticus* can hydrolyze various α- and β-linked di-, oligo- and polysaccharides, such as starch, maltose, sucrose, pullulan, pectin, trehalose, xylan and (hemi)celluloses [57]. So far, *C. saccharolyticus* has been reported to grow and produce H_2 on hydrolysates of wheat straw [19], Miscanthus [58], paper sludge [59], barley straw and corn stalk [60], juices of sweet sorghum [61] and sugar beet [62], as well as untreated wheat straw, sugar cane bagasse, leaves of maize or *Silphium trifoliatum* [61], and potato steam peels [63].

6.3 Absence of Carbon Catabolite Repression

The products of hydrolyzed complex carbohydrates, i.e. the soluble mono-, di- or oligo-saccharides should then be assimilated for which organisms should be equipped with transporters in their cell membrane. *C. saccharolyticus* achieves this via ABC transporters at the expense of ATP. Of 177 annotated ABC transporters, only 24 have been assigned with substrate specification, meaning that most ABC transporters have a broad substrate range and also some substrates can be transported by multiple transporters [64].

In addition, the organism should preferably be able to metabolize these sugars simultaneously, but this is usually hindered by carbon catabolite repression (CCR). When *C. saccharolyticus* was grown on a mixture of sugars, including pentoses and

hexoses, it displayed the ability of co-utilization of all these sugars confirming the absence of CCR [19, 64, 65]. The co-utilization of sugars was also observed with the hydrolysates of renewable feedstock [19, 58, 66]. Thus, the absence of CCR is an important property making *C. saccharolyticus* desirable as an industrial biohydrogen producer.

6.4 Ability to Withstand High P_{H2}

Hydrogenases catalyze the reduction of proton to H_2. NADH or reduced ferredoxin is the main electron donor, which are derived during the catabolism of substrate(s) [10]. As discussed above, from a strict thermodynamic perspective, the possession of a ferredoxin-dependent hydrogenase enables organisms to tolerate high P_{H2}, albeit reducing the H_2 yield by half [47]. Nevertheless, from an industrial perspective this means the removal of H_2 from DF reactor is not necessary. However, due to a variety of reasons, as argued by Willquist and co-workers, a thermodynamic constraint alone cannot be a criterion to determine the critical P_{H2} affecting H_2 production [49].

6.5 Ability to Grow in a Minimal Medium

In a detailed techno-economic analysis of a biohydrogen production process, Ljunggren and co-workers estimated that the use of additive nutrient such as yeast extract make the process very expensive [40]. Therefore, organisms capable of growing in a minimal medium would aid in improving the process economics further. In a previous study it was experimentally proved that *C. saccharolyticus* is prototrophic to all the amino acids required in protein synthesis or other cellular functions and thus, does not need the addition of complex substrates such as yeast extract and/or peptone in its growth medium [67].

In addition to complex substrates, cysteine HCl is also an expensive ingredient used traditionally in the cultivation medium of strictly anaerobic H_2 producers as a: (i) reducing agent [68] and a (ii) sulphur source [69]. The evaluation of assimilatory sulphur metabolism in *C. saccharolyticus* revealed that, not only can cysteine HCl cause emissions of hazardous H_2S gas, but also it is not essential for growth and H_2 production [46]. Moreover, relatively inexpensive inorganic sulphate salts could successfully replace cysteine HCl as a primary sulphur source in the growth medium of *C. saccharolyticus* without any apparent emission of H_2S, thus improving safety and economic feasibility [46].

6.6 Feasibility of Strain Improvement

The research and development pertaining to the physiology of popular microbes such as *Saccharomyces cerevisiae* and *Escherichia coli* has improved by leaps and bounds in the past few decades creating numerous industrial applications. Arguably, the development of various kinds of genetic tools for these microbes has played a major role in their individual development as an industrial workhorse. However, so far only few tools have been successfully obtained for genetic modification of the known thermophilic H_2 producers (Table 3, for a complete list see [54]).

Moreover, these tools are mostly organism specific, thus limiting their application in other H_2 producers. Researchers face a number of challenges in developing tools for genetic modification in thermophilic H_2 producers. Nevertheless, development of genetic tools for H_2 producing organisms may facilitate their development as an efficient H_2 producer.

6.7 Ability to Withstand High Osmotic Pressure

Over the years cultures of mainly thermophilic H_2 producers have been associated with low Q_{H2}. This is not only due to the low cell densities but also due to low initial substrate concentrations [52]. Certainly, increasing the initial substrate concentrations may improve the Q_{H2} but it will also increase the osmolality of the medium, which can be fatal to the growth of organisms such as *C. saccharolyticus* [44, 51]. Tools of strain improvement may help develop strains able to withstand the high substrate concentrations in the medium.

Table 3 Examples of the tools developed for genetic modification in thermophilic H_2 producers

Plasmid	Description	Host	Gene of interest	Gene source	References
pIKM3	ColEH1; ORF2; Amp^r; MLS^r	*T. saccharolyticum* JW/SL-YS485	*manA*	*manA*: *Caldicellulosiruptor* Rt8B4	[70]
pUDT2	Replicating; *pyrF*; double cross-over	*T. kodakarensis* KOD1	*trpE*	*trpE:T. kodakarensis* KOD1	[71]
pDCW89	Replicating; *pyrBCF*	*C. hydrothermalis* Δ*pyrBCF*	*pyrBCF*	*pyrBCF:C. bescii*	[72]
pDCW121	pDCW88; Apr^r; Δ*ldh*	*C. bescii* Δ*pyrBCF*	*ldh (deletion)*	*pyrBCF:C. bescii*	[73]
pDH10	pRQ7; Amp^r; Kan^r	*T. neapolitana, T. maritima*	*kan*	NA[a]	[74]
pYS3/4	pYS2; HMG CoA *reductase* (*hcr*)	*P. furiosus*	*hcr*	*hcr:P. furiosus*	[75]

[a]Purchased from Biotools, BM labs, Madrid, Spain

7 Conclusions

So far, the biohythane process, i.e. biohydrogen production accompanied with biogas production, presents as the best possible option for a complete conversion of biomass into energy carriers. Hence, further research should be encouraged to develop the biohythane process. Similarly, the features discussed above (and more) may also be used to determine the potential of H_2 producing microorganisms isolated in the future. Undeniably, H_2 is an important commodity and a potential fuel of the future.

References

1. Balat M (2008) Potential importance of hydrogen as a future solution to environmental and transportation problems. Int J Hydrogen Energy 33:4013–4029
2. Balat M, Balat M (2009) Political, economic and environmental impacts of biomass-based hydrogen. Int J Hydrogen Energy 34:3589–3603
3. Jacobson MZ, Delucchi MA (2011) Providing all global energy with wind, water, and solar power, Part I: Technologies, energy resources, quantities and areas of infrastructure, and materials. Energy Policy 39:1154–1169
4. Turner J, Sverdrup G, Mann MK, Maness P-C, Kroposki B, Ghirardi M, Evans RJ, Blake D (2008) Renewable hydrogen production. Int J Energy Res 32:379–407
5. Lee H-S, Vermaas WFJ, Rittmann BE (2010) Biological hydrogen production: prospects and challenges. Trends Biotechnol 28:262–271
6. Hallenbeck PC, Benemann JR (2002) Biological hydrogen production; fundamentals and limiting processes. Int J Hydrogen Energy 27:1185–1193
7. Liu H, Grot S, Logan BE (2005) Electrochemically assisted microbial production of hydrogen from acetate. Environ Sci Technol 39:4317–4320
8. Chaubey R, Sahu S, James OO, Maity S (2013) A review on development of industrial processes and emerging techniques for production of hydrogen from renewable and sustainable sources. Renew Sustain Energy Rev 23:443–462
9. Hallenbeck PC, Abo-Hashesh M, Ghosh D (2012) Strategies for improving biological hydrogen production. Bioresour Technol 110:1–9
10. Kengen SWM, Goorissen HP, Verhaart M, Stams AJM, van Niel EWJ, Claassen PAM (2009) Biological hydrogen production by anaerobic microorganisms. In Biofuels. Wiley, New York, pp 197–221
11. Nath K, Das D (2004) Improvement of fermentative hydrogen production: various approaches. Appl Microbiol Biotechnol 65:520–529
12. Ghimire A, Frunzo L, Pirozzi F, Trably E, Escudie R, Lens PNL, Esposito G (2015) A review on dark fermentative biohydrogen production from organic biomass: process parameters and use of by-products. Appl Energy 144:73–95
13. Claassen PAM, van Lier JB, Lopez Contreras AM, van Niel EWJ, Sijtsma L, Stams AJM, de Vries SS, Weusthuis RA (1999) Utilisation of biomass for the supply of energy carriers. Appl Microbiol Biotechnol 52:741–755
14. Hamelinck CN, Hooijdonk GV, Faaij APC (2005) Ethanol from lignocellulosic biomass: techno-economic performance in short-, middle- and long-term. Biomass Bioenergy 28:384–410
15. Naik SN, Goud VV, Rout PK, Dalai AK (2010) Production of first and second generation biofuels: a comprehensive review. Renew Sustain Energy Rev 14:578–597

16. Chandra R, Takeuchi H, Hasegawa T (2012) Methane production from lignocellulosic agricultural crop wastes: a review in context to second generation of biofuel production. Renew Sustain Energy Rev 16:1462–1476
17. Sarkar N, Ghosh SK, Bannerjee S, Aikat K (2012) Bioethanol production from agricultural wastes: an overview. Renew Energy 37:19–27
18. Sultana A, Kumar A (2011) Optimal configuration and combination of multiple lignocellulosic biomass feedstocks delivery to a biorefinery. Bioresour Technol 102:9947–9956
19. Pawar SS, Nkemka VN, Zeidan AA, Murto M, van Niel EWJ (2013) Biohydrogen production from wheat straw hydrolysate using Caldicellulosiruptor saccharolyticus followed by biogas production in a two-step uncoupled process. Int J Hydrogen Energy 38:9121–9130
20. Lo Y-C, Lu W-C, Chen C-Y, Chang J-S (2010) Dark fermentative hydrogen production from enzymatic hydrolysate of xylan and pretreated rice straw by Clostridium butyricum CGS5. Bioresour Technol 101:5885–5891
21. Zhang M-L, Fan Y-T, Xing Y, Pan C-M, Zhang G-S, Lay J-J (2007) Enhanced biohydrogen production from cornstalk wastes with acidification pretreatment by mixed anaerobic cultures. Biomass Bioenergy 31:250–254
22. Lo YC, Huang C-Y, Fu T-N, Chen C-Y, Chang J-S (2009) Fermentative hydrogen production from hydrolyzed cellulosic feedstock prepared with a thermophilic anaerobic bacterial isolate. Int J Hydrogen Energy 34:6189–6200
23. Talluri S, Raj SM, Christopher LP (2013) Consolidated bioprocessing of untreated switchgrass to hydrogen by the extreme thermophile Caldicellulosiruptor saccharolyticus DSM 8903. Bioresour Technol 139:272–279
24. Su H, Cheng J, Zhou J, Song W, Cen K (2010) Hydrogen production from water hyacinth through dark- and photo-fermentation. Int J Hydrogen Energy 35:8929–8937
25. Pattra S, Sangyoka S, Boonmee M, Reungsang A (2008) Bio-hydrogen production from the fermentation of sugarcane bagasse hydrolysate by Clostridium butyricum. Int J Hydrogen Energy 33:5256–5265
26. Himmel ME, Ding S-Y, Johnson DK, Adney WS, Nimlos MR, Brady JW, Foust TD (2007) Biomass recalcitrance: engineering plants and enzymes for biofuels production. Science 315:804–807
27. Ren N, Wang A, Cao G, Xu J, Gao L (2009) Bioconversion of lignocellulosic biomass to hydrogen: potential and challenges. Biotechnol Adv 27:1051–1060
28. Mosier N, Wyman C, Dale B, Elander R, Lee YY, Holtzapple M, Ladisch M (2005) Features of promising technologies for pretreatment of lignocellulosic biomass. Bioresour Technol 96:673–686
29. Kumar P, Barrett DM, Delwiche MJ, Stroeve P (2009) Methods for pretreatment of lignocellulosic biomass for efficient hydrolysis and biofuel production. Ind Eng Chem Res 48:3713–3729
30. Hahn-Hägerdal B, Galbe M, Gorwa-Grauslund MF, Lidén G, Zacchi G (2006) Bio-ethanol—the fuel of tomorrow from the residues of today. Trends Biotechnol 24:549–556
31. Klinke HB, Thomsen AB, Ahring BK (2004) Inhibition of ethanol-producing yeast and bacteria by degradation products produced during pre-treatment of biomass. Appl Microbiol Biotechnol 66:10–26
32. Hendriks ATWM, Zeeman G (2009) Pretreatments to enhance the digestibility of lignocellulosic biomass. Bioresour Technol 100:10–18
33. Liu Z, Zhang C, Wang L, He J, Li B, Zhang Y, Xing X-H (2015) Effects of furan derivatives on biohydrogen fermentation from wet steam-exploded cornstalk and its microbial community. Bioresour Technol 175:152–159
34. Veeravalli SS, Chaganti SR, Lalman JA, Heath DD (2013) Effect of furans and linoleic acid on hydrogen production. Int J Hydrogen Energy 38:12283–12293
35. Lin C-Y, Cheng C-H (2006) Fermentative hydrogen production from xylose using anaerobic mixed microflora. Int J Hydrogen Energy 31:832–840

36. Anastas P, Eghbali N (2010) Green chemistry: principles and practice. Chem Soc Rev 39:301–312
37. Hallenbeck PC (2009) Fermentative hydrogen production: principles, progress, and prognosis. Int J Hydrogen Energy 34:7379–7389
38. Claassen PAM, de Vrije T, Koukios E, van Niel E, Eroglu I, Modigell M, Friedl A, Wukovits W, Ahrer W (2010) Non-thermal production of pure hydrogen from biomass: HYVOLUTION. J Clean Prod 18(Supplement 1):S4–S8
39. Özgür E, Afsar N, de Vrije T, Yücel M, Gündüz U, Claassen PAM, Eroglu I (2010) Potential use of thermophilic dark fermentation effluents in photofermentative hydrogen production by Rhodobacter capsulatus. J Clean Prod 18(Supplement 1):S23–S28
40. Ljunggren M, Zacchi G (2010) Techno-economic evaluation of a two-step biological process for hydrogen production. Biotechnol Prog 26:496–504
41. Ljunggren M, Wallberg O, Zacchi G (2011) Techno-economic comparison of a biological hydrogen process and a 2nd generation ethanol process using barley straw as feedstock. Bioresour Technol 102:9524–9531
42. Willquist K, Nkemka VN, Svensson H, Pawar SS, Ljunggren M, Karlsson H, Murto M, Hulteberg C, van Niel EWJ, Liden G (2012) Design of a novel biohythane process with high H_2 and CH_4 production rates. Int J Hydrogen Energy 37:17749–17762
43. Pauss A, Andre G, Perrier M, Guiot SR (1990) Liquid-to-gas mass transfer in anaerobic processes: inevitable transfer limitations of methane and hydrogen in the biomethanation process. Appl Environ Microbiol 56:1636–1644
44. Ljunggren M, Willquist K, Zacchi G, van Niel E (2011) A kinetic model for quantitative evaluation of the effect of H_2 and osmolarity on hydrogen production by Caldicellulosiruptor saccharolyticus. Biotechnol Biofuels 4:31
45. Pawar SS, Vongkumpeang T, Grey C, van Niel EW (2015) Biofilm formation by designed co-cultures of Caldicellulosiruptor species as a means to improve hydrogen productivity. Biotechnol Biofuels 8:19
46. Pawar SS, van Niel EWJ (2014) Evaluation of assimilatory sulphur metabolism in Caldicellulosiruptor saccharolyticus. Bioresour Technol 169:677–685
47. Willquist K, Pawar SS, van Niel EWJ (2011) Reassessment of hydrogen tolerance in Caldicellulosiruptor saccharolyticus. Microb Cell Fact 10:111
48. Bielen AAM, Verhaart MRA, van der Oost J, Kengen SVM (2013) Biohydrogen production by the thermophilic bacterium Caldicellulosiruptor saccharolyticus: current status and perspectives. Life 3:52–85
49. Willquist K, Zeidan AA, van Niel EWJ (2010) Physiological characteristics of the extreme thermophile Caldicellulosiruptor saccharolyticus: an efficient hydrogen cell factory. Microb Cell Fact 9:89
50. van Groenestijn JW, Hazewinkel JHO, Nienoord M, Bussmann PJT (2002) Energy aspects of biological hydrogen production in high rate bioreactors operated in the thermophilic temperature range. Int J Hydrogen Energy 27:1141–1147
51. Willquist K, Claassen PAM, van Niel EWJ (2009) Evaluation of the influence of CO_2 on hydrogen production in Caldicellulosiruptor saccharolyticus. Int J Hydrogen Energy 34:4718–4726
52. Pawar SS, van Niel EWJ (2013) Thermophilic biohydrogen production: how far are we? Appl Microbiol Biotechnol 97:7999–8009
53. Rittmann S, Herwig C (2012) A comprehensive and quantitative review of dark fermentative biohydrogen production. Microb Cell Fact 11:115
54. Raj SM, Talluri S, Christopher LP (2012) Thermophilic hydrogen production from renewable resources: current status and future perspectives. BioEnergy research 5:515–531
55. Blumer-Schuette SE, Lewis DL, Kelly RM (2010) Phylogenetic, microbiological, and glycoside hydrolase diversities within the extremely thermophilic, plant biomass-degrading genus Caldicellulosiruptor. Appl Environ Microbiol 76:8084–8092

56. Blumer-Schuette SE, Kataeva I, Westpheling J, Adams MWW, Kelly RM (2008) Extremely thermophilic microorganisms for biomass conversion: status and prospects. Curr Opin Biotechnol 19:210–217
57. Rainey FA, Donnison AM, Janssen PH, Saul D, Rodrigo A, Bergquist PL, Daniel RM, Stackebrandt E, Morgan HW (1994) Description of Caldicellulosiruptor saccharolyticus gen-nov, sp. nov. an obligately anaerobic, extremely thermophilic, cellulolytic bacterium. FEMS Microbiol Lett 120:263–266
58. de Vrije T, Bakker RR, Budde MAW, Lai MH, Mars AE, Claassen PAM (2009) Efficient hydrogen production from the lignocellulosic energy crop Miscanthus by the extreme thermophilic bacteria Caldicellulosiruptor saccharolyticus and Thermotoga neapolitana. Biotechnol Biofuels 2:12
59. Kadar Z, De Vrije T, Budde MAW, Szengyel Z, Reczey K, Claassen PAM (2003) Hydrogen production from paper sludge hydrolysate. Appl Biochem Biotechnol 105–108:557–566
60. Panagiotopoulos IA, Bakker RR, Budde MAW, de Vrije T, Claassen PAM, Koukios EG (2009) Fermentative hydrogen production from pretreated biomass: a comparative study. Bioresour Technol 100:6331–6338
61. Ivanova G, Rákhely G, Kovács KL (2009) Thermophilic biohydrogen production from energy plants by Caldicellulosiruptor saccharolyticus and comparison with related studies. Int J Hydrogen Energy 34:3659–3670
62. Panagiotopoulos JA, Bakker RR, de Vrije T, Urbaniec K, Koukios EG, Claassen PAM (2010) Prospects of utilization of sugar beet carbohydrates for biological hydrogen production in the EU. J Clean Prod 18(Supplement 1):S9–S14
63. Mars AE, Veuskens T, Budde MAW, van Doeveren PFNM, Lips SJ, Bakker RR, de Vrije T, Claassen PAM (2010) Biohydrogen production from untreated and hydrolyzed potato steam peels by the extreme thermophiles Caldicellulosiruptor saccharolyticus and Thermotoga neapolitana. Int J Hydrogen Energy 35:7730–7737
64. VanFossen AL, Verhaart MRA, Kengen SWM, Kelly RM (2009) Carbohydrate utilization patterns for the extremely thermophilic bacterium Caldicellulosiruptor saccharolyticus reveal broad growth substrate preferences. Appl Environ Microbiol 75:7718–7724
65. van de Werken HJG, Verhaart MRA, VanFossen AL, Willquist K, Lewis DL, Nichols JD, Goorissen HP, Mongodin EF, Nelson KE, van Niel EWJ et al (2008) Hydrogenomics of the extremely thermophilic bacterium Caldicellulosiruptor saccharolyticus. Appl Environ Microbiol 74:6720–6729
66. de Vrije T, Budde MAW, Lips SJ, Bakker RR, Mars AE, Claassen PAM (2010) Hydrogen production from carrot pulp by the extreme thermophiles Caldicellulosiruptor saccharolyticus and Thermotoga neapolitana. Int J Hydrogen Energy 35:13206–13213
67. Willquist K, van Niel EWJ (2012) Growth and hydrogen production characteristics of Caldicellulosiruptor saccharolyticus on chemically defined minimal media. Int J Hydrogen Energy 37:4925–4929
68. Sissons CH, Sharrock KR, Daniel RM, Morgan HW (1987) Isolation of cellulolytic anaerobic extreme thermophiles from New Zealand thermal sites. Appl Environ Microbiol 53:832–838
69. Zeidan AA (2011) Hydrogen production by Caldicellulosiruptor species: the organism and the metabolism. PhD thesis, Lund University, Sweden, Applied Microbiology
70. Mai V, Wiegel J (2000) Advances in development of a genetic system for Thermoanaerobacterium spp.: expression of genes encoding hydrolytic enzymes, development of a second shuttle vector, and integration of genes into the chromosome. Appl Environ Microbiol 66:4817–4821
71. Sato T, Fukui T, Atomi H, Imanaka T (2003) Targeted gene disruption by homologous recombination in the hyperthermophilic archaeon thermococcus kodakaraensis KOD1. J Bacteriol 185:210–220
72. Chung D, Farkas J, Huddleston JR, Olivar E, Westpheling J (2012) Methylation by a unique α-class N_4-Cytosine Methyltransferase is required for DNA transformation of Caldicellulosiruptor bescii DSM6725. PLoS ONE 7:e43844

73. Cha M, Chung D, Elkins J, Guss A, Westpheling J (2013) Metabolic engineering of Caldicellulosiruptor bescii yields increased hydrogen production from lignocellulosic biomass. Biotechnol Biofuels 6:85
74. Han D, Norris SM, Xu Z (2012) Construction and transformation of a Thermotoga-E. coli shuttle vector. BMC Biotechnol 12:2
75. Waege I, Schmid G, Thumann S, Thomm M, Hausner W (2010) Shuttle vector-based transformation system for Pyrococcus furiosus. Appl Environ Microbiol 76:3308–3313

Purification of Hydrogen-Methane Mixtures Using PSA Technology

Rosaria Augelletti, Sara Frattari and Maria Anna Murmura

Abstract Mixtures of hydrogen-methane (hydromethane), composed of 20–30 % vol. hydrogen, are considerably interesting, especially in the field of sustainable mobility, because their energy content is higher than that of pure methane; moreover, the carbon dioxide emissions due to the combustion are reduced. The production of such mixture can be effectively carried out by means of steam reforming of natural gas (97 % methane and 3 % carbon dioxide) at 500–550 °C. However, the reformed gas must be purified in order to reduce the carbon dioxide concentration (lower than 3 %). The pressure swing adsorption technology, which uses activated carbon as adsorbent material, may be employed to remove carbon dioxide and to obtain a high recovery of hydrogen and methane. To improve the recovery of methane, a second pressure swing adsorption unit, which uses carbon molecular sieve as an adsorbent, can be introduced.

Keywords Hydrogen-methane mixture separation · Pressure swing adsorption · Activated carbon · Carbon dioxide removal

List of symbols

A	Skarstrom PSA cycle
B	Modified Skarstrom PSA cycle
b	Temperature-dependent Langmuir isotherm parameter
k	Mass transport coefficient
p	Partial pressure
P	Total pressure
q	Amount absorbed on absorbent material
q_{max}	Maximum absorbable amount
S	Selectivity
T	Temperature

R. Augelletti · S. Frattari (✉) · M.A. Murmura
Department of Chemical Engineering Materials Environment,
Sapienza University of Rome, Rome, Italy
e-mail: sara.frattari@uniroma1.it

M. De Falco and A. Basile (eds.), *Enriched Methane*,
Green Energy and Technology, DOI 10.1007/978-3-319-22192-2_8

Subscripts and superscripts

i, *J*	component
kin	Kinetic
LDF	Linear driving force
thermo	Thermodynamic

Acronyms and abbreviations

BD	Blow-down step
CHP	Cogeneration system
CMS	Carbon molecular sieve
EQ	Equalization step
FE	Feed step
MOF	Metal organic framework
PR	Pressurization step
PSA	Pressure swing adsorption
PU	Purge step
RPSA	Rapid pressure swing adsorption
SAPO	Silico aluminate phosphate
VPSA	Vacuum pressure swing adsorption

1 Introduction

The hydrogen-methane mixtures (hydromethane), composed by 20–30 %vol. of hydrogen in methane, are considerably interesting, mainly in the field of sustainable mobility, for the reason that their energy content is higher than that of the pure methane. Furthermore it can be considered a green fuel, as the combustion of these mixtures releases a lower amount of CO_2 than the case in which hydrogen is not present. For instance, the combustion of 1 kg of hydromethane with 30 %vol. of hydrogen (typical composition of hydrometane), produces 2.61 kg of CO_2 against 2.75 kg products from natural gas. Moreover, the hydromethane standard heat combustion is −52 kJ/g versus −49 kJ/g of that of natural gas.

The required methane-hydrogen ratio depends on the technical applications of the mixture and suggests its production mode. The production of hydrogen from natural gas is generally based on the steam-reforming reaction.

This process allows the conversion of methane in a gaseous mixture—containing methane, hydrogen, and carbon oxides—having energy content greater than the starting natural gas. The reactions are globally endothermic and require a heat input that can be provided through different energy sources, depending on the temperature of reforming and therefore the degree of conversion can be achieved.

As an example, Table 1 shows the equilibrium compositions obtained from steam reforming at 15 atm of natural gas with 3 % of carbon dioxide and a steam-to-carbon ratio 3.

Table 1 Typical equilibrium composition of reacted natural gas at two different temperatures and at pressure equal to 15 atm

	1173 K	788 K
CH_4	0.9	18.8
H_2	52.7	15.8
CO	11.3	0.2
CO_2	5.2	4.5
H_2O	29.9	60.7

Compositions are expressed in terms of volumetric percent

For example, a mixture with a quantity of hydrogen equal to 53 %vol. can be obtained at reaction temperature of at least 1173 K, with an almost complete methane conversion (see the first column of Table 1); in this case, the most appropriate type of energy source is of thermal nature.

If, instead, the required hydrogen content for the reformed gas is about 16 %, the reaction temperature can be lower than the first case mentioned (788 K compared to 1173 K, as shown in Table 1) and the heat input may be provided through concentrated solar energy and can be stored, for example, in a molten salts tank.

It is worth noting that in the case of high temperature steam reforming, a consistent amount of CO is present, which has to be converted into CO_2 in a second reactor, working at lower temperature in order to promote the water-gas shift reaction [1].

The development of a system to enrich methane with hydrogen, using solar energy, promises interesting applications in the transport sector, combining the advantages of using a fuel "partially" generated from solar energy—a renewable source—with the use of methane-hydrogen blends having an energy content greater than the starting methane; moreover, a hydromethane mixture with H_2 content of 20–25 %vol. does not require expensive, technical modifications of the engine setup, being able to be burned in the already existing internal combustion engine for the combustion of natural gas [2, 3].

In both the cases described in Table 1, the mixture is formed not only by methane and hydrogen but also by CO, CO_2, and unreacted H_2O. These last three components should be present in limited amounts, in particular, for application in the automotive field; indeed, the specific regulation for blends for this application requires the complete removal of water (dew point of −5 °C at 70 bar) and CO_2 content lower than the 3 %. Therefore, together with the total removal of water, a process to separate CO_2 produced in the steam-reforming process from the gas mixture is required.

In the following, CO_2 removal from gas mixture produced from low temperature, solar-driven steam reforming is considered; as previously discussed, after dehydration, this is a three component mixture with about 50 % of CH_4, 40 % of H_2, and 10 % of carbon dioxide.

CO_2 removal through chemical absorption in solutions of amines is an interesting solution because of their high selectivity towards carbon dioxide. It is a continuous process, so the design and operation of plants is quite simple. However, these solvents are toxic and corrosive and require high temperature and energy

consumption for their regeneration. Therefore, they are not a sustainable solution for small installations.

An interesting alternative is represented by pressure swing absorption (PSA), because of its low energy consumption and low costs of investment. This technology is based on the different selectivity of an adsorption material towards one or more components from a mixture, alternating adsorption phases at high pressure with regeneration phases at low pressure.

Here PSA is studied for the separation of carbon dioxide from the reformed gas. General information on PSA processes is reported and subsequently the removal of CO_2 by PSA, from a mixture produced in a solar-driven reformer is studied.

2 The PSA Process

PSA is a very versatile technology for the separation of gaseous mixtures based on physical adsorption. Conceptually, the process is based on two fundamental elements:

- the separation of components of a gaseous mixture is obtained by exploiting the selectivity of a solid adsorbent, which can be determined by different adsorption capacities of the components present in the gas on the solid, a thermodynamic property (equilibrium adsorbents), and/or by the different diffusion rates of the components inside the solid particles—a kinetic property (kinetic adsorbents). In some cases, the difference in diffusion rates can be so high that the species which diffuse more slowly is effectively, totally excluded from the adsorbent; thus the adsorbent works as a sieve allowing to obtain high degree of separation;
- the regeneration of the absorbent is obtained by reducing the total pressure in the column without increasing the temperature. The regeneration by depressurization is energetically more convenient than the one obtained raising the temperature of the bed; depressurization is also rapider than the heating of the column and can operate with very fast cycles. The capacity of the column is given by the difference in the amount of the heavy component adsorbed between the pressure conditions corresponding to the adsorption and regeneration phases.

The operation is carried out by alternating phases of adsorption and regeneration in a cyclic manner. In the adsorption phase at high pressure, in the column output, a gas enriched in the lighter component and purified from the heavier component (which is adsorbed preferentially) is obtained, while the gaseous stream desorbed during the regeneration phase at low pressure is enriched in the heavier component. Although for applications of very small potentiality it is possible to provide a PSA unit that uses a single column with a storage tank in which the produced gas is accumulated in a discontinuous manner, PSA is normally realized by using multiple columns in which the same cycle is reproduced with an appropriate phase shift, so as to emulate a continuous process.

The simplest cycle, proposed by Skarstrom in 1960s [4], includes four phases:

1. Pressurization (PR): the column is pressurized without removing output currents;
2. Feed or adsorption (FE): the gas to be treated is fed into the column at high pressure, obtaining an output gas enriched in the lighter component;
3. Blow down (BD): the column is depressurized by removing the gases present in the voids of the column and the adsorbed gas;
4. Purging (PU): the removal of the heavy component is completed by feeding to the column a stream enriched in the light component (usually a part of the product of adsorption phase) at low pressure and recovering an output gas enriched in the heavy component.

The cycle can be implemented with two columns, which operate with shifted phases (as shown in Fig. 1):

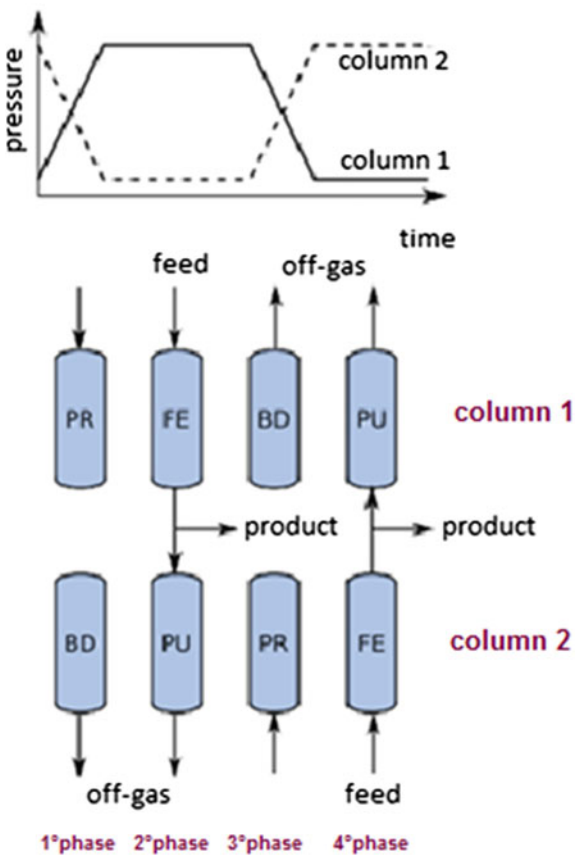

Fig. 1 Skarstrom cycle for a two-column system: Pressurization (PR), Feed (FE), Blow-down (BD), Purge (PU). The pressurization is co-current, blow-down and purge are counter-current with respect to feed

- in the first phase, column 1 is pressurized to the adsorption pressure, while the pressure in column 2 is reduced to the lowest value;
- in the second phase, column 2 is fed with the mixture to be separated at high pressure, obtaining an output gas enriched in the lighter component; at this stage a part of the product is used to purge column 2 at the lower operating pressure;
- the steps 3 and 4 repeat the same operations of steps 1 and 2, but with the columns exchanged.

Several variations to the described scheme are possible, for example:

- pressurization can be obtained using the gas to be treated or the product obtained in the feeding phase, in co-current or counter-current respect to the feed step;
- to reduce the losses with the off-gas, the blow-down can be performed together with the depressurization stages, by recirculating to the feed phase the gas released during the first depressurization. This gas, in fact, contains significant amounts of the light component, which in this way can be significantly recovered;
- the blow-down step of a column can be combined with the pressurization phase of another, thus introducing a pressure equalization phase—reducing energy consumption and improving the recovery.

A possible variant of the basic process can be represented by the choice of operating the regeneration step at a pressure lower than the atmospheric one (Vacuum PSA, VPSA). This solution may be advantageous if the adsorption isotherm of the heavy component is strongly nonlinear and the regeneration of the column can be obtained only at very low pressure. Another interesting alternative is the rapid PSA (RPSA), which uses a single column with very small adsorbent particles (order of magnitude of 100–500 m), with cycle times (3–10 s) significantly lower than those of a conventional PSA; as a result, the productivity is much higher, but the energy consumption is also generally higher.

3 PSA for the CO_2 Removal from CO_2–CH_4–H_2 Mixture Produced by Solar Steam Reforming of Natural Gas

3.1 Process Definition

Figure 2 shows the block diagram of the hydromethane production and purification process analyzed in this work; the reforming reactor operates in the range of 500–517 °C with a steam-to-carbon ratio 3; the details of the hydromethane production are reported in a previously published work [5]. Here reference will be made to the gas produced in the reforming reactor.

In Table 2 the characteristics of the main upstream streams of the PSA unit are reported.

Natural gas and water streams entering the reformer are considered to be previously heated in the solar energy exchanger, not shown in the block diagram.

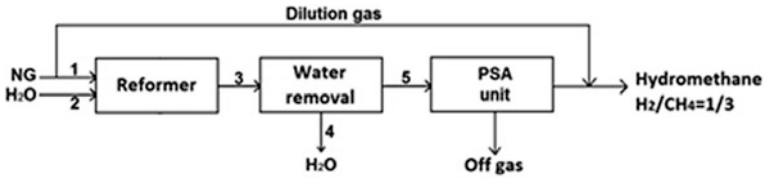

Fig. 2 Production and purification process of hydromethane mixture

Table 2 Main characteristics of process streams

	Flow rate		Composition (%)				T (°C)	P (atm)
	kg/h	Nm^3/h	CH_4	CO_2	H_2	H_2O		
1	157.8	210	97	3	–	–	500	15
2	490.7	611	–	–	–	100	500	15
3	648.5	891.6	18.9	4.6	15.6	60.9	514	14.5
4	435.8	542.7	–	–	–	100	–	–
5	212.7	34	48.3	11.9	39.8	–	25	13

At the end of the present work, the characteristics of the remaining streams will be reported; however, considering the conversion obtained in the solar reactor and the expected efficiency of the separation steps required, it is possible to make an estimate of the order of magnitude of the hydromethane flow rate, which will be about 340 kg/h.

The CO content in the reformed gas has been neglected and a complete water removal has been assumed; as can be observed from the figure, a dilution current of natural gas is necessary in order to obtain the requested hydrogen-to-methane ratio (H_2/CH_4 = 1/3) in the hydromethane stream.

The separation of CO_2 by the PSA unit produces an off-gas, which can be sent to a cogeneration system or burned in flares depending on its methane content.

Here the design of a PSA process has been developed to treat a three-component mixture (the reformed gas represented by stream 4 in Fig. 2), to reduce its carbon dioxide content to <3 %, and to obtain at the same time high recoveries for both hydrogen and methane. Indeed, high recoveries of hydrogen and methane are desirable for the economic convenience of the process; in this work many efforts have been addressed to obtain an almost complete hydrogen recovery and a good methane recovery, at the same time maintaining low energy consumption.

3.2 PSA Simulation Model

A realistic simulation model able to describe the dynamic behavior of a PSA unit is necessary; the model must also be used to evaluate the process performances in

terms of purity, recovery, and energy requirement, and then for screening between different adsorbent materials and process cycle or scheduling.

In this chapter a dynamic nonisothermal model, previously reported in literature is used [6]. This model is based on the linear driving force approximation for the adsorption/desorption kinetics with a single lumped transport parameter for each component, $k_{\mathrm{LDF;}}$ thermal equilibrium between gas and solid phase and no heat exchange with the external environment are assumed; further details on the mathematical model are reported in the original paper [7].

The model development also requires adsorption equilibrium information, which in the present case has been described by multicomponent Langmuir adsorption isotherm.

$$\frac{q_i}{q_{\mathrm{max,i}}} = \frac{b_i p_i}{1 + \sum_j b_j p_j} \tag{1}$$

where q_i and p_i are the adsorbed amount and the partial pressure, respectively, of the ith component and $q_{\mathrm{max,}}$ and b_i are temperature-dependent isotherm parameters.

3.3 Adsorbent Materials

The most commonly used materials for separation by adsorption are activated carbon, zeolite, and carbon molecular sieves. Other materials, such as the more innovative metal organic frameworks (MOFs) or silico aluminate phosphates (SAPOs), can also be used to remove one or more components from a gas stream.

As previously mentioned, adsorbent materials can be classified based on the underlying mechanism of selectivity towards the components in the gas phase:

- equilibrium adsorbents, whose selectivity is related to the different capacity of adsorption of the different components on the solid, therefore to thermodynamic phase equilibrium properties
- kinetic adsorbents, whose selectivity is mainly due to the different diffusion rate of the components inside the solid particles, therefore to kinetic properties.

The classification depends on the type of gas system to be treated and can change from one system to another.

Since the goal of the process is the separation of CO_2 from a CH_4–H_2–CO_2 mixture, a material with high adsorption capacity together with high selectivity toward carbon dioxide is desirable. In fact, selectivity is the primary requirement to obtain the required purity while capacity determines the size and therefore the cost of the adsorbents beds.

A useful and rapid screening on the suitability of an adsorbent material towards the preferential adsorption of one component (component i) over the other (component j) may be effected by the assessment of selectivity. If the equilibrium

conditions are expressed by means of the Langmuir isotherm (1), the thermodynamic selectivity is given by

$$S_{i/j}^{\text{thermo}} = \frac{b_i q_{\text{max,i}}}{b_j q_{\text{max,j}}} \tag{2}$$

In this case, thermodynamic selectivity is independent of the operating pressure and gas composition.

If the adsorption/desorption kinetics is described in the framework of linear driving force approximation, the kinetic selectivity is given by

$$S_{i/j}^{\text{kin}} = \frac{K_{\text{LDF},i}}{K_{\text{LDF},j}} \tag{3}$$

where k_{LDF} is the lumped mass transfer coefficient.The overall selectivity is then given by

$$S_{i/j} = S_{i/j}^{\text{thermo}} S_{i/j}^{\text{kin}} \tag{4}$$

Table 3 shows the selectivity calculated at 25 °C for the three binary systems of three different adsorption materials.

As it can be observed, from the thermodynamic point of view, the preferential adsorption by the activated carbon follows the order $CH_4 > CO_2 > H_2$. The thermodynamic selectivity between CO_2 and CH_4, however, is not high. From the kinetic point of view, instead, it is highlighted that diffusion into the particle of solid adsorbent is faster for H_2 compared to CH_4 and even more with respect to CO_2; it is therefore clear that the thermodynamic selectivity for this system is not enhance by selectivity. The total selectivity shows that the separation of CH_4 from H_2 is rather facilitated, while the separation of CO_2 from H_2 is less easy. The separation of CO_2 from CH_4 is difficult as shown by the value of the total selectivity for the CO_2–CH_4 system, which is not far from unit.

Table 3 Selectivity values of three adsorption materials for the three binary systems

	$S_{i/j}^{\text{thermo}}$	$S_{i/j}^{\text{kin}}$	$S_{i/j}$	Adsorbent material
CO_2–H_2	60.9	0.051	3.1	Activated carbon [8]
CH_4–H_2	29	0.28	8.12	
CO_2–CH_4	2.1	0.18	0.378	
CO_2–H_2	1052.46	0.019	20	Zeolite 5A [8]
CH_4–H_2	33.98	0.21	7.14	
CO_2–CH_4	30.97	0.092	30.97	
CO_2–H_2	46	0.32	14.7	MOF [9]
CH_4–H_2	8.8	0.37	3.26	
CO_2–CH_4	5.24	0.9	4.72	

With regards to the zeolite, Table 3 shows the high thermodynamic selectivity towards the CH_4 and even more towards CO_2 in the binary systems CH_4–H_2 and CO_2–H_2. A good thermodynamic selectivity towards CO_2 in the CO_2–CH_4 is also noticeable. From the kinetic point of view, the rate of diffusion of the three components follows the order $H_2 > CH_4 > CO_2$ and the behavior is not very different from that of the activated carbon. Overall, the separation of the H_2 from CH_4 and CO_2 seems easily achievable while the separation of CH_4 from CO_2 is difficult.

The thermodynamic behavior of the MOF, for the CH_4–H_2 and CO_2–H_2 binary systems is qualitatively similar to that of zeolite, with a preferential adsorption of CH_4 and CO_2 with respect to H_2. From the kinetic point of view, the same behavior may be observed for the two systems, with the hydrogen diffusing more rapidly than CO_2 and CH_4.

For the CO_2–CH_4 system, the thermodynamic selectivity is in favor of CH_4, while kinetically the solid is not selective. Overall, the MOF seems to be the most suitable material for the complete separation of the three components.

In this chapter, the activated carbon reported in [8] has been chosen as adsorbent material; Fig. 3 shows the adsorption isotherms of the three pure components on the activated carbon at 25 °C; the figure shows that under equilibrium conditions the most adsorbed component is CO_2, which is also the component to be separated. Methane is adsorbed in a comparable amount as has been predicted by the rather low value of the thermodynamic selectivity towards the two components.

The nonlinearity of the adsorption isotherm of CO_2 in the pressure range that can interest an operation of separation by PSA can also be observed; in practice, with such adsorption isotherm, regeneration must be carried out under vacuum, thus realizing a VPSA.

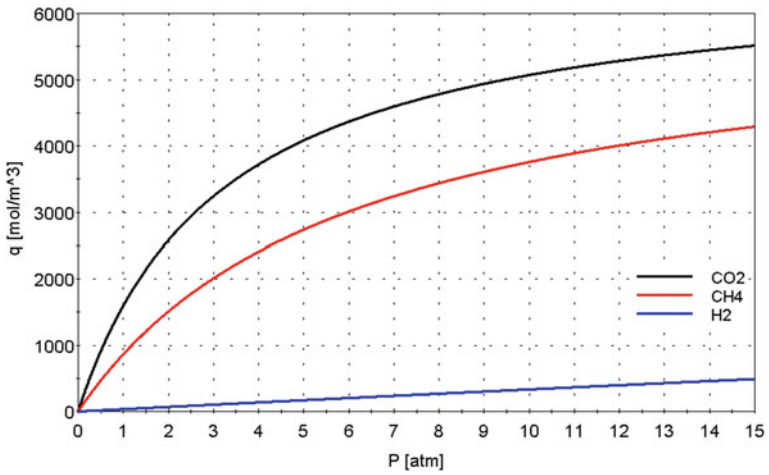

Fig. 3 Adsorption isotherm of CO_2, CH_4, and H_2 on activated carbon at 25 °C

Further properties of the adsorbent material and the simulation parameters are reported in the original paper [7].

3.4 PSA Cycles for CO_2 Separation from CH_4–CO_2–H_2 Mixture

The work presented below has been aimed to identifying cycles to be implemented in multibed systems that allow to obtain the specific separation required (CO_2 < 3 %) with high recoveries of H_2 (>95 %) and possibly with good recovery of methane. Both the cycles introduced operate with a VPSA system at a minimum pressure of 0.1 atm and the maximum pressure of 13 atm; the maximum pressure value has been chosen accounting for the pressure in the reforming reactor (15 atm) and the pressure drops in the dehydration unit and in the connecting pipelines.

3.4.1 Cycle A

The first identified cycle (cycle A) is a classical Skarstrom cycle (see Fig. 4) and consists of four phases:

1. Feed (FE), where the reformed gas is fed at 13 atm; during this phase, preferential adsorption of carbon dioxide takes place.

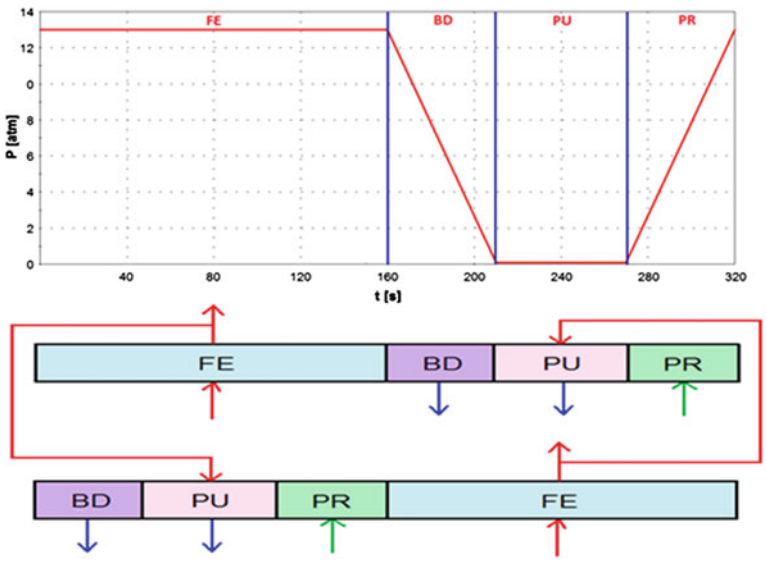

Fig. 4 Pressure profile, phase sequence, and interconnections between the columns of the cycle A

2. Blow-down in counter-current with FE (BD), where the pressure is reduced to 0.1 atm; during this phase, a first partial regeneration of the column occurs.
3. Counter-current purge (PU), where part of the produced gas is fed at low pressure to the column in order to complete the column regeneration;
4. Co-current pressurization (PR), during which the column is pressurized with the reformed gas up to 13 atm.

In order to make the gas production continuous, the PSA unit is composed of two interconnected columns; Fig. 4 shows the pressure profile in the first column and the interconnections between the columns.

In Table 4, the column size, operating conditions, and cycle timing are specified. To achieve the specific separation, it has been decided to divide the reformed gas between two PSA units operating in parallel; it is also noted that, for each unit, the second column operates with a phase shift of 160 s (of the duration of the phase of feed) relative to the first to ensure the continuous production product stream.

Table 5 shows the performance and the energy consumption (for kg of hydrogen in the product) of cycle A; it must be noted that the energy consumption is only due to the vacuum pump, since the reformed gas is already at the pressure at which the PSA unit operates.

Table 5 shows that this cycle allows to reach the required on CO_2 separation, with quite low energy consumptions; unfortunately both hydrogen and methane recoveries are low, making the process unsuitable for hydromethane production from an economical point of view.

Therefore, a different, modified PSA cycle is considered in order to improve the hydrogen and methane recovery.

Table 4 Column sizes, operating conditions, and timing of proposed cycles

Cycle			A	B
PSA unit			2	1
Number of columns per unit of PSA			2	4
Column sizes				
	Diameter	m	0.35	0.44
	Length	m	1.3	1.5
	Bed porosity	–	0.43	0.43
	Bed density	kg/m^3	484.5	484.5
	Activated carbon per column	kg	60.6	110.5
Cycle timing				
	Feed	s	160	160
	Equalization	s	–	20
	Blow-down	s	50	140
	Purge	s	60	160
	Pressurization	s	50	140

Table 5 Performances and energy consumption of the proposed cycles

	Composition			Recovery		Energy consumption (kJ/kg_{H2})	Electric power (kW)
	Feed (%)	Product (%)	Off-gas (%)	Product (%)	Off-gas (%)		
Cycle A							
CH_4	48	16	72.6	14.6	–	2700	4.5
CO_2	12	1.8	19.1	–	89.1		
H_2	40	82.2	8.3	88.2	–		
Cycle B							
CH_4	48	30.6	73.2	37.2	–	1300	4.5
CO_2	12	2.5	25.3	–	87.8		
H_2	40	66.9	1.5	98.4	–		

3.4.2 Cycle B

Cycle B is derived from the classical Skarstrom cycle (cycle A) with the addition of a pressure equalization before the blow-down, as shown in Fig. 5. The equalization step consists of connecting a column that is at the end of the feeding step at high

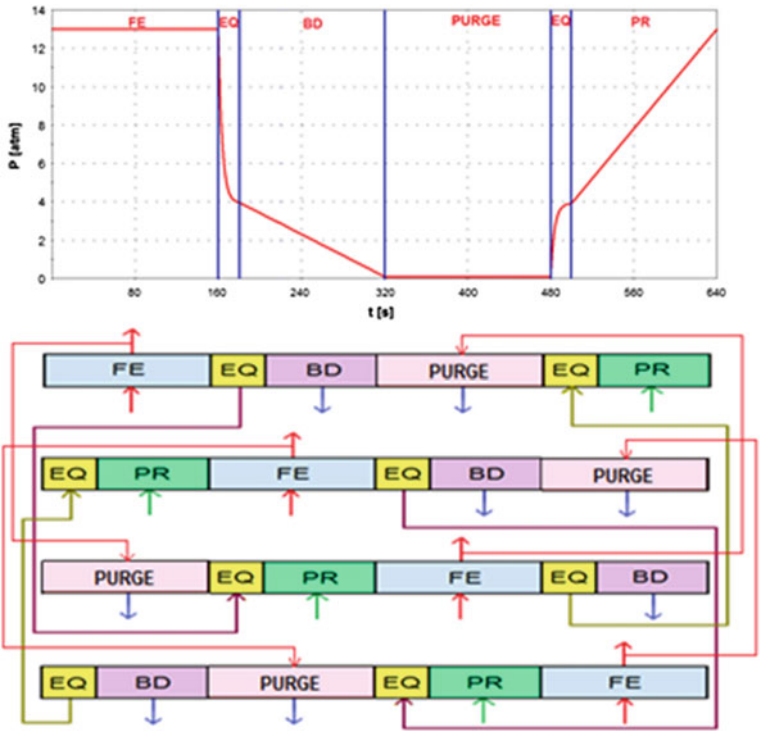

Fig. 5 Phases sequence and interconnections between the columns of the cycle B

pressure, with the one that is at the end of the purge phase at low pressure; in this way the gas exiting the first column is used to pressurize the second column, until the two columns are brought practically at the same pressure. This operation allows to recover part of the hydrogen-rich gas that would otherwise be lost with the off-gas and at the same time to reduce the energy consumption due to the lower energy requirement to pressurize the column after the purge step. On the other hand, as shown in Fig. 5, the introduction of the equalization step forces to work with four columns in order to ensure a continuous production.

In Table 4, the column sizes and other operating conditions of this cycle are reported; a single PSA unit of four columns has been used, but with columns larger than those of the previous cycle. The timing ensures the continuity of production. In this case columns work shifted at 160 s compared to each other.

In Table 5, the cycle performances and the energy consumption of the cycle are shown.

The significant increase in hydrogen recovery (which is recovered almost completely) due to the equalization step is immediately evident; methane recovery has increased by 23 %, even if more than 60 % of methane is still present in the off-gas. The energy consumption, referred to the produced hydrogen, is significantly decreased, due to the reduced energy consumption caused by the introduction of the equalization step, and also due to the increase in hydrogen recovery. For this cycle, a single vacuum pump is required, since only a single PSA unit is provided.

3.5 The Off-gas

Both the analyzed cycles have allowed the achievement of the specified separation of CO_2 and in particular the second cycle has shown a very good result in terms of hydrogen recovery and a great improvement in methane recovery, even if the reached value is rather still low. Indeed in both cycles an off-gas with high methane content has been produced. This stream, mainly composed by CH_4 and CO_2 with methane content >70 %, is therefore an excellent fuel that can be earmarked for a cogeneration system (CHP) for the combined production of thermal and electrical energy.

Considering the off-gas produced in cycle B and assuming an electrical power generation efficiency of 35 % and a thermal power generation efficiency of 70 %, it is possible to recover 0.37 MW of electric power (which corresponds to 108.2 MJ/kgH_2 in the product) and 0.48 MW of thermal power. Therefore, a small portion of the electrical energy (<2 %) obtained from the cogeneration system is used for the PSA operation, and the remaining part can be fed into the local power grid.

As an alternative to the CHP, the off-gas can be treated to recover methane in a gas stream with carbon dioxide content lower than 3 %; again such a separation can be carried out in a PSA unit, using an adsorbent material with high selectivity for carbon dioxide adsorption.

3.6 PSA for CH_4 Recovery

In order to recover methane from the off-gas, a PSA unit with carbon molecular sieve (CMS) as adsorbent material is considered. Equilibrium and kinetic parameters for CH_4 and CO_2 adsorption on this material are reported in [10]; these values have been used to evaluate the thermodynamic and kinetic selectivity reported in Table 6. It is worth noting that selectivity is mainly due to the difference in the adsorption kinetics; in fact in this case the difference in diffusion rate is so high that methane is totally excluded from the adsorbent. Moreover, the thermodynamic selectivity for carbon dioxide strengthens the separation capability of CMS.

In Fig. 6 the adsorption isotherms of the two pure components on CMS at 25 °C are shown; also for this material, the nonlinearity of the adsorption isotherm of CO_2 requires to operate the regeneration of the adsorption column under vacuum.

Due to the very low hydrogen content in the off-gas, PSA unit for methane recovery is designed referring to a two-component system (CO_2 and CH_4); design has been carried out in order to obtain a product gas with CO_2 content lower than 3 %, which can be used as diluent gas to reach the optimal hydrogen-to-methane ratio in the hydromethane stream. In Table 7, the column size, operating conditions, and cycle timing are specified; a pressure of 4 bar has been set during the adsorption phase, while the minimum pressure of the cycle has been set equal to 0.1 bar.

Table 8 shows the cycle performances in terms of gas composition and methane recovery. The energy consumption (for kg of recovered methane) is also evaluated, taking into account both the energy required to compress the feed up to maximum

Table 6 Selectivity values of CMS for the three binary systems at 25 °C (from thermodynamic and kinetic parameters reported in ([11])

	$S_{i/j}^{thermo}$	$S_{i/j}^{kin}$	$S_{i/j}$	Adsorbent material
CO_2–CH_4	5.2	173.3	901.3	CMS [11]

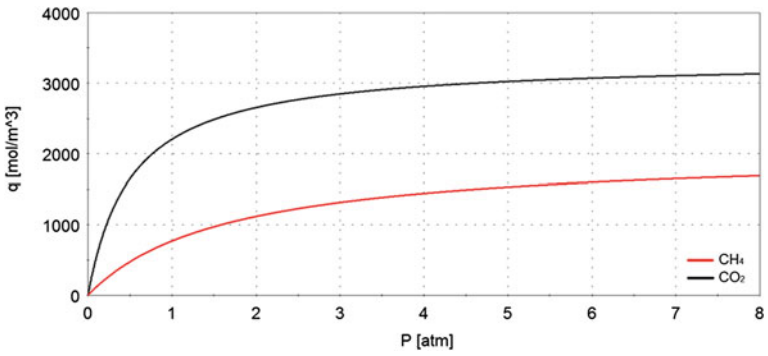

Fig. 6 Adsorption isotherm of CO_2, CH_4 on CMS at 25 °C

Table 7 Column sizes, operating conditions, and timing

PSA unit			1
Number of columns per unit of PSA			4
Column sizes			
	Diameter	m	0.65
	Length	m	2
	Bed porosity	–	0.41
	Bed density	kg/m^3	683.2
	Activated carbon per column	kg	453.4
Cycle timing			
	Feed	s	90
	Equalization	s	20
	Blow-down	s	70
	Purge	s	90
	Pressurization	s	70

Table 8 Performances and energy consumption

	Composition			Recovery		Energy consumption (kJ/kg_{CH4})	Electric power (kW)
	Feed (%)	Product (%)	Off-gas (%)	Product (%)	Off-gas (%)		
CH_4	74	97.1	38	80	–	1220	21
CO_2	26	2.9	62	–	93.2		

pressure of the PSA cycle (4 bar) and the energy required to compress the produced gas up to pressure of the hydrogen-rich gas to be diluted to obtain the optimal H_2–to–CH_4 ratio in the hydromethane (13 bar).

It is worth noting that a methane recovery of 80 % is obtained; on the other hand, the off-gas has a methane content (38 %) high enough to be burned without external fuel.

3.7 Overall Process

The overall process scheme is shown in Fig. 7, while mass balances and operating conditions are reported in Table 9.

The overall process operate with a complete hydrogen recovery and a methane recovery >88 %. The energy consumption is about 270 kJ/kg of produced hydromethane.

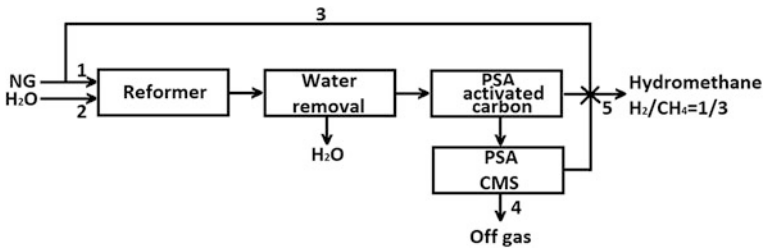

Fig. 7 Process of production and purification of hydromethane mixture

Table 9 Streams' characteristics of the process

	Flow rate		Composition (%)				T (°C)	P (atm)
	kg/h	Nm^3/h	CH_4	CO_2	H_2	H_2O		
1	157.8	210	97	3	–	–	500	15
2	490.7	611	–	–	–	100	500	15
3	208.7	277.8	97	3	–	–	25	15
4	81.8	55.2	62	38	–	–	25	1
5	341.1	571.55	72.9	2.8	24.3	–	25	13

4 Conclusions

In the context of production of a hydrogen-methane mixture (20–30 %vol. of H_2) by solar-driven steam reforming of natural gas, the use of the PSA technology for the reformed gas purification seems very interesting; the reformed gas, in fact, needs to be purified to reduce the CO_2 content to <3 %, in order for it to be used in an internal combustion engine; on the other hand, for the process to be economically convenient, the separation process must have high hydrogen and methane recovery.

In this work, the first PSA unit, using an activated carbon as adsorbent material, has been designed to reduce the carbon dioxide content to <3 %. The off-gas obtained has still high methane content and can be used for combined heat and electrical energy production in a CHP unit or can be sent to the second PSA unit, using carbon molecular sieve as adsorbent material, to recover methane. In the last case, the whole process allows to obtain a complete hydrogen recovery and a methane recovery of 88 %, with a low energy consumption of 270 kJ/kg of produced hydromethane.

References

1. Dufour J, Martos C, Ruiz A (2012) Water gas shift reaction, Nova Science Publishers
2. Villante C, Genovese A (2012) Hydromethane: A bridge towards the hydrogen economy or un unsustainable promise? Int J Hydrogen Energy 37:11541–11548
3. Tirler W, Voto G, Donegà M, Mair K, Gallmetzer M, Klauser T, Huber W, De Sangro G, Capoccia M, Rampelotto F, Fazzari G, Grimolizzi L (2012) The use of methane-hydrogen mixtures in buses. In: 16th ETH-Conference on combustion generated nanoparticles
4. Skarstrom CW (1958) Patent 2,944,627, Feb 1958
5. De Falco M, Caputo G, Frattari S, Gironi F, Annesini M (2014) Solar steam reforming for enriched methane production: reactor configuration modeling and comparison. Int J Hydrogen Energy 39:13979–13990
6. Ruthven D, Farooq S, Knaebel K (1994) Pressure swing adsorption, VCH Publishers
7. Annesini M, Augelletti R, Frattari S, Gironi F, Murmura M, CO_2 removal by pressure swing adsorption from CO_2–CH_4–H_2 mixture produced by naturala gas steam reforming at low temperature
8. Ahn S, You YW, Lee DG, Kim KH, Oh M, Lee CH (2012) Layered two- and four-bed PSA processes for H2 recovery from coal gas. Chem Eng Sci 68:413–423
9. Silva B, Solomon I, Ribeiro AM, Lee UH, Hwang YK, Chang JS, Loureiro JM, Rodrigues AE (2013) H_2 purification by pressure swing adsorption using CuBTC. Sep Purif Technol 118:744–756
10. Annesini M, Augelletti R, De Falco M, Frattari S, Gironi F, Murmura MA (2015) Production and purification of hydrogen-methane mixtures utilized in internal combustion engines. In: 7th WIT-International conference on sustainable development and planning, Istanbul
11. Kapoor A, Yang RT (1989) Kinetic separation of methane- carbon dioxide mixture by adsorption on molecular sieve carbon. Chem Eng Sci 44(8):1723–1733

Emissions and Efficiency of Turbocharged Lean-Burn Hydrogen-Supplemented Natural Gas Fueled Engines

James S. Wallace

Abstract The use of hydrogen fuel to supplement conventional hydrocarbon engine fuels is of interest as a means of developing hydrogen supply infrastructure, without the challenges of developing dedicated hydrogen-fueled vehicles. Mixing hydrogen with natural gas is the most straightforward means of implementation as both can be mixed and stored in conventional high pressure compressed gas cylinders. The primary benefit of hydrogen supplementation for IC engines is to allow leaner operation than with operation on natural gas alone while maintaining high combustion efficiency. Results from both engine and vehicle studies confirm that hydrogen supplementation improves the NO_x–hydrocarbon emission trade-off compared to natural gas as a result of leaner operation. The difference between the leanest air–fuel ratio for hydrogen-containing mixtures and the leanest air–fuel ratio for natural gas decreases with engine load. Thus, the extent of improvement in the NO_x–hydrocarbon trade-off diminishes at high loads. As a result, the extent of improvement in real-world use will depend on driving cycle. Finally, fuel consumption is a third dimension in the NO_x–hydrocarbon trade-off. As a result, not only the emissions but also the impact on fuel consumption must be taken into account in selecting the air–fuel ratio, spark timing, and other factors that constitute an engine calibration.

Keywords IC engines · Enriched methane use · NO_x–hydrocarbon emissions · Engine calibration

List of Acronyms

BMEP	Brake mean effective pressure
BSCO	Brake specific carbon monoxide
BSTHC	Brake specific total hydrocarbon
$BSNO_x$	Brake specific oxides of nitrogen
CO	Carbon monoxide

J.S. Wallace (✉)
Department of Mechanical and Industrial Engineering, University of Toronto,
5 King's College Road, Toronto, ON M5S 3G8, Canada
e-mail: wallace@mie.utoronto.ca

M. De Falco and A. Basile (eds.), *Enriched Methane*,
Green Energy and Technology, DOI 10.1007/978-3-319-22192-2_9

CO_2	Carbon dioxide
CSHVR	City–Suburban Heavy Vehicle Route
H2NG	Mixture of hydrogen and natural gas
HxxNG	Mixture with xx % hydrogen and (1-xx) % natural gas by volume
IC	Internal combustion
MBT	Minimum timing for best torque
NG	Natural gas
NO	Nitric oxide
NO_2	Nitrogen dioxide
NO_x	Oxides of nitrogen, the sum of NO and NO_2
OCTA	Orange County Transit Authority
PM	Particulate matter
THC	Total hydrocarbon

1 Introduction

The use of hydrogen fuel as a supplement to conventional hydrocarbon engine fuels has been extensively investigated by numerous research groups. A strong motivation for using hydrogen fuel supplementation is to begin developing hydrogen infrastructure, without the challenges associated with a dedicated hydrogen-fueled vehicle. One of those challenges is onboard storage. Hydrogen storage systems have significant size, weight, and energy penalties compared to common liquid vehicle fuels [1]. Mixing hydrogen with natural gas is the most straightforward means of implementing hydrogen supplementation. Both hydrogen and natural gas are in the gaseous state at normal ambient conditions and can be mixed easily. Both hydrogen and natural gas are commonly stored on vehicles in high pressure gas cylinders [2]. As long as the proportion of hydrogen in the fuel remains relatively small, the loss of range compared to compressed natural gas is small enough be tolerated. For example, there is about a 15 % loss of range for a mixture of 20 hydrogen and 80 % natural gas by volume compared to 100 % natural gas [3] assuming equal engine efficiency on both fuels.

From the standpoint of an internal combustion engine, the primary benefit of hydrogen-supplemented natural gas arises from the increase in laminar flame speed and widening of the lean flammability limit that occur as hydrogen is added. These factors enable operation at a leaner overall air–fuel ratio, which improves the trade-off between oxides of nitrogen (NO_x) emissions and total hydrocarbons (THC) in the exhaust. In the context of greenhouse gas emissions, the addition of hydrogen to natural gas increases the hydrogen-to-carbon ratio in the fuel. This reduces the CO_2 emissions per unit of fuel energy.

As well, by limiting the amount of hydrogen present in the fuel, the combustion difficulties, especially surface ignition, that occur with 100 % hydrogen fueling can

be avoided. This eliminates the need for the engine modifications typically required for a dedicated hydrogen IC engine [4, 5].

Numerous studies have been conducted in an effort to assess the potential of hydrogen-supplemented natural gas [6–20]. These studies can essentially be divided into two groups according to the fueling strategy employed: stoichiometric operation or lean-burn operation. This chapter focusses on lean-burn operation.

The studies that explored lean-burn operation (e.g. [6–10]) found similar results, namely that for a given fuel–air equivalence ratio, THC emissions are substantially lower, NO_x emissions are higher, and CO emissions are about the same when hydrogen-supplemented natural gas was used compared to natural gas only. In practice, the main benefit of hydrogen supplementation arises from the extended lean operating limit enabled by the hydrogen. Strothers [8], for example, found that the lean operating limit is 6.3–12.5 % leaner with hydrogen supplementation than with natural gas only. NO_x levels at the lean operating limit with hydrogen-supplemented fuels can be reduced below the levels of NO_x at the lean operating limit of natural gas, with low CO emissions and equivalent or lower THC emissions. Two of the studies [8, 9] also reported that hydrogen supplementation improved engine efficiency.

Most of the previous research was conducted with naturally aspirated engines. As will be demonstrated in the next section, turbocharging is required with lean-burn engines to achieve the required torque and power output. The objective of this chapter is to review and compare the exhaust emissions and efficiency of lean-burn turbocharged engines operating on hydrogen-supplemented natural gas to operation on natural gas only.

2 The Need for Turbocharging

The relative air–fuel ratio, λ (lambda), quantifies lean mixtures. Lambda is the actual air–fuel ratio divided by the stoichiometric air–fuel ratio for that fuel. Values greater than one indicate a lean mixture.

The lean-burn operating strategy has been widely employed for natural gas fueled stationary engines, as well as in some medium and heavy-duty vehicles. However, the volumetric energy content of the intake fuel–air mixture decreases as the mixture is made leaner (λ increased). It is therefore necessary to boost the intake manifold pressure of lean-burn engines by turbocharging or supercharging in order to maintain a given torque output as the mixture is leaned. Figure 1 shows the relative intake manifold absolute pressure required to maintain a constant torque output as a function of lambda. The lines represent theoretical values where 100 % methane is used to represent natural gas. The reference torque output is for operation on natural gas at $\lambda = 1.4$. Note that additional boost is required for hydrogen containing mixtures compared to 100 % methane. The symbols on the figure are actual intake manifold absolute pressure data for a lean-burn turbocharged engine operating at 5.2 bar bmep on 100 % natural gas, NG, as well as on a mixture of

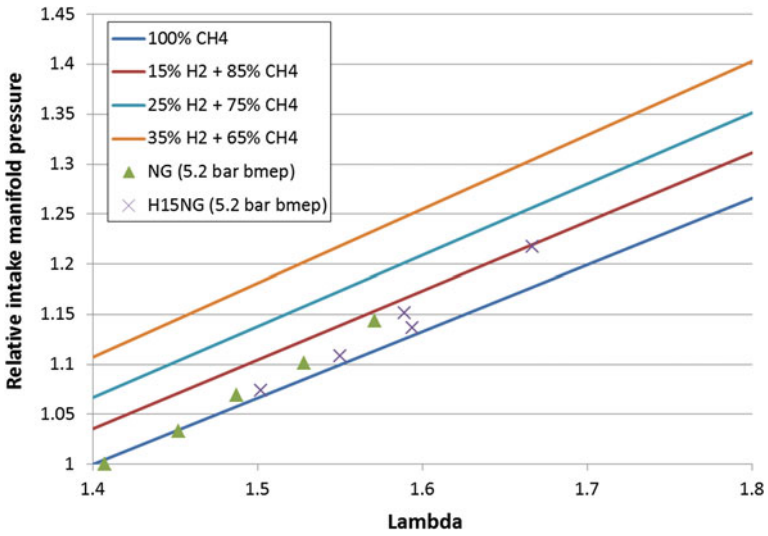

Fig. 1 Relative intake manifold absolute pressure required to maintain torque output at the level for natural gas operation at $\lambda = 1.4$. The *lines* are calculated values; the *points* are experimental measurements

15 % hydrogen in natural gas, H15NG [12]. MBT timing (minimum timing for best torque) was used. The reference condition for these experimental results is also operation on natural gas at $\lambda = 1.4$. While many factors affect the torque output, the experimental data show good agreement with the projections.

Figure 1 illustrates that maintaining torque output even at a very modest 5.2 bar bmep requires boosting as the mixture is leaned. This is true even for natural gas, but the introduction of hydrogen increases the pressure boosting requirements. While there have been many studies of lean-burn hydrogen-supplemented natural gas engines, most have been conducted with naturally aspirated engines. Consequently, the results obtained with naturally aspirated engines may not be fully representative of the turbocharged engines needed to have sufficient torque for practical applications.

3 Turbocharged Lean-Burn Engine Studies

The most comprehensive studies of turbocharged lean-burn hydrogen-supplemented natural gas fueled engines are the studies carried out by Larsen and Wallace [12], Saanum et al. [18] and Munshi et al. [3]. Table 1 compares test engine parameters for these three studies. The engine used by Larsen and Wallace was converted from gasoline operation, so it does not have a rated output for natural gas operation.

Table 1 Test engine parameters for lean-burn turbocharged H_2NG studies

	Larsen and Wallace [12]	Saanum et al. [18]	Munshi et al. [3]
Manufacturer and model	GM 3.2	–	–
Number of cylinders	V-6	I6	I6
Displacement (liters)	3.2	9.6	5.9
Bore (mm)	89	120.7	102
Stroke (mm)	84	140	120
Compression ratio	8.8:1	11.8:1	10.5:1
Rated power	–	184 kW at 2000 rpm	172 kW@ 2800 rpm
Rated torque	–	1150 N-m @ 1150 rpm	677 N-m @ 1600 rpm

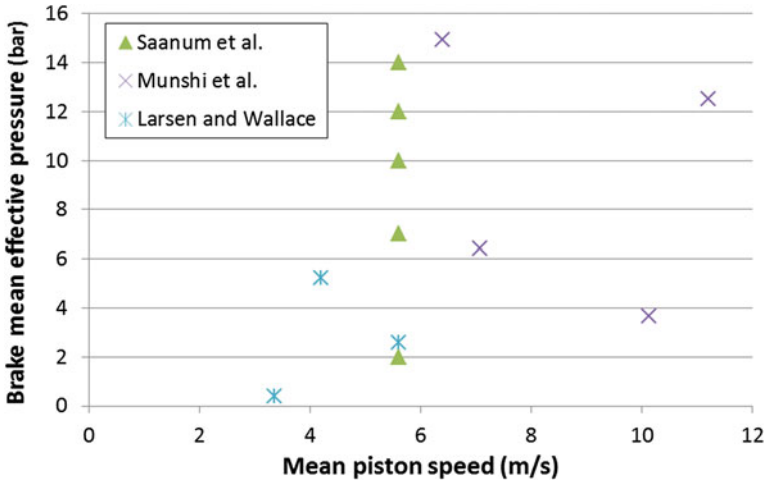

Fig. 2 Engine test conditions employed by various lean-burn hydrogen-supplemented turbocharged natural gas engine researchers

Figure 2 summarizes the test points chosen by each of these three research groups. Due to the different engine sizes, the test points are expressed in terms of the size independent parameters of brake mean effective pressure (bmep) and mean piston speed. The results of Saanum et al. [18] and Munshi et al. [3] cover a range up to 14 bar bmep, a much more practical output level for current engines. Note that the engine test results published by Munshi et al. are presented primarily in the form of relative changes with respect to a baseline condition, which makes comparison to other data sets more difficult. The subsequent discussion will focus on the results of these three research groups to illustrate the opportunities and challenges associated with hydrogen supplementation of natural gas in lean-burn turbocharged engines.

Results are also available for transient testing of transit buses. Using a heavy-duty chassis dynamometer, Munshi et al. [3] tested four 40 ft. transit buses

powered by Cummins-Westport B5.9 Gas Plus natural gas engines, the same engine used for their engine dynamometer tests (Table 1 and Fig. 2). Two of the buses were operated on natural gas and two of the buses were operated on H20NG fuel. Two transient test procedures were used: the Orange County Transit Authority (OCTA) cycle representing intermediate speed heavy-duty vehicle operation and the City-Suburban Heavy Vehicle Route (CSHVR) cycle, representing heavy-duty vehicle operation in delivery areas between expressways and stop-and-go downtown areas. Higher engine power levels are achieved during the CSHVR test compared to the OCTA cycle. The transit bus test results will be discussed along with the engine dynamometer test results.

4 Comparison and Discussion of Published Results

The discussion of results will begin by examining the effect of hydrogen supplementation on MBT spark timing requirements. Emissions of NO_x, CO, and THC will be compared and data on particulate matter emissions presented. Finally, the effect of hydrogen supplementation on engine efficiency will be identified.

To simplify fuel description, hydrogen-containing mixtures will be denoted by "HxxNG", where the "xx" indicates the percentage by volume of hydrogen "H" contained in the fuel gas mixture and the "NG" indicates that natural gas is the balance of the fuel gas. For example, "H15NG" identifies a fuel gas consisting of 15 % hydrogen and 85 % natural gas. The symbol "NG" without a prefix denotes 100 % natural gas.

5 Amount of Hydrogen Supplementation

The rational for hydrogen supplementation is to allow leaner engine operation, which in turn should reduce NO_x emission and reduce fuel consumption on an energy basis. The ability to operate leaner depends on engine load. Figure 3 shows the lambda values that produce the best efficiency at different loads for natural gas and a mixture containing 25 % hydrogen [18]. Note that at the highest load, the effect of hydrogen supplementation diminishes to effectively zero. Two factors may contribute to this effect: the higher in-cylinder temperatures and pressures at high load reduce the impact of hydrogen on reaction kinetics and the greater air flow through the engine at high loads may result in increased combustion chamber turbulence, which would reduce the impact of kinetics on combustion rate.

Figure 4 shows the difference—the lambda offset—between the two curves in Fig. 3 plotted as a function of load. The individual lambda offset points shown at a load of 12.5 bar bmep are results obtained by Munshi et al. for fuel gas mixtures containing varying amounts of hydrogen. Their results suggest little benefit of increasing the hydrogen concentration beyond 25 %. They also did a weighted

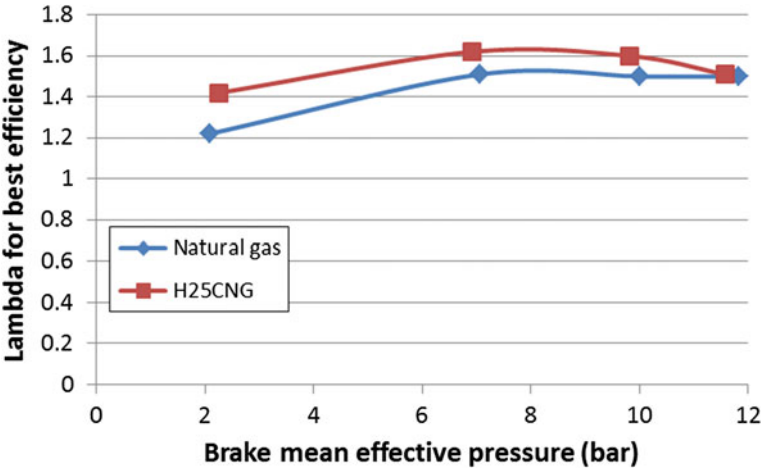

Fig. 3 Best efficiency lambda values as a function of engine load (bmep) [18]

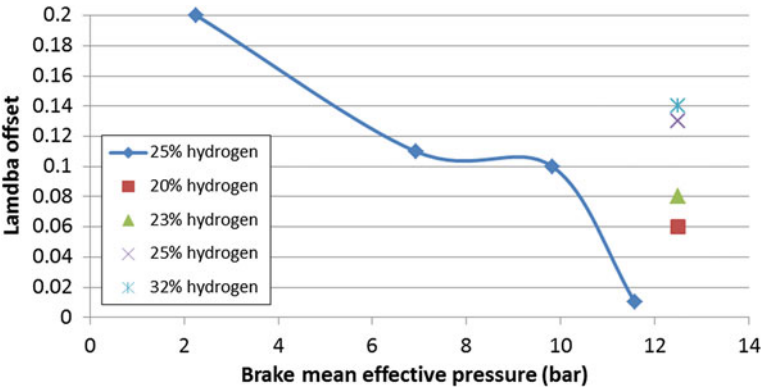

Fig. 4 Lambda offset as a function of engine load for mixture containing various amounts of hydrogen. Data sources: *line* Saanum et al. [18]; individual *points* Munshi et al. [3]

factor analysis to determine the optimum hydrogen concentration. Taking four factors into consideration, (1) NO_x reduction ability, (2) ability to maintain engine performance, (3) ease of vehicle conversion for hydrogen-containing mixtures, and (4) economics, fuel blends with a concentration in the range of 20–23 % by volume were determined to be optimal for this particular project and a 20 % concentration of hydrogen was used in all of their subsequent tests [3]. Although this finding applies to a particular application, a transit bus, it illustrates that a point of diminishing returns is reached as the hydrogen concentration in the fuel gas is increased. The optimum concentration may well be lower for other applications, but given the relatively high loads considered in their optimization, a concentration of about 25 % could be regarded as an upper bound.

6 MBT Spark Timing

It is well known that the addition of hydrogen to natural gas increases the burning velocity. A more rapid burning velocity reduces the combustion duration, which in turn reduces the need for spark advance. Figure 5 shows MBT timing requirements as a function of lambda for both natural gas and 15 % hydrogen in natural gas for two different test conditions [12]. At a given value of lambda, the addition of 15 % hydrogen to the fuel reduces the MBT timing by as much as 10° compared to operation on 100 % natural gas.

Munshi et al. [3] explored the effect of the amount of hydrogen supplementation on MBT spark advance at a high load test condition (the operating point 12.5 bar bmep, 11.2 m/s mean piston speed in Fig. 2). Figure 6 shows that their engine consistently required 3.6° less spark advance for mixtures containing up to 32 %

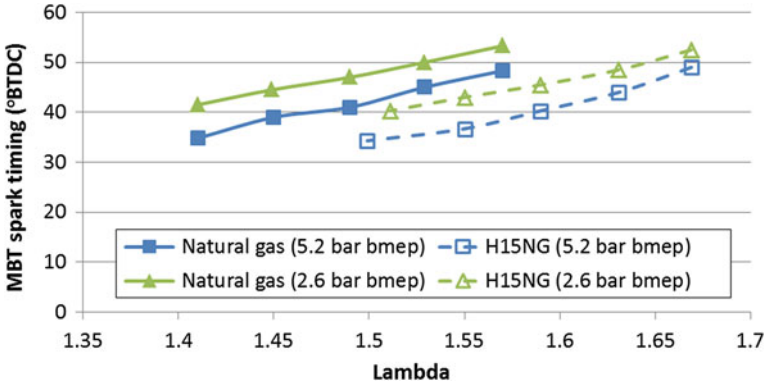

Fig. 5 MBT timing as a function of lambda for operation on natural gas and on mixtures of 15 % hydrogen in natural gas [12]

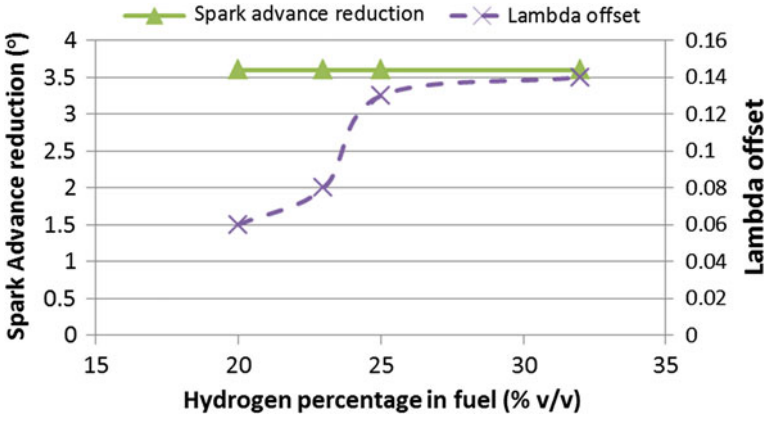

Fig. 6 Effect of fuel gas hydrogen content on MBT spark advance and lambda. Data from Munshi et al. [3]

hydrogen by volume. Note also in Fig. 6 that larger amounts of hydrogen in the fuel allow operation with leaner mixtures (higher lambda). Lambda offset refers to the difference in lambda between operation on the hydrogen-containing mixtures and operation on natural gas only.

7 Oxides of Nitrogen Emissions (NO_x)

The formation of nitric oxide (NO) is favored by high temperatures and the availability of oxygen. Since oxygen is readily available in a lean-burn engine, peak combustion temperature is the primary determinant of the level of NO_x emissions. For lean-burn engines, control of peak temperature is accomplished by control of air–fuel ratio by dilution with excess air. Because NO formation is rate limited, the temperature–time history is also important in addition to the magnitude of the peak temperature. Temperature–time history depends on details of the combustion process, especially combustion duration. Combustion duration also has some dependence on air–fuel ratio as well as on engine specific combustion chamber characteristics.

Consider first peak temperature. As a frame of reference, the adiabatic flame temperature for an atmospheric pressure stoichiometric hydrogen–air mixture is 2384 versus 2227 K for a stoichiometric methane air mixture [21]. Thus, a hydrogen-supplemented natural gas–air mixture would be expected to have a higher flame temperature in an engine than a natural gas–air mixture having the same lambda. This suggests higher NO_x emissions for the hydrogen-supplemented mixture, without taking combustion duration into account.

Figure 7 shows brake-specific NO_x emissions ($BSNO_x$) at MBT as a function of lambda for the two fuels (NG and H15NG) at two different load conditions [12]. At 65 N-m load, the H15NG fuel does, as expected, have higher $BSNO_x$ emissions than NG at the same value of lambda. However, the H15NG mixture allows the engine to be operated leaner overall (greater lambda), which can achieve lower $BSNO_x$ emissions than the leanest NG operating point. At the 130 N-m load, $BSNO_x$ for the two fuels are very comparable in the region where lambda values overlap, with the H15NG mixture even having lower $BSNO_x$ in some cases. This is likely a result of short combustion duration at the higher temperatures associated with the higher load. At 130 N-m load, the H15NG mixture can be operated at a much leaner condition than NG, and this results in significantly lower $BSNO_x$ emissions. However, there is a trade-off between $BSNO_x$ and BSTHC with increasing lambda and this tradeoff will be discussed in a subsequent section.

Figure 7 shows total oxides of nitrogen (NO_x), where NO_x consists of two species, nitric oxide (NO) and nitrogen dioxide (NO_2). NO typically accounts for 80 or 90 % of the total NO_x. However, Fig. 8 shows that the proportion of NO_2 increases sharply as the overall level of NO_x decreases below 200 ppm [12]. Note that the NO_2/NO_x ratio is independent of fuel type (NG or H15NG) and appears to depend only on overall NO_x concentration.

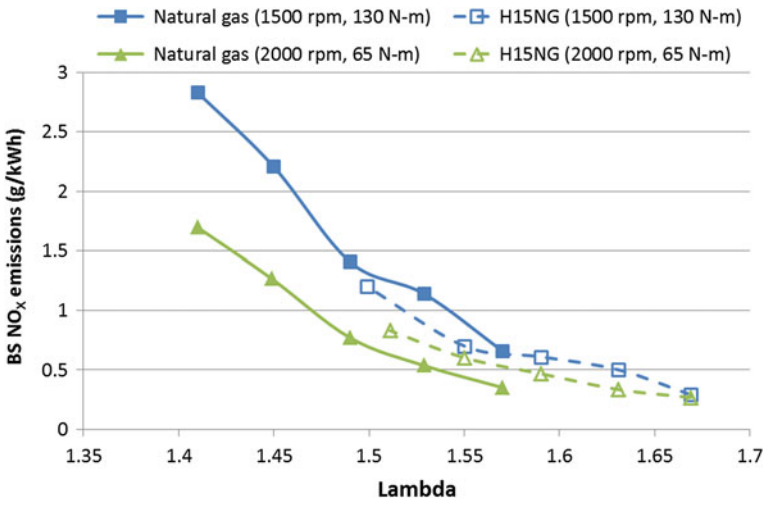

Fig. 7 Brake-specific oxides of nitrogen ($BSNO_x$) emissions at MBT as a function of lambda [12]

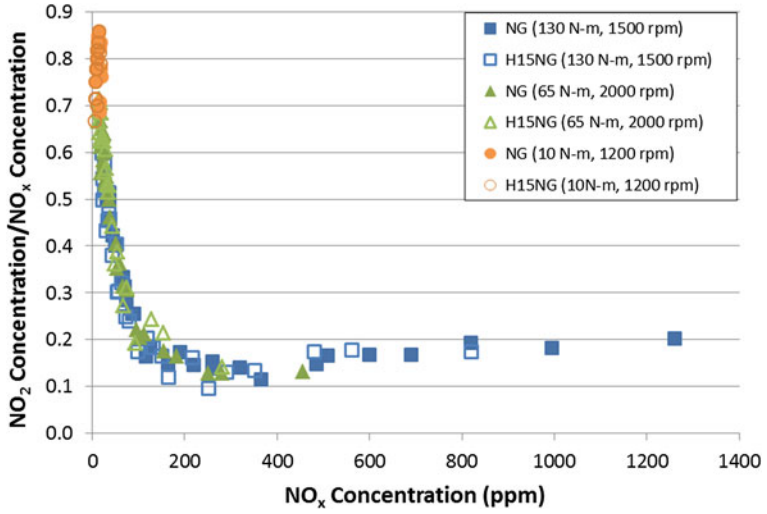

Fig. 8 NO_2/NO_x ratio as a function of overall NO_x concentration (ppm by volume) [12]

7.1 Vehicle Emissions of NO_x

In their chassis dynamometer tests of transit buses, Munshi et al. found that use of H20NG fuel resulted in a significant reduction in NO_x emissions compared to NG over both transient test cycles, as shown in Fig. 9 [3]. On average, NO_x emissions were reduced by 56 and 57 % on the CSHVR and OCTA cycle tests respectively.

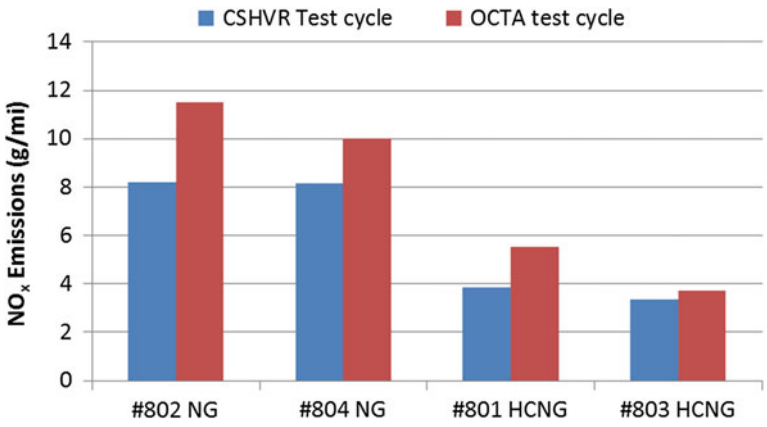

Fig. 9 Transit bus NO_x emissions over two different transient test cycles [3]

This is a result of leaner operation and less advanced spark timing with the hydrogen containing mixture, although specific values are not provided. The lambda and spark timing offsets used for engine dynamometer testing and shown in Fig. 6 are likely representative of changes made for the H20NG fuel.

8 Total Hydrocarbon (THC) Emissions

The brake-specific total hydrocarbon emissions (methane equivalent) are plotted against lambda in Fig. 10. The effect of hydrogen addition to the fuel gas is clear for both of the load conditions tested. At a fixed value of lambda, the hydrogen-containing fuels significantly reduce brake-specific total hydrocarbon emissions.

The reduction in hydrocarbon emissions is much larger than would be expected solely on the basis of the reduced hydrocarbon fraction in the hydrogen-containing fuels. Larsen and Wallace [12] singled out the two largest sources of hydrocarbon emissions relevant to their test engine as (1) crevice hydrocarbon storage and (2) bulk quenching that occurs as a result of partial burning or misfire. They analyzed their data to assess the relative contribution of crevice storage and flame quenching and to elucidate how hydrogen acts to reduce hydrocarbon emissions so effectively. In the absence of in-cylinder temperature measurements, exhaust port gas temperature provides an estimate of the relative temperature environment for oxidation of the returning crevice flow late in the expansion stroke. Figure 11 shows exhaust port temperature for MBT operation as a function of lambda [12]. At both loads tested, the exhaust port temperature is essentially independent of fuel type. This suggests that both fuels encounter a similar oxidation environment.

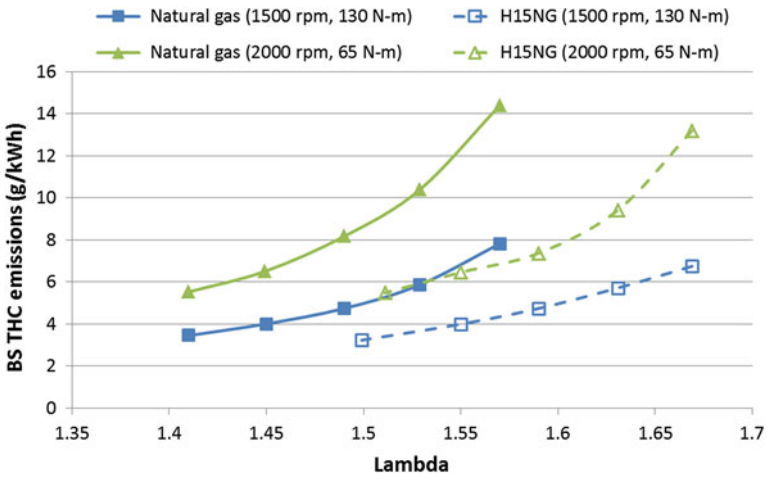

Fig. 10 Brake-specific total hydrocarbon (BSTHC) emissions at MBT as a function of lambda [12]

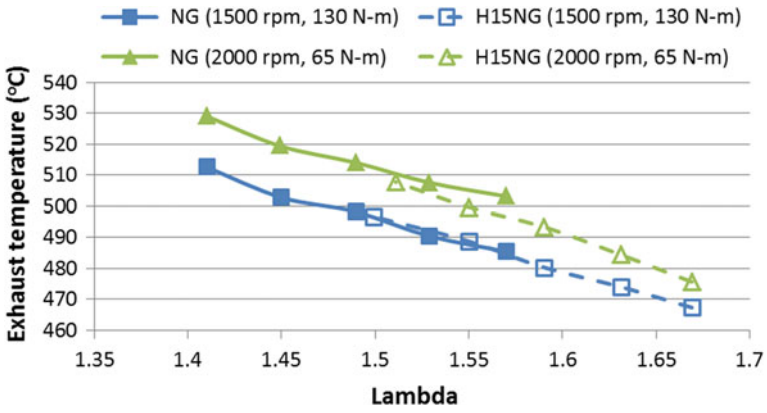

Fig. 11 Exhaust port temperature at MBT as a function of lambda [12]

Consider the case of an engine with high combustion efficiency, where limited bulk quenching occurs. Thompson and Wallace [22] showed that most of the hydrocarbon emissions in a natural gas fueled SI engine arise from storage of fuel–air mixture in crevices and their subsequent return to the cylinder. The temperature of the in-cylinder gases is a key determinant of the extent to which the returning crevice gases are oxidized. Jaaskelainen and Wallace [23] were able to demonstrate the effect of oxidation in a natural gas fueled engine by correlating increased gas temperatures in the exhaust port, a proxy for late cycle in-cylinder temperatures, with a reduction in hydrocarbon emissions. In those tests with a stoichiometric mixture, varying amounts of EGR were used to vary the exhaust port temperature.

A similar effect occurs with a lean-burn engine, where dilution with air rather than EGR also reduces the exhaust port temperature.

Figures 12 and 13 illustrate the dependence of BSTHC emissions on exhaust port temperature for all test conditions, not just the MBT conditions. The multiple points shown for each lambda value cover a range of spark timing settings. For both load conditions, BSTHC emissions increase with increasing exhaust port temperature, which is contrary to what would be expected if the returning crevice flow was the largest contributor to hydrocarbon emissions. In that case, higher temperature would lead to more oxidation that would result in lower hydrocarbon emissions. The observed results suggest that bulk flame quenching, especially slow or partial burning but possibly also misfire, are the main contributor to hydrocarbon emissions at these very lean operating conditions.

The slope of each curve in Figs. 12 and 13 can be viewed as a qualitative measure of the relative contribution of bulk quenching compared to crevice storage, a ratio of the two sources of hydrocarbon emissions. Larsen and Wallace [12] characterized this slope as the *partial burn index*. For the two fuels at both loads, leaner operation (increasing lambda) increases the partial burn index (slope). Moreover, the partial burn index (slope) for H15NG and NG is similar for similar levels of BSTHC emissions. This suggests that the extent of partial burning is similar for the two fuels at equivalent levels of BSTHC.

Figure 14, a plot of BSTHC versus MBT spark timing, compares the total hydrocarbon emissions of the two fuels at equivalent spark timing. The natural gas and H15NG results are equivalent at each of the two load conditions. MBT spark timing can be taken as a relative indicator of combustion duration, with more spark advance need to compensate for a longer duration. The results of Fig. 14 suggest that at the same combustion duration (represented by the same MBT spark timing), the total hydrocarbon emissions of the two fuels are the same. The reduction in THC emission shown in Fig. 10 for the H15NG fuel compared to NG can therefore be explained in terms of combustion duration. The addition of hydrogen reduces the

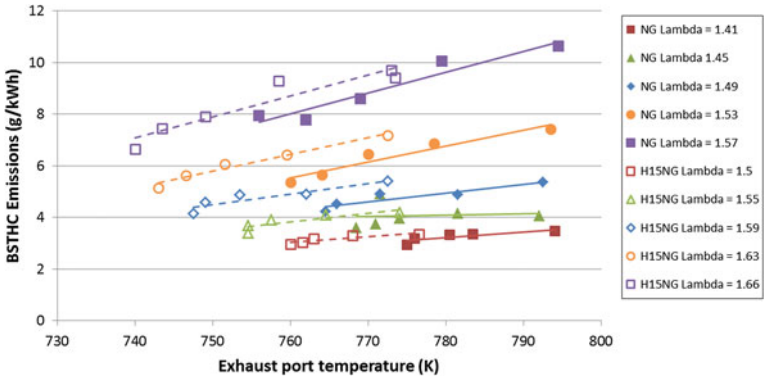

Fig. 12 Dependence of BSTHC emissions on exhaust port temperature at the full-load (130 N-m, 1500 rpm) test condition [12]

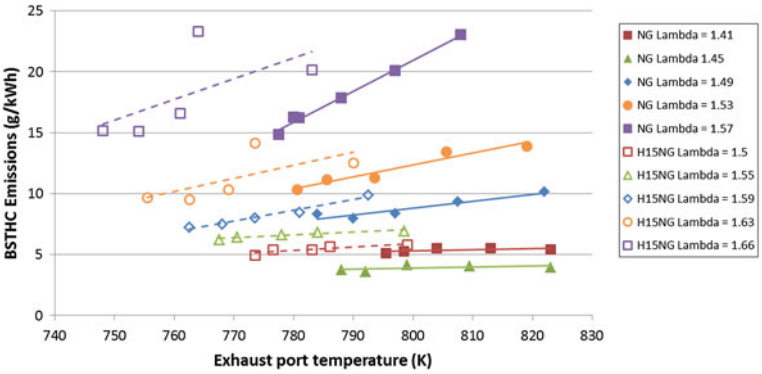

Fig. 13 Dependence of BSTHC emissions on exhaust port temperature at the half-load (65 N-m, 2000 rpm) test condition [12]

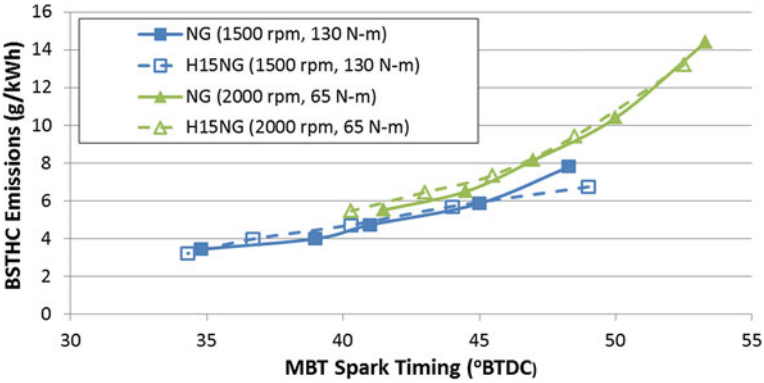

Fig. 14 Dependence of BSTHC on MBT spark timing [12]

combustion duration (Fig. 5 shows the reduction in MBT spark timing for H15NG fuel) and that in turn reduces the total hydrocarbon emissions by reducing the extent of partial burning.

8.1 Catalytic After Treatment of Hydrocarbon Emissions

Lean-burn engines typically employ an oxidation catalyst. Methane, the main component of natural gas, is particularly difficult to oxidize. Few tests of catalyst efficiency have been conducted with hydrogen-supplemented natural gas fueling. Saanum et al. used a standard 3-way catalyst and measured catalyst efficiency at a relatively high engine load of 10 bar bmep over the range of lambda 1.1–1.6 [18].

They found that THC conversion efficiency falls sharply with leaner mixtures (increasing lambda) to below 30 % for lambda greater than 1.4. The THC conversion efficiency was slightly higher for the H25NG mixture than for NG. An oxidation catalyst specifically formulated for natural gas engines would likely have demonstrated higher conversion efficiency.

8.2 Vehicle THC Emissions

In their chassis dynamometer tests of transit buses over two different transient test cycles, Munshi et al. compared post catalyst hydrocarbon emissions for both H20CNG and NG fueling over two different transient test cycles [3]. In this case, the oxidation catalyst fitted to the buses was specifically formulated for natural gas engine service. The results were somewhat dependent on test cycle. Figures 15 and 16 compare methane and non-methane hydrocarbon emissions, respectively, of the four buses operating on the two fuels. On the CSHVR test cycle, methane emissions fell from an average of 14.4 g/mi for natural gas to an average of 12.3 g/mi for the H25NG fuel mixture. There was little difference, however, on the OCTA test cycle, with averages of 16.8 and 16.2 g/mi for NG and H25NG respectively. Similarly, for NMHC, average emissions improved from 0.415 g/mi for NG to 0.285 g/mi for H25HG over the CSHVR test cycle, but the values were similar for the OTCA test cycle, 0.486 g/mi for NG and 0.55 g/mi for H25NG.

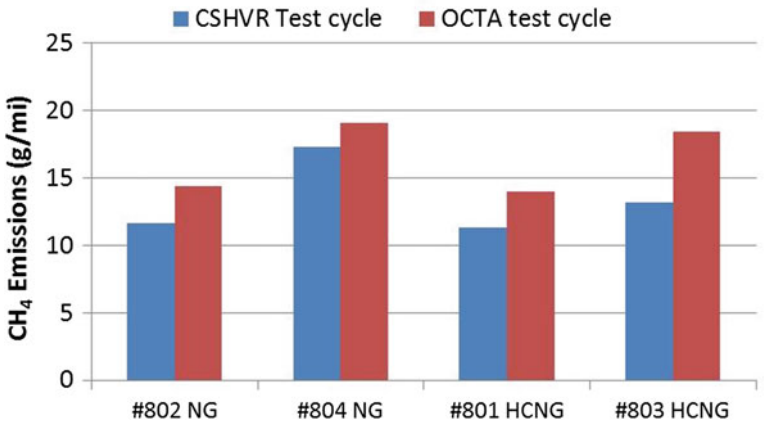

Fig. 15 Transient cycle methane emissions comparison between natural gas and 25 % hydrogen in natural gas [3]

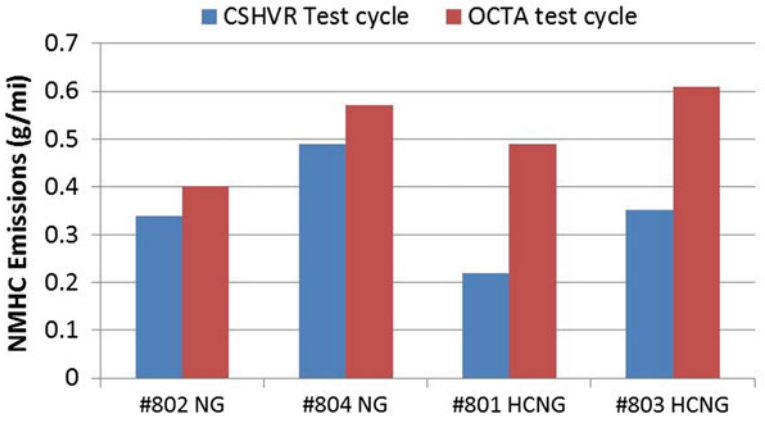

Fig. 16 Transient cycle non-methane hydrocarbon emissions comparison between natural gas and 25 % hydrogen in natural gas [3]

9 Carbon Monoxide Emissions

The brake-specific carbon monoxide (BSCO) emissions at MBT spark timing are plotted in Fig. 17 versus equivalence ratio for H15NG and NG fuels at full-load and half-load operating conditions [12]. The trends at both operating conditions are similar; relative to natural gas and in common with the effect observed on total hydrocarbon emissions, the hydrogen containing fuel results in substantially reduced brake-specific CO emissions for a given equivalence ratio. At the high load

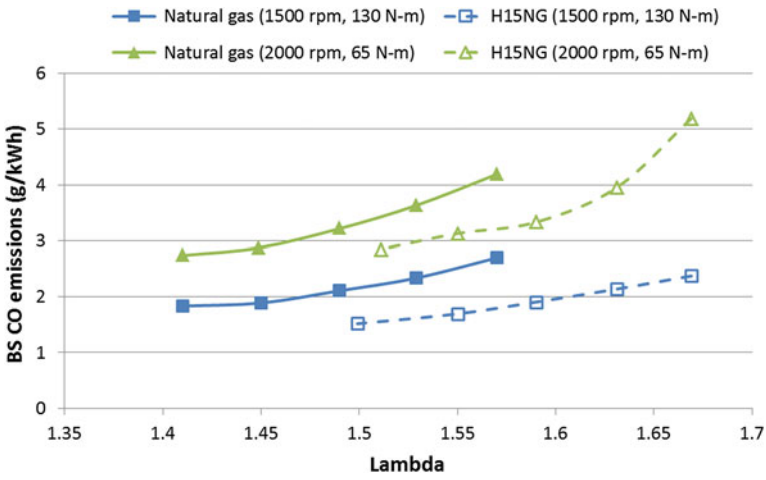

Fig. 17 MBT BSCO emissions versus lambda for full- and half-load test conditions [12]

condition, the CO emissions for the hydrogen containing fuel are lower even at the leanest value of lambda attainable.

The dominant oxidation path for CO in the combustion process can be represented by the following reaction:

$$CO + OH \leftrightarrow CO_2 + H \tag{1}$$

Reaction (1) is slow in comparison with other reactions of OH with various hydrocarbon species, which puts it at a disadvantage in the competition for available OH radicals. CO oxidation is therefore delayed until the original fuel hydrocarbons and subsequent intermediate species are largely consumed. With less competition for OH radicals, the rate of reaction (1) improves relative to that of the remaining hydrocarbons with the result that CO oxidation proceeds late in the combustion process.

A consequence of the competition of reaction (1) with hydrocarbon species for OH radicals is that the presence of unburned hydrocarbons in reacting products of combustion inhibits the oxidation of CO. Figure 18 plots the dependence of the ratio of the CO to CO_2 in the exhaust emissions to the concentration of total hydrocarbon (THC) emissions in the exhaust. The former ratio shows the progress in oxidizing CO to CO_2; ideally the ratio would be reduced to zero. Figure 18 shows that the ratio CO/CO_2 increases as the exhaust THC concentration increases, a clear illustration of the THC inhibiting effect.

Figure 18 also shows that the presence of hydrogen in the fuel changes the slope of the THC inhibiting effect, increasing the inhibiting effect. This suggests that another mechanism beyond inhibition by hydrocarbons is involved. Reaction (1)

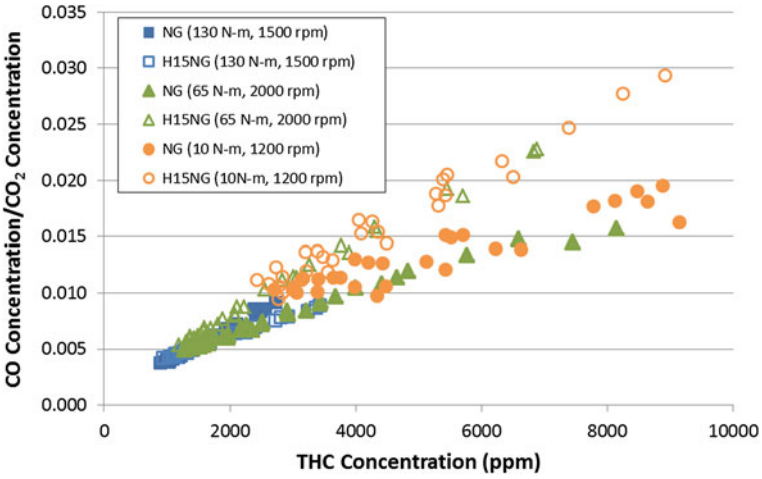

Fig. 18 Ratio of CO/CO_2 versus total hydrocarbon (THC) concentration [12]. All concentrations by volume

shows that the ratio of CO to CO_2 depends on the concentrations of the radical species H and OH:

$$\frac{[CO]}{[CO_2]} = \frac{1}{K}\frac{[H]}{[OH]} \tag{2}$$

where K is the equilibrium constant for reaction 1 and [CO], [CO_2], [H] and [OH] are the concentrations of carbon monoxide, carbon dioxide, monatomic hydrogen, and hydroxyl radicals, respectively. The H and OH radical concentrations are governed by the partial equilibrium established by the following sequence of bimolecular reactions [24]:

$$OH + H \leftrightarrow H_2 + O \tag{3}$$

$$OH + O \leftrightarrow O_2 + H \tag{4}$$

$$OH + H_2 \leftrightarrow H_2O + H \tag{5}$$

$$OH + OH \leftrightarrow H_2O + O \tag{6}$$

Any kinetic limitation on this system arises from limitations on the availability of the reacting species as both the forward and reverse reactions for 3 through 6 are inherently extremely fast. There is a difference in the availability of molecular hydrogen from the two fuels, NG and H15NG, and this difference shows up in the measured exhaust hydrogen concentrations.

Figure 19 illustrates that measured exhaust hydrogen concentration correlates strongly with measured total hydrocarbon concentration (both concentrations are ppm by volume). Moreover, the slope of the correlation (0.194) is very close to the

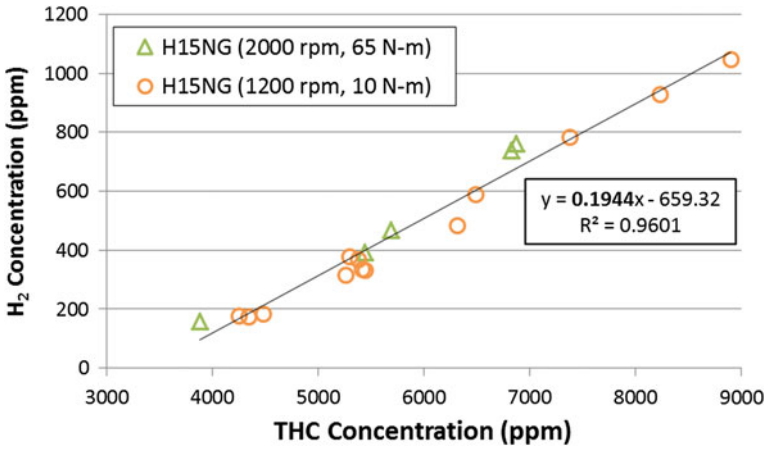

Fig. 19 Measured hydrogen concentrations (ppm by volume) versus measured THC concentrations [12]

ratio (0.176) of hydrogen to natural gas in the fuel. Note that measureable quantities of hydrogen could only be detected in the exhaust for the 10 and 65 N-m operating conditions with 15 % hydrogen in the fuel gas. Hydrogen was not detected at the same operating conditions with 100 % natural gas fueling and none was detected at the highest load of 130 N-m for either fuel. The combination of these three observations suggest that partial burn is the dominant mechanism contributing to both hydrogen and THC emissions at the 10 and 65 N-m operating conditions. While a returning crevice flow would have the same ratio of hydrogen to hydrocarbons as the fuel gas, hydrogen and natural gas would be expected to have different oxidation rates (hydrogen faster than methane) as the crevice flow mixes with the hot products of combustion in the cylinder, which would reduce the proportion of hydrogen to hydrocarbons.

Figure 19 illustrates that the H_2 concentration rises linearly with increasing hydrocarbon concentration. The fact that measureable quantities of hydrogen appear only during half- and low-load hydrogen-supplemented operation, and that H_2 emissions correlate so well with THC concentration, suggests that partial burn (as opposed to a hydrogen producing chemical reaction) is the dominant mechanism regulating exhaust H_2 levels.

The presence of unburned hydrogen in the post combustion products suggests that the partial equilibrium between reactions (3) through (6) could shift to increase the ratio of H-atoms to OH radicals. Reaction (5) in particular produces H-atom from molecular hydrogen while consuming OH. The effect of the amount of hydrogen in the fuel gas may manifest itself through the increase in availability of molecular hydrogen, which increases the ratio of H-atoms to OH radicals through reactions (3) through (6) and that in turn increases the ratio of CO to CO_2 through reaction (2). The rising H_2 concentrations that occur with rising THC concentrations shown in Fig. 19 should increase the ratio of H-atoms to OH radicals which is then responsible for the divergence of the H15NG and NG CO/CO_2 versus THC curves in Fig. 18.

9.1 Catalytic Aftertreatment of CO

Lean-burn engines typically employ an oxidation catalyst that can be expected to convert most of the CO emitted by the engine to CO_2. Saanum et al. [18] conducted tests of catalyst efficiency at a relatively high engine load of 10 bar bmep and found that CO conversion efficiency was on the order of 96 % for lean mixtures over the range of lambda 1.1–1.6, with no difference in efficiency between H25CNG and NG.

9.2 Vehicle Emissions of CO

In their chassis dynamometer tests of transit buses on both H20CNG and NG over two different transient test cycles, Munshi et al. [3] found that post catalyst CO

emissions for 5 of the 8 tests were below the detection limits and the remaining three were very low (0.17 g/mi for NG and 0.076 and 0.045 g/mi for H20CNG). Overall, CO emissions are minimal for NG engines equipped with an oxidation catalyst and the presence of hydrogen does not appear to degrade the ability of the catalyst to oxidize CO emissions.

10 Engine Efficiency

Figure 20 shows the dependence of brake thermal efficiency on lambda for H15NG mixtures compared to pure natural gas at MBT spark timing for two load conditions [12]. At the full-load condition, the efficiency is essentially the same for both fuels. There is a slight improvement with H15NG at the part load condition. Larsen and Wallace demonstrated that the difference in efficiency between the two fuels observed at the half-load condition could be entirely attributed to the level of unoxidized carbon monoxide, hydrocarbons and hydrogen in the exhaust gas. The longer combustion duration of natural gas compared to the H15NG mixture results in increased hydrocarbon and carbon monoxide emissions as previously described. Those emissions are wasted fuel energy that could have been utilized in the engine. The emissions therefore represent a loss of efficiency.

Similar results were obtained by Saanum et al. [18]. Figure 21 shows the dependence of brake thermal efficiency on lambda for an H25NG mixture compared to natural gas for the leanest of the range of lambda values they tested. At all loads tested the H25HG mixture shows an improvement in efficiency compared to

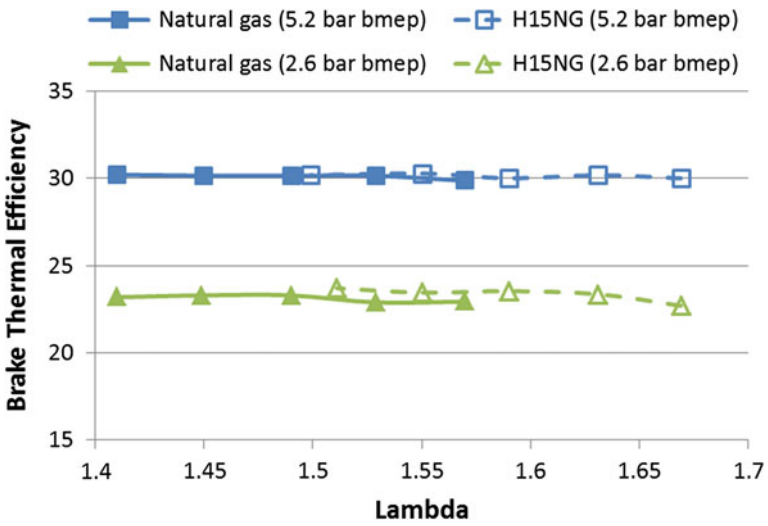

Fig. 20 Brake thermal efficiency dependence on lambda for mixtures containing 15 % hydrogen by volume [3]

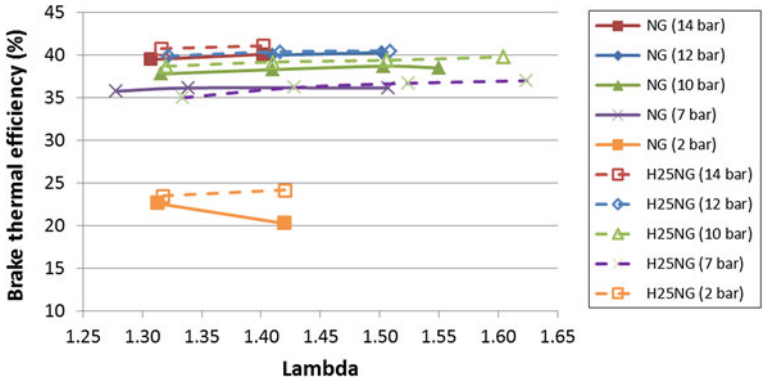

Fig. 21 Brake thermal efficiency dependence on lambda for mixtures containing 25 % hydrogen by volume [18]

natural gas at the leanest values of lambda. At the highest loads the improvement is modest but, consistent with the results of Larsen and Wallace [12], the improvement for the hydrogen-containing mixture is greatest at the lightest load condition.

10.1 Vehicle Fuel Efficiency

In their chassis dynamometer tests of transit buses, Munshi et al. [3] found that use of H20NG fuel resulted in a slight reduction in fuel economy, expressed as mpg diesel equivalent, compared to NG over both transient test cycles, as shown in Fig. 22. On average, fuel economy was reduced by 9.5 and 13.6 % (i.e. fuel consumption increased) on the CSHVR and OCTA cycle tests, respectively.

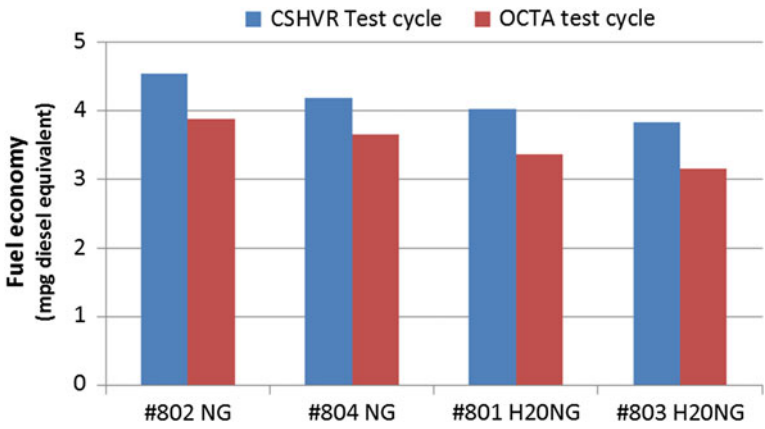

Fig. 22 Transient cycle fuel economy comparison between natural gas and 25 % hydrogen in natural gas [3]

The CSHVR test utilizes higher engine power levels than the OCTA cycle, so the smaller reduction in fuel economy for the CSHVR test is qualitatively consistent with the results of Figs. 20 and 21 where hydrogen addition has a smaller impact on brake thermal efficiency at high loads.

11 NO_x–THC Trade-off

The choice of engine operating parameters, especially the value of lambda, involves a decision about the NO_x–THC trade-off that exists for lean-burn engines. This trade-off arises because the same conditions that minimize NO_x, e.g., lean mixtures, retarded spark timing, are conditions that contribute to high hydrocarbon emissions. Larsen and Wallace [12] explored this tradeoff for mixtures containing 15 % hydrogen in natural gas. Their results are shown in Fig. 23 for both load conditions with MBT spark timing. These results clearly show that hydrogen supplementation has improved the NO_x–THC trade-off. At both loads the curve for the hydrogen containing mixture lies below and to the left of the curve for 100 % natural gas. Thus, for a given level of hydrocarbon emissions, switching to the 15 % hydrogen blend results in significantly reduced NO_x emissions. For example, at a BSTHC emission level of 6 g/kWh, use of H15HG reduces NO_x by 60 and 50 % at the 130 and 65 N-m loads, respectively.

Figure 24 shows that a similar improvement in the NO_x-THC tradeoff can be observed in the results of Saanum et al. [18] for a fuel mixture containing 25 % hydrogen (v/v). It can be seen that the use of hydrogen supplementation improves the NO_x–THC trade-off at all three load conditions, e.g., at the same level of total

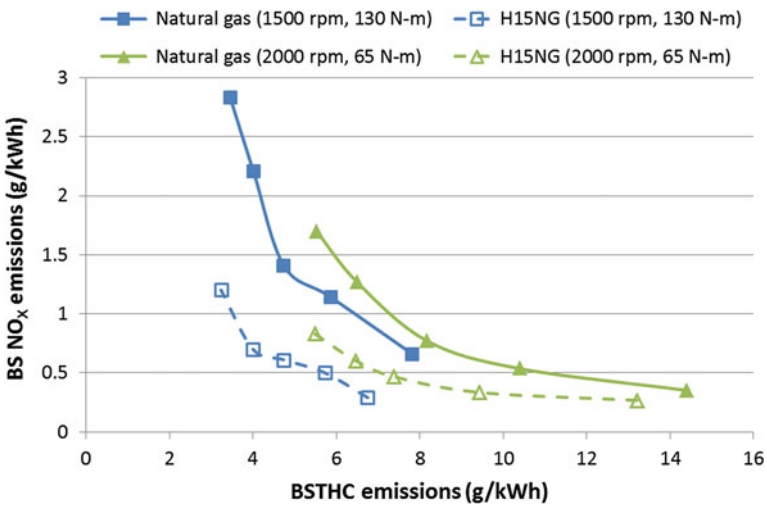

Fig. 23 $BSNO_x$ versus BSTHC emissions trade-off. Results of Larsen and Wallace [12] for mixtures containing 15 % (v/v) hydrogen

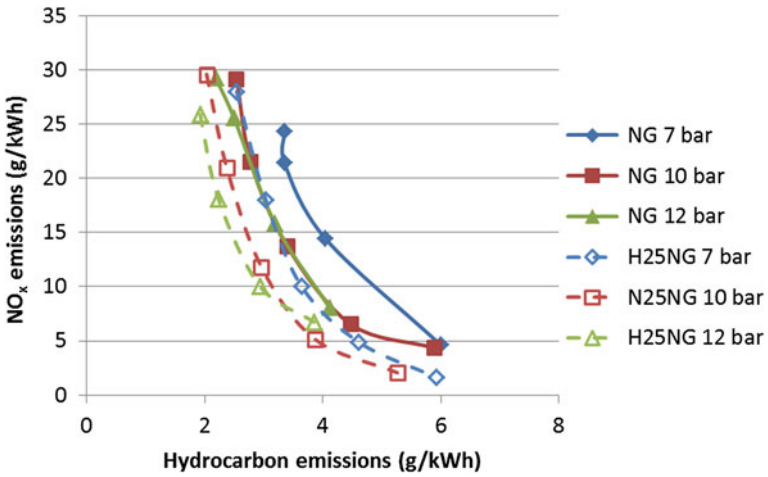

Fig. 24 $BSNO_x$ versus BSTHC emissions trade-off. Results of Saanum et al. [18] for mixtures containing 25 % (v/v) hydrogen

hydrocarbon emissions, use of hydrogen-supplemented natural gas results in lower NO_x emissions. For example at a level of 4 g/kWh BSTHC emissions, NO_x emissions are reduced by 48, 49, and 31 % at the 7, 10, and 12 bar bmep loads respectively. This reduction occurs as a result of being able to operate leaner with hydrogen supplementation.

12 Particulate Matter Emissions

Particulate matter (PM) emissions from vehicles are of tremendous current interest due to their impact on health. Diesel engines have historically been a much larger source of PM emissions than spark ignition engines and diesel exhaust is associated with adverse health effects. For example, exposure to diesel exhaust leads to cardiopulmonary and immune system responses in mice [25] and diesel exhaust has been associated with lung cancer risk in humans [26].

There are two sources of PM emissions from IC engines, fuel and lubricating oil. PM emissions typically consist of a combination of solid carbon, elemental carbon with a graphitic structure, and adsorbed organic compounds, organic carbon. PM may also contain sulfates, nitrates and metals. Metals originate from organometallic compounds added to lubricating oil base stock to reduce wear, reduce friction, as well as from metal-containing dispersants and detergents in the oil.

Lean-burn spark ignition engines should produce only very low level of PM emissions from the fuel due to their homogeneous pre-mixed combustion. However, there is still a contribution to PM from the lubricating oil, some of which escapes past the piston rings into the combustion chamber where it is consumed.

As PM emission standards tighten, this contribution from lubricating oil becomes more important.

Miller et al. isolated the lubricating oil contribution to PM emissions by studying an engine fuelled by hydrogen [27]. Since hydrogen combustion does not produce any carbon-containing species, the possibility of fuel-derived particulate matter emissions is eliminated and any PM emissions can be attributed to the lubricating oil. The results showed that fine particles, with geometric mean diameters from 18 to 31 nm were generated. The particles were mainly organic carbon, with little elemental carbon and contained a much higher percentage of metals than particles from diesel engines. This characterization is certainly consistent with what might be expected of particles formed from lubricating oil [27]. These results from an engine fueled by pure hydrogen demonstrate that a certain level of PM emissions can be expected from engines fueled by hydrogen-supplemented natural gas mixtures.

Particulate matter emissions from lean-burn natural gas engines are typically quite low. PM emissions are formed in rich mixtures so a lean homogeneous mixture of natural gas and air would not be expected to produce any PM emissions. Once again, PM emissions also arise from lubricating oil and this is the dominant source of PM emissions in lean-burn natural gas engines.

12.1 Vehicle Emissions of PM

There are very few published measurements comparing PM emissions from engines fueled by hydrogen-supplemented natural gas with engines operating on natural gas. Using a chassis dynamometer Munshi et al. [3] measured emissions from four identical transit buses equipped with an oxidation catalyst over two different test cycles. Two buses were operated on CNG and two on H20CNG. Figure 25

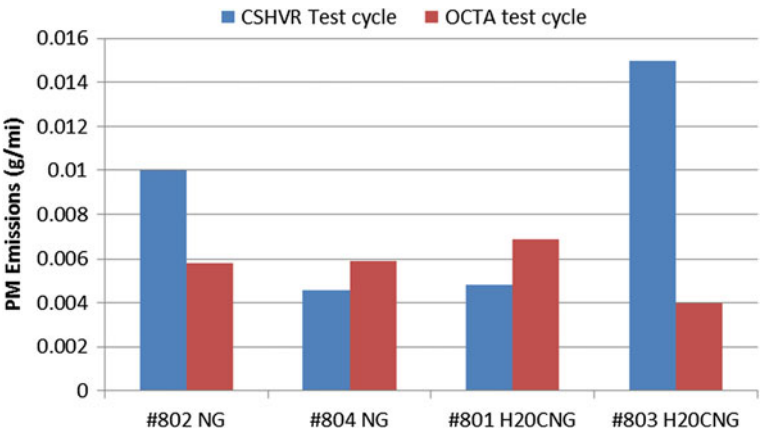

Fig. 25 PM emissions from four identical transit buses operated on a chassis dynamometer over two different transient test cycles [3]

compares the results. Overall PM emissions are low. Results from the OCTA test are more consistent, with the average PM emissions for the two CNG buses differing from the two H20CNG buses by less than 7 %. Results for the CSHVR cycle are highly variable, and the authors attribute the variability to the individual bus operating conditions rather than to the fuel. On the whole these results suggest that PM emissions from HCNG fueled engines will be similar to those of the same engine fueled by natural gas.

13 Conclusions

Engine dynamometer tests consistently show that hydrogen supplementation of natural gas fuel improves the NO_x–THC trade-off that is a characteristic of lean-burn SI engines. The key implication is that NO_x emissions can be reduced for the same level of THC emissions. Engine dynamometer tests show NO_x reductions between 30 and 60 % at a constant THC emission level, depending on load. This is an important result, as THC emissions can be further reduced by oxidation catalysts, but there are very limited options for catalytic reduction of NO_x emissions from lean-burn engines.

The improved NO_x–THC trade-off arises from the ability to operate at a leaner air–fuel ratio with hydrogen. The difference between the leanest air–fuel ratio for hydrogen-containing mixtures and the leanest air–fuel ratio for natural gas only decreases with load. Thus, the extent of improvement in the NO_x–THC trade-off diminishes at high loads. As a result, the extent of improvement in real-world use will depend on driving cycle.

The third factor in the trade-off is fuel consumption. While most of the engine tests cited showed a reduction in fuel consumption, the H20NG transit bus study found an increase in fuel consumption with H20NG compared to operation on natural gas [3]. The increase was attributed to choices of air–fuel ratio and spark timing that minimized NO_x emissions. Equivalent fuel consumption could be achieved with a revised engine calibration by accepting a smaller reduction in NO_x emissions. Thus, not only the emissions but also the impact on fuel consumption must be taken into account in developing the engine calibration.

Acknowledgments The author gratefully acknowledges the outstanding work of John Larsen who carried out the original study that is extensively cited in this chapter. That study was funded by the Alternative Energy Division of CANMET, part of Natural Resources Canada.

References

1. Wallace JS, Ward CA (1983) Hydrogen as a fuel. Int J Hydrogen Energy 255–268
2. Wallace JS (1984) A comparison of compressed hydrogen and CNG storage. Int J Hydrogen Energy 609–611

3. Munshi S, Nedeicu C, Harris J, Edwards T, Williams J, Lynch F et al (2004) Hydrogen blended natural gas operation of a heavy-duty turbocharged lean burn spark ignition engine. SAE technical paper no 2004-01-2956
4. Swain MR, Swain MN, Adt RR (1988) Considerations in the design of an inexpensive hydrogen-fueled engine. SAE technical paper series, 881630, 1–15
5. Tang X, Kabat DM, Natkin RJ, Stochhausen WF (2002) Ford P2000 hydrogen engine dynamometer development. SAE technical paper series, 2002-01-0242
6. Eccleston D, Fleming RD (1972) Clean automotive fuel. US Bureau of Mines Automotive Exhaust Emissions Program. Technical progress report 48
7. Foute S, Knowlton T, Lynch F, Ragazzi R, Raman V (1992) The Denver Hythane project—recent progress. In: Presented at the tenth anniversary conference, industry and hydrogen, Kananaskis, Alberta, Canada
8. Strothers R (1993) Hythane—its potential as a fuel for internal combustion engines. Final report for ORTECH corporation project number 600197
9. Swain MR, Yusuf MJ, Dulger Z, Swain MN (1993) The effects of hydrogen addition on natural gas engine operation. SAE technical paper no 932775
10. Hoekstra RL, Collier K, Mulligan DN (1994) Demonstration of hydrogen mixed gas vehicles. In: Proceedings of 10th world hydrogen energy conference, pp 1781–1796. Cocoa Beach, Florida, 20–14 June 1994
11. Cattelan AI, Wallace JS (1994) Hythane and CNG fuelled engine exhaust emissions and engine efficiency comparison. In: Proceedings of 10th world hydrogen energy conference, Cocoa Beach, Florida
12. Larsen JF, Wallace JS (1997) Comparison of emissions and efficiency of a turbocharged lean-burn natural gas and hythane-fueled engine. J Eng Gas Turbines Power 119(1):218–226
13. Sierens R, Rosseel E (2000) Variable composition hydrogen/natural gas mixtures for increased engine efficiency and decreased emissions. J Eng Gas Turbines Power 122(1):135–140
14. Bauer CG, Forest TW (2001) Effect of hydrogen addition on the performance of methane-fueled vehicles. Part I: effect on SI engine performance. Int J Hydrogen Energy 26:55–70
15. Li H, Karim GA (2005) Exhaust emissions from an SI engine operating on gaseous fuel mixtures containing hydrogen. Int J Hydrogen Energy 30:1491–1499
16. Li H, Karim GA (2005) An experimental investigation of S.I. engine operation on gaseous fuels lean mixtures. SAE technical paper no 2005-01-3765
17. Huang Z, Liu B Zeng, Huang Y, Jiang D, Wang X, Miao H (2006) Experimental study on engine performance and emissions for an engine fueled with natural gas-hydrogen mixtures. Energy Fuels 20(5):2131–2136
18. Saanum I, Bysveen M, Tunestal P, Johansson B (2007) Lean burn versus stoichoimetric operation with EGR and 3-way catalyst of an engine fueled with natural gas and hydrogen enriched natural gas. SAE technical paper No. 2007-01-0015. Cape Town, South Africa: SAE
19. Li H, Karim GA, Sohrabi A (2009) The lean mixture operational limits of a spark ignition engine when operated on fuel mixtures. J Eng Gas Turbines Power 131(1):012801-1–012801-7
20. Li H, Karim GA, Sohrabi A (2010) An experimental and numberical investigation of spark ignition engine operation on H_2, CO, CH_4 and their mixtures. J Eng Gas Turbines Power 132 (3):032804-1–032804-8
21. Reynolds W, Perkins HC (1977) Engineering thermodynamics, 2nd edn. McGraw-Hill, New York
22. Thompson N, Wallace JS (1994) Effect of engine operating variables and piston and ring parameters on crevice hydrocarbon emissions. SAE technical paper no 940480
23. Jaaskelainen H, Wallace JS (1994) Examination of charge dilution with EGR to reduce NOx emissions from a natural gas fueled 16 valve DOHC four-cylinder engine. SAE technical paper no 942006
24. Newhall H (1969) Kinetics of engine-generated nitrogen oxides and carbon monoxide. In: Proceedings of 125 h symposium on combustion, pp 603–613. The Combustion Institute

25. McDonald JD, Campen MJ, Harrod KS, Seagrave J-C, Seilkop SK, Mauderly JL (2011) Environ Health Perspect 119(8):1136–1141
26. Hesterberg TW, Long CM, Bunn WB, Lapin CA, McCelellan RO, Vaberg PA (2012) Inhalation Toxicol 24(S1):1–45
27. Miller AL, Stipe CB, Habjan MC, Ahlstrand GG (2007) Role of lubrication oil in particulate emissions from a hydrogen-powered internal combustion engine. Environ Sci Technol 41:6828–6835

Using Natural Gas/Hydrogen Mixture as a Fuel in a 6-Cylinder Stoichiometric Spark Ignition Engine

Luigi De Simio, Michele Gambino and Sabato Iannaccone

Abstract Hydrogen added to natural gas improves the process of combustion with the possibility to develop engines with higher performance and lower environmental impact. In this chapter, experimental analyses on multi-cylinder heavy duty engines, fuelled with natural gas–hydrogen blends, are reported. Theoretical aspects on engine performance are illustrated and a formula to evaluate the benefit of H_2 addition on NG combustion is defined. Experimental data on the effects of air index and exhaust gas recycling on combustion with different NG/H_2 blends are discussed followed by an experimental comparison of stoichiometric and lean-burn strategies on the European transient cycle for heavy duty emission certification. Results of the study indicate that a right metering of hydrogen into the natural gas and an optimization of the charge dilution provides not only a reduction in tailpipe CO_2 emissions and a more complete combustion process with a lower formation of THC and CO, but also a possible increase in engine efficiency, avoiding abnormal combustion phenomena.

List of Acronyms

BGC	Burning gravity centre
BMEP	Brake mean effective pressure
BSEC	Brake specific energy consumption
BSFC	Brake specific fuel consumption
CAD	Crank angle degree
CNG	Compressed natural gas
ECU	Electronic control unit
EEV	Enhanced environmentally friendly vehicle
EGR	Exhaust gas recycling
ETC	European transient cycle
FID	Flame ionization detector
HCNG	Hydrogen-enriched compressed natural gas
HD	Heavy duty

L. De Simio (✉) · M. Gambino · S. Iannaccone
Istituto Motori–National Research Council, Viale Marconi, 4, 80125 Naples, Italy
e-mail: l.desimio@im.cnr.it

M. De Falco and A. Basile (eds.), *Enriched Methane*,
Green Energy and Technology, DOI 10.1007/978-3-319-22192-2_10

HR	Heat release
ID	Incubation duration
LHV	Lower heating value
MAP	Manifold absolute pressure
MCD	Main combustion duration
MV	Mean value
NG	Natural gas
NG_{up}	Natural gas unburned percentage
NMHC	Non-methane hydrocarbons
PT	Particulate matter
SA	Spark advance
SD	Standard deviation
SI	Spark ignition
THC	Total hydrocarbons
TWC	Three-way catalyst
UEGO	Universal exhaust gas oxygen
WG	Wastegate
WOT	Wide open throttle

List of Symbols

T_{TS}	Energy content of the air–fuel stoichiometric mixture
y_{H2}	Mass fraction of H_2 in the NG/H2 blend
$\dot{m}$	Mass flow rate
P	Power

List of Greek Symbols

$\rho_{mix,st}$	Density of the air–fuel stoichiometric mixture
α_{st}	Stoichiometric air–fuel ratio

1 Introduction

Hydrogen has the potential to become a valid alternative to conventional fuels, since it is completely carbon-free and easy to produce, if primary energy is available at low cost. As instance, hydrogen production could be suitable for energy storage in future electricity grid which is a key challenge in Europe to enable developing of renewable sources. The electricity network should manage in an intelligent way different energy vectors, distributed power generators and dispersed energy storage devices, instead of the electricity alone [1]. In fact, solar and wind energy are abundant and distributed, but are also intermittent and characterized by poor ability to control and predict the amount of electricity that can be produced.

Distributed generation also implies that the grid should become bidirectional. Therefore, the distribution network will switch from a passive to an active role [2–4], changing the way in which electricity is produced, transmitted and consumed. In this scenario also a flexible coproduction of hydrogen as energy carrier could be a viable solution [5–8]. Hydrogen production is also the best way of coal use (the most abundant fossil fuel), if CO_2 capture and storage is achieved [9].The technologies of gas powered vehicles, that have made the compressed natural gas (CNG) a concrete alternative to gasoline and diesel fuels for vehicle propulsion, can be used also for NG/H_2 blends.

The use of pure hydrogen in internal combustion engines amplifies the problem of the operative range for gas-powered vehicles. In fact, the range operation with pure hydrogen would be reduced by about 70 %, compared to that of pure methane, due to the lower density of the fuel energy stored on board at parity of tank volume and pressure. Hydrogen addition reduces the methane number, which is expressed as percentage of methane in a methane/hydrogen mixture and is related to the knock resistance [10]. Furthermore, the lower ignition energy in air, of H_2 respect to CH_4 (0.02 mJ vs. 0.29, at stoichiometric conditions [11]) helps to burn very lean mixtures but makes the mixture subject to pre-ignition phenomena by contact with hot spots or residual gas. The pre-ignition, unlike knocking, cannot be controlled with the ignition timing, but requires substantial modifications to the engine. The use of NG/hydrogen mixtures offers instead the opportunity to exploit the positive aspects related to the hydrogen without substantial modification of already existing natural gas engines avoiding the drawbacks of the use of pure hydrogen.

A turbulent flame front speed propagation increasing in internal combustion engine is achieved when H_2 is added to NG [12, 13], in accordance with the stoichiometric laminar velocity which is 1.9 m/s for H_2, while only 0.38 m/s for CH_4. Moreover, H_2 added to NG gives the possibility to expand the lean burn limit, [14–16], due to a more stable combustion, [17]. A more stable combustion permits a reduction of CO and total hydrocarbons (THC), contributing to increase thermodynamic efficiency. On the contrary, NO_x emissions could be higher for more elevated temperatures at stoichiometric conditions, while addition of hydrogen to natural gas permits to reduce NO_x emission of a lean-burn combustion reducing the gap with a stoichiometric operation with exhaust gas recycling (EGR) and a three-way catalyst [18]. At the same time the use of higher exhaust gas recirculation to optimize the engine is possible with H_2 addition [19–21].

The use of such mixtures in heavy duty (HD) gas-powered vehicles belonging to fleets instead of private light duty passenger cars could be more interesting because the overcoming of the refuelling problems could be simplified being, in this case, well defined the refuelling points.

In this chapter the NG/H_2 fuelling of 6-cylinder turbocharged engines for buses application is considered. Starting from theoretical aspect on engine performance and from a definition of a formula to evaluate the benefit of H_2 addition on NG combustion, experimental data on effect of air index and exhaust gas recycling on

combustion with different NG/H_2 blends will be presented. Finally, an experimental comparison of stoichiometric and lean-burn strategies on the European transient cycle (ETC) for heavy duty emission certification is reported.

2 Theoretical Effects of Hydrogen Content on Engine Performance and Vehicle Range Operation

As hydrogen is a carbon-free fuel, the reduction in tank to wheel CO_2 emissions, at parity of engine efficiency, is a direct function of H_2 content in a CH_4/H_2 blend, as shown in Fig. 1a. For CH_4/H_2 mixtures containing 20 % by volume of H_2 (equivalent to about 3 % by mass), there is a reduction of CO_2 of almost 7 %.

In a port fuel injection engine, the maximum engine performance depends from the volumetric energy content of the air–fuel stoichiometric mixture (T_{TS}) calculated as:

$$T_{TS} = \rho_{mix,st} \cdot \frac{LHV}{1 + \alpha_{st}} \tag{1}$$

The presence of H_2 determines a small variation of this parameter, therefore the influence on maximum power can be considered negligible even for high percentages of hydrogen. In the case of CH_4/H_2 mixtures the lower density of the stoichiometric air–fuel mixture ($\rho_{mix,st}$) and the higher air to fuel stoichiometric equivalence ratio (α_{st}) are balanced by the increased lower heating value (LHV) of the blend. In the case of 50 % hydrogen in the mixture, the rated power reduction compared to a natural gas engine would be around 1.6 %, at the same engine efficiency.

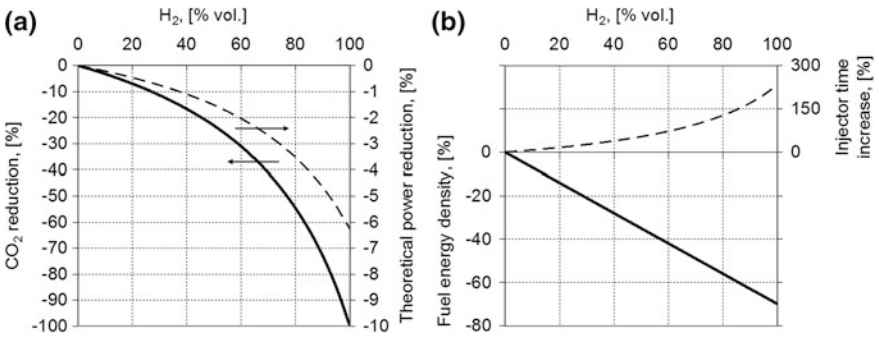

Fig. 1 Effect of the hydrogen percentage in a CH_4/H_2 mixture, on fuel energy density and CO_2 emission, maximum power and fuel injection volume calculated at parity of engine thermal efficiency

With the increase of hydrogen content, the energy per unit of mixture volume is reduced compared to pure methane, as reported in Fig. 1b. As a result, at parity of tank volume, a lower energy than pure methane is stored on board. This implies a lower operative range and the necessity to increase injector volumetric flow rate. For pure H_2 the vehicle operative range is reduced by almost 70 %, while the volumetric flow rate at the injectors to maintain the same performance should be more than double respect to pure CH_4 case.

The increasing of H_2 in the mixture causes also a direct reduction of THC emission at the exhaust due to substitution of part of CH_4 with H_2. However, a global combustion improvement could be achieved with H_2 addition. Therefore, to better explain this effect, a parameter which correlates THC emissions with the NG fraction really burned has been defined. It was named NG_{up} (natural gas unburned percentage) and was calculated as the ratio between unburned hydrocarbon and natural gas mass flow rate:

$$NG_{\mathrm{up}} = \frac{\dot{m}_{\mathrm{THC}}}{\dot{m}_{\mathrm{NG}}} = \frac{\dot{m}_{\mathrm{THC}}/P}{BSFC \times (1 - y_{\mathrm{H2}})} \times 100 \tag{2}$$

where P is the actual power, BSFC the brake specific fuel consumption and y_{H2} is the mass fraction of H_2 in the NG/H_2 blend. The formula compares the specific THC emission with the specific consumption of natural gas fuel, not considering the consumption of hydrogen. The NG_{up} parameter can range from 0 % (complete NG combustion) to 100 % (all natural gas unburned). It gives a quantification of completeness of combustion starting from THC measurable with a FID (flame ionization detector) analyzer that does not take in consideration unburned H_2 in the exhaust. Therefore, a reduction of NG_{up} with H_2 content indicates a better combustion efficiency, that reduces THC emissions in larger quantity than substitution of NG with H_2 does.

3 Experimental Data on Effect of Air Index and EGR on Combustion

Experimental tests with different NG/H_2 blends on the engine at test bed are presented. The engine used for experimental tests was a heavy duty spark ignition turbocharged engine, which was equipped with a low pressure cooled EGR route. The main engine characteristics are shown in Table 1.

In a low pressure system the exhaust gas are spilled after the turbine and introduced into the intake manifold before the compressor. Moreover, EGR was cooled in order to reduce temperature and knocking tendency [22]. A research electronic control unit (ECU) enabled the access to the main control parameters (air/fuel mixture, spark advance, wastegate duty cycle, etc.) and allowed to change them during engine operation. Performances were tested on an asynchronous alternating current motor. Fuel flow rate was measured with a Coriolis mass flow

Table 1 Main characteristics of the reference HD SI CNG engine

Type	6-cylinder in line
Displacement	7.8 L
Bore × stroke	115 × 125 mm
Compression ratio	11:1
Rated power	200 kW @ 2100 rpm
Max. torque	1100 Nm @ 1100–1650 rpm
Boost pressure	0.8 relative bar, with waste gate valve
Intercooler	Air to water (external line)
NG feeding system	Electronic timed multi-point injection
Power density	25.6 kW/L

meter. The pressure cycles have been measured into combustion chamber with a KISTLER piezoelectric pressure transducer (sensitivity 26 pC/bar). Each pressure cycle was acquired as mean values of 100 consecutive cycles. The apparent heat release (HR) curves were used to calculate the incubation duration (ID), as the period from the spark advance (SA) to 10 % HR, the main combustion duration (MCD), as the period from 10 to 90 % HR and the burning gravity centre (BGC) as the angle at which 50 % of heat is released. This last parameter was used to set the SA in each conditions, in fact all test cases refer to a BGC close to 8° before top dead centre, which gives an optimal combustion phasing with respect to indicated engine efficiency. A list of the main instrumentation used is reported in Table 2.

Table 2 Instrumentation for emission and performance measurement

Unit	Type	Range	Accuracy
Torque	Torque flange HBM T 10F	2000 Nm	±0.2 % of range
Speed	Encoder heidenhain	3500 rpm	<±1 rpm
Power	AFA AVL dinamometer	280–315 kW @ 2000–3500 rpm	±0.2 % of reading
Fuel	Micro motion elite	50 kg/h	<1 % of reading
Air	ABB sensy flow P	1200 kg/h	±1 % of reading
THC	MULTIFID 14 EGA	0–10,000 ppm C3	0.5 % of range
CH_4		0–10,000 ppm C1	
CO	URAS 14 EGA	0–10 %	<1 % of range
NO_X	CLD ecophysics	0–5000	<1 % of range
CO_2	URAS 14 EGA	0–20 %	1 % of range
O_2	MACROS 16 EGA	0–25 %	0.5 % of range
Particulate sampling system	Control system PSS20	1.5 m3/h	±0.2 % of range
PT electronic balance	Sartorius 4503 Micro	4.1 g	±5 ng

Temperature and pressure transducers in different points of the inlet and exhaust systems were installed.

A first experimental activity was carried out at stoichiometric air-to-fuel ratio condition with closed-loop control and at different EGR rate, fuelling the engine with NG and with two blends of NG and 20 and 40 % of H_2 by volume. The characteristics of the fuels used in the tests are reported in Table 3. The EGR rate refers to the EGR mass flow rate respect to the whole mass (air and EGR) entering the cylinders and it was calculated starting from the CO_2 concentration in the exhaust and in the intake manifold.

Due to knocking phenomena with NG/H_2 40 % at full load (in NG fuelling setting up) the turbocharged stoichiometric heavy duty engine was tested at a lower load. This reduced load was settled in order to compare the three tested fuels at parity of engine volumetric efficiency. Therefore the maximum boost pressure was reduced acting on the turbine wastegate valve retaining the wide open throttle (WOT) condition. The wastegate (WG) valve lets a share of exhaust gas to not expand in turbine reducing the boost pressure. Therefore the wastegate valve was set in fixed open position and this implies a lower engine turbocharging but does not set it to zero. In fact, the turbine has two inlets, only one of which with the wastegate. In NG fuelling, the ECU controls the wastegate electronically in closed loop to realize a target boost pressure at each speed on the full torque curve. Setting the wastegate in fixed open position, and retaining the WOT condition, it was possible to reduce the rated torque of about 35 % without throttling the engine. In this way, the comparison with the different fuelling was performed at a load lower than 100 %. Tests were carried out at 1100, 1500 and 1900 rpm. Despite the before established reduction of the engine maximum load, frequent knocking cycles (rate of pressure rise significantly higher than 10–15 bar/CAD) occurred (Fig. 2) with NG/H_2 40 % but only at the maximum tested speed (1900 rpm). The abnormal combustion at 1900 rpm with high pressure gradient was attributed to pre-ignition from hot spots, more than to end-gas self-ignition. This deduction is based on the fact that not knocking cycles were observed at lower engine speeds (1100 and 1500 rpm) despite the higher brake mean effective pressure (BMEP) (Fig. 3) and longer duration of combustion (Fig. 5), both of these more favourable conditions for the auto ignition of end gas. Instead, the higher frequency of combustion phases at 1900 rpm, respect to lower engine speeds, could be the cause of ignition by hot spots. Mixtures with lower H_2 content or with inert gas dilution did not give pre-ignition phenomena thanks to the increased minimum ignition energy. Therefore for the NG/H_2 40 % blend, the engine was tested at different EGR rate at the three considered engine speeds, but at 1900 rpm no data without EGR were acquired.

Data show a load reduction when increasing the EGR. This behaviour is well illustrated in Fig. 3, where BMEP is represented for three different speeds at variable EGR rate. This is due to the substitution of part of the inlet air with exhaust gases, therefore also the fuel flow rate have to be reduced to retain stoichiometric conditions. Instead, the effect of an increasing EGR on the manifold absolute pressure (MAP) is relatively low, because in a low pressure route EGR system,

Table 3 Tested fuels characteristics

Fuel	CH_4 (% vol.)	H_2 (% vol.)	y_{H2} (kg/kg)	α_{st} (kg/kg)	LHV (MJ/kg)	P (kg/Nm3)	H/C (n/m)	C (% mass)	H (% mass)
NG	85	0	0.000	15.7	45.9	0.83	3.7	71.0	22.3
NG/H_2 20 %	68	20	0.026	16.2	47.8	0.64	4.1	69.2	24.3
NG/H_2 40 %	51	40	0.067	17.0	50.9	0.50	4.9	66.2	27.6
HCNG	85	15	0.022	17.3	50.7	0.62	4.3	73.2	26.8

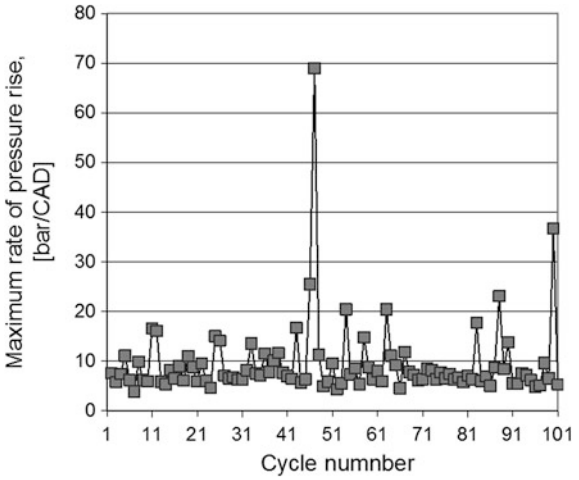

Fig. 2 Maximum rate of pressure rise due to knocking cycles with NG/H_2 40 % at 1900 rpm without EGR

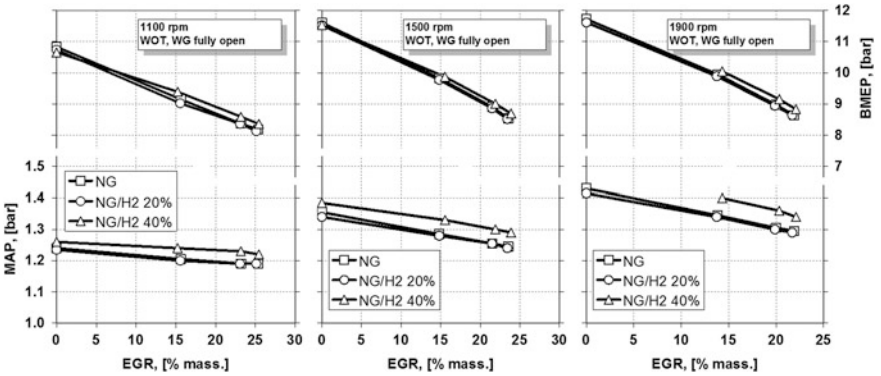

Fig. 3 BMEP and MAP at the three tested speeds varying hydrogen content and EGR rate

where the exhaust gas is taken after the turbine and introduced before the compressor, the boost pressure does not substantially changes if part of the air, which expands in turbine, is substituted with EGR. Anyway, from Fig. 5 it can be noted that at the same EGR rate, almost the same BMEP was obtained with the three blends. In particular, only small reductions of BMEP were observed with H_2 admission and therefore a comparison at parity of load can be done.

At H_2 increasing in the blends SA has to be reduced, while at EGR rate increasing, a higher SA is necessary to retain the same BGC. Furthermore, at a fixed EGR rate, it was observed that a higher H_2 content requires a lower increment of the spark advance (respect to the case without EGR), Fig. 4.

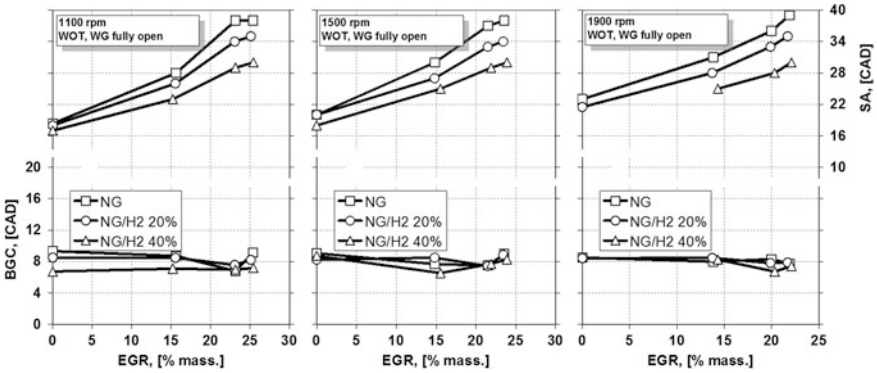

Fig. 4 SA and BGC at the three tested speeds varying hydrogen content and EGR rate

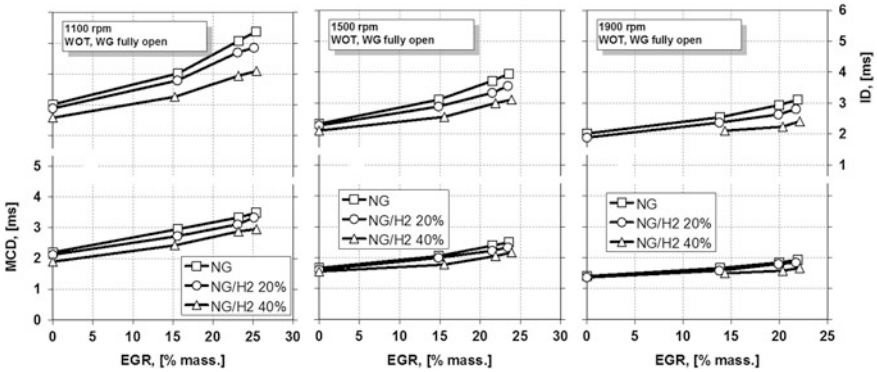

Fig. 5 Incubation duration and main combustion duration at the three tested speeds varying hydrogen content and EGR rate

A faster combustion was achieved with H_2 addition. A stronger effect of H_2 as combustion boosting is visible at lower speed during the first part of combustion, ID. In particular, at EGR rate increasing, the combustion conditions become worse and a positive effect of H_2 on the ignition process in all the tested operating points is highlighted, Fig. 5. A less evident effect has been observed on MCD especially at higher speed. This indicates that the combustion speed increasing due to turbulent intensity is higher than that due to hydrogen addition.

The faster combustion gives a higher peak pressure and pressure rise, Fig. 6, despite SA was reduced to retain the BGC position.

With EGR rate ranging from 0 to 25 %, an increasing of THC, both upstream and downstream the three-way catalyst (TWC) was observed for all the three tested fuels. However, with blends containing higher amount of H_2, THC increasing was less marked. Consequently, a higher hydrogen content in the blend provides benefits on THC emission reduction, both upstream and downstream the catalyst, at

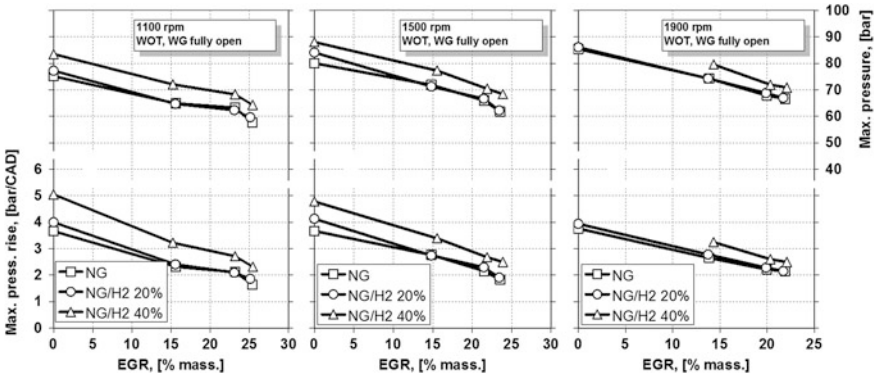

Fig. 6 Maximum in-cylinder pressure and pressure rise at the three tested speeds varying hydrogen content and EGR rate

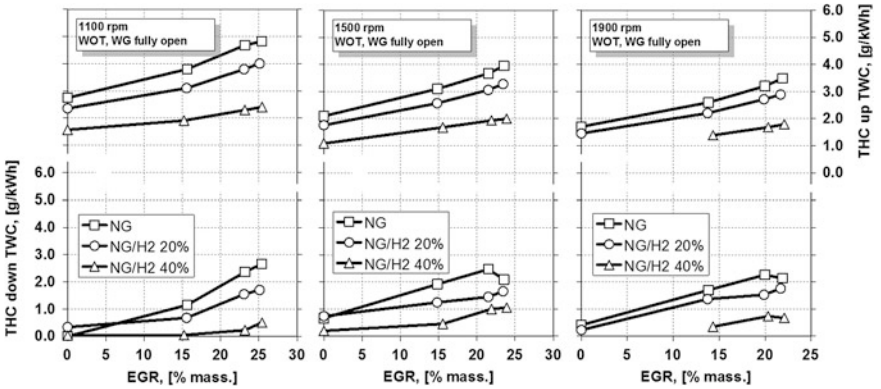

Fig. 7 THC upstream and downstream the catalyst at the three tested speeds varying hydrogen content and EGR rate

each EGR percentage, as shown in Fig. 7. Anyway, it has to be mentioned that THC emissions downstream the catalyst are largely dependent on engine operative conditions as well as catalyst characteristics and operative temperatures.

THC reduction, showed in Fig. 7, is not only due to the substitution of part of CH_4 with H_2, but also to a more complete combustion, as indicated by NG_{up} decreasing with H_2 content, Fig. 8. Anyway, since combustion efficiency is close to 98–99 %, the benefit of H_2 on NG_{up} does not affect the overall engine efficiency (Fig. 8). It can be assumed that NG_{up} is mainly affected by the effect of H_2 on the reduction of the quenching zone [23], which is just very small in the NG case. The faster combustion with H_2 did not give a higher global efficiency, even if the combustion becomes closer to the ideal constant volume one. To explain this behaviour, overcoming the limits of the experimental activity and extending the

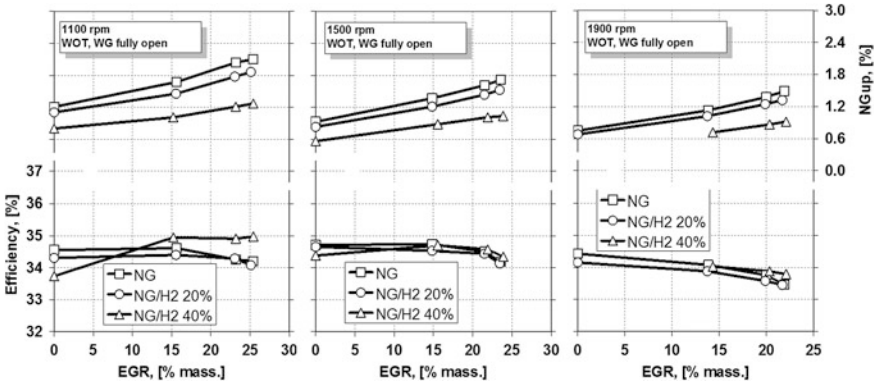

Fig. 8 Efficiency and NG_{up} at the three tested speeds varying hydrogen content and EGR rate

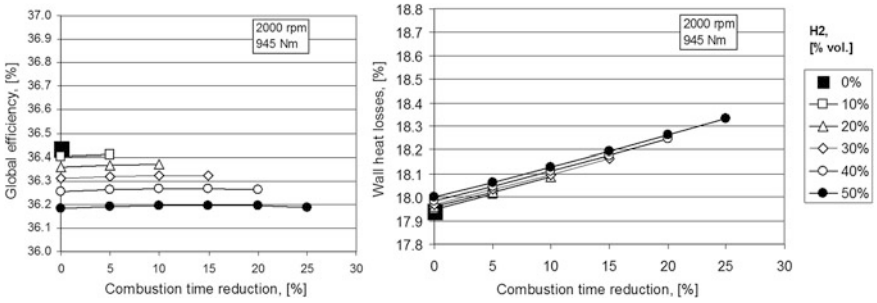

Fig. 9 Calculated effect of hydrogen content and shorter combustion duration on engine global efficiency and wall heat losses (adopted from [24])

analysis at full load condition and assuming higher hydrogen content a specific modelling of the reference engine was developed. The main results of the simulation are reported in Fig. 9. Detailed activity is reported in [24]. A reduction of the combustion duration, due to the use of CH_4/H_2 mixtures, may not give any benefit for the overall engine efficiency. In fact, the shorter duration of combustion, even if implies a higher thermodynamic efficiency, also causes an increase in heat loss for greater heat transfer to the walls. This gives a reduction on global efficiency at H_2 content increasing. In the experimental activity, without EGR, a reduction of global efficiency even higher than calculated by the model was observed in some conditions. This could be justified with the NG_{up} measured trends that were in accordance with a lower quenching distance which gives higher wall heat losses. The model, instead, considering a complete combustion did not take into account this effect. At EGR increasing the lower combustion temperature mitigate the higher engine wall heat losses, therefore higher thermal efficiency with H_2 addition have been measured.

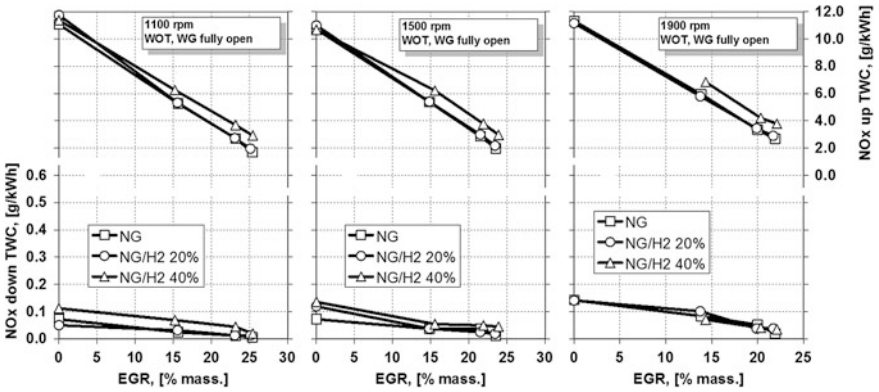

Fig. 10 NO_x upstream and downstream the catalyst at the three tested speeds varying hydrogen content and EGR rate

The EGR rate has a significant impact on NO_x formation reduction (measured upstream the TWC) through lower combustion temperature, while a slight trend in increasing NO_x concentration inside the combustion chamber is observed when increasing H_2 fraction in the blend due to temperature increasing connected to faster combustion, as shown in Fig. 10. Downstream the TWC catalyst NO_x emissions are less influenced by the fuel mixture composition.

A second activity was then performed at 1100 and 1900 rpm increasing the air index up to 1.5–1.7 with different EGR rate and with the same BGC, throttle and WG condition of the previous activity. The results are report in the Figs. 11 and 12. It is evident the effect of H_2 on the lean burn combustion improving both with and without EGR. At H_2 increasing it is possible to extend the zone of higher efficiency in lean conditions (refer to Fig. 11).

The dilution of mixtures with excess of air acts as dilution with EGR as regard in-cylinder combustion temperatures decreasing. Thus the negative effect of faster combustion on wall heat losses are mitigate. Therefore a more complete combustion addicted by a lower NG_{up} gives also a higher engine thermal efficiency.

These data highlight the possibility of optimizing engine efficiency acting on air index, as it is for current NG lean-burn engines, and also on H_2 content and EGR. To make this possible, the issue of NO_x reduction in lean condition should be afforded. In fact NO_x emissions, reported in Fig. 13, are higher than that of TWC stoichiometric case even if high EGR rate are set. Anyway, to increase the maximum power achievable with high H_2 content, avoiding abnormal combustion, also an engine redesign should be considered (combustion chamber shapes, ignition systems, etc.).

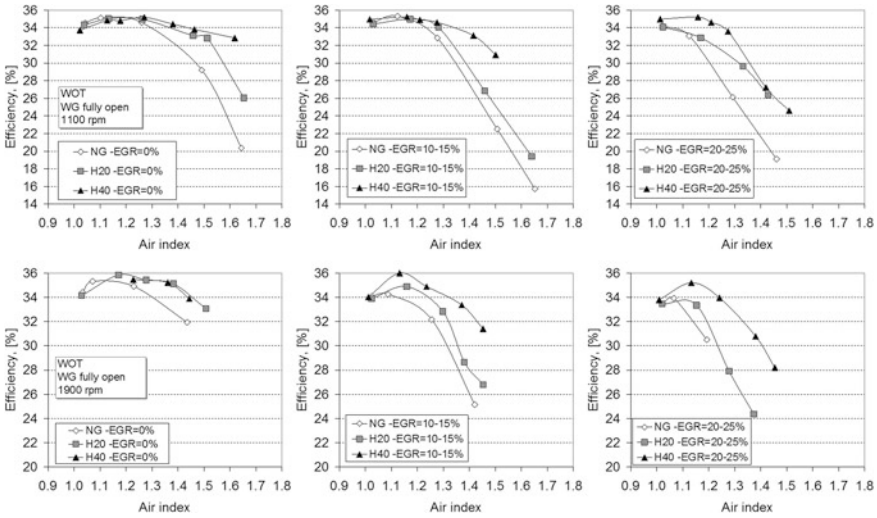

Fig. 11 Engine global efficiency at 1100 and 1900 rpm varying air index, hydrogen content and EGR rate

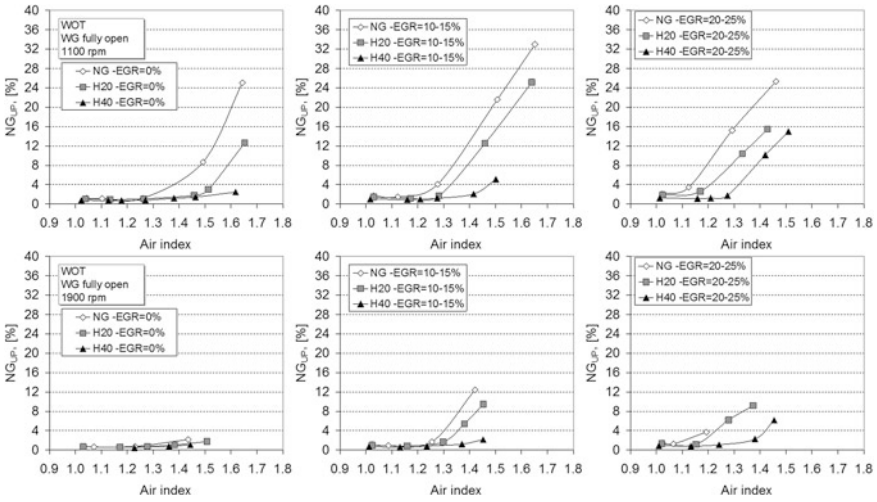

Fig. 12 NG_{up} at 1100 and 1900 rpm varying air index, hydrogen content and EGR rate

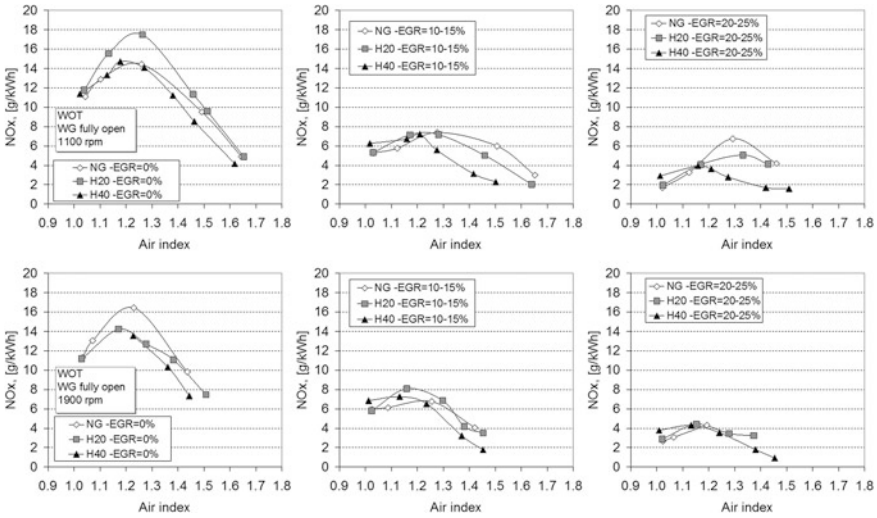

Fig. 13 NO_x at 1100 and 1900 rpm varying air index, hydrogen content and EGR rate

4 Experimental Comparison of Stoichiometric and Lean Burn on the ETC Cycle

In this section a comparison between stoichiometric and lean burn fuelling with a CH_4/H_2 mixture on the ETC is reported. ETC is the reference cycle for HD gas engines emission measurement in the steps EURO III, IV, V, and EEV (Enhanced environmental friendly vehicles). The comparison is referred to two different HD SI dedicated NG engines. The stoichiometric one is the same of Table 1 equipped with a TWC and an oxygen lambda sensor while the lean burn is a 170 kW engine (Table 4) equipped with an oxidant catalyst and a UEGO lambda sensor which indicates the oxygen content in the exhaust gas and allows a more accurate air-to-fuel ratio in lean conditions.

Table 4 Main characteristics of the lean burn SI CNG engine

Type	6-cylinder in line
Displacement	6.9 L
Bore × stroke	106 × 130 mm
Compression ratio	10.5:1
Rated power	170 kW @ 2200 rpm
Max. torque	810 Nm @ 1200–1800 rpm
Boost pressure	124 kPa @ 2200 rpm
Intercooler	Air to air
NG feeding system	Electronic timed multi-point injection
Power density	24.6 kW/L

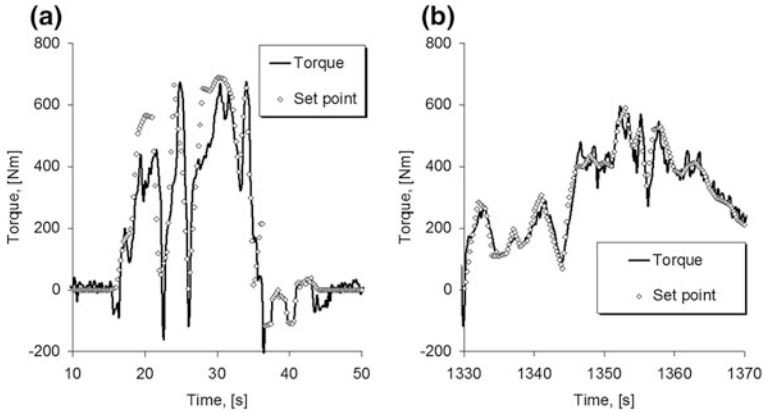

Fig. 14 Torque performed by for the lean burn engine compared with the set point of the ETC cycle: **a** part of urban phase, **b** part of motorway phase

The engines were fuelled with NG and with a blend of pure methane and 15 % of H_2 by volume named HCNG. The NG used has 85 % of methane content while the rest is principally constituted by ethane and inert gases. The HCNG, represents instead an enriched NG in which substances different from methane were replaced by hydrogen.

Transient tests were carried out on an AVL Puma 5 dynamic test bed, integrated with an emission test bench, able to control the engine and carry out continuous measurements during the ETC. The ETC test approval for gaseous SI HD engines is fixed through a table of normalized values of speed and torque. The full torque curve of the engine is used to denormalize that table. The dynamic test has a duration of 1800 s and can be split in three subsets of 600 s: in the first there are very sudden changes of speed and load typical of the operation in urban areas, with continuous phases of "stop and go". The second subset is related to rural roads with less intensive variations of speed and load, while the last is representative of motorway running. Two short sections relating to the torque profile of the urban phase in the range 10–50 s of the ETC test (a) and of the motorway in the range of 1330–1370 s (b) are plotted in Fig. 14. The figure highlights that the engine must operate with considerable variations in performance, which require a very fast and accurate control for a correct execution of the cycle.

With the stoichiometric engine, the comparison between the two test fuels has been carried out without changing the ECU calibration. Therefore the same SA map was used for both NG and HCNG fuelling. For the lean burn engine, instead, the SA map requires a reduction, in order to avoid much elevated NO_x emissions. The experimental activity determined a SA reduction of 2.5 CAD on the whole engine map as a good compromise among performance, emissions and efficiency.

In Table 5 the comparison among the results on the ETC test with the two engines and the two tested fuels is reported. CO, NMHC and NO_x emissions were lower than EEV limits in all the cases. Particulate matter (PT) emissions were very

Table 5 Comparison of results of the ETC tests for both the stoichiometric and the lean-burn engine with the EEV limits

	CO (g/kWh)	NMHC (g/kWh)	CH_4 (g/kWh)	NO_x (g/kWh)	PT (g/kWh)	CO_2 (g/kWh)	BSEC (MJ/kWh)
Stoichiometric 200 kW NG	2.36	0.07	0.68	0.49	<0.01	714	12.5
Stoichiometric 200 kW HCNG	2.15	<0.01	0.67	0.52	<0.01	670	12.7
Lean burn 170 kW NG	<0.01	0.06	2.32	1.37	<0.01	705	12.4
Lean burn 170 kW HCNG	<0.01	0.00	2.26	1.64	<0.01	643	12.2
Limits							
EURO III	5.45	0.78	1.60	5.00	0.16	–	–
EURO IV	4.00	0.55	1.10	3.50	0.03	–	–
EURO V	4.00	0.55	1.10	2.00	0.03	–	–
EEV	3.00	0.40	0.65	2.00	0.02	–	–

under the limits, especially for lean burn engine. The control of CH_4 emission is critical and strongly dependent from the exhaust temperature which is higher in case of stoichiometric fuelling. Slightly lower energy consumption was obtained with the lean burn engine. Using HCNG a reduction of CO_2 emission due to a higher H/C was obtained. With the stoichiometric engine the CO emissions are the most critical. Therefore the changing from CNG to HCNG gives some benefits, in fact the reduction of H/C of the fuel permits also a reduction of CO emissions. High TWC NO_x conversion efficiency permits to not increase NO_x emission downstream the catalyst when HCNG is used, although NO_x emissions increase upstream the catalyst, due to a faster combustion that, at parity of SA, gives higher combustion temperatures.

With the lean-burn engine, NO_x control is possible only in the combustion chamber, not being coupled a post-reduction system of exhaust gas. Moreover, the lowest exhaust temperature makes more variable the conversion efficiency of the oxidation catalyst respect to the stoichiometric engine. In Table 6 it is possible to analyse both the two mentioned problems for the lean burn engine.

Looking at the first and the second lines, CO and NMHC conversion is almost complete while CH_4 are reduced of about 50 %. Considering the standard deviation of results, there is a low variation of engine CH_4 exhaust emission upstream the catalyst and a high variation downstream the catalyst. This is due to the efficiency of the conversion system, in particular in the first phase of the ETC cycle, influenced by the initial catalyst temperature, which is a fundamental parameter on CH_4 oxidation. In fact, for this kind of engine also the presence of insulation on the exhaust could influence the CH_4 conversion efficiency of the catalyst. Thus the results on CH_4 obtained could be reduced with a more efficient aftertreatment exhaust system. About NO_x emission, from the second and the third lines an

Table 6 Results of the ETC tests for the lean burn engine with different conditions

	CO MV (g/kWh)	SD (%)	NMHC MV (g/kWh)	SD (%)	CH_4 MV (g/kWh)	SD (%)	NO_x MV (g/kWh)	SD (%)
NG Up. Cat.	2.74	0.7	0.91	4.7	5.16	2.6	1.40	7.1
NG Down. Cat.	<0.01	0.1	0.06	0.1	2.32	26.9	1.37	6.9
HCNG Down. Cat.	<0.01	0.1	<0.01	0.1	2.10	20.1	2.45	8.1
HCNG SA Optimized Down. Cat.	<0.01	0.1	<0.01	0.1	2.26	18.3	1.64	7.8

increase of more than 80 % with HCNG is evident when the ECU SA calibration is not adjusted. Therefore an optimization of the SA calibration is necessary to retain the same level of NO_x emission of the CNG case (forth line).

5 Conclusions

In this chapter an analysis of the effect of hydrogen addition to natural gas on the performance and emission of heavy duty engines is carried out. The discussion is based on experimental data on heavy duty engines fuelled with NG and some NG/hydrogen blends. A faster combustion derives from H_2 addition. In fact, in order to retain the same peak pressure position of NG operation, SA is reduced at H_2 content increasing. Although the faster combustion development, the global efficiency is only marginally influenced by hydrogen content in the blends in the case of stoichiometric fuelling. In particular, a more complete combustion process with a lower formation of THC and CO causes also a reduction of the quenching zone. This, together with the higher in-cylinder temperature due to the faster combustion results in higher gas cylinder wall thermal exchange. Therefore the tailpipe CO_2 emission reduction is strictly related to the amount of NG substitution with H_2 content. The possibility of charge dilution, instead, could reduce this negative aspect. In fact, thanks to hydrogen characteristics, a more relevant amount of EGR rate or charge dilution are tolerated by the engine and a strong reduction of maximum in-cylinder temperature is possible. Therefore a right metering of hydrogen content and charge dilution could lead to a more complete combustion and also to higher engine global efficiency, avoiding abnormal combustion phenomena.

European transient cycle tests on two dedicated HD engines, highlight that with a stoichiometric engine no particular attention should be placed when the engine is switched from CNG to HCNG, in fact the NO_x increasing happens only upstream the three-way catalyst. With a lean-burn engine ECU SA adjustment should be required when the engine is fuelled with HCNG with the aim of not compromising the very low engine-out emissions with NO_x increasing.

References

1. Orecchini F, Santiangeli A (2011) Beyond smart grids—the need of intelligent energy networks for a higher global efficiency through energy vectors integration. Int J Hydrogen Energy 36(13):8126–8133
2. Battaglini A, Lilliestam J, Haas A, Patt A (2009) Development of SuperSmart grids for a more efficient utilisation of electricity from renewable sources. J Clean Prod 17(10):911–918
3. Hammons T (2008) Integrating renewable energy sources into European grids. Int J Electr Power Energy Syst 30(8):447–462
4. Crossley P, Beviz A (2010) Smart energy systems: transitioning renewables onto the grid. Renew Energy Focus 11(5):54–59
5. Hemmes K, Guerrero JM, Zhelev T (2011) Highly efficient distributed generation and high-capacity energy storage. Chem Eng Process 51:18–31
6. Delucchi M, Jacobson MZ (2011) Providing all global energy with wind, water, and solar power, Part II: reliability, system and transmission costs, and policies. Energy Policy 39 (3):1170–1190
7. Kelly N, Gibson TL, Cai M, Spearot J, Ouwerkerk DB (2010) Development of a renewable hydrogen economy: optimization of existing technologies. Int J Hydrogen Energy 35(3):892–899
8. Barton J, Gammon R (2010) The production of hydrogen fuel from renewable sources and its role in grid operations. J Power Sources 195(24):8222–8235
9. De Simio L, Gambino M, Iannaccone S (2013) Possible transport energy sources for the future. Transp Policy 27:1–10
10. Forschungsberichte Verbrennungskraftmaschinen Heft 120, 1997, 'Erweiterung der Energieerzeugung durch Kraftgase, Teil3
11. Chapman KS, Patil A (2008) Performance, efficiency, and emissions characterization of reciprocating internal combustion engines fuelled with hydrogen/natural gas blends. Technical report DOE award DE-FC26-04NT42234. http://www.osti.gov/scitech/servlets/purl/927586
12. Boulouchos K, Dimopoulos P, Hotz R, Rechsteiner C, Soltic P (2007) Combustion characteristics of hydrogen-natural gas mixtures in passenger car engines. SAE paper no. 2007-24-0065
13. Andersson T (2002) Hydrogen addition for improved lean burn capability on natural gas engine. Rapport SGC 134. http://www.sgc.se/ckfinder/userfiles/files/SGC134.pdf
14. Park C, Kim C, Choi Y, Won S, Moriyoshi Y (2011) The influences of hydrogen on the performance and emission characteristics of a heavy duty natural gas engine. Int J Hydrogen Energy 36(5):3739–3745
15. Xu J, Zhang X, Liu J, Fan L (2010) Experimental study of a single-cylinder engine fueled with natural gas–hydrogen mixtures. Int J Hydrogen Energy 35(7):2909–2914
16. Ma F, Wang M, Jiang L, Deng J, Chen R, Naeve N et al (2010) Performance and emission characteristics of a turbocharged spark-ignition hydrogen-enriched compressed natural gas engine under wide open throttle operating conditions. Int J Hydrogen Energy 35(22):12502–12509

17. Wang J, Chen H, Liu B, Huang Z (2008) Study of cycle-by-cycle variations of a spark ignition engine fueled with natural gas–hydrogen blends. Int J Hydrogen Energy 33(18):4876–4883
18. Saanum I, Bysveen M (2007) Lean burn versus stoichiometric operation with EGR and 3-way catalyst of an engine fueled with natural gas and hydrogen enriched natural gas. SAE paper no. 2007-01-0015
19. Hu E, Huang Z, Liu B, Zheng J, Gu X (2009) Experimental study on combustion characteristics of a spark-ignition engine fueled with natural gas–hydrogen blends combining with EGR. Int J Hydrogen Energy 34(2):1035–1044
20. Dimopoulos P, Rechsteiner C, Soltic P, Laemmle C, Boulouchos K (2007) Increase of passenger car engine efficiency with low engine-out emissions using hydrogen–natural gas mixtures: a thermodynamic analysis. Int J Hydrogen Energy 32(14):3073–3083
21. Dimopoulos P, Bach C, Soltic P, Boulouchos K (2008) Hydrogen–natural gas blends fuelling passenger car engines: combustion, emissions and well-to-wheels assessment. Int J Hydrogen Energy 33(23):7224–7236
22. Ibrahim A, Bari S (2008) Optimization of a natural gas SI engine employing EGR strategy using a two–zone combustion model. Fuel 87:1824–1834
23. Heffel JW, Durbin TD, Tabbara B, Bowden JM, Montano MC, Norbeck JM (1996) Hydrogen fuel for surface transportation. SAE, Warrendale
24. De Simio L, Gambino M, Iannaccone S (2013) Experimental and numerical study of hydrogen addition in a natural gas heavy duty engine for a bus vehicle. Int J Hydrogen Energy 38 (16):6865–6873

Enriched Methane for City Public Transport Buses

Antonino Genovese and Fernando Ortenzi

Abstract Hydrogen is seen as an alternative strategy to overcome the energy dependence on fossil fuels. The epochal change recognized by the "hydrogen revolution" has not yet occurred; however, many efforts toward carbon-free energy development have been made. In the world of transportation, hydrogen as a fuel, has demonstrated reduction of pollutant emissions and better energy efficiency. Although low temperature fuel cells (FC) allow using FC generators on board of vehicles, there are still some open issues regarding FC generator durability and hydrogen storage. Furthermore, some manufacturers have already designed and produced vehicles powered by internal combustion engines fueled with hydrogen. As a matter of fact for both technologies, the major obstacle consists in the lack of a hydrogen distribution network. While awaiting for satisfactory solutions to the large availability of hydrogen at gas stations an intermediate step toward a carbon- free mobility is achievable with the mixtures of hydrogen and methane. These blends represent an interesting application to take advantage of conventional combustion engines and to promote the transition toward hydrogen mobility. The higher combustion characteristics of hydrogen result in a higher combustion efficiency that is able to reduce energy consumption and CO_2 emission due to the lower presence of carbon in the mixture. The Mhybus project demonstrates the feasibility of using hydrogen-methane blends as fuel in public transportation and highlights energy and environmental advantages.

Keywords Hydrogen · Methane · Hydro-methane · CO_2 · Emissions · Enriched methane for public transport · Mhybus project · IC engine · Engine performance

List of Symbols

CNG	Compressed natural gas
CPA	Center of testing vehicles
ECU	Engine control unit

A. Genovese (✉) · F. Ortenzi
ENEA Italian National Agency for New Technologies, Energy and Sustainable Economic Development, Rome, Italy
e-mail: antonino.genovese@enea.it

M. De Falco and A. Basile (eds.), *Enriched Methane*,
Green Energy and Technology, DOI 10.1007/978-3-319-22192-2_11

ETC	European transient cycle
EU	European Union
FC	Fuel cell
GHG	Greenhouse gases
GWP	Global warming potential
HCNG	Hydrogen-compressed natural gas
HNG	Hydrogen-natural gas
ICE	Internal combustion engine
IPCC	International panel on climate change
KIMM	Korea Institute of Machinery and Materials
LNG	Liquefied natural gas
OECD	Organization for Economic Co-operation and Development
P2G	Power to gas
PEMS	Portable emissions measurement systems
PV	Photovoltaic

1 Introduction

The CO_2 concentration in the atmosphere has increased noticeably from the beginning of the Industrial Age. The Working Group I of IPCC (International Panel on Climate Change) proved that CO_2 level in atmosphere until the eighteenth century was around 280 ppm with a deviation of ±10 ppm [1]. The massive exploitation of fossil fuels after the Industrial Revolution has rapidly increased the concentration of CO_2 to reach 390 ppm currently. In the year 2012, the CO_2 concentration was reported to be 394 ppm, which represents an increase of 40 % compared to the pre-industrial age [2]. Along with CO_2, the presence of other anthropogenic gases such as methane (CH_4) and nitrogen protoxide (N_2O) has grown drastically. These gases contribute to global warming with different potential (GWP) evaluated in 21 and 310 times the CO_2 respectively. The growth of CO_2 and other greenhouse gases (GHG) concentration in the atmosphere is attributable mostly to human activities (energy production, industrial processes, agriculture, waste).The International Energy Agency (IEA) evaluated in 49,503 megatons of CO_2 the equivalent of global emission of GHG in 2010 [2] of which 76 % is ascribed to CO_2 as shown in Fig. 1. In OECD (Organization for Economic Co-operation and Development) countries, this percentage is further increased achieving 82 % of the GHG emissions.

The role of CO_2 as anthropogenic cause in climate change is now an indisputable fact and fossil fuels are pointed as the main source of CO_2 resulting in 82 % of global CO_2 emission [2]. Segmenting by sectors the greatest CO_2 emissions come from energy production (electric generation and heat), which along with the transport sector represents 63 % of global CO_2 emissions (see Fig. 2).

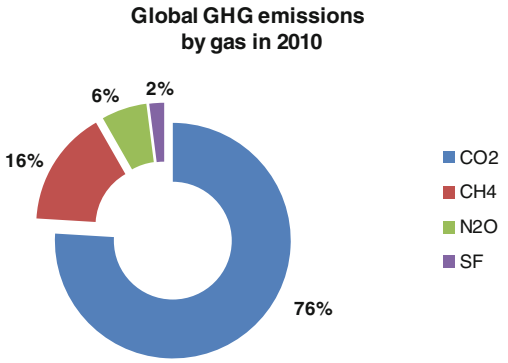

Fig. 1 GHG emission in 2010 by gas

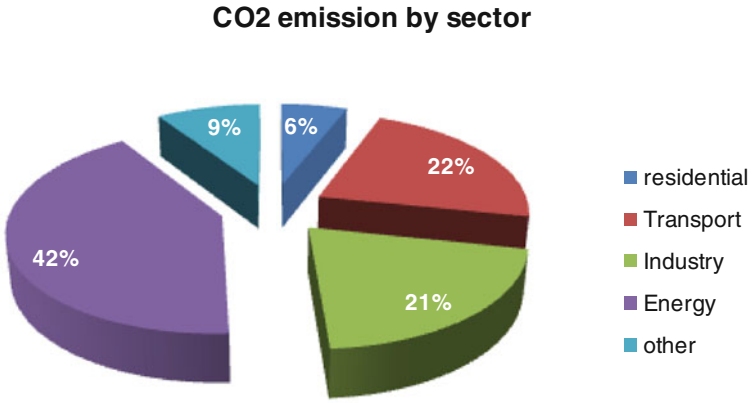

Fig. 2 World CO_2 emissions by sector

In 2011 the transport sector emitted 7,001 megatons of CO_2 of which 74 % (5,172 megatons) was caused from road transport. In road transport, liquid fuels (gasoline and diesel) combustion was the main source of CO_2 emissions being responsible for 96 % of the total. In EU countries, the CO_2 emissions by transport were greater reaching 31 % of global fossil fuel emissions with a share of 71 % of road transport [3].

Decreasing of GHG emissions requires a resolute intervention toward the reduction of fossil fuels consumption currently used to satisfy the world energy demand. Renewable energy sources (wind, solar) are a solution going in the right direction toward cutting down CO_2 emissions. However, they still carry a degree of uncertainty due to their intermittent nature and the supply–demand discontinuity. These limitations can be overcome with the adoption of high efficiency energy storage systems able to store energy surplus produced at time of low consumption

and made available at time of high user's demand. The direct storage of electric energy produced by wind or photovoltaic (PV) power plants is now under development in the new smart grid concept using Li-ion batteries as means of temporary storage. Nevertheless, electric storage is not the only energy storage system available to receive the energy from renewable power plants. An alternative can be actuated by storing hydrogen (and its derivatives such as synthetic natural gas) generated from electrolytic process energized with renewable sources as currently expressed within the "power to gas" (P2G) paradigm [4].

The age of "easy oil" is foreseen close to the end with estimated reserve between 50 [5] and 75 years. In this scenario, hydrogen is often referred as a potential substitute for oil and it is seen as a key element to change the economic structure of modern society based on fossil fuels toward a carbon free economy [6]. However, despite the efforts, hydrogen technology is not yet completely mature to suggest itself as full substitute of oil. Although significant progress in fuel cells (FCs) technology has been achieved, there are still problems regarding reliability and durability. Moreover, the absence of a widespread hydrogen network increases the difficulties of supplying it everywhere without expensive investments. Studies [7] demonstrated that up to 50 % of hydrogen could be injected in existing NG pipelines depending on the steel kind and the operating conditions without embrittlement or safety problems. However, (domestic) end-users could manifest problems of slight backfire with fuel rich combustion if hydrogen share is over 10 %, while in lean fuel conditions hydrogen share can be as high as 50 % [8]. In the transportation sector technological constraints jointly with infrastructural lacks retarded the commercial diffusion of hydrogen FC vehicles. Many car manufacturers have already developed hydrogen FC vehicles with interesting results in energy consumption. However, the shortage of infrastructures necessary to support their daily use (filling stations, hydrogen distribution networks) confines these efforts to concept level only useful to confirm the technological feasibility of hydrogen vehicles. Instead, substantial financial investments are required to implement a widespread hydrogen network in order to expand the automotive FC market. The Japanese car manufacturer Toyota, aware of the effort needed to enlarge the automotive market to FCs vehicles, invited a free use of over 5,000 FC-related patents including technologies developed for the new Toyota Mirai [9].

Waiting for the implementation of an extensive network of hydrogen gas station able to refuel the hydrogen fueled vehicles, an interesting chance is given by Enriched Methane mixture as fuel in internal combustion engine (ICE). The hydrogen-natural gas (HNG) blends offer a ready use of hydrogen in NG engines already existing in the automotive market without heavy changes in engine designs but only operating small adaptations on engines and adjustments on combustion control. Distribution of HNG blend can be made through the NG network at low hydrogen rate or alternatively the mixture may be produced directly at the refilling station. Ready-use and low investment costs make HNG mixtures a bridging solution toward the full hydrogen age.

2 NG and H_2 as Clean Fuel in ICE

NG has proven to be a concrete alternative to gasoline and diesel fuels for vehicle propulsion. NG is a blend of different hydrocarbons (methane, propane, butane) and other gases (nitrogen, carbon dioxide, argon) with a wide methane share ranging from 85 to 99 % according to extraction site. NG, often incorrectly called methane, is a clean fuel since toxic compounds such as sulfur, or potentially toxic, such as benzene and higher molecular weight hydrocarbons, or highly reactive such as olefins, are absent. Even particulate matter in exhaust gas emissions of NG vehicles is very poor compared to diesel fueled vehicles. The low carbon content in NG makes it a fuel with a low CO_2 emission level. The specific emission of CO_2 per mass unit in NG combustion is 2.75–2.85 versus 3.15 kg_{CO_2}/kg_{fuel} of diesel fuel combustion.

Nowadays, most NG engines operate in spark -ignition (SI) mode, for both light and heavy-duty applications. Usually, NG is stored as compressed gas at high pressure (200–300 bar) (CNG) in steel or composite vessels. An alternative storage of natural gas is possible as liquid (LNG), but it requires a cryogenic temperature (−162 °C) to keep NG at liquid state. At present only heavy-duty vehicles with LNG tanks have been developed for commercial use. The CNG vehicles technology is widely established, especially in countries with a large distribution network of NG. In Italy, for example, over 1,000 filling stations, about one-third of European CNG filling stations, offer natural gas in addition to gasoline and diesel fuels. The main disadvantages of CNG fuel is the weight and size of storage tanks in comparison with gasoline or diesel fuel. As shown in Table 1, 100 l of CNG (@ 200 bar) has an energy content 5 times lower than the same volume of gasoline or diesel fuel. To keep the same vehicle range CNG storage tanks should be about 5 times larger than diesel tanks. This results in additional weight and space required to fit on board CNG tanks. Typical weight of CNG tanks range between 0.2 and 1 kg per liter depending on cylinder composition (composite, steel composite, steel).

In heavy-duty vehicles, the disadvantages represented by greater fuel tank weight and volume are reduced because of the wide space availability and the small relative weight increase. Moreover, public transportation routes in urban areas are scheduled, therefore the size of NG tanks can be chosen according to the required range. For transit buses the roof usually offers the opportunity to place cylinders

Table 1 Fuel characteristics

Fuel (100 l)	Weight (kg)	Energy (MJ)	Specific energy (MJ/l)
Gasoline	75	3,260	32.6
Diesel	83	3,530	35.3
CNG (200 bar)	13.5	650	6.5
LNG	44	2,100	21
Hydrogen (200 bar)	1.54	185	1.85

Fig. 3 CNG bus with roof-mounted NG cylinder

(Fig. 3), saving more space for passengers and helping in distributing weight over axles evenly.

The 100 % H_2 as fuel in ICE was demonstrated to be an alternative to gasoline or diesel fuel. BMW presented in 2007 the Hydrogen 7 model based on conventional 730i model. Model 7 is a dual fuel vehicle that can be powered by gasoline and/or hydrogen. Only 100 hydrogen vehicles were produced to test the technology and they cumulate 3 million km ran in real-world testing. However, the lack of infrastructures and the high cost of conversion halted the real-world testing [10]. The use of 100 % H_2 as fuel, in substitution of NG, in an SI engine, drastically reduces vehicle operating range (by about 70 % compared to NG) due to its lower energy density by volume. Furthermore, H_2 has a low ignition energy in air (0.02 vs. 0.22 mJ of CH_4, at stoichiometric conditions, [11]), which ensures the combustion even with very lean mixtures but makes it subject to pre-ignition phenomena by contact with hot spots or residual gas. The effect of pre-ignition is that the event will produce an advance in start of combustion. This results in an increased heat release rate with higher peak pressure and higher in-cylinder surface temperature. The pre-ignition, unlike the knocking, cannot be controlled only with the ignition timing, but it requires substantial modifications to the engine and the control strategies. In [12], the use of cold spark plugs, low coolant temperature, and injection timing tuning are indicated as solutions to decrease the pre-ignition together with variable valve timing, intake charge cooling, and direct fuel ignition.

In H_2 ICE exhaust emissions are limited to NO_x as no hydrocarbons are present. Unfortunately, the high temperature produced by H_2 combustion increases production of NO_x. In order to control the level of NO_x, ultra lean combustion is adopted to decrease combustion temperature. H_2 ICE is susceptible to operating under highly diluted conditions and this strategy can decrease NO_x emission when air/fuel ratio referred to stoichiometric air/fuel (λ) is higher than 2. An alternative strategy to the above is the exhaust gas recirculation (EGR), where the exhaust gas is used to dilute the fresh charge and then decrease the temperature. For this solution a stoichiometric combustion is adopted with a three-way catalyst.

3 Enriched NG for H_2 Ready Fueled Vehicles

The transition toward a 100 % hydrogen mobility results attractive for the benefits which go along with it, however, it requires significant efforts in research and development. An effective way to shorten this transition is offered by the adoption of hydrogen-NG mixture as fuel. The HNG fuel is suitable to be used in existing NG vehicles, requiring only minor adaptations in engine settings or replacing some mechanical parts that are not suitable or compatible with hydrogen. The addition of H_2 to NG strengthens its advantage in low pollutant emissions at local level and also lowers the impact at global level decreasing CO_2 emissions. In comparison to FC and H_2 ICE, HNG technology is less costly, easier to apply, and can be used for revamping of CNG vehicles.

The use of NG-H_2 mixtures containing H_2 between 10 and 30 % per volume offer the opportunity to exploit the positive aspects related to the hydrogen without substantial modification of already existing natural gas engines, avoiding the drawbacks caused by use of pure hydrogen. Scientific literature data highlight an increase in flame front speed when H_2 is added to NG [13–15] and benefits on thermal efficiency. At the same time, a reduction of CO and unburned hydrocarbons (THC) occurs. On the contrary, NO_x emissions could be higher for more elevated temperatures at stoichiometric conditions [16]. H_2 added to NG gives the possibility to expand the lean burn limit [16, 17] due to a more stable combustion [18, 19]. A more stable combustion allows using higher exhaust gas recirculation to reduce the NO_x produced by the engine [17, 20, 21]. As hydrogen is a carbon-free fuel, the reduction of CO_2 emissions is a direct function of H_2 content in the mixture, at the same engine efficiency. For mixtures containing a 30 % in volume of H_2, more than 10 % CO_2 reduction is expected. In any case the way of H_2 production is a crucial aspect for additional CO_2 emitted.

First experiences of HNG mixture as fuel for buses were carried out within a research program in 1995 in Montreal (Montreal Hythane Bus Project). A 10–20 % vol. of a hydrogen blended with NG was used in a modified Cummins L-10 natural gas engine (Hythane® is a trademark registered by Hydrogen Components Inc). It was observed that NO_x emission decreased to about 45 %, compared to the emissions of NG buses, due to the more lean operation and the less spark advance of HNG [22]. The bus demonstration project at SunLine Transit Agency in California exhibited 50 % of reduction in NO_x emission using a 20 % vol. of H_2/NG blend. In Sweden, operation with HNG 20/80 % had been compared for a heavy-duty natural gas engine and the study had revealed a small increase in efficiency. Based on success with HNG buses, and the cost-effectiveness of HNG compared to available fuel cell technology, a number of projects are currently carried out all around the world, like the Beijing Hythane Bus Project, whose demonstration phase will be to adapt several natural gas engines for HNG operation. In Italy, a first experimental test aimed to evaluate the potential use of HNG in ICE was carried out in the framework of the EU Interreg IIIC project BONG-HY (Blends of Natural Gas and Hydrogen in internal combustion engines). The tested

vehicle was a light-duty commercial vehicle Euro III with a three-way catalytic converter, IVECO Daily 2.8 CNG originally fuelled with natural gas. Tests were carried out at chassis dynamometer using the ECE15 driving cycle and comparing the emissions levels of the CNG configuration with the results obtained with different HNG blends and control strategies as well. Using the optimized engine maps, the emissions levels were lower than the original CNG ones, especially for NO_x. In 2008, ENEA had already carried out an experimental campaign aimed to evaluate benefits of HNG blends as fuel in NG vehicle for public transport [23, 24]. Results were used to assess the most favorable percentage of H_2 to decrease CO_2 emission and the energy consumption. An 8 m long bus was fueled with several HNG blends (5, 10, 15, 20, and 25 % of H_2) and tested in an urban simulated driving cycle on road in ENEA Casaccia facilities. Test on HNG blends indicated that HC and CO decreased with the increase of H_2 percentages, although a fine-tuning in both ignition advance timing and leaning air-fuel ratio is necessary to decrease the NO_x emissions. The best blend resulted in 15 % of H_2 volume content.

4 Mhybus Experience

In the framework of European Life + program, Mhybus project (2009–2013) has provided the technical and administrative steps to bring the first HNG fueled bus in Italy to circulate on public roads. Mhybus can be considered a pioneer project for further spreading of HNG mixtures not just in public transport application, but also for private and goods transportation. Starting from the results of previous first on road experiences, a mixture of 15/85 HNG was selected as testing fuel in Mhybus project.

In Mhybus project, an urban bus (Fig. 4), equipped with a lean burn spark-ignition (SI) NG engine, has been adapted to be fueled with a mixture of H_2 and NG (15/85 by volume).

Fig. 4 Mhybus project bus

Table 2 NG heavy-duty engine main characteristics

Turbocharged intercooler 6-cylinder in line	
Total displacement	6883 cm^3
Bore × stroke	106 × 130 mm
Compression ratio	10.5:1
Rated power	170 kW @ 2200 rpm
Rated torque	810 Nm @ 1200÷1800 rpm
Boost pressure	124 kPa @ 2200 rpm
Intercooler	Air to air
NG feeding system	Electronic timed multi-point injection
Exhaust treatment	Two way catalyst
Power density	24.7 kW/dm^3

Engine maps for the HNG configuration have been tuned in with ENEA facilities, then, for approval purposes, the engine has been tested on the European transient cycle (ETC) at Istituto Motori (Naples, Italy) of the Italian National Research Council. Finally, the vehicle, equipped with the adapted engine, has been put in regular transport service in Ravenna and monitored during its real-world usage. The urban bus was powered by an NG lean burn engine with rated power of 170 kW and equipped with an oxidation catalyst (Table 2).

4.1 Approval Procedure

The state of the art for regulations displayed the absence of specific type-approval procedure for HNG mixtures. Instead vehicles that run on compressed natural gas (CNG) had to meet the requirements of Regulation UNECE 110 and hydrogen-powered vehicles had to meet for type-approval procedures of the Regulation EC 79/2009 [25]. The regulation EC 79/2009 points out HNG mixtures as a transition fuel toward the use of pure hydrogen to facilitate the introduction of hydrogen-powered vehicles in Member States where the NG infrastructure is good. The regulation states that the European Commission should develop requirements for the use of HNG mixtures especially on the mixing ratio that takes account of technical feasibility and environmental benefits. The application of hydrogen regulation can be more stringent for HNG vehicles and conversely NG regulations can neglect some hydrogen properties, which may be important even if hydrogen is present in small volumes [26]. In the Mhybus project, in order to obtain permission to use the bus in regular service on the roads, a test protocol was agreed with the Ministry of Transport by way of the Center of testing vehicles (CPA) in Bologna. The request for specific tests was motivated by the need to evaluate the behavior of HNG blend as regards energy consumption, pollutant emissions, safety, and refueling operation. The experimental context was stressed by the main disposition of approval protocol that pointed out a minimum mileage of at least 45,000 km of

which the first 5,000 km is run without passengers. This claim was mandatory before to authorize the transit company to make use of the HNG vehicle out of experimental framework. In order to gain the final permission for each indicated area different tests were agreed and carried out as follows.

4.1.1 Energy Consumption

The use of hydrogen mixed with methane can result in a decrease in fuel consumption because hydrogen improves the combustion process as the flame front spreads more quickly allowing a more complete carbon oxidation. To evaluate the effect of hydrogen on energy consumption test at engine test bench was planned before and after road test. The ETC testing cycle was adopted to verify the energy consumption and compared with the energy consumption detected with the same engine powered by NG. For all time duration of road tests, HNG consumption was calculated from measured gas pressure/temperature in the vehicle tanks before and after each refueling. On road fuel consumption was compared with an equal NG fueled vehicle used as benchmark.

4.1.2 Exhaust Emissions

At present, Regulation EU 630/2012 sets the procedures for type-approval of motor vehicles fueled by hydrogen and mixtures of hydrogen and natural gas with respect to emissions limits. Failing of specific regulation when Mhybus operated the pollutant emissions were measured adopting the ETC cycle. Two ETC tests were scheduled: the first one before the on road testing in order to check compliance with the emission limits and a second one at the end of on road test to verify that hydrogen does not cause engine abnormalities that increase pollutant emissions. In addition, three emission measurement tests were operated during on road test using a Portable Emissions Measurement Systems (PEMS). Information about vehicle speed, rpm, torque, power, cooling temperature, oil pressure, and temperature was continuously monitored in order to detect the occurrence of anomalies.

4.1.3 Safety

To provide the same safety quality achieved in NG vehicles, the protocol established a set of requirements which HNG bus had to comply: use of materials compatible with hydrogen, endurance to electric and thermal operating conditions, safe refueling operation, protection from over-pressure, and incidental leaks. To gain these goals an analysis concerning the safety of 15/85 HNG mixture was carried out [27]. The flammability limits of methane/air and hydrogen/air are, respectively, 5–15 and 4–75 % while for 15/85 HNG/air they are 4.8–17.6 %, slightly different from methane. At 200 °C the flammability limits of HNG increase

Table 3 Ignition energy for HNG mixtures

Fuel mixture	Minimum ignition energy (mJ)
100 % CH_4–0 % H_2	0.22
75 % CH_4–25 % H_2	0.10
50 % CH_4–50 % H_2	0.09
25 % CH_4–75 % H_2	0.07
0 % CH_4–100 % H_2	0.02

at 3.8–17.5. The minimum ignition energy is 0.2 and 0.02 mJ for NG and hydrogen respectively. For HNG the minimum ignition energy is a function of volumetric concentration of hydrogen as shown in Table 3: for 15/85 mixture ignition energy is 0.14 mJ, close to the methane.

Specific focus was reserved to investigate the separation of the mixed gas and the behavior during an accidental release. Results on dispersion and the long-term stratification of hydrogen–methane mixture are reported in [28]. With the presented experiment configurations and measurement time (1 h), no separation between hydrogen and methane was observed in case of dispersion in air. For gas separation inside the pressurized vehicle tank no meaningful separation between hydrogen and methane was detected on long term [27]. The jet fire produced by ignition of a released mixture of 15/85 hydrogen/methane was indicated close to that of methane. A review of materials component the storage and supply circuit (from bottles to engine) was carried out to check the compliance with hydrogen in order to avoid leakage from gaskets or mechanical failure due by hydrogen embrittlement. A program of periodic inspections was implemented to control gas leaks and to replace suspected parts.

The bus under test was equipped with gas sensors placed inside the engine compartment and in the tank compartment on the roof. Relief valves in case of over-pressure and fire were already placed on the gas bottles as indicated by ECE110 regulation. Operating and safety manuals were released in order to train drivers and technicians on what to do in case of gas leak or fire. In the refilling operation no special action was indicated but only to make a ground connection of vehicle chassis to avoid static charge build up and let engine compartment open.

4.1.4 Refilling Operation

A dedicated filling station for the HNG blend has been designed and built within the premises of a hydrogen production plant in Ravenna (Fig. 5). A specific mixing unit has been designed to provide the bus daily with the necessary fuel. During refilling, hydrogen and methane are mixed according to the fixed ratio (15 % H_2 in volume with a tolerance of ±2 %) within a mixing unit tailor-made for the project.

The filling station was built according to the safety standards for fire and explosion and received the authorization to operate from Fire Brigade.

Fig. 5 HNG refilling operation

5 Mhybus Testing Results

At test rig (Fig. 6) the engine was fueled a first time with NG using the original ECU map in order to define the actual benchmark. Afterward, the engine was fueled with the blend of H_2 and NG (15/85 % vol). The testing activity was carried out on an AVL Puma 5 dynamic test bed, integrated with an emission test system, able to control the engine and carry out continuous measurements during the ETC respecting all the constraints imposed by the legislation. The ETC cycle, which is the test approval for gaseous SI heavy-duty engines, is fixed through a table of

Fig. 6 Tested engine on the test bed

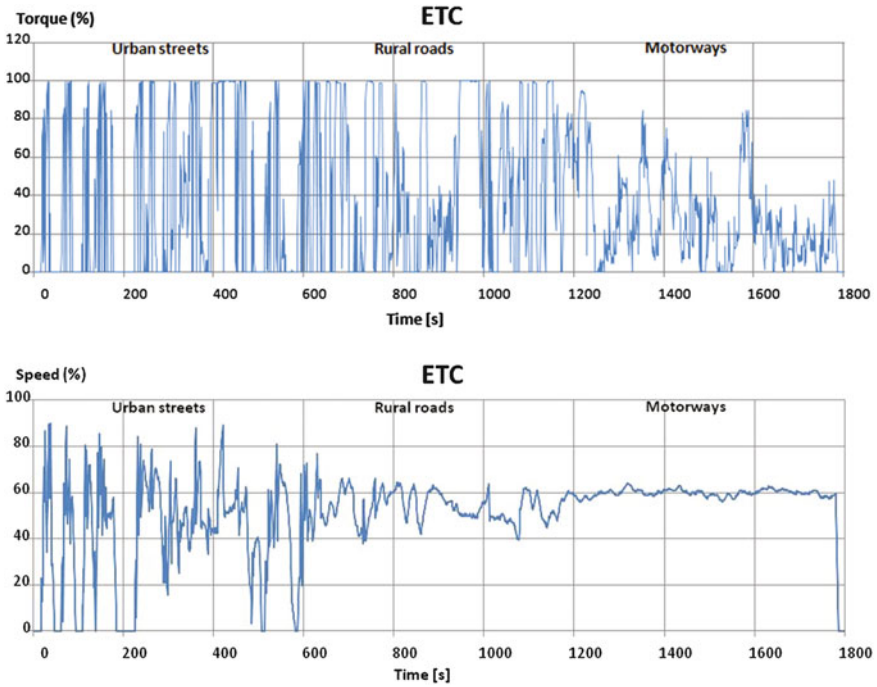

Fig. 7 ETC dynamometer engine speed and torque

normalized values of engine speed and torque. The full-load torque curve of the engine is used to de-normalize that table. Figure 7 shows the profiles of normalized torque and speed during the ETC.

The dynamic test has a duration of 1800 s and can be split into three subsets of 600 s: in the first, there are very sudden changes of speed and load typical of the operation in urban areas, with continuous phases of "stop and go." The second subset is related to rural roads with less intensive variations of speed and load, while the last is representative of motorway running. As already stated testing at test rig were carried out twice: before and after the 45,000 km covered on road.

In Table 4 the fuel consumption and CO_2 emitted on ETC driving cycle has been reported: a reduction of about 7.6 % in CO_2 has been measured using HNG instead of NG. The engine does not produce appreciable values of CO and PM. The NG

Table 4 Results of ETC tests

	CO_2 (g/kWh)	BSEC (g/kWh)	BSEC (MJ/kWh)	NO_x (g/kWh)	THC (g/kWh)	CO (g/kWh)
CNG	703	265	12.4	1.44	3.19	0
HNG before	649	244	12.2	1.41	2.47	0
HNG after	645	242	12.1	1.58	2.65	0

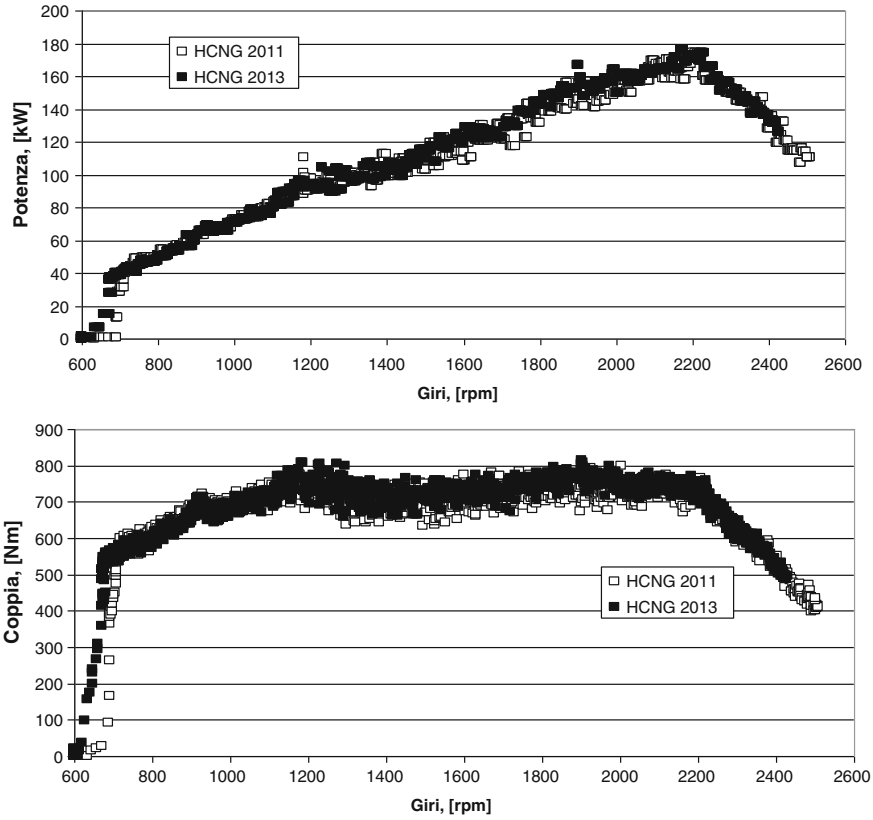

Fig. 8 Engine power and torque with HNG before and after 45,000 km

used as fuel for benchmark was derived by gas network and resulted composed of a gas mixture consisting mainly of methane (86 %) including varying amounts of other gases (ethane 6 %, propane 2 %, and other inert gases). The NG used for the HNG mixture production was rich in methane gas (99 %) as usually occurs in the NG extracted in Italy. Figure 8 shows the engine power and torque provided with HNG fuel before and after the 45,000 km covered with no appreciable change in performance.

From January to September 2013, the HNG bus ran on normal service along line 8 in Ravenna. It ran on average 200 km per day, for a total of 45,000 km. In this long time real-world measurements the bus was fueled with the 15–85 % mixtures of H_2–CH_4 in volume and fuel consumption was compared with that of another bus (same model) running the same mission and fueled with NG.

The fuel consumption was detected using the pressure-temperature method with real compression factor correction. Fuel mass consumption for NG bus was about 0.322 kg/km while for HNG was 0.282 kg/km, (−13 %). Energy consumption was 16 MJ/km for CNG bus and 14.4 MJ/km for HNG bus (−10 %). The CO_2 produced

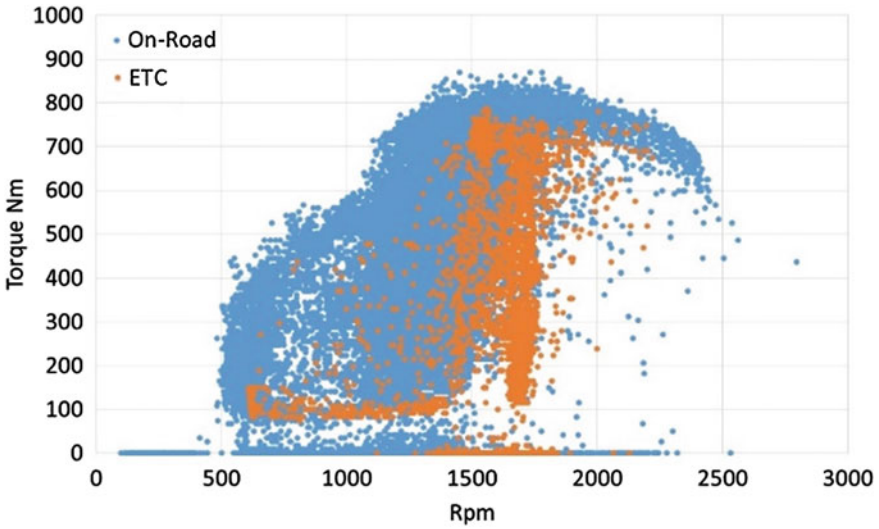

Fig. 9 rpm-torque comparison between the ETC and real-world use (fueled with HNG)

was 0.885 kg/km for CNG and 0.753 kg/km for HNG. The benefits of the HNG blends are about −15 % of CO_2 emitted on road. However, the H_2 production through SR produce a CO_2 emission that decreases the advantage gained on road. The net CO_2 emission in a Well to Wheel path was calculated in −8 %.

Real-world driving cycles are quite different from the ETC cycle and more severe in terms of power, but also more dispersed in terms of engine rpm and load as shown in Fig. 9. The average engine power on the ETC driving cycle is 20 kW while on road the average power supplied by the engine, considering the whole test data available, was 36.1 kW. The engine, during the ETC driving cycle, runs mainly in the range of rpm from 1400 to 1800, while on-the-road running is in a wider range. These results, however, are much similar to those obtained in the previous experimentation [23] in which the same vehicle, with 15 % of hydrogen percentage, we obtained a 16 % reduction of CO_2 emissions.

The absence of technical problems and the monitoring data about the engine performance demonstrated that the use of the HNG blend does not hinder the vehicle performances. In the endoscopic inspections are not recognizable signs of damages, but are visible deposits as shown in Fig. 10a. The same deposits are shown in Fig. 10b for an engine piston fueled with NG after a mileage of 150,000 km.

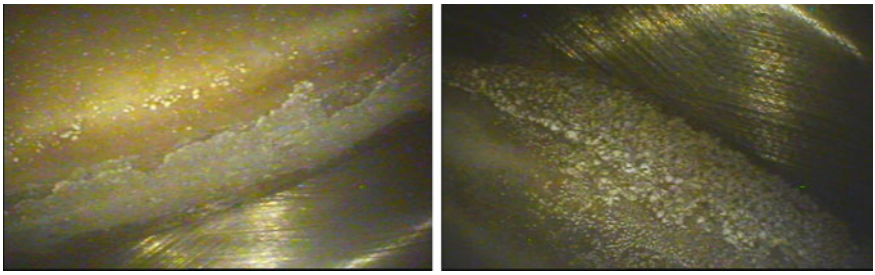

Fig. 10 HNG engine piston after 45,000 km and CNG engine piston after 150,000 km

6 Economic Evaluation

Economic and environmental sustainability of HNG mixtures are dependent on the cost, safety, and environmental impacts of H_2 production. The clear definition of the financial aspects of H_2 production and distribution is not easy to assess because it depends on a set of multiple items whose variations are relevant. This variability can lead to significant changes in the H_2 cost, even of some tens of percents. The production of H_2 can be made either on a centralized large size facility or on smaller plants placed on-site. The latter provision appears to be the one able to help in the short term, the development of an H_2 economy by limiting the investment costs for infrastructure, transport, and distribution. Conversely, plants of large size appear to be more convenient in H_2 production for the scale economy advantages offered only in case of high volumes of H_2 production. A nonexhaustive list of the main elements which contribute to the final cost of H_2 includes investment and maintenance cost for production plant differentiated by pathways (steam reforming from NG, electrolysis, coal gasification,….), cost of raw materials (mainly hydrocarbons, energy, demineralized water), hydrogen volume produced, distance of dispatching, type and size of transport and storage means, size of storage system at the user site. For on-site plants the distance of dispatching and transport system size is ineffective but secondary subsystems such as compressors, buffers, and local back-up storage have to be considered. To these factors must be added, of course, the cost of any taxes and excise.

The evaluation of economic sustainability of HNG has been made comparing the NG cost with the HNG cost. To carry out this comparison the hydrogen cost was estimated as indicated in ZeroRegio project for different pathways and plant capacity [29]. A Steam Reforming (SR) centralized power plant was considered in H_2 production with 200 Nm^3/h of nominal capacity, efficiency higher than 70 % and a NG price of 4 €/GJ was used. With these assumptions the hydrogen cost is indicated in 0.65 €/Nm^3 (60.3 €/GJ). The plant capacity selected is able to produce over 400 kg/day of hydrogen useful to fuel a fleet of 250 buses with the 15/85 mixture of HNG for a daily mileage of 200 km all. SR plants with higher capacity (over 56,000 Nm^3/h) can give H_2 at lowest cost of 0.06 €/Nm^3. The specific

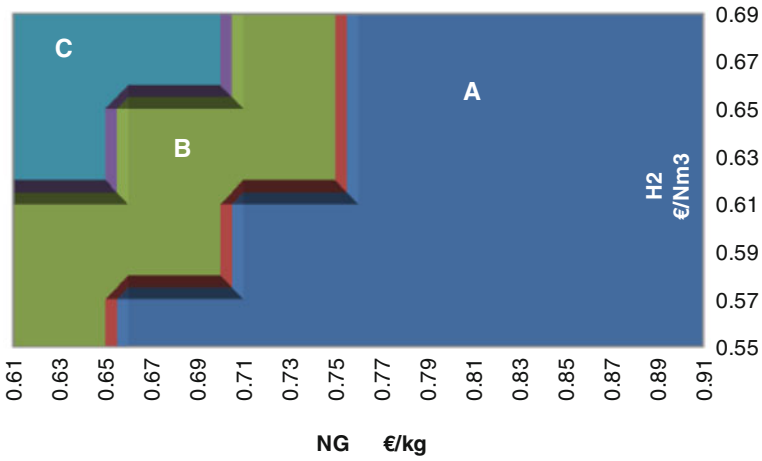

Fig. 11 HNG versus NG (at refilling station) additional cost

situation in Mhybus project related to the refilling station placed inside the H_2 production plant (centralized plant, no shipping cost, infrastructure available by the project partner) allowed an estimated saving of 0.10 €/Nm^3 thereby bringing the hydrogen cost to 0.55 €/Nm^3. With the fuel consumption data detected in real driving conditions, it is possible to identify three different areas as the function of NG cost at final users (tax included) and the H_2 cost (Fig. 11): in area *A* there is not much difference in fuel cost (within the measurement error of fuel consumption) for daily transit service, in area B the extra cost of HNG is limited within the 5 % with an annual additional cost of 500 €/year for each bus, in area C the additional cost have a maximum value of 700 €/year for each bus.

7 Conclusion

Mhybus demonstrated that using the HNG mixture in public transport significantly increases its sustainability. This is due to a reduction in CO_2 emissions and to a decrease in fuel consumption. During the road test operations, 5.98 tons (3.19 tons taking into account the emissions from SR H_2 production) of CO_2 emissions were saved on 45,000 km. The project had a pioneering aspect for the definition of the approval procedures to be applied for a public transport vehicle and for technical features. The project was an example of a possible solution to contrast climate change and to improve air quality. Under tested conditions it was estimated that the maximum annual fuel extra costs for an HNG fueled bus were 800–1000 €/vehicle without the cost for the infrastructures. This estimate takes into account fuel consumptions and costs for hydrogen production. However, while fuel costs are the charge of the local transport company, the CO_2 emissions involve costs for the

whole society, and thus are expressed as indirect costs. Recent studies evaluate for every ton of CO_2 emitted by the transport sector an external cost of 20–70 € [30]. But recently a 200 € per ton was indicated as more real value for externalities cost. Thus, the higher yearly costs could be partially balanced by local or regional policy incentives as part of an overall strategy to increase the sustainability of transport. The extension of the technology to other NG fueled fleets is thus already a feasible and interesting solution compared to other emerging technologies that reduce urban transport's environmental impacts.

Mhybus also demonstrated that a smooth transition toward hydrogen age is possible without the need for heavy financial investment by adapting vehicles already in circulation. The next step must be made to design and commercialize HNG powered vehicles optimized for HNG mixtures. In this direction, the Korean government funded a project that aims to develop a bus powered by a Euro VI-compliant HCNG engine with the objective of reducing CO_2 emissions by more than 10 % compared to a CNG bus. Partners include KOGAS, Korea Gas Safety Corporation, Daewoo Bus, and Korea Institute of Machinery and Materials (KIMM) [31] and the budget available to gain the goal was of 13 M$ [32].

References

1. Forster P, Ramaswamy V, Artaxo P, Berntsen T, Betts R, Fahey DW, Haywood J, Lean J, Lowe DC, Myhre G, Nganga J, Prinn R, Raga G, Schulz M, Van Dorland R (2007) Changes in atmospheric constituents and in radiative forcing. In: Solomon S, Qin D, Manning M, Chen Z, Marquis M, Averyt KB, Tignor M, Miller HL (eds) Climate change 2007: the physical science basis. Contribution of working group I to the fourth assessment report of the intergovernmental panel on climate change. Cambridge University Press, Cambridge, p 996
2. CO_2 emissions from fuel combustion highlights (2013 Edition)—International Energy Agency. www.iea.org
3. Energy consumption and CO_2 emissions—Railway handbook 2012—International Energy Agency. www.iea.org
4. Lehner M, Tichler R, Steimuller H, Kpooe M (2014) Power to gas: technology and business models. Springer. ISBN 978-3-319-03995-4
5. http://www.bp.com/en/global/corporate/about-bp/energy-economics/statistical-review-of-world-energy/review-by-energy-type/oil/oil-reserves.html. Accessed 28 Dec 2014
6. Rifkin J (2003) The hydrogen economy. Tarcher 1st edn. ISBN 978-1585422548
7. NaturalHy Project—Final publishable activity report. Accessed 25 Mar 2010
8. De Vries H, Florisson O, Tiekstra GC (2007) Safe operation of natural gas appliances fueled with hydrogen/natural gas mixtures (progress obtained in the NaturalHy-project). In: International conference on hydrogen safety (ICHS 2007), San Sebastian, Spain
9. http://pressroom.toyota.com/article_display.cfm?article_id=4901. Accessed 09 Jan 09 2015
10. http://www.greencarreports.com/. BMW Halts 7 Series Hydrogen Vehicle Real World Testing Program Dec 21 2009
11. Chapman KS et al (2008) Performance, efficiency, and emissions characterization of reciprocating internal combustion engines fuelled with hydrogen/natural gas blends. Final Technical Report, DOE Award DE-FC26-04NT42234
12. White CM, Steeper RR, Lutz AE (2006) The hydrogen-fueled internal combustion engine: a technical review. Int J Hydrogen Energy 31:1292–1305

13. Hu E et al (2009) Experimental study on combustion characteristics of a spark-ignition engine fueled with natural gas–hydrogen blends combining with EGR. Int J Hydrogen Energy 34 (2):1035–1044
14. Dimopoulos P et al (2007) Increase of passenger car engine efficiency with low engine-out emissions using hydrogen–natural gas mixtures: a thermodynamic analysis. Int J Hydrogen Energy 32(14):3073–3083
15. Dimopoulos P et al (2008) Hydrogen–natural gas blends fuelling passenger car engines: combustion, emissions and well-to-wheels assessment. Int J Hydrogen Energy 33(23):7224–7236
16. Park C et al (2011) The influences of hydrogen on the performance and emission characteristics of a heavy duty natural gas engine. Int J Hydrogen Energy 36(5):3739–3745
17. Bysveen M (2007) Engine characteristics of emissions and performance using mixtures of natural gas and hydrogen. Energy 32(4):482–489
18. Ma F et al (2010) Performance and emission characteristics of a turbocharged spark-ignition hydrogen-enriched compressed natural gas engine under wide open throttle operating conditions. Int J Hydrogen Energy 35(22):12502–12509
19. Wang J et al (2008) Study of cycle-by-cycle variations of a spark ignition engine fueled with natural gas–hydrogen blends. Int J Hydrogen Energy 33(18):4876–4883
20. Boulouchos K et al (2007) Combustion characteristics of hydrogen-natural gas mixtures in passenger car engines. SAE paper-24-0065
21. Andersson T (2002) Hydrogen addition for improved lean burn capability on natural gas engine. Rapport SGC 134. Lund Institute of Technology. ISSN 1102-7371
22. Raman V, Hansel J, Fulton J, Lynch F, Bruderly D (1994) Hythane: an ultraclean transportation fuel. In: Proceedings of 10th world hydrogen energy conference, vol 3, Cocoa Beach, pp 1797–1806
23. Genovese A, Contrisciani N, Ortenzi F, Cazzola V (2011) On road experimental tests of hydrogen/natural gas blends on transit buses. Int J Hydrogen Energy 36:1775–1783
24. Pede G, Rossi E, Chiesa M, Ortenzi F Test of blends of hydrogen and natural gas in a light duty vehicle. SAE Technical Paper 2007-01-2045
25. Regulation (EC) No 79/2009 of the European parliament and of the council of 14 January 2009 on type-approval of hydrogen-powered motor vehicles, and amending Directive 2007/46/EC-L 35/32 Official Journal of the European Union 4.2.2009
26. Visvikis C, Pitcher M, Hardy B (2010) Hydrogen-powered vehicles: review of type-approval legislation on vehicle safety. Final report (TRL)
27. Carcassi M (2011) Caratteristiche e pericolosità di miscele di gas infiammabili Idrogeno/Metano (characteristics and dangerousness of hydrogen/methane gas mixtures). Mhybus internal project report
28. Marangon A, Carcassi MN (2014) Hydrogen-methane mixtures: dispersion and stratification studies. Int J Hydrogen Energy 39:6160–6168
29. Project no. 503190 Project ZERO REGIO Deliverable 7.1. Work plan competitiveness November 2005
30. Maibach M, Schreyer C, Sutter D, van Essen HP, Boon BH, Smokers R, Schroten A, Doll C, Pawlowska B, Bak M (2008) Handbook on estimation of external costs in the transport sector. Report internalisation measures and policies for all external cost of transport (IMPACT), Delft
31. http://www.ngvglobal.com/ngv-growth-and-development-ongoing-in-korea-0111. Accessed 11 Jan 2013
32. Han JO, Lee YC, Chae JM, Hong SH (2012) Introduction to Korean NGV industry and hydrogen blended CNG project for coping with euro 6 emission. In: World gas conference, Kuala Lampur

Exploring New Production Methods of Hydrogen/Natural Gas Blends

Kas Hemmes

Abstract In this chapter, we present concepts for hydrogen production technologies that create mixtures of hydrogen with natural gas, for either the gas grid or the standalone fuel; enriched methane. In the production of hydrogen from the natural gas itself, full conversion of methane into hydrogen is no longer necessary, as it is in conventional hydrogen production technologies, because the hydrogen is to be mixed with natural gas. In this study explored the production of hydrogen/natural gas blends through steam reforming of natural gas and through thermal and plasma decomposition of methane. The production methods considered are assessed on a conceptual design level. An interesting option is the production of hydrogen/natural gas blends by an internal reforming fuel cell, whereby effective heat integration is applied and at the same time electricity is produced at high total efficiency. We also investigate potentially simplified conversion routes from biomass compared to current conversion routes that aim at the production of pure hydrogen. Two examples, supercritical gasification and a bio-technological route, illustrate the production of hydrogen/natural gas blends from biomass.

Keywords Thermal and plasma decomposition of methane · Distribution grids · Enriched methane production processes · Production from biomass

List of Symbols

ΔG (J/mol)	Change in Gibbs free energy
ΔH (J/mol)	Change in enthalpy
η	Efficiency
η_{fc}	Fuel cell efficiency
ΔS (J/mol K)	Change in entropy
T (K)	Temperature
V (Volt)	Volt
i (A/m^2)	Current density

K. Hemmes (✉)
TU Delft, Mekelweg 2, 2628 CD Delft, The Netherlands
e-mail: k.Hemmes@tudelft.nl

M. De Falco and A. Basile (eds.), *Enriched Methane*,
Green Energy and Technology, DOI 10.1007/978-3-319-22192-2_12

r (Ω m^2)	Specific internal resistance
u_f	Fuel utilization
α (Volt)	Slope of local Nernst potential as a function of u_f

List of Acronyms

CHP	Combined heat and power
CSP	Concentrated solar power
DCFC	Direct carbon fuel cell
HHV	Higher heating value
EM	Enriched methane
ICE	Internal combustion engine
IR	Internal reforming
MCFC	Molten carbonate fuel cell
NG	Natural gas
SMR	Steam methane reforming
SOFC	Solid oxide fuel cell

1 Introduction

The significance of mixing hydrogen with methane or natural gas for the production of hydrogen is that by relaxing the constraints on the purity of the hydrogen, the production process can be simplified and optimized so that more cost-effective technologies dedicated to the production of hydrogen/natural gas (H_2/NG) or H_2/methane mixtures may be explored. In specific cases, for the H_2/NG blends, the final separation step may be completely eliminated because the product already has a suitable composition. We will explore the opportunities for synergy by focusing on both conventional and more innovative examples of hydrogen production processes, first using NG as a feedstock and second using biomass as a feedstock. The two main application areas for hydrogen/methane mixtures are the use of the mixture as a new standard gas composition in the natural gas grid and second as a fuel for internal combustion engines in cars and buses and other vehicles in the transport sector.

1.1 Mixing Hydrogen into the Natural Gas Grid

This chapter is partly based on an earlier conference paper written in the framework of the Dutch national 'Greening of Gas' project in which the feasibility of mixing hydrogen into the natural gas network was studied [1]. It explored new production methods for hydrogen natural gas blends as in this chapter. The possibility of

adding H_2 directly to the natural gas network leads us to explore innovative, low-cost and partial conversion methods. In contrast to pure hydrogen, as an end product, the hydrogen produced for introduction into the natural gas network need not be as pure. Using the existing natural gas grid as an infrastructure for the introduction of hydrogen by mixing hydrogen with the natural gas in the grid has been explored in a Dutch national project 'The Greening of Gas' as well as in the European project NATURALHY [2]. The main argument for mixing hydrogen into the natural gas grid is the cost-savings of building a separate hydrogen infrastructure by effectively using the existing natural gas infrastructure.

It is emphasized that there still is a large gap in the order of magnitude between the production capacity of the innovative production technologies explored here and the capacity needed to convert the whole NG network into a H_2/NG network. This chapter explores possible benefits on the production side should the H_2/NG network be realised.

1.2 Enriched Methane

Blends of hydrogen and natural gas have been studied for their suitability in internal combustion engines as used in cars, buses and trucks [3–6]. For suitable mixtures of around 20 % hydrogen by volume or 5–7 % hydrogen by energy, the term Hythane© (or Enriched Methane—EM) has been coined [7]. So as an alternative to mixing hydrogen or hydrogen natural gas blends into the natural gas grid, the hydrogen natural gas blend could be used directly in transport applications.

Lynch and Marmaro [6] have patented a process for the direct conversion of methane to gaseous mixtures of H_2 and methane, called Hythane©. They claim to have achieved an effective combustion rate similar to that of gasoline, thereby creating a potentially promising substitute for conventional fuels in spark ignition internal combustion engines as well as in compression ignition engines. The pollution emissions from EM powered vehicles have been shown to be well below that of gasoline and methane fuelled engines, due to the clean-burning characteristics of the components of EM.

2 Production of H_2/NG Mixtures from NG

2.1 Production of H_2/NG Using Incomplete SMR

Steam reforming of NG (Steam Methane Reforming or SMR) is a well-known process that is applied on a large industrial scale. The steps in this process are: (i) desulphurization of the feedstock; (ii) reaction of methane with steam to produce syngas (a mixture of hydrogen, carbon monoxide and carbon dioxide)

$$2CH_4 + 3H_2O \Leftrightarrow 7H_2 + CO + CO_2 \quad (\Delta H = 206\ \text{kJ/mol}) \tag{1}$$

(iii) the water gas shift reaction:

$$CO + H_2O \Leftrightarrow H_2 + CO_2 \quad (\Delta H = -41\ \text{kJ/mol}) \tag{2}$$

and (iv) separation and purification of hydrogen. The reactions take place at temperatures of 800–1000 °C and pressures of 15–30 bar.

The natural gas contains small quantities of sulphur compounds, which are added as odorant for safety reasons. However, these sulphur containing odorants are detrimental to the cobalt–molybdenum catalysts used in the reforming process and must first be removed.

A simple way to produce a H_2/NG blend would be to use a standard SMR production process with a poor conversion ratio. However, there are some issues that must be addressed before this alternative can be adopted.

First, in the conventional SMR process, temperatures are quite high and heating up the feedstock requires a large amount of energy. The whole feedstock is heated up to the reactor temperature while only a relatively small part of the heat is used in the endothermic reforming reaction. The rest of the heat must be used to preheat the feedstock as much as possible before it enters the steam methane reformer reactor. This will manifest itself in a different heat balance.

Second, the physical flows in the incomplete SMR process are quite large, since a large part of the methane will not be converted. Larger piping and reactors are needed to cope with the larger physical flows in the incomplete SMR process for the same amount of hydrogen produced compared to conventional SMR.

However, because full conversion of methane into hydrogen is not required, a lower catalytic activity is tolerable or actually desired (refer to Chap. 4). Therefore, the use of cheaper sulphur-tolerant, yet less effective, catalysts for the reforming reaction might provide a more cost effective alternative. Given the scale of this process, the cost of desulphurization is significant and can be reduced when H_2/NG blends are to be produced. Of course, fractions of sulphur will than remain in the H_2/NG blend and must be tolerable in the application of the blend or otherwise have to be removed still.

A lower conversion ratio also allows for a lower reaction temperature, thereby reducing the heat exchange capacity needed in the process.

In summary, the direct production of H_2/NG blends with significant NG concentration seems unlikely to be feasible due to the inefficiency of heating and cooling large amounts of NG in the process. However, as a remedy some natural gas can be bypassed to prevent unnecessary heat exchange and the composition of the final product can easily be adjusted by regulating the amount of natural gas that is bypassed. Furthermore, the relaxed constraints on the purity of the produced hydrogen allows for the use of cheaper catalysts and/or lower operating temperature because full conversion is no longer necessary. Furthermore, catalysts with high sulphur tolerance can be selected because a lower activity for the reforming reaction can be tolerated, thereby reducing the constraints on the sulphur removal

equipment. Alternatively, large-scale central reforming before the sulphur-containing odorants are added to the natural gas can be applied in some cases depending on where the H_2/NG blends are to be consumed.

2.2 Production of H_2/NG Mixtures Using an Internal Reforming Fuel Cell

High-temperature fuel cells fuelled by hydrogen suffer from large thermodynamically determined (reversible) heat production due to entropy changes ($T{\cdot}\Delta S$). Therefore, the reversible fuel cell efficiency is significantly lower than one hundred percent for a hydrogen oxygen fuel cell especially at higher temperatures since it is defined as [8]

$$\eta_{\mathrm{fc}} = \frac{\Delta G}{\Delta H} = \frac{\Delta H - T \cdot \Delta S}{\Delta H} = 1 - \mathrm{T}\frac{\Delta S}{\Delta H}. \tag{3}$$

The change in Gibbs free energy (ΔG) is the maximum amount of the heating value or enthalpy change of the reaction (ΔH) that can be converted into electricity. From the second law of thermodynamics, we know that an amount of heat equal to $T.\Delta S$ must be produced and from the first law of thermodynamics, we know this amount of heat has to be subtracted from the available amount of chemical energy (ΔH). Furthermore, there is the Nernst loss caused by the fact that less fuel is available near the outlet of the fuel cell; the partial pressure of hydrogen has decreased, whereas the partial pressures of the reaction product steam (and in case of the MCFC also carbon dioxide) has increased. This Nernst loss is proportional to temperature too and also the utilization of the fuel gas. More on fuel cell theory and Nernst loss can be found in literature [8]. Using algebraic modelling, Standaert et al. [9–11] found a simple, yet quite accurate formula, for the cell voltage as a function of current density and fuel utilization,

$$V = V(0) - i.r - \frac{1}{2}\alpha.u_{\mathrm{f}} \tag{4}$$

in which $V(0)$ is the open cell voltage, i the current density, r internal specific resistance (representing all loss processes) and u_{f} the fuel utilization. The inlet gas composition and fuel cell operating temperature determine α: the slope of local Nernst potential as a function of u_{f}.

The total of reversible heat together with irreversible heat can be used for the endothermic reforming of natural gas. Irreversible heat being caused by the polarization processes at the electrodes and limited conductivity of the electrolyte and electron conducting materials as approximated by the second term in Eq. (4). There are two concepts developed for fuel cells with natural gas as a fuel: internal- and external- reforming. In external reforming, a standard reformer unit is placed

before the fuel cell while in internal reforming (IR), the H_2 for the fuel cell anode reaction is produced from natural gas inside the fuel cell stack itself. The reforming reaction consumes a significant amount of the reversible and irreversible heat produced in the cell, yet the cell still needs to be cooled. Often, the remaining heat is transferred to a bottoming (steam) cycle for conversion into power. Although, in principle, high system efficiencies can be obtained in such a hybrid fuel cell heat engine combination, it requires two conversion steps, while each step is associated with large investment costs. Here, we will explore the option to use an IR fuel cell to produce a surplus of H_2 above the amount for its own consumption, thus using the surplus of heat effectively and circumventing the need for a costly bottoming cycle. A beneficial side effect is the increase in electric efficiency of the fuel cell due to the lower utilization of the fuel gas and thus a lower Nernst loss according to the third term in Eq. (4). Vollmar et al. [12] noted the flexibility of such a system for producing hydrogen and electricity in various ratios. Operating conditions can be relatively rapid, adjusted to meet changing demands and hence a better economic optimisation can be achieved. In a first order, but good approximation, the cell voltage can be calculated by Eq. (4) above. The Nernst loss is given by the third term on the right hand side. For high-temperature fuel cells in which internal reforming is possible, the Nernst loss is significant. Since α is of the order of 200 mV, Nernst loss approaches 100 mV for near 100 % fuel utilization; hence it is of the same order of magnitude as all irreversible losses ($i.r$) together. So, by using the fuel cell as a reformer and producing hydrogen (or H_2/NG blends), the fuel utilization is reduced. Hence, proportional to the fuel utilization, the Nernst loss is reduced and efficiency of the fuel cell is increased. This concept is worked out in detail in earlier work using the flowsheeting program Cycle Tempo [1]. The program calculates proper mass and energy balances and assumes chemical equilibrium in the gas compositions. For simplicity, the fuel cell is modelled as a SOFC (solid oxide fuel cell) in the flowsheet modelling and allowed to operate in the temperature range 600–1000 °C. However, in practice, an IR-MCFC (internal reforming molten carbonate fuel cell) might be used as well. The MCFC is ahead of the solid oxide fuel cell in market share, production capacity and size of the fuel cell units. The first calculations focused on the fuel cell only, while the surroundings were modelled using sources and sinks, where the sources provide gas streams of the appropriate temperature chosen as 600, 800 and 1000 °C, respectively. The oxidant utilization is fixed at 50 % and the fuel utilization is adjusted so that the temperature of the output gases equals the operating temperature. In Fig. 1, the schematic of the fuel cell with sources and sinks is shown.

Sufficient steam is added to the NG to prevent carbon deposition in the fuel cell. Carbon deposition inside the fuel cell is disastrous for the proper functioning of the anode. However, the process of carbon deposition itself is highly desired in the context of our study where we are looking at decreasing the carbon content of the NG by proposing the introduction of H_2/NG blends. If it were possible to deposit the carbon in a controlled manner in a separate unit, this concept would be important enough to explore further (see Sect. 2.6). In Figs. 2 and 3, the gas

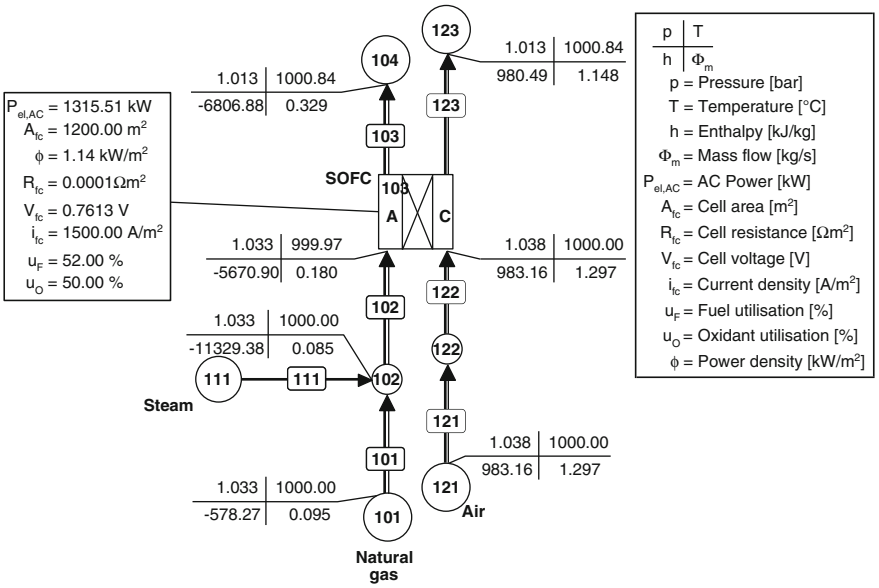

Fig. 1 Solid oxide fuel cell used in the co-production of H_2/NG blends and electricity from NG

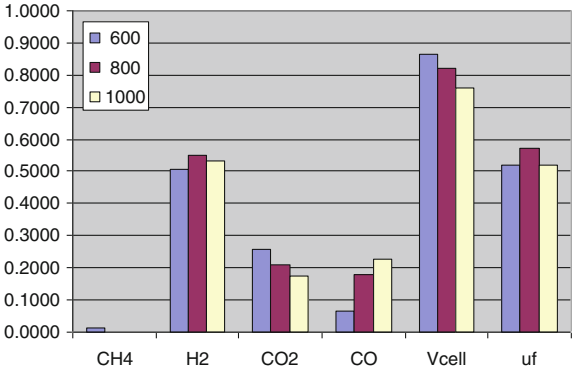

Fig. 2 Fuel cell anode output dry-gas compositions at atmospheric pressure for three operating temperatures (600, 800 and 1000 °C). Cell voltage (in Volts) and dimensionless fuel utilization; U_f are also indicated

compositions as calculated are indicated for three operating temperatures (600, 800 and 1000 °C) at a pressure of 1 and 30 bar, respectively. Also, the calculated cell voltage and the adjusted fuel utilization are shown. The off-gas typically contains 50 % of steam, but in the figures the dry gas compositions are indicated.

Under all these conditions, an almost full conversion of methane to hydrogen occurred except that at the highest pressure and lowest operating temperature a

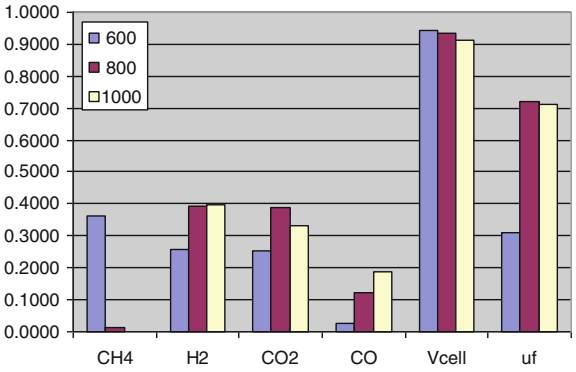

Fig. 3 Fuel cell anode output dry-gas compositions at $P = 30$ bar for three operating temperatures (600, 800 and 1000 °C). Cell voltage (in Volts) and dimensionless fuel utilization; U_f, are also indicated

mixture containing a significant amount of methane is created. In the calculations equilibrium is assumed, so in practice methane concentrations may be higher. As for conventional reforming, a further shift of CO to H_2 is necessary as well as separation of CO_2 for sequestration or for use as feedstock in a chemical process.

We have continued calculations on the complete fuel cell system with a solid oxide fuel cell at standard operating temperature of 1000 °C and have shown that total efficiency for hydrogen (+CO) and power production can reach more than 90 %, meaning that less than 10 % waste heat is produced [13–15]. In this case, nearly all methane is converted because of the high operating temperature. We will further discuss this hydrogen and power co-production system below.

2.3 *Solving the Chicken and Egg Problem in Hydrogen for the Transport Sector*

The flexible hydrogen and power co-production system based on an internal reforming fuel cell can be seen as a stepping stone towards a hydrogen economy, because of its flexibility and combined hydrogen and power production [16]. In particular, in the hydrogen production for the transport sector, the well-known chicken and egg problem between hydrogen infrastructure and penetration of fuel cell vehicles can largely be solved with this flexible coproduction system based on an internal reforming fuel cell. The unit can be operated at or near by a gas station to which it can supply hydrogen for cars and buses. The fuel cell can be operated in standard mode as a conventional combined heat and power plant and -whenever more hydrogen is needed- , be switched to a lower fuel utilization so that hydrogen is produced. This can be done by either increasing the natural gas input or decreasing the electric power output. Therefore, the unit does not stand idle if no

hydrogen is needed, as would be the case for dedicated hydrogen production technologies such as electrolysis or conventional steam methane reforming (SMR). Only the hydrogen separation and purification equipment after the internal reforming fuel cell would still stand idle of course, if no hydrogen is needed.

Adding EM as a transport fuel further helps solving the chicken and egg problem because, the fuel cell unit can also produce EM to be sold at the same gas station next to hydrogen. Here, the advantage of fuel cells that they have a high efficiency more or less independent of their size and capacity allows for distributed generation on-site using the existing natural gas infrastructure that in most European countries brings natural gas almost everywhere. Thereby, the need for a separate hydrogen transportation grid is circumvented.

The fuel cell unit can be seen as a power plant also producing hydrogen as a by-product, or alternatively we can see it as a SMR producing electricity as a by-product. As for EM production in an SMR, we can try to operate the fuel cell as to reach incomplete methane conversion by lowering the operation temperature or using less active catalyst. Both have their limitations, however, because the anode electrode inside the fuel cell also serves as a catalyst. In MCFC's as well as SOFC's nickel is the preferred choice for the anode material with good electrochemical catalytic performance for the hydrogen oxidation reaction and nickel is well known for its catalytic properties for the steam methane reforming reaction. MCFC's normally work at 650 °C and lowering the temperature is limited by the melting point of the carbonate used. Solid oxide fuel cells have much higher operating temperatures starting at around 1000 °C with the tendency to become lower because SOFC producers want to avoid material problems caused by these high temperatures. As Patakangas et al. [17] write in their recent review on SOFC's: "Research on thin electrolytes and/or new electrolyte materials suitable for lower operating temperatures (300–800 °C) is highly motivated". These low temperature SOFC's designed as internal reforming fuel cells would be very suitable for Hythane production from natural gas by having an incomplete reforming reaction inside the fuel cell.

Furthermore, the flexibility allows for efficient adaption to fluctuating renewable energy sources (solar and wind) and integration of these sources into the electricity grid as will be explained in the next paragraph.

2.4 *Integrating Fluctuating Renewable Energy Sources into the Electricity Grid*

The flexibility of the hydrogen and power production units can also be used to adapt to fluctuating electricity production devices and fluctuating electricity demand. As an example, we will discuss an operating mode of the internal reforming fuel cell in which we keep the natural gas input constant and decrease the electricity output in order to compensate for a peak in wind energy that is not

needed because demand is also assumed constant. All the natural gas will still be reformed in the high-temperature internal reforming fuel cell but not all the hydrogen will be electrochemically converted, since less current is drawn from the fuel cell to compensate for the peak in wind energy. The hydrogen that is not converted will leave the fuel cell (fuel utilization decreases) and hydrogen is produced for external use. The interesting thing that flowsheet calculations have shown is that by decreasing the electric power output by one unit we can increase the hydrogen[1] output by 3–4 units. This is not a violation of the first law of thermodynamics since the heat output from the fuel cell is decreased accordingly. Because of the lower power and current density, the internal losses in the fuel cell (ohmic, kinetic and diffusion losses) decrease. Moreover, because more hydrogen is available at the outlet side of the fuel cell also the Nernst loss is decreased. Hence, overall much less heat is produced but the same amount of heat is used for the endothermic reforming reaction, since we have kept the input of natural gas constant and all natural gas will be reformed at this standard operating temperature of the fuel cell. Seen from a system perspective, we see that a peak in wind energy disappears in the system and a peak in hydrogen emerges that is 3–4 times larger, while all other inputs and outputs are kept constant (only the heat output decreases in accordance with the first law of thermodynamics; energy conservation). It looks as if a peak in wind energy has been converted into hydrogen with an efficiency of 300–400 %. Compared to standard operation, we are able to decrease waste heat from the fuel cell by operating at a lower power density but still let the fuel cell produce valuable products, i.e. hydrogen production next to electricity. In spite of the fact that less power is produced, which in standard CHP operation of a fuel cell would not be economic (less power and less heat, so less profit), in the described hydrogen power coproduction mode in total more high-value products are produced instead of less. The hydrogen plus electric power output in total has increased and waste output has decreased. Overall system efficiency therefore has increased and we have calculated that at a fuel utilization of 60 %, the system efficiency for the coproduction of hydrogen plus electric power is larger than 90 %, implying that less than 10 % waste heat exits the fuel cell system. At the same time, integration of renewable energy into the electricity grid has been facilitated.

2.5 *Production of EM for the Transport Sector*

Based on our flow sheet calculations, we distinguish three operation modes: (1) high efficiency mode; (2) high power mode and (3) an intermediate constant current mode [13]. With the production of H_2/NG mixtures, we can add an additional operation mode to increase even further the flexibility of the system. In addition to hydrogen

[1]It is assumed that in the reformed natural gas the CO is completely converted into hydrogen by the water gas shift reaction.

for fuel cell vehicles that may be seen as a final goal, also EM for internal combustion engine vehicles can be produced as an intermediate step in the transition towards hydrogen as a fuel in the transport sector. This can be done by simply mixing the hydrogen with natural gas from the source that is available since it is used as a fuel for the fuel cell or by operating the fuel cell at a lower temperature and operating it at lower fuel utilization.

2.6 *Production of H_2/NG Mixtures by Methane Decomposition*

The decomposition of methane is an interesting alternative for SMR, since it circumvents the need for gas (H_2/CO_2)–gas separation. At high temperatures, either with or without the assistance of a plasma, methane is decomposed into carbon and hydrogen:

$$CH_4 = > C + 2H_2\,(+75.3\ \mathrm{kJ/mol}). \tag{5}$$

Compared to steam methane reforming, less hydrogen is produced from a mole of methane, because approximately one-third of the energy is contained in the carbon that is precipitated. For an economically feasible exploitation of this process, a useful purpose for the carbon should be found as we will discuss later.

Because of the high temperature of the decomposition, the production of blends with significant NG concentrations require a large heat exchange capacity to both preheat and cool unconverted NG in the inlet, respectively, outlet stream of any reactor. However, a 'slip' of unconverted NG is now tolerated.

From an energy point of view, one cannot see the disadvantage of thermal decomposition. It appears beneficial because heat is converted into chemical energy in the hydrogen and carbon that is formed. The sum of these heating values is larger than the heating value of the methane that enters the reaction. However, because of the entropy production in the reaction, exergy is lost and as we know from thermodynamics, exergy can never be recovered. In the thermal decomposition reaction, entropy is produced as we can deduce from thermodynamic tables, but it is also easily seen from the reaction equation in which two moles of the gas hydrogen are formed out of one mole of methane gas. The carbon in the reaction is a solid, therefore representing little entropy compared to the gas state and entropy being a measure of disorder. Therefore, in the decomposition reaction disorder has been created: in other words, entropy has been produced and exergy destroyed. A thorough entropy or exergy analysis of the thermal decomposition process in concentrated solar reactors has been made recently [18, 19]. These scholars conclude that indeed the major part of the entropy production is caused by the chemical reaction described above, as we deduced above by simple argumentation.

Still the decomposition of methane by concentrated solar power is an interesting process in which solar energy is both used effectively and stored in chemical form

and the carbon is separated from the hydrogen. Because carbon is a solid, instant separation is implemented in the process or, in other words, separation is inherent to the decomposition process. No gas separation equipment is necessary thus simplifying the hydrogen production process greatly.

An extensive review on the decomposition of methane is given by Abbas et al. [20].

In the next paragraphs, we will first explore uses of carbon and describe the current commercial production of carbon black, based on the combustion of natural gas as the source of heat and next we look at alternative heat and energy sources for the decomposition of the methane molecules.

2.7 Use of Carbon Black

The thermal decomposition of NG on a large-scale produces significant amounts of carbon that must be taken into consideration if applying the process on a large scale. The carbon that is produced, known as carbon black, is quite pure and used in ink for printers and on a larger scale in car tyres. In the conventional production process of carbon black, natural gas is allowed to decompose under the influence of heat. However, production processes for these existing markets could be replaced by solar thermal decomposition with the simultaneous production of hydrogen methane blends. In addition to the replacement of these conventional processes, additional markets for carbon black would be necessary to utilize the amounts of carbon produced if the (solar) decomposition process were adopted on a large-scale. In literature, several suggestions have been made for the economic use of carbon black from future NG decomposition processes. Muradov et al. [21] have proposed several ways of using solid carbon in the amounts necessary. They propose application areas such as structural materials, power generation, soil amendment and environmental remediation. One of these future markets might involve the use of Direct Carbon Fuel Cells (DCFC's) as also proposed by Cinti and Hemmes [22].

A new application for carbon black is found in the direct electrochemical conversion of carbon into carbon dioxide in a fuel cell known as the Direct Carbon Fuel Cell or DCFC. After pioneering work around 1900 in early fuel cell developments by Jacques, interest in the DCFC arose in the early 1990s, among others, by Gur [23]. More recently, Hemmes and Cooper [24, 25] have revived interest in the DCFC. We now see a serious increase in interest for this type of fuel cell with a solid fuel in contrast to conventional fuel cells based on gaseous or liquid fuel [26, 27]. Cooper et al. [28] have experimentally shown that direct conversion of carbon black in a Direct Carbon Fuel Cell (DCFC) producing pure CO_2 is possible. They derived an efficiency of 67 % (HHV) for the complete conversion route from NG to electricity via decomposition and subsequent conversion of the carbon in a DCFC and in parallel for the hydrogen in a Solid Oxide Fuel Cell (SOFC) or a molten carbon fuel cell (MCFC). Alternatively, the hydrogen can also be added to the NG network or used as transport fuel in fuel cell vehicles.

2.8 Commercial Carbon Black Production

Currently, carbon black intended for the printer and tyre industries is produced from methane decomposition. In two parallel batch processes, a stone is heated by the combustion of natural gas and, in the next step natural gas is brought into contact with the hot stone upon which methane decomposes into hydrogen and carbon. The carbon is removed. Meanwhile, in the parallel batch reactor, the stone is heated and can now be used as the heat source for decomposition of methane. By swinging from one to the other batch, a semi-continuous production of carbon black is obtained. As a by-product, hydrogen containing some unreacted methane is released from the two batch reactors. Rather than recycling the gases back into the batch process or combust it to heat the stones in the batch reactors, one could use this mixture of hydrogen and natural gas, for example, to feed it into the natural gas grid. The commercial process can also be modified as to deliver H_2/NG blends of the right composition for a certain application, as EM to be applied as a fuel for the transport sector next to the production of carbon black. In this way, the production can be optimized and made more profitable.

2.9 Thermal Decomposition of Methane by CSP

Thermal decomposition of methane using concentrated solar power has been studied as a way of capturing solar energy by producing hydrogen and carbon. Solar decomposition of methane has been studied in the laboratory and it was found to be difficult to obtain full conversion [29–31].

The thermal decomposition reaction is endothermic like the steam reforming reaction and heat is converted into chemical energy. Note that also steam methane reforming reaction can be performed by using heat from concentrated solar power. Both are an alternative for using the high temperature heat from concentrated solar for electricity production through a steam cycle and have been the subject of studies in literature [32–35].

The experimental fact that it is difficult to get full conversion in solar reactors can be seen as a disadvantage for hydrogen production from methane decomposition by concentrated solar power. However, for the production of H_2/NG blends, this is not a problem at all. In fact, exactly the product that we desire is produced after the easy removal of the solid carbon. Process parameters can be adjusted in such a way as to obtain the required composition of the natural gas hydrogen blend, including bypassing part of the methane along the concentrated solar reactor.

2.10 Decomposition of Methane in High-Temperature Fuel Cells

In high-temperature internal reforming fuel cells fed by natural gas, one must exercise care in operating the fuel cell to prevent carbon deposition. Deposition can be avoided by the introduction of enough steam to the fuel gas. A high steam carbon ratio thermodynamically prevents carbon deposition. However, adding steam, for example, by recycling the anode off gas decreases the hydrogen partial pressure. As a result, the open cell voltage or thermodynamic driving forces for the electrochemical fuel cell reactions and hence fuel cell efficiency, are all decreased.

Instead of seeing carbon deposition as a problem, we could see it as a solution that creates a marketable product and circumvents the disadvantages of internal reforming. Presently, the problem with internal reforming is that the reaction normally is fast at the conventional high fuel cell operating temperatures. This results in the reaction of all the natural gas in the beginning of the cell near the inlets, whereby the inlet side is overly cooled due to the endothermic nature of the reforming reaction and thereby introducing thermal stress. Systems used to prevent this include pre-reforming, which requires additional equipment such as a separate pre-reformer and heat exchanger.

It is proposed here that separate channels can be added to the fuel cell through which the methane fuel is heated to such temperatures that carbon deposition can take place in a controlled manner and the carbon can be removed by special constructions and/or gravity. In the 'decomposition channel', a mixture of hydrogen and natural gas is formed from which any remaining solid carbon particles can easily be separated. This mixture is then sent to the anode inlet. To make sure that the carbon deposition process is not continued in the anode inlet, some anode off-gas recycling may still be applied or some steam can be added, yet in low amounts. Surplus waste heat is carried away from the fuel cell by the decomposition channel and the heat is converted into chemical energy of the hydrogen and carbon thus upgrading the fuel and partly compensating for removing part of the heating value of the fuel through the carbon. This proposed process only makes sense if economically attractive applications for carbon exist (see Sect. 2.7).

Moreover, some of the outlet gas of the decomposition channels can be used externally as it is a hydrogen natural gas blend after the carbon particles have been removed. Depending on operating conditions such as temperature and gas flow rate, the composition of the blend can be adjusted. This should be matched with a proper heat balance in the fuel cell to maintain a constant temperature and limit the temperature difference between inlet and outlet. The new process proposed here requires further design engineering and optimization. However, calculations on the hydrogen and power co-producing internal reforming fuel cells have shown that they are capable of producing hydrogen as an additional product. Therefore, it is shown that sufficient surplus heat is available for sustaining an endothermic reaction, i.e. the steam methane reforming reaction in internal reforming fuel cells and methane decomposition in the newly proposed fuel cell concept with separate

decomposition channels as described above. So, by allowing for controlled methane decomposition, hydrogen natural gas blends are produced as a by-product of the high-temperature fuel cell and the fuel cell itself can operate at a higher cell voltage, thus increasing its efficiency. That is to say the efficiency of the conversion of that part of the fuel that is converted (not counting the hydrogen/methane fuel blend and the carbon black that is co-produced). Please note that the system has become a so-called multisource multiproduct energy system for which conversion efficiency should be defined carefully as explained elsewhere [36].

It is expected that as for hydrogen power coproduction with an internal reforming fuel cell, high total efficiencies of near 90 % can be achieved with the here proposed 'Internal Thermal Decomposition Fuel Cell' because of the analogies between the two systems that both effectively convert waste heat from the fuel cell into chemical energy [12, 37].

2.11 Plasma Decomposition of Methane

In a plasma-arc process at elevated temperatures, hydrocarbons can be separated into pure carbon and hydrogen. But using methane also higher order hydrocarbons can be formed in the process under certain conditions. In a recent paper, Lee et al. [38] compared the characteristics of methane activation by diverse plasma sources. They focus on the electron energy and degree of thermal activation in evaluating the cost-effectiveness of methane decomposition. The high-temperature process needs an energy source to sustain the plasma and therefore is similar to thermal decomposition discussed above. Bypassing some of the methane can prevent unnecessary heating and cooling of converted methane. As they state: "Among the tested plasma sources, those that provide a somewhat thermal environment have a rather high degree of warmness, resulting in higher methane conversion and lower operational costs. As the non-thermal characteristics of the plasma sources become stronger, the selectivity of C_2H_6 increases. This reflects C_2H_6 formation from the direct collision of CH_4 with high-energy electrons".

They demonstrate that; the higher the plasma temperature, the more the process looks like thermal decomposition of methane. At lower plasma temperatures, lower methane conversion ratios are obtained which would be more suitable for the production of hydrogen methane blends. However, in that case, some formation of higher order hydrocarbons such as C_2H_6 takes place. It depends on the application of the produced blend, whether or not the formation of C_2H_6 is advantageous for the application process, or just an undesirable component in the end product.

3 Hydrogen/Methane Blends from Biomass

For producing H_2/NG blends in the future, innovative processes using renewable energy sources may be adopted. Above we have discussed the use of concentrated solar energy; biomass provides another potential energy source for the production of hydrogen/methane blends.

3.1 Bioreactors

Biological hydrogen production suffers from a negative feedback from the produced hydrogen on the hydrogen production by the bacteria [39–41]. The production process in the bacteria is stopped at a certain partial pressure of hydrogen [41]. To let the bacteria continue the production of hydrogen, the partial pressure of hydrogen must thus be kept low. This can be done by using fuel cells that consume the hydrogen or by pumping out the hydrogen through a membrane. However, biological H_2 production can also continue without the use of fuel cells, hydrogen membrane pumps or other capital-intensive equipment by simply purging the bio-reactor with natural gas. Hereby, the hydrogen is removed and it's partial pressure is kept low enough (<0.2 bar) for continued bio-hydrogen production at a high production rate. The potential disadvantage is that no pure hydrogen is produced but instead a mixture of hydrogen and natural gas. However, if the applications for hydrogen natural gas blends as proposed in this chapter have matured and an economic demand for H_2/NG has developed, this inexpensive process would be advantageous.

3.2 Supercritical Gasification of Biomass

Wet biomass and organic residues can be treated in supercritical water ($T > 374$ °C, $P > 22$ MPa) to produce a clean fuel gas rich in hydrogen and methane [42, 43]. The first step in the process is to prepare a transportable slurry of water with bio-mass and pressurize it to about 300 bar. The pressurized feedstock is heated by the reactor outlet stream in a heat exchanger. This heat exchange is essential for the process to achieve high thermal efficiencies. The reactor operating temperature is typically between 600 and 650 °C; the operating pressure is around 300 bar. The biomass reacts with the supercritical water and produces a gas mixture containing hydrogen, carbon dioxide, methane, carbon monoxide and traces of ethane [44]. A residence time of 0.5–2 min is probably needed to achieve complete carbon conversion [43]. The two-phase product stream containing liquid water together with steam and production gases is released from the reactor and is separated in a high-pressure gas–liquid separator ($T = 25$–300 °C). Because of these conditions, a

significant part of the CO_2 remains in the water phase. Theoretically, possible contaminants like H_2S, NH_3 and HCl are even more likely to be captured in the water phase due to their higher solubility. In fact, in situ gas scrubbing is part of the process. It is therefore expected that the gas stream from the separator contains mainly the H_2, CO and CH_4 and only part of the CO_2.

Depending on the application, the fuel gas can be further conditioned in downstream equipment or in the process itself. By adding an appropriate shift catalyst (for example NaOH or KOH), nearly all CO is shifted towards H_2 [45, 46]. Furthermore, the high process pressure favours the formation of methane.

High methane concentrations (30–40 %) were achieved by Waldner and Vogel [47] using Raney nickel catalysts. Overall, thermal efficiencies above 70 % can be achieved. So, in this process methane/hydrogen blends are produced, but further scrubbing of CO_2 is needed depending on the application of the produced gas mixture.

4 Conclusions

The concept of using H_2/NG blends instead of NG in the national NG network is an interesting option in the pathway to a sustainable hydrogen society. It offers a whole new perspective on the hydrogen society and the hydrogen production technologies needed. Since the constraints are relaxed, the production processes can be operated in more efficient and cost effective ways offering positive incentives for market introduction of these production technologies.

We have investigated various possible and advantageous processes for producing H_2/NG mixtures. Advantages include cheaper production, higher efficiency of the total process and in some cases the use of renewable energy sources.

Directly using a H_2/NG blend in the gas grid would provide a huge demand for these blends and promote a transition to low carbon fuels in our energy system.

Alternative applications for the H_2/NG blends can be found in the transport sector, where EM is proposed as an alternative fuel for ICE's (Internal Combustion Engines) in cars, buses and trucks.

Acknowledgments This chapter is based on the research performed in the framework of the Dutch national project "The Greening of Gas" Project number EETK01011. The author acknowledges the contribution of his co-authors in this early article [1]. The work has partly been financed by a grant of the Energy Delta Gas Research (EDGaR) program. EDGaR is co-financed by the Northern Netherlands Provinces, the European Fund for Regional Development, the Ministry of Economic Affairs, Agriculture and Innovation and the Province of Groningen.

References

1. van de Beld L, Bouwmans I, Claassen PAM, Hemmes K, de Wit JHW, Woudstra N et al (2003) Exploring new production methods of hydrogen/natural gas blends for mixing into the natural gas network of the Netherlands. In: Houbak N, Elmegaard B, Qvale B, Moran MJ (eds) Technical University of Denmark, Lyngby, pp 55–62
2. Florisson O (2004) NATURALHY EU Cordis Internet database. http://cordis.europa.eu/project/rcn/73964_en.html
3. Sisiopiku VP, Rousseau A, Fouad FH, Peters RW (2006) Technology evaluation of hydrogen light-duty vehicles. J Environ Eng ASCE 132(6):568–574
4. Wright S, Pinkelman A (2008) Natural gas internal combustion engine hybrid passenger vehicle. Int J Energy Res 32(7):612–622
5. Villante C, Genovese A (2012) Hydromethane: a bridge towards the hydrogen economy or an unsustainable promise? Int J Hydrogen Energy 37(15):11541–11548
6. Lynch FE, Marmaro RW (1992) Special purpose blends of hydrogen and natural gas. US patent
7. Larsen JF, Wallace JS (1997) Comparison of emissions and efficiency of a turbocharged lean-burn natural gas and hythane-fueled engine. J Eng Gas Turbines Power Trans ASME 119 (1):218–226
8. Hemmes K (2004) Fuel cells. In: White RE, Conway BE, Vayenas CG (eds) Fuel cells; in modern aspects of electrochemistry, vol 37. Kluwer Academic/Plenum Publishers, New York, pp 131–251
9. Au SF, Peelen WHA, Standaert FRAM, Hemmes K, Uchida I (2001) Verification of analytical fuel cell models by performance testing at a 110 cm(2) molten carbonate fuel cell. J Electrochem Soc 148(10):A1051–A1057
10. Standaert F, Hemmes K, Woudstra N (1998) Analytical fuel cell modeling; non-isothermal fuel cells. J Power Sources 70(2):181–199
11. Standaert F, Hemmes K, Woudstra N (1996) Analytical fuel cell modeling. J Power Sources 63(2):221–234
12. Vollmar HE, Maier CU, Nolscher C, Merklein T, Poppinger M (2000) Innovative concepts for the coproduction of electricity and syngas with solid oxide fuel cells. J Power Sources 86(1–2): 90–97
13. Hemmes K, Patil A, Woudstra N (2005) Internal reforming SOFC system for flexible co production of hydrogen and power. In: Proceedings of the third international Conference on Fuel Cell Science, Engineering and technology, Ypsilanti, Michigan
14. Hemmes K, Patil A, Zachariah JL (2004) Flexible co-production of hydrogen and power using fuel cells. In: Conference proceedings of the international gas research conference. Vancouver, Canada
15. Hemmes K, Patil A, Woudstra N (2008) Flexible coproduction of hydrogen and power using internal reforming solid oxide fuel cells system. J Fuel Cell Sci Technol 5(4): 041010-1–041010-6
16. Hemmes K, Kamp LM, Vernay ABH, de Werk G (2011) A multi-source multi-product internal reforming fuel cell energy system as a stepping stone in the transition towards a more sustainable energy and transport sector. Int J Hydrogen Energy 36(16):10221–10227
17. Patakangas J, Ma Y, Jing YF, Lund P (2014) Review and analysis of characterization methods and ionic conductivities for low-temperature solid oxide fuel cells (LT-SOFC). J Power Sources 263:315–331
18. Zedtwitz PV, Petrasch J, Trommer D, Steinfeld A (2006) Hydrogen production via the solar thermal decarbonization of fossil fuels. Sol Energy 80(10):1333–1337
19. Hirsch D, Epstein M, Steinfeld A (2001) The solar thermal decarbonization of natural gas. Int J Hydrogen Energy 26(10):1023–1033
20. Abbas HF, Daud WMAW (2010) Hydrogen production by methane decomposition: a review. Int J Hydrogen Energy 35(3):1160–1190

21. Muradov NZ, Veziroglu TN (2005) From hydrocarbon to hydrogen-carbon to hydrogen economy. Int J Hydrogen Energy 30(3):225–237
22. Cinti G, Hemmes K (2011) Integration of direct carbon fuel cells with concentrated solar power. Int J Hydrogen Energy 36(16):10198–10208
23. Gur TM, Huggins RA (1992) Direct electrochemical conversion of carbon to electrical energy in a high-temperature fuel-cell. J Electrochem Soc 139(10):L95–L97
24. Peelen WHA, Hemmes K, De Wit JHW (1998) Carbon a major energy carrier for the future? Direct carbon fuel cells and molten salt coal/biomass gasification. High Temp Mater Process (New York) 2(4):471–482
25. Cherepy N, Krueger R, Cooper JF (2001) Direct electrochemical conversion of carbon anode fuels in molten salt media. In: Power sources for the new millennium, proceedings, vol 2000, no 22, pp 64–66
26. Hemmes K, Cooper JF, Selman JR (2013) Recent insights concerning DCFC development: 1998–2012. Int J Hydrogen Energy 38(20):8503–8513
27. Gur TM (2013) Critical review of carbon conversion in "carbon fuel cells". Chem Rev 113 (8):6179–6206
28. Cherepy NJ, Krueger R, Fiet KJ, Jankowski AF, Cooper JF (2005) Direct conversion of carbon fuels in a molten carbonate fuel cell. J Electrochem Soc 152(1):A80–A87
29. Maag G, Zanganeh G, Steinfeld A (2009) Solar thermal cracking of methane in a particle-flow reactor for the co-production of hydrogen and carbon. Int J Hydrogen Energy 34(18): 7676–7685
30. Steinfeld A (2005) Solar thermochemical production of hydrogen: a review. Sol Energy 78(5):603–615
31. Hirsch D, Epstein M, Steinfeld A (2001) The solar thermal decarbonization of natural gas. Int J Hydrogen Energy 26(10):1023–1033
32. Petrasch J, Steinfeld A (2007) Dynamics of a solar thermochemical reactor for steam-reforming of methane. Chem Eng Sci 62(16):4214–4228
33. Wang ZL, Naterer GF (2014) Integrated fossil fuel and solar thermal systems for hydrogen production and CO_2 mitigation. Int J Hydrogen Energy 39(26):14227–14233
34. De Falco M, Caputo G, Frattari S, Gironi F, Annesini MC (2014) Solar steam reforming for enriched methane production: reactor configurations modeling and comparison. Int J Hydrogen Energy 39(26):13979–13990
35. Gokon N, Nakamura S, Hatamachi T, Kodama T (2014) Steam reforming of methane using double-walled reformer tubes containing high-temperature thermal storage Na_2CO_3/MgO composites for solar fuel production. Energy 68:773–782
36. Hemmes K (2009) Multi-source multi-product and other integrated energy systems. Int J Integr Energy Syst 1(1): 1–15
37. Hemmes K, Patil A, Woudstra N (2008) Flexible coproduction of hydrogen and power using internal reforming solid oxide fuel cells system. J Fuel Cell Sci Technol 5(4)
38. Lee DH, Song YH, Kim KT, Lee JO (2013) Comparative study of methane activation process by different plasma sources. Plasma Chem Plasma Process 33(4):647–661
39. Claassen PAM, de Vrije T, Koukios E, van Niel E, Eroglu I, Modigell M et al (2010) Non-thermal production of pure hydrogen from biomass: HYVOLUTION. J Clean Prod 18: S4–S8
40. Claassen PAM, van Lier JB, Contreras AML, van Niel EWJ, Sijtsma L, Stams AJM et al (1999) Utilisation of biomass for the supply of energy carriers. Appl Microbiol Biotechnol 52(6):741–755
41. van Niel EWJ, Claassen PAM, Stams AJM (2003) Substrate and product inhibition of hydrogen production by the extreme thermophile, Caldicellulosiruptor saccharolyticus. Biotechnol Bioeng 81(3):255–262
42. Reddy SN, Nanda S, Dalai AK, Kozinski JA (2014) Supercritical water gasification of biomass for hydrogen production. Int J Hydrogen Energy 39(13):6912–6926

43. Matsumura Y, Minowa T, Potic B, Kersten SRA, Prins W, van Swaaij WPM et al (2005) Biomass gasification in near- and super-critical water: status and prospects. Biomass Bioenergy 29(4):269–292
44. Antal MJ, Allen SG, Schulman D, Xu XD, Divilio RJ (2000) Biomass gasification in supercritical water. Ind Eng Chem Res 39(11):4040–4053
45. Boukis N, Abeln J, Kruse A, Schmieder H, Dinjus E (2008) Biomass treatment in supercritical water. The way from total oxidation to the gasification. In: Bridgwater AV (ed) Progress in thermochemical biomass conversion. Wiley, pp 109–121
46. Watanabe M, Inomata H, Arai K (2002) Catalytic hydrogen generation from biomass (glucose and cellulose) with ZrO2 in supercritical water. Biomass Bioenergy 22(5):405–410
47. Waldner MH, Vogel F (2005) Renewable production of methane from woody biomass by catalytic hydrothermal gasification. Ind Eng Chem Res 44(13):4543–4551

Explosion Risks of Hydrogen/Methane Blends

Prankul Middha

Abstract Hydrogen is the next frontier and there is a concerted push to include hydrogen as an energy carrier. The main benefit is emissions reduction—eventually by 100 %. When used as a fuel, hydrogen supplies more energy per unit mass than the popular fuels used today. However, in the near term, there is a very significant cost differential between fossil fuels and hydrogen. Therefore, proposals have been made for the use of hydrogen as an additive to hydrocarbon fuels as a practical approach to the introduction of hydrogen in the energy mix. Enriched Methane (EM, a blend of hydrogen and natural gas) can presage a gradual transition to an eventual hydrogen economy. Besides the techno-commercial challenges for introducing hydrogen (or for that matter a hydrogen–methane blend), another key issue is that of the comparative safety between natural gas and hydrogen concerning the application, storage, transport, etc. Due to prior experience with, e.g. the process or petrochemical industries, it is well known that accidental releases of flammable substances are one of the largest contributors to the hazards of most industrial, domestic, and infrastructure facilities. Assessing the consequences and risks of such accidental releases is thus crucial. The consequences of a release such as cloud size and subsequent explosion like overpressure are dependent on several parameters such as fuel type, concentration, leak rate/direction, environmental conditions, cloud size, ignition location, and presence of any mitigation measures. More importantly, geometrical effects—including congestion and confinement, as well as layout of objects and walls—plays a key role in determining the magnitudes of gas cloud size (following a release) and overpressure/drag loads (following an explosion). Therefore, simple analysis techniques are generally not applicable as these may provide inaccurate results. 3D modelling based on Computational Fluid Dynamics (CFD) needs to be used. The current chapter describes the safety aspects of EM. In general, it can be expected that EM is relatively safer to handle (compared to hydrogen), thus significantly reducing the risk of fire and explosion. This chapter also seeks to evaluate whether EM may be safer than both hydrogen and methane under certain conditions. This is due to the fact EM combines the positive

P. Middha (✉)
Gexcon UK, Wembley, Greater London HA9 9NP, UK
e-mail: prankul.middha@gmail.com

M. De Falco and A. Basile (eds.), *Enriched Methane*,
Green Energy and Technology, DOI 10.1007/978-3-319-22192-2_13

safety properties of hydrogen (strong buoyancy, high diffusivity) and methane (much lower flame speeds and narrower flammability limits as compared to hydrogen). Nonetheless, the explosion risk is by no means insignificant. The work is performed using the CFD software FLACS that has been well validated for safety studies of both natural gas/methane and hydrogen systems. Validation for EM–air explosions is also demonstrated. Practical systems such as vehicular tunnels, garages, etc., are used to demonstrate positive safety benefits of EM with comparisons to similar simulations for both hydrogen and methane.

Keywords Enriched methane safety · Explosion dynamics · Computational fluid dynamics · Explosion risks

List of Abbreviations

BFETS	Blast and Fire Engineering for Topside Structures
BLEVE	Boiling Liquid Expanding Vapour Explosion
CEA	Commissariat à l'énergie atomique et aux énergies alternatives (English: Atomic Energy and Alternative Energies Commission)
CFD	Computational Fluid Dynamics
CMR	Christian Michelsen Research
DDT	Deflagration to Detonation Transition
EN	European Norm
ER	Equivalence Ratio
EU	European Union
FhICT	Fraunhofer Institute for Chemical Technology
FLACS	CFD tool for ventilation, dispersion, explosion, and fire modelling (by Gexcon)
FZK	Research Centre Karlsruhe (now KIT)
HSE	Health and Safety Executive
HSL	Health and Safety Laboratory
EM	Natural gas–hydrogen blend
ISO	International Standardisation Organisation
KIT	Karlsruhe Institute of Technology
LFL	Lower Flammability Limit
LNG	Liquefied Natural Gas
LPG	Liquefied Petroleum Gas
PRD	Pressure Relief Device
QRA	Quantitaitive Risk Assessment/Analysis
TNO	Nederlandse Organisatie voor Toegepast Natuurwetenschappelijk Onderzoek (English: Netherlands Organisation for Applied Scientific Research)
TNT	Tri-Nitro Toluene (Explosive)
UFL	Upper Flammability Limit

List of Symbols

ε Turbulent dissipation
k Turbulent kinetic energy
λ Detonation cell size

1 Introduction

Substitution of conventional fuels (e.g. coal, gasoline) by natural gas has already occurred on a large scale in the global energy mix. Its use is not limited to industry and domestic, but also extends to the transport sector, especially in Europe and some parts of Asia. Hydrogen is the next frontier and there is a concerted push to include hydrogen as an energy carrier. The main benefit is emissions reduction—eventually by 100 %. When used as a fuel, hydrogen supplies more energy per unit mass than the popular fuels used today. However, in the near term, there is a very significant cost differential between fossil fuels and hydrogen. Therefore, proposals have been made for the use of hydrogen as an additive to hydrocarbon fuels as a practical approach to the introduction of hydrogen in the energy mix. EM (a blend of hydrogen and natural gas) can presage a gradual transition to an eventual hydrogen economy.

It is a fuel blend consisting of 8–30 % hydrogen in methane by volume. Addition of hydrogen to natural gas engines can have beneficial effects in terms of the improvement of combustion properties and can reduce emissions of pollutants such as NO_x (and greenhouse gases such as CO_2), especially in lean-burn operation, while not requiring significant changes to existing infrastructure. This is due to the fact that the broad flammability range and fast flame propagation velocity of hydrogen aids in more complete combustion of the fuel blend, and allows the engine to operate at extended lean-burn ranges leading to reduction in emissions. Further, it also reduces the ignition energy of the fuel (the ignition energy of hydrogen is an order of magnitude smaller than methane, while the laminar burning velocity is an order of magnitude larger). The use of hydrogen also accelerates the methane combustion and increases the efficiency of catalysis at lower exhaust temperatures. The use of EM also results in no knock or backfire and increases power output. It also does not lead to a significant loss of range as the blend only corresponds to 5–7 % hydrogen by energy.

The use of EM is the most "cost-effective" use of hydrogen that is available today. It uses infrastructure that builds on and coexists with natural gas stations. This infrastructure will continue to be useful in the ultimate hydrogen economy and a pre-approval of "EM" is a good way to satisfy all regulatory and public perception requirements. A transportation system using natural gas and hydrogen mixtures can thus be an effective way of mitigating environmental issues as well as paving the way for introducing hydrogen into the energy supply infrastructure.

2 Safety Challenges and Risk Assessments

Besides the techno-commercial challenges for introducing hydrogen (or for that matter a hydrogen–methane blend), another key issue is that of the comparative safety between natural gas and hydrogen (and EM) concerning the application, storage, transport, etc.

Due to the inherent hazard of any system employing EM (e.g. refuelling station, storage system, etc.), a risk assessment is required under various national and international regulations (such as EN or ISO). A general scheme for such a risk assessment is presented in Fig. 1. It basically involves identification of the hazards and then an evaluation of the probability and consequence of each potential incident where the hazard is realised.

Due to prior experience with, e.g. the process or petrochemical industries, it is well known that accidental releases of flammable substances are one of the largest contributors to the hazards of most industrial, domestic, and infrastructure facilities. Assessing the consequences and risks of such accidental releases is thus crucial. A typical event tree following an accidental release can be represented as shown in Fig. 2. Often, one of the most severe hazards associated with flammable materials is an explosion event. This happens when the flammable fuel–air cloud is allowed to premix and is followed by a delayed ignition.

The main damage in accidental explosions is caused by pressure increase, blast wave, fragment scattering, and so on. The damage caused by a blast wave can spread quickly and widely, and become a significant consequence of the accidental explosion. It can lead to structural collapse, loss of life, and more.

Hydrogen is the lightest gas (14 times lighter than air), highly flammable, odourless, and burns with a colourless flame. The hazards from hydrogen primarily stem from its wide flammability range, extremely fast burning rate (order of

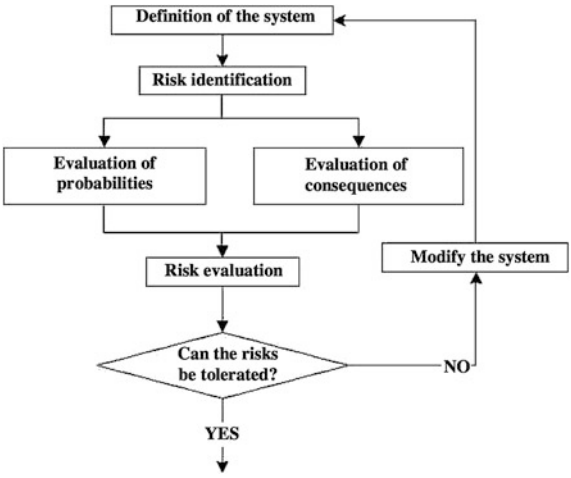

Fig. 1 Typical steps of a risk assessment process

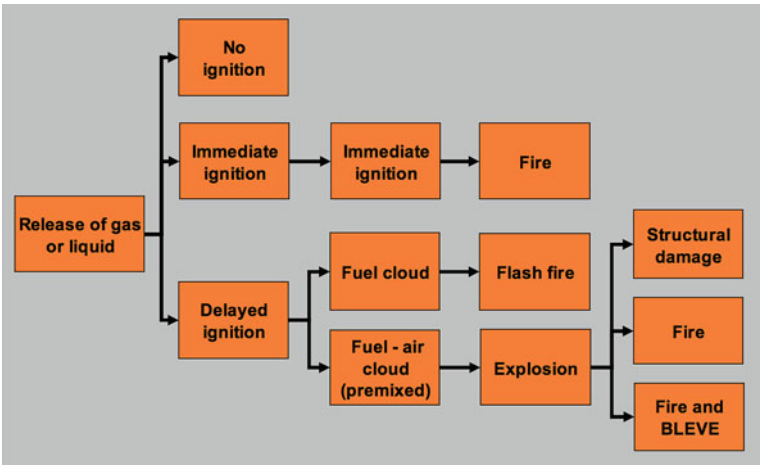

Fig. 2 Typical event tree following the release of a flammable gas or liquid. BLEVE stands for "boiling liquid expanding vapour explosion"

magnitude larger compared to natural gas), and the considerable amount of energy released when it burns or explodes. It also has a lower minimum ignition energy compared to natural gas. This leads to an increased risk and consequences that are much more severe as compared to hydrocarbons. This is clearly shown by experiments carried out in the late 1980s in a wedge-shaped geometry [1] that show the overpressures generated on the combustion of a stoichiometric fuel–air mixture for various gases (results are shown in Fig. 3).

Hydrogen is also quite different from natural gas in certain other ways, some of which actually help to reduce the risk of using the gas. Hydrogen is much lighter than air and, therefore, has very strong buoyancy that will quickly lift and disperse small leaks of the gas in an unconfined situation. However, any leakage of hydrogen in confined spaces frequented by motor vehicles such as parking garages

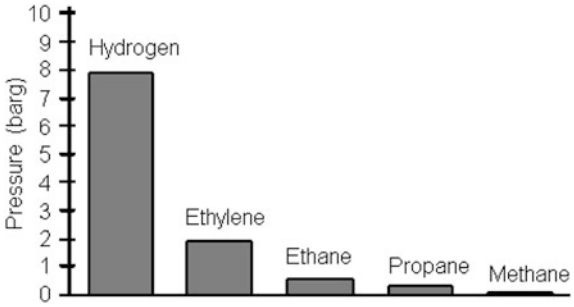

Fig. 3 Comparison of explosion overpressure for various stoichiometric gas–air mixtures in a 10 m wedge-shaped vessel (from [1])

Table 1 Comparison of combustion and physical properties of hydrogen and methane (natural gas)

Property	Hydrogen	Methane (natural gas)
Density at NTP (kg/m^3)	0.0838	0.6512
Heat of combustion (MJ/kg)	129–152	55–61
Flammability range in air (%)	4–75	5–15
Stoichiometric composition in air (%)	29.53	9.48
Minimum ignition energy (mJ)	0.02	0.29
Maximum laminar burning velocity (cm/s)	~300	~40

and tunnels poses a significant hazard. The safety issue is further worsened by the wide detonability limits and the propensity of flames to accelerate rapidly due to the very high laminar burning velocity of hydrogen. Clearly, hydrogen has many characteristics that are significantly different from conventional gaseous fuels such as natural gas, propane, gasoline, etc. A comparison of properties between hydrogen and natural gas is given in Table 1.

There are many models for the determination of explosion consequences ranging from calculations using a simple expression (e.g. TNT equivalency) to complex numerical formulations based on CFD (Computational Fluid Dynamics). Selecting and using appropriate models for the problem at hand are important, as the information requirements and efforts to run the models increase with the demand of accuracy.

Several research activities have been carried out in order to develop techniques for the determination of consequences of explosion of hydrogen–air mixtures (e.g. [2–4]). For instance, [4] proposed a simple approximate method for evaluation of blast effects and safety distances related to unconfined hydrogen explosions. The proposed method determines the blast damage based on the flame speeds depending on the cloud size, composition, and obstacle geometry. These can be applicable for EM as well.

The consequences of a release such as cloud size and subsequent explosion like overpressure are dependent on several parameters such as fuel type, concentration, leak rate/direction, environmental conditions, cloud size, ignition location, and presence of any mitigation measures. More importantly, geometrical effects—including congestion and confinement, as well as layout of objects and walls—plays a key role in determining the magnitudes of gas cloud size (following a release) and overpressure/drag loads (following an explosion). Therefore, simple analysis techniques are generally not applicable as these may provide inaccurate results.

The current chapter describes the safety aspects of EM. In general, it can be expected that EM is relatively safer to handle (compared to hydrogen), thus significantly reducing the risk of fire and explosion. This chapter also seeks to evaluate whether EM may be safer than both hydrogen and methane under certain conditions. This is due to the fact EM combines the positive safety properties of hydrogen (strong buoyancy, high diffusivity) and methane (much lower flame

speeds and narrower flammability limits as compared to hydrogen). Nonetheless, the explosion risk is by no means insignificant.

Further, the analyses of explosions are still essential in order for appropriate mitigation measures to be designed such that the explosion risk is reduced to an acceptable level.

3 Combustion Properties of Hydrogen–Methane Blends

Laminar burning velocity is a fundamental property of a combustible mixture. It is the speed at which an unstretched laminar flame will propagate through a quiescent mixture of unburned reactants, and is a measure of the reactivity and hence the potential for generation of fast flame speeds.

Ilbas et al. [5] have studied the effect of hydrogen enrichment on the natural gas laminar flame properties experimentally. They stated that increasing the hydrogen concentrations in a mixture causes an increase in the resultant burning velocity and also widens the flammability limits. The results of their study are presented in Fig. 4, clearly depicting the rise of the laminar burning velocity as the hydrogen concentration is increased. This rise is exponential for hydrogen concentrations larger than 50 %.

Di Sarli and Di Benedetto [6] have calculated the laminar burning velocities of methane–hydrogen/air premixed flames by means of the CHEMKIN PREMIX code with a detailed reaction mechanism. A wide range of blend compositions was explored. Their data also supported the experimental measurements reported above. In particular, they found that the laminar burning velocity of the blend was smaller

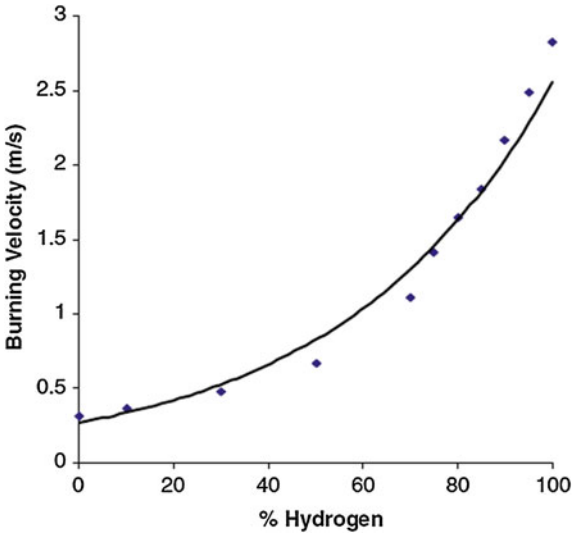

Fig. 4 Burning velocity of hydrogen–methane mixtures (ER = 1.0) for different percentages of hydrogen (taken from [5])

than that obtained by averaging the corresponding values of the pure fuels in the correct proportion, but a Le Chatelier-based model could be developed to correlate the calculated values of the laminar burning velocity.

Auto-ignition times of methane/hydrogen mixture have been measured in a rapid compression machine and a shock tube for varying pressure, equivalence ratio, and temperature (Huang et al. [7]). For instance, Huang et al. (8) have reported that the auto-ignition times of methane–hydrogen/air mixtures (15 or 35 mol% H_2) at 16 and 40 atm, and a temperature between 1000–1300 K. The effect of hydrogen is very visible at high temperature; for example, the auto-ignition delays of the mixture CH4/35 % H_2 at 1300 K and 40 atm are reduced by a factor of 1.5 compared to self-ignition delays of methane.

El-Ghafour et al. [9] have investigated the effect of hydrogen addition on combustion characteristics of EM turbulent diffusion flame at a fixed Reynolds number (4000). They found that the addition of hydrogen sustains a progressive improvement in flame stability and reduction in flame length.

Yon and Sautet [10] have studied experimentally the influence of hydrogen addition and the equivalence ratio on the structure of a turbulent diffusion oxy-flame of EM. They confirmed that, in an oxy-fuel burner, hydrogen addition and a lean condition allow an early combustion, a better flame stability, and a decrease of fuel consumption.

It should be noted that the pressure loading following an ignition/combustion event depends strongly on its mode, either deflagration or detonation. In case of a (subsonic) deflagration of a hydrogen–air mixture, a structure of a building may be able to withstand the pressure rise of the combustion process. Although a direct ignition of a detonation is very unlikely due to the required high energy source, a deflagration can turn into a detonation by a deflagration to detonation transition (DDT) process, which can cause very severe damage. DDT can lead to very high pressures (16–20 barg) and flame speeds (1,600–2,000 m/s) even outside congested regions and has a significant impact on the severity of the near-field and far-field explosion loads.

DDT may be a significant threat for hydrogen explosions. The detonability limits of hydrogen lie in the range of 18 % (as low as 11 % in some experiments) to 59 % of hydrogen concentration in air by volume. A measure of the detonation sensitivity of a mixture is the detonation cell size (see Fig. 5). The lower the detonation cell size, the more the likelihood of a transition to detonation. The detonation cell size for a stoichiometric hydrogen–air mixture is of the order of 10–15 mm. In comparison, the value for a methane–air mixture is as large as 330 mm. Due to the high reactivity of hydrogen, DDT is likely in a variety of scenarios involving H_2–air mixtures and result in large-scale damage.

A recent study by Eder et al. [11] has studied the detonability limits of pure hydrogen–air mixtures at ambient temperature and pressure as well as for hydrogen–methane blends. Hydrogen–air detonability studies have been carried out by several previous researchers and Eder et al. [11] have confirmed their conclusions regarding the detonability limits which can occur between ca. 11–60 % hydrogen concentration depending on the conditions.

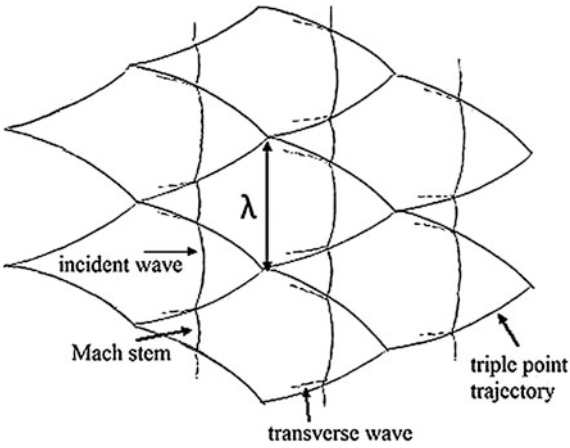

Fig. 5 Typical cellular pattern of a detonation wave

They observed very unexpected combustion behaviour for EM–air mixtures. It was found that due to the lower equivalence ratio of methane–air mixtures, that is the most sensitive to detonation, the minimum mole fraction for detonation onset for EM–air mixtures was in fact 4 % lower for EM–air mixtures than for pure hydrogen–air mixtures for an equivalence ratio of 0.8. Therefore, this indicates EM–air mixtures can be more dangerous than pure hydrogen–air mixtures, if the detonability of both mixtures is concerned! However, further research is required to confirm this statement.

4 CFD Modelling—Explosion Analyses

There are several kinds of tools available to assess the various scenarios associated with a loss of containment, leading to a release. A release can then get ignited and may lead to an ignition event.

Simplified tools based on integral models are unable to account for the geometry, while tools based on CFD are able to include the geometry and its effect on the complex interaction of flow, turbulence, reaction, and combustion. These tools provide a much more accurate estimate of the explosion consequences and are also able to realistically account for the effect of environmental conditions, release parameters, mitigation measures, and more. CFD is therefore an integral part of consequence modelling studies and, if undertaken correctly, can produce a vital design input, leading to safer, more effective designs for various kinds of infrastructure.

CFD modelling is used extensively, e.g. for explosion consequence analyses for petrochemical facilities. However, explosion risk associated with hydrogen and other compressed gas infrastructure is handled very differently at the present time. There is a significant focus on regulations, codes, and standards, e.g. safety distance

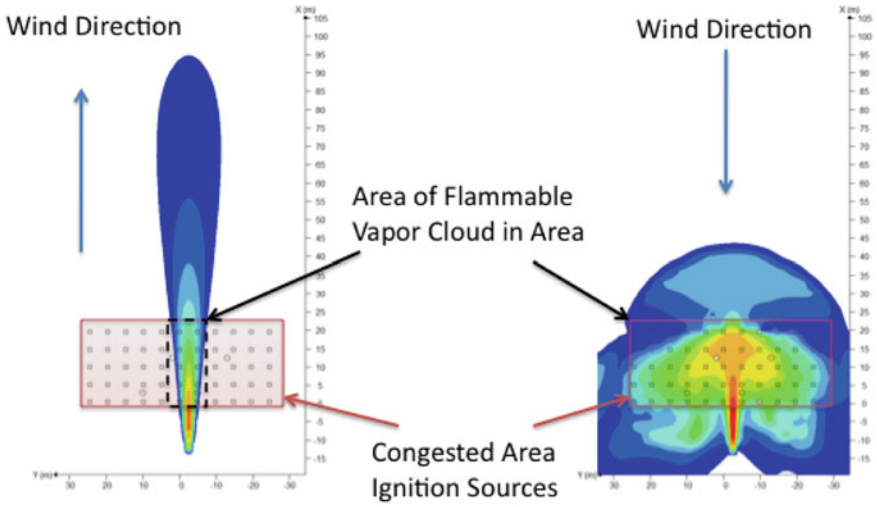

Fig. 6 Gas release in the direction of the wind and not accounting for obstacles (*left*). Same release against the wind and accounting for congestion (*right*). Coloured region of the release is the flammable gas region

rules. CFD is used only occasionally, and mainly for worst-case evaluations. We must accept that it is not realistic to perform an extensive quantitative risk assessment similar to what is required for large petrochemical installations for most applications, but we need to choose the correct methodologies to reduce potential inaccuracies when assigning the risk/safety levels. More details on a potential approach for explosion risk assessments are given in [12].

As an example, Fig. 6 presents the simulation of a gas release in a congested geometry using a simple model (obstacles are not accounted for and wind is only in the direction of the leak) and a CFD simulation for comparison, which takes into account various wind directions and geometry details. The figure shows that the development of the cloud (and hence where/when it might encounter an ignition source) is very dependent on the details of the scenario (geometry, terrain, etc.). The figure also shows that the size of the flammable cloud within the congested/ignition source region is very different in the two cases (CFD shows it to be 20 times larger for this particular case).

The 3D representation of the results, as well as the depth of the analysis, helps engineers to understand the governing physical phenomena that can improve their ability to make critical decisions regarding the explosion risk and how to mitigate it. However, one needs to remember that just applying a CFD tool is not sufficient in itself. One needs to make sure that the tool is applicable (i.e. the problem at hand is within the validation and application envelope of the tool) and also to ensure that best practice guidance is applied in the definition of the scenario, geometry, and mesh.

5 CFD Tool FLACS

The computational fluid dynamics (CFD) software FLACS, developed and maintained by Gexcon in Norway (www.gexcon.com), is an advanced tool for the modelling of ventilation, gas dispersion, gas/vapour cloud explosions, fire (jet and pool), and explosion/blast in complex process areas. The tool is used extensively for simulating scenarios relevant to process safety. It has specifically been designed for modelling the consequences of a flammable gas release in a semi-confined and/or congested region. FLACS solves the compressible Navier–Stokes equations on a 3-D Cartesian grid using the finite volume method. FLACS accounts for the interaction between the flow (including the flame) and complex geometries such as structure, equipment, and pipework. In order to simulate these interactions for realistic geometries without introducing unreasonable demands on the computer resources, a distributed porosity concept is used for representing the geometry on a Cartesian grid. A good description of geometry and the coupling of geometry to the flow, turbulence, and flame are key elements in the modelling.

The numerical model uses a second-order central differencing scheme for resolving diffusive fluxes and a second-order "kappa" scheme (hybrid scheme with weighting between second-order upwind and second-order central difference, with delimiters for some equations) to resolve the convective fluxes. The solver is implicit in nature. The time-stepping scheme used in FLACS is a first-order backward Euler scheme. The discretized equations are solved using the BiCGStab in the SIMPLE pressure correction algorithm [13]. The SIMPLE algorithm has been extended to handle compressible flows with additional source terms for the compression work in the enthalpy equation.

FLACS uses a k–ε model in order to model the convection, diffusion, production, and dissipation of turbulence (see, e.g. [14]). However, the standard k-ε model has been modified by adding source terms for (a) turbulence production by velocity gradients to achieve independent and rapid build-up of the turbulent flow field and (b) representative turbulence production from objects not resolved by the computational grid (subgrid objects). In addition, several other modifications have been implemented [15].

For the combustion modelling, the burning velocity model consists of the following three models [15]:

(a) A laminar burning velocity model that describes the laminar burning velocity as a function of gas mixture, concentration, temperature, pressure, oxygen concentration in air, and amount of inert diluents. One-step reaction kinetics is assumed and a chemical equilibrium model is used to estimate the composition of the combustion products.
(b) A model describing quasi-laminar combustion in the first phases of flame propagation after ignition (and flame instabilities).
(c) A model that describes turbulent burning velocity as a function of turbulence parameters (intensity and length scale). The model is based on a broad range of experimental data [16] and the correlation by Bray (1990).

5.1 Validation for Methane (Natural Gas), Hydrogen, and EM Explosions

We need to be very careful before applying a CFD tool to carry out consequence analyses. The tool needs to be well validated against a range of relevant experiments. The validation should be an integrated part of the tool development, and not be the responsibility of the end user. Validation is key since the physical phenomena that are being studied occur over a wide range of spatial and temporal scales and the models have to be robust enough to capture enough level of detail such that a reasonable predictive capability can be achieved. This is also because it is said, "No one believes an analysis except the analyst" unless it can be demonstrated that the modelling results have a grounding in "reality" which can only be achieved through validation against experimental data.

Significant experimental validation activity has contributed to the wide acceptance of FLACS as a reliable tool for the prediction of natural gas explosions in real process areas offshore and onshore [17]. This has included ventilation, dispersion, and explosion studies.

An accurate description of ventilation characteristics also plays an important role in the estimation of the shape, size, and location of the flammable gas cloud. Through the 1990s, several ventilation validation studies were performed on actual offshore oil installations and large-scale test sites, including Oseberg-C (Hydro), Beryl-B (Mobil), Nelson (Enterprise Oil), and Spadeadam. At the Nelson platform, on-site wind measurements for all major platform areas were performed for a range of different wind conditions and compared to simulations.

The validation activity for dispersion has included experiments involving dispersion of natural gas (and other hydrocarbons) and ignition of a non-homogeneous gas cloud (Gexcon experiments and large-scale experiments as a part of the Phase 3B full-scale tests 18], which is highly relevant for QRA studies performed towards offshore oil and gas industry and elsewhere [18–20]). Since then, FLACS has been used and validated for a growing number of gas dispersion applications, ranging from toxic gas releases (e.g. chlorine, hydrogen sulphide) to liquefied gases (e.g. LNG, LPG). More recently, FLACS was validated against over 30 different dense gas dispersion experiments (involving releases of LNG, H_2S, and CO_2, both from wind tunnels and field-scale tests) that were included in the Model Evaluation Protocol for LNG Vapour Dispersion Models [21].

Some of the noteworthy efforts for natural gas and hydrocarbon explosions include simulations of the 180 m^3 British Gas (Advantica) box [22], 27 m^3 CMR (GexCon) 3D-corner, 50 m^3 CMR (GexCon) M24 module [23, 24], Shell SOLVEX chambers (2.5, 550 m^3), 1–250 m^3 TNO and British Gas MERGE experiments [25], and 1600–2700 m^3 British Gas (Advantica) BFETS [26]/HSE Phase 3A [27].

In the same way, significant validation work for explosion studies for scenarios relevant to hydrogen safety has been carried out in which results obtained with FLACS have been compared with results from hundreds of experiments. This includes tests in tunnels, channels, unconfined geometries (balloons, refueling

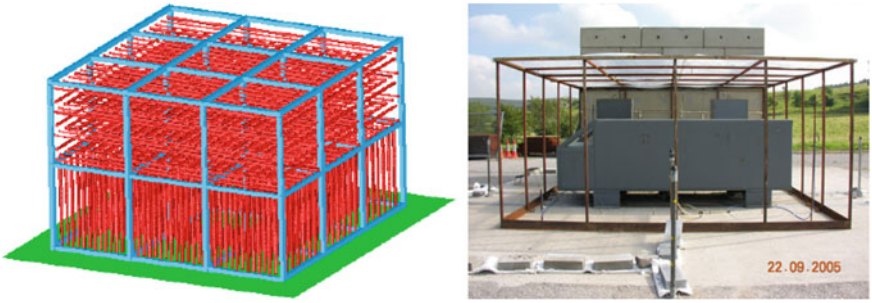

Fig. 7 Examples of geometries used for hydrogen explosion validation: (*left*) highly congested repeated pipe grid and (*right*) Mock hydrogen refueling station

station), highly congested rigs, smooth and obstructed geometries, vented geometries, jet ignition scenarios, and more. Some of the noteworthy efforts for explosion simulations have included 2094 m^3 unconfined balloon tests [28], 136 m^3 Sandia FLAME facility [29], hydrogen refueling station (Fig. 7) [30], highly congested repeated pipe grid (Fig. 7) [30], 108 m^3 Fh-ICT lane geometry with a driver chamber [31], several different experiments (different hydrogen concentrations) involving hydrogen explosions in a tunnel with and without vehicles (Groethe et al. [32]), etc.

Likewise, a large amount of validation has been performed for hydrogen release and dispersion. This has included tests in the 80 m^3 INERIS gallery facility [33], 40 m^3 CEA garage facility [34], and several high-pressure free jet releases (e.g. [35, 36]).

Other validation efforts have included tests involving combined release and dispersion experiments, e.g. FZK/KIT workshop experiments [35] that included nine different vertical leaks (varying nozzle size, release rate, and momentum) impinging on a plate in two configurations. The resulting gas cloud was ignited and overpressures were recorded at various different locations. Simulations (both dispersion and explosion) reported in [37].

Other organisations such as Sandia National Laboratories (USA) and Hydrogen Research Institute (Canada) have also contributed to the validation database for FLACS. For instance, [38] have described a combined experimental and modelling study involving releases from three hydrogen fuel cell vehicles (FCV) inside a tunnel (see Fig. 8). Other studies have included experiments on forklifts in enclosed spaces [39] and experiments on use of barrier walls for mitigation [40].

In addition several validation exercises for liquid hydrogen have been carried out. A detailed summary for most of the hydrogen validation tests described above is given in [41].

Since the validation status for natural gas/methane and hydrogen–air explosions has been established, the next step involved validating the overpressures predicted by the CFD tool for combustion of premixed mixtures of methane and hydrogen

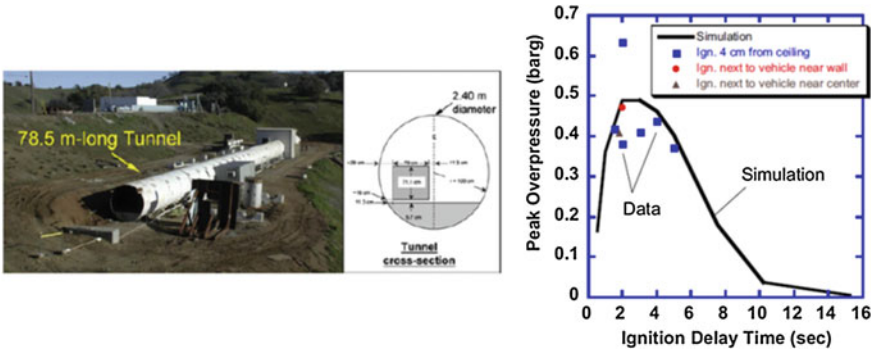

Fig. 8 Tunnel release and explosion experiments at Sandia/SRI and comparison of simulations (FLACS) and experimental data [38]

with air against available experimental data. Shell and HSL have recently performed large-scale explosion experiments with mixtures of hydrogen and methane in a congested volume as part of the NaturalHy project [42]. The main objective of the NaturalHY project was to prepare EU countries for the hydrogen economy by identifying and removing potential barriers regarding the introduction of hydrogen into society, using the extensive existing natural gas system. The basic concept of the project was the smooth and short-term introduction of hydrogen, at relatively low cost, by using the existing natural gas system to carry and distribute mixtures of natural gas and hydrogen. The research focused on investigating how hydrogen will affect the integrity and durability of pipelines in particular crack growth and corrosion.

The hydrogen, introduced into the pipeline network, would mix with the natural gas. This mixture could then be used directly by consumers as a fuel within existing gas powered equipment, with the benefit of lower carbon emissions. In addition, hydrogen could be extracted from the mixture for use in hydrogen-powered engines or for hydrogen fuel cell applications. Using the existing pipeline network to convey hydrogen in this way would enable hydrogen production and hydrogen-fuelled applications to become established prior to the development of a dedicated hydrogen transportation system.

In the safety work package, explosion experiments were performed on a large scale, paying particular attention to the potential for transition from deflagration to detonation. Herein, field-scale experiments were performed to measure the explosion overpressures generated by methane–hydrogen–air mixtures in well-understood repeated pipe congestion. The geometry for the experimental tests is shown in Fig. 9. The pipe array had dimensions 3 m × 3 m × 2 m. In the lower 1 m there were 9 rows of vertical pipes (26 mm diameter) in each direction outward (typical spacing 0.15 m), whereas in the upper 1 m there were 7 layers of horizontal pipes of the same diameter and spacing. Five different methane/hydrogen gas mixtures were applied in the tests; these were 0, 25.5, 51, 75 and 100 % hydrogen.

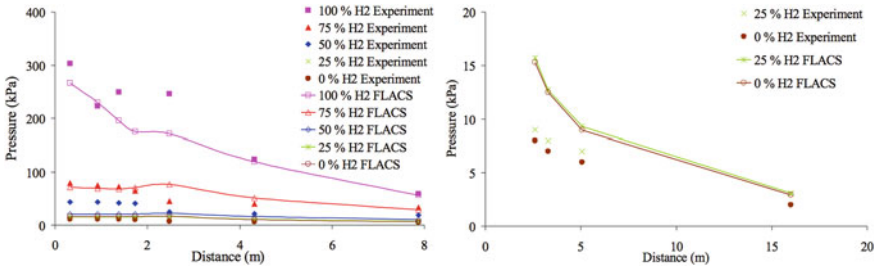

Fig. 9 Pressure recordings (*filled markers*) versus FLACS simulations (*lines*) in monitor arrays parallel to the wall (*left*) and sensors away from wall (*right*) for methane- and EM–air mixtures. Experimental observations are found in [42]. Figure taken from [43]

The pure hydrogen–air mixture had an equivalence ratio of 1.28 (fuel-rich), while the other mixtures were closer to stoichiometry (ER = 1.06–1.09). The ignition source was placed in the middle of the lower part (0.5 m above ground). More details can be found in [42].

Simulations were carried out with FLACS using the experimental conditions. The first part of the work involved validating the flame speeds and flammability limits predicted by FLACS against values available in literature (described above). The laminar burning velocities calculated by FLACS were compared to data obtained experimentally by Ilbas et al. [5] and that obtained using numerical simulations with a detailed reaction mechanism by Di Sarli and Di Benedetto [6]. It was found that the predictions using the mixing rules available in FLACS based on oxygen consumption for each fuel were reasonable. In particular, FLACS predicts an increase of 10 % in the laminar burning velocity of methane–air mixture with the addition of 8 % hydrogen while the increase becomes 30 % with the addition of 20 % hydrogen. Thus, the laminar burning velocity values were used as such and no modifications were carried out.

Subsequently, the geometry was built and the hydrogen–methane mixture combustion was described at the correct stoichiometry. A comparison of experimental and simulation results are shown in Fig. 9 where the pressure decay with distance for various sensors is shown. The top plot shows the results for sensors placed parallel to the wall and the bottom plot presents the results for sensors placed perpendicular to the wall at different distances.

It can be seen that the pressure levels in the explosion are well reproduced for most mixtures. For the pure hydrogen mixture very high pressures were seen at when the flame exited the pipe array (due to a potential DDT). Also the simulation gave very high pressures at the edge of the pipe array, but since DDT was not modelled, this did not yield the observed local pressure increase at the sensor array parallel to the wall. In general, simulated pressure levels corresponded well to the experimental curves; however, in the case with 50 % hydrogen the pressure level seen in the experiment was almost a factor of 2 higher inside the pipe array (the discrepancy outside was less). The second plot in Fig. 9 shows the pressure decay

up to 16 m away from the wall for the cases with pure methane and EM with 25 % hydrogen. The FLACS simulations predicted somewhat higher pressures than seen in the experiments for both cases, but the relative effect of the addition of 25 % hydrogen was found to be very similar to observed giving only a marginal pressure increase. It may therefore be concluded that most experiments are reproduced reasonably well with FLACS, and that the relative effect of adding 25 % hydrogen to methane seems to be well predicted.

6 Practical Explosion Studies for Enriched Methane

A practical study to determine the relative risk of methane, hydrogen, and EM (a blend of hydrogen and methane) is described next. Typical transport infrastructure such as vehicular tunnels, garages, etc., has been used to demonstrate positive safety benefits of EM with comparisons to similar simulations for both hydrogen and methane (all the gases were under high pressure or compressed). For this purpose, several different mixture compositions (e.g. 8, 20, and 30 % hydrogen) were considered. The evaluation of (a) dispersion characteristics (which are more positive than for methane due to increased buoyancy), (b) combustion characteristics (which are closer to methane than hydrogen), and (c) Combined dispersion + explosion risk was performed. The explosion consequences for EM are expected to be comparable to that of pure methane, possibly lower in some situations, and definitely lower than for pure hydrogen.

All details of this work are provided in [43]. Rosas et al. [44] have also performed CFD simulations of explosions of methane–hydrogen mixtures and validated them with experimental data available in the literature.

In the study described below, three different release scenarios were evaluated, all originating from a pressure relief device (PRD) on a vehicle using compressed gas as fuel.

These included:

- Gas release from a car in a private garage
- Gas release from a car in a public parking garage (two release locations)
- Gas release from a bus in a typical tunnel

The simulations were performed to evaluate potential worst-case scenarios, which was a PRD release that was allowed to mix with air to form a premixed fuel–air cloud, followed by a delayed ignition leading to an explosion event. Note that no analysis was carried out herein to determine the likelihood or probability of such an event.

In order to determine a leak profile (leak rate as a function of time), the car used in the study was assumed to contain 4 kg hydrogen (at 700 bar) or 26 kg methane (at 200 bar). The city bus was assumed to contain 20 kg hydrogen (at 350 bar) or 104 kg methane (at 200 bar). EM was assumed to be using methane storage

systems, with 20 % of the natural gas replaced with hydrogen. The amounts were determined based on the same range/energy content.

The first scenario was a two-car private parking garage attached to a house, with a floor area of 35 m^2. Dispersion simulations were performed for each of methane, hydrogen, and EM PRD releases from a "parked" vehicle. The simulations clearly showed that the PRD release would quickly fill up the available volume. The concentration in the room was almost uniform due to a high flow velocity and ensuing mixing.

For hydrogen, the mixture was found to be close to stoichiometric (approx. 30 % volume fraction) after less than 5 s. After 20 s, the hydrogen concentration was around 60 % by volume (but still within the flammability limits). When the release ended, hydrogen gradually flowed out of the upper vent opening and was replaced by air (after 500 s half the volume was still flammable). Because of the very wide flammability limits for hydrogen (between 4 and 75 %), practically all of the room was within the flammability limits for the first 4 min, and thereafter, cold air pushed the buoyant hydrogen out of the upper vent opening over the next 10 min.

For the methane and EM scenarios, the development was quite different. After around 15 s, very reactive concentrations of gas could be seen in most of the room. The flammable range for both methane and EM is much smaller compared to hydrogen. Therefore, within a short period of time (roughly 30 s), the whole garage reached concentrations above the upper flammability limit (UFL) and could not be ignited. At the end of the release phase, a similar venting mechanism was evident where cold air diluted the rich mixture. During the venting/dilution phase, a thin layer of gas (diluted by air) became flammable again (representing around 20–25 % of the volume of the garage). The flammable cloud volume as a function of time for all three gases is shown in Fig. 10. It can be seen that the flammable cloud resulting from an EM release was initially larger than that from a methane release, but the values were very similar during the venting process afterwards.

Explosion calculations were carried out for each of these scenarios in order to estimate the expected worst-case explosion loads that could be expected if such a

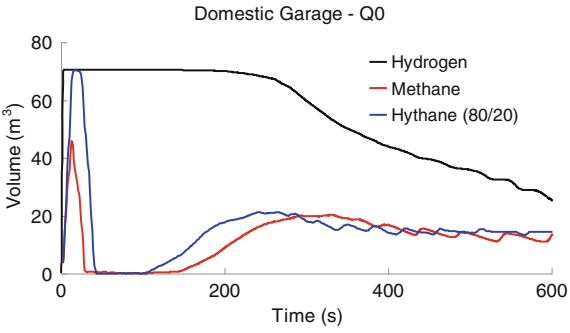

Fig. 10 Flammable gas cloud volume for hydrogen, methane, and EM mixtures for releases from a PRD from a vehicle in a private garage. Figure taken from [43]

scenario would occur. The largest gas clouds were ignited for each of the release scenario (for hydrogen, methane, and EM). The overpressures following a hydrogen explosion were very high (4 barg or 400 kPa), and had the potential to destroy the adjacent house. However, the methane (0.11 barg or 11 kPa) and EM (0.15 barg or 15 kPa) overpressures were much lower and therefore less of a concern. These can destroy the garage, but the damage to the adjacent house is expected to be insignificant. The reason for the slightly higher pressure seen in the explosion with EM compared to methane in this case was mainly the larger gas cloud as seen in Fig. 10, and not necessarily the higher reactivity of EM.

Calculations were also carried out for potential releases in a typical public parking garage (it was assumed to have three decks). The release scenarios considered were PRD releases from a car either in the middle of a large open area with flat ceiling (2.75 m height) or in a more confined corner with lower ceiling (2.50 m height) in which some significant structural beams in the ceiling give some extra confinement. Both release scenarios were assumed to occur on the middle deck.

In this case, it was seen that the maximum flammable clouds for hydrogen (200–500 m^3, the values being higher for the corner release) were much larger than that of methane and EM (8–40 m^3). Most of the cloud volume was, however, quite dilute with concentrations near the lower flammable limit and is therefore of low reactivity (this behaviour can be pretty typical for hydrogen due to the very high buoyancy). For the centre release scenario no accumulation of gas was found to take place, and thus the hazard is quite limited. However, due to higher confinement for the corner release scenario, it took somewhat longer for the gas to disperse, leading to a greater exposure time for the cloud to encounter a potential ignition source.

Hydrogen explosions using the gas cloud sizes generated resulted in significant explosion overpressures of the order 0.5 barg (50 kPa). This is due to high reactivity as well as contribution from jet-induced turbulence to flame acceleration. However, the pressures quickly decayed with distance due to a relatively small cloud size (and hence limited energy). However, due to much smaller clouds and also a lower reactivity, the explosion overpressures for scenarios with both methane and EM were predicted to be very low (less than 10 mbarg).

The third scenario that was considered was a road tunnel (see also validation work presented earlier, for pure hydrogen–air mixtures). This was a one-way tunnel with two lanes, and a cross section of about 6 m × 4 m (rectangular). The tunnel was assumed to be full of vehicles (with a mix of cars, buses, and trucks based on traffic data).

The release scenario was a PRD release from a city bus in the centre of the tunnel (releases from a car were not considered here). The results are shown in Fig. 11. It can be seen that the volume of the flammable cloud predicted following a hydrogen release was twice as high as that for methane or EM, but most of this cloud was again found to be very dilute. It was seen that the volumes near stoichiometry (about 10 % volume fraction) were much higher for methane and EM (approx. 5 times higher) than for hydrogen.

There was also a significant difference in the time for reaching the “most severe” cloud size. This was only 20 s for hydrogen but up to 100 s for methane and EM.

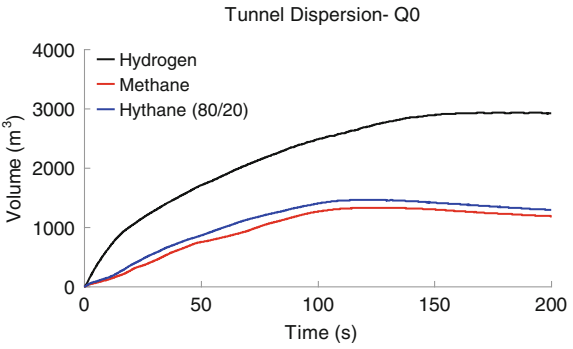

Fig. 11 Flammable gas cloud volume for hydrogen, methane, and EM mixtures for releases from a PRD from a city bus in a typical tunnel. Figure taken from [43]

The main reasons for the difference was that the hydrogen leak profile decayed faster (larger initial release rate due to higher pressure), larger mixing/dilution for hydrogen (due to higher release velocity and more buoyancy), and the lower buoyancy of methane and EM that makes it more likely to generate a dangerous gas cloud through the full cross section.

The gas clouds were subsequently ignited (using the largest or worst-case cloud sizes) for each of the release scenarios. As expected and seen earlier, hydrogen still yielded the highest overpressure (2.2 barg or 220 kPa) due to its higher reactivity. However, the methane overpressure was found to be comparable in this case (1.6 barg or 160 kPa). This is because the methane–air clouds were much closer to stoichiometry compared to the hydrogen cloud, which was much more dilute (due to more mixing), as mentioned above.

It was also seen that the methane explosion overpressure was in fact higher than the EM pressure (0.97 barg or 97 kPa) for the tunnel release scenario. This is the first instance where the positive dispersion properties of EM have resulted in a lower explosion consequence. In Fig. 11, it can be seen that the EM and methane gas clouds are of comparable size. However, the methane cloud was found to be somewhat closer to stoichiometry than EM, thus having higher reactivity. Two possible explanations for this are that the EM release rates decay somewhat towards the end of the release due to a higher flow rate initially, and also that the early jet momentum and thus mixing/dilution is somewhat higher for EM than for methane.

Kang et al. [45] have also performed consequence analysis for a gas explosion and a jet fire following a release in a typical high-pressure gas filling station using CFD/FLACS. The gases in question were compressed natural gas or methane (CNG), hydrogen and a hydrogen–natural gas blend (containing 30 % hydrogen). The explosion event resulted in a maximum overpressure of 0.3 barg (30 kPa) for hydrogen while the overpressures for CNG was minimal (4 mbarg or 0.4 kPa). EM explosions led to an overpressure of 35 mbarg (3.5 kPa). EM explosions were thus about 8 times stronger than a CNG/methane explosion but about 9 times smaller than a hydrogen explosion. The flame propagation velocity was also much smaller for methane and EM compared to hydrogen. The estimated jet flame length was,

however, comparable: 5.5 m for hydrogen, 3.4 m for CNG, and 3.9 m for EM. The results for this work are comparable to the ones reported above.

Dan et al. [46, 47] have carried out a quantitative risk analysis of filling stations using EM. They have also looked at different kinds of explosion models (simple as well as CFD) and provided guidelines for when a certain model can be used. For instance, simple models can provide a sufficient level of detail if only far-field pressures are of interest. It was also predicted that conventional gas filling stations would be converted as new energy stations without any additional explosion risk.

Therefore, it can be postulated that, in general, EM explosions are somewhat stronger than methane explosions, and that both of these give significantly lower pressures compared to pure hydrogen (as expected). In the tunnel case, however, somewhat higher pressures were seen with methane compared to EM (see plausible explanations above).

7 Conclusions

It has been established that the use of EM represents a plausible and reasonable step towards the development of an ultimate "hydrogen economy". This infrastructure will continue to be useful in the future and a pre-approval of "EM" is a good way to satisfy all regulatory and public perception requirements. However, the use of EM carries many potential hazards due to its flammable nature, and the addition of hydrogen to methane does increase the explosion risk. This points to the need for establishing viable tools to carry out the required safety and risk analyses connected with the use of EM infrastructure. It is possible to use both simplified methods (venting guidelines, etc.) and advanced tools such as those based on Computational Fluid Dynamics (CFD) in order to carry out the required safety analyses. However, only CFD tools have the potential to model the relevant physics involved in safety analyses. With CFD, it is possible to take account of effects of buildings, mitigation measures, piping and vessel arrangements, etc., which have been found to have a strong influence on the consequences of any accident or unwanted incident. A primary requirement for the use of any such tool, in addition to the models capturing the correct physics, is extensive validation against available small- and large- scale experiments (with studies on variations of various important parameters that may affect explosion loads and hence risk).

The chapter has described one such tool (FLACS) and established its validation database for the simulation of methane, hydrogen, and EM explosions. Further, simulation studies have been described in practical systems such as a private garage, a parking house, a tunnel, and a refuelling station. These have been performed in order to evaluate the safety aspects of EM relative to methane and hydrogen. In general, it has been found that EM explosions would be marginally stronger than methane explosions, and that both of these will give significantly lower pressures compared to pure hydrogen. In the tunnel case, however, somewhat higher pressures were seen with methane compared to EM. However, all these studies have

been based on a "worst-case analysis" and no proper quantitative risk assessment has been carried out.

These studies have shown that the EM explosion risk is manageable and hence the use of EM does not offer any significant disadvantage with respect to explosion safety.

References

1. Bjerketvedt D, Bakke JR, van Wingerden K (1997) Gas explosion handbook. J Hazard Mat 52:1–150
2. Dobashi R, Kawamura S, Kuwana K, Nakayama Y (2011) Consequence analysis of blast wave from accidental gas explosions. Proc Comb Inst 33:2295–2301
3. Lobato J, Cañizares P, Rodrigo MA, Sáez C, Linares JJ (2006) A comparison of hydrogen cloud explosion models and the study of the vulnerability of the damage caused by an explosion of H2. Intl J Hyd Ener 31(12):1780–1790
4. Dorofeev SB (2007) Evaluation of safety distances related to unconfined hydrogen explosions. Intl J Hyd Ener 32:2118–2124
5. Ilbas M, Crayford AP, Yilmaz I, Bowen PJ, Syred N (2006) Laminar-burning velocities of hydrogen-air and hydrogen-methane-air mixtures: an experimental study. Intl J Hyd Ener 31:1768–1779
6. Di Sarli V, Di Benedetto A (2007) Laminar burning velocity of hydrogen-methane/air premixed flames. Intl J Hyd Ener 32:637–646
7. Gersen S, Anikin NB, Mokhov AV, Levinsky HB (2008) Ignition properties of methane/hydrogen mixtures in rapid compression machine. Int J Hydrogen Energy 33 (7):1957–1964
8. Huang J, Bushe W K, Hill P G, et al. (2006) Experimental and kinetic study of shock initiated ignition in homogeneous methane-hydrogen-air mixtures at engine-relevant conditions. Int J Chem Kinet 38 221–233
9. El-Ghafour SAA, El-dein AHE, Aref AAR (2010) Combustion characteristics of natural as-hydrogen hybrid fuel turbulent diffusion flame. Intl J Hyd Ener 35(6):2556–2565
10. Yon S, Sautet JC (2012) Flame lift off height, velocity flow and mixing of EM in oxy-combustion in a burner with two separated jets. Appl Therm Eng 32(1):83–92
11. Eder A, F Pingten, Mayinger F (2001) Propagation of fast deflagrations and marginal detonations in hydrogen–air-additive mixtures. In: Proceedings of 18th international colloquium on the dynamics of explosions and reactive systems, Seattle, Washington, vol 181
12. Hansen OR, Middha P (2008) CFD-based risk assessment for hydrogen applications. Proc Saf Prog 27(1):29–34
13. Patankar SV (1980) Numerical heat transfer and fluid flow. Hemisphere Publishing, ISBN: 0070487405
14. Launder BE, Spalding DP (1974) The numerical computation of turbulent flows. Comp Meth Appl Mech Eng 3(2):269–289
15. Arntzen BJ (1998) Modelling of turbulence and combustion for simulation of gas explosions in complex geometries. Dr. Ing. Thesis, NTNU, Trondheim, Norway
16. Abdel-Gayed RG, Bradley D, Lawes M (1987) Turbulent burning velocities: a general correlation in terms of straining rates. Proc R Soc Lond A 414:389–413
17. Hansen OR, Storvik I, van Wingerden K (1999) Validation of CFD-models for gas explosions, FLACS is used as example. Model description, experiences and recommendations for model evaluation. Presented at the 'European meeting on chemical Industry and Environment', Krakow, Poland, pp 1–3

18. Johnson DM, Cleaver RP, Puttock JS, van Wingerden CJM (2002) Investigation of Gas Dispersion and Explosions in Offshore Modules, Offshore Technology Conference, Paper 14134. Houston, TX
19. Hansen OR, Gavelli F, Davis SG, Middha P (2011/2013) Equivalent cloud methods used for explosion risk and consequence studies, Mary Kay O'Connor process safety center 2011 international symposium, College Station, TX, USA, 25–27 October 2011. J Loss Prev Process Ind, 26(3), 511–527
20. Hansen OR, Renoult J, Bakke JR (2001) Explosion risk assessment: how the results vary with the approach chosen. fall symposium proceedings, Mary Kay O' Connor Process Safety Centre, Department of Chemical Engineering, Texas A&M University, 3122 TAMU, College Station, TX 77843–3122, pp 395–410
21. Hansen OR, Gavelli F, Ichard M, Davis SG (2010) Validation of FLACS against experimental data sets from the model evaluation database for LNG vapour dispersion. J Loss Prev Process Ind 23:857–877
22. Catlin C, Gregory CAJ, Johnson DM, Walker DG (1993) Explosion mitigation in offshore modules by general area deluge, Trans. IChemE, 71, Part B
23. Hjertager BH, Bjørkhaug M, Fuhre K (1988) Gas explosion experiments in 1:33 scale and 1:5 scale; offshore separator and compressor modules using stoichiometric homogeneous fuel–air clouds. J Loss Prev Process Ind 1:197–205
24. Hjertager BH, Bjørkhaug M, Fuhre K (1988) Explosion propagation of non- homogeneous methane-air clouds inside an obstructed 50 m3 vented vessel. J Haz Mater 19:139–153
25. Mercx WPM (1996) Extended modelling and experimental research into gas explosions, CEC EMERGE project final summary report, EV5VCT930274 (TNO)
26. Selby C, Burgan B (1998) Blast and fire engineering for topside structures, phase 2, final summary report, SCI Publication 253, Steel Construction Institute, UK
27. Al-Hassan T, Johnson DM (1998) Gas explosions in large-scale offshore module geometries: overpressures, mitigation and repeatability, presented at OMAE-98. Lisbon, Portugal
28. Schneider H, Pförtner H (1983) PNP-Sichcrheitssofortprogramm, Prozebgasfreisetzung-Explosion in der gasfabrik und auswirkungen von Druckwellen auf das Containment
29. Sherman MP, Tieszen SR, Benedick WB (1989) FLAME facility, the effect of obstacles and transverse venting on flame acceleration and transition to detonation for hydrogen- air mixtures at large scale, Sandia National Laboratories, Albuquerque, NM 87185, NUREG/CR-5275, SAND85–1264, R3, USA
30. Shirvill LC, Royle M, Roberts TA (2007) Hydrogen releases ignited in a simulated vehicle refuelling environment. In: Proceeding of the 2nd international conference for hydrogen safety, San Sebastian, Spain, pp 11–13
31. Pförtner H, Schneider H (1984) Tests with jet ignition of partially confined hydrogen air mixtures in view of the scaling of the transition from deflagration to detonation. Final Report for Interatom GmbH, Bergisch Gladbach, Germany, (Fraunhofer ICT Internal Report)
32. Groethe M, Merilo E, Colton J, Chiba S, Sato Y, Iwabuchi H (2007) Large-scale hydrogen deflagrations and detonations. International Journal of Hydrogen Energy 32, 2125–2133
33. Lacome JM, Dagba Y, Jamois D, Perrette L Proust Ch. (2007). Large-scale hydrogen release in an isothermal confined area. In: 2nd International conference on hydrogen safety, 11–13 September 2007, San Sebastian, Spain
34. Gupta S, Brinster J, Studer E, Tkatschenko I (2007) Hydrogen related risks within a private garage: concentration measurements in a realistic full-scale experimental facility. In: Proceedings of the 2nd international conference on hydrogen safety, San Sebastian, Spain
35. Friedrich A, Grune J, Kotchourko N, Kotchourko A, Sempert K, Stern G, Kuznetsov M (2007) Experimental study of jet-formed hydrogen-air mixtures and pressure loads from their deflagrations in low confined surroundings. In: Proceedings of 2nd international conference on hydrogen safety, San Sebastian, Spain
36. Shirvill LC, Roberts PT, Roberts T A, Butler CJ Royle M (2006) Dispersion of hydrogen from high-pressure sources. In: Proceedings of hazards XIX conference. Manchester, UK, pp 27–30

37. Middha P, Hansen OR, Grune J, Kotchourko A (2010) CFD calculations of gas leak dispersion and subsequent gas explosions: validation against ignited impinging hydrogen jet experiments. J Hazard Mater 179:84–94
38. Houf WG, Evans GH, Merilo E, Groethe M, James SC (2012) Releases from hydrogen fuel-cell vehicles in tunnels. Intl J Hyd Ener 37(1):715–719
39. Houf WG, Evans GH, Ekoto IW, Merilo E, Groethe M (2013) Hydrogen fuel-cell forklift vehicle releases in enclosed spaces. Intl J Hyd Ener 38(19):8179–8189
40. Houf WG, Evans GH, Schefer RW, Merilo E, Groethe M (2011) A study of barrier walls for mitigation of unintended releases of hydrogen. Intl J Hyd Ener 36(3):2520–2529
41. Middha P (2010) Development, use and validation of the CFD tool FLACS for hydrogen safety studies. PhD Thesis, Institute of Physics and Technology, University of Bergen, Bergen, Norway
42. Royle M, Shirvill LC, Roberts TA (2007) Vapour cloud explosions from the ignition of methane/hydrogen/air mixtures in a congested region. In: Proceedings of 2nd international conference of hydrogen safety, San Sebastian, Spain, pp 11–13
43. Middha P, Engel D, Hansen OR (2011) Can the addition of hydrogen to natural gas reduce the explosion risk? Intl J Hyd Ener 36(3):2628–2636
44. Rosas C, Nayak S, Munoz F, Mannan MS (2011) Simulation and validation of methane and hydrogen mixtures explosion using CFD models. In: Mary Kay O´Connor process safety centre 2011 international symposium, College Station, TX, USA
45. Kang S-K, Bang H-J, Jo H-J (2013) Consequence analysis of hydrogen blended natural gas (HCNG) using 3D CFD Simulation. J Korean Inst Gas, 17(5)
46. Dan S-K, Moon D-J, Yoon E-S, Shin D-I (2013) Analysis of gas explosion consequence models for the explosion risk control in the new gas energy filling stations. Ind Eng Chem Res 52(22):7265–7273
47. Dan S-K, Park K-J, Kim T-O, Shin D-I (2011) Explosion simulations for the quantitative risk analysis of new energy filling stations. J Korean Institute Gas 15(1):60–67
48. Groethe M, Merilo E, Colton J, Chiba S, Sato Y, Iwabuchi H (2005) Large-scale hydrogen deflagrations and detonations. In: Proceedings of the 1st international conference on hydrogen safety, Pisa, Italy
49. www.edenenergy.com.au/pdfs/20061101%20EM%20presentation.pdf
50. www.EM.com/system.html